
Synthesis of New Functional Molecules for Molecular Electronics

Inaugural Dissertation

Zur

Erlangung der Würde eines Doktors der Philosophie

vorgelegt der

Philosophisch-Naturwissenschaftlichen Fakultät

der Universität Basel



von

Nicolas Jenny

aus

Basel (BS), Schweiz

Basel 2012

Genehmigt von der Philosophisch-Naturwissenschaftlichen Fakultät der Universität Basel auf Antrag
von

Prof. Dr. Marcel Mayor

Prof. Dr. Thomas Ward

Basel, den 26 Juni 2012

Prof. Dr. Martin Spiess

Originaldokument gespeichert auf dem Dokumentenserver der Universität Basel
edoc.unibas.ch



Dieses Werk ist unter dem Vertrag „Creative Commons Namensnennung-Keine
kommerzielle Nutzung-Keine Bearbeitung 2.5 Schweiz“ lizenziert. Die vollständige Lizenz
kann unter
creativecommons.org/licences/by-nc-nd/2.5/ch
eingesehen werden.

Acknowledgments

I would like to thank Prof. Dr. Marcel Mayor for giving me the opportunity to work on such an interesting project. I am especially thankful for his help and guidance during my PhD-work.

I would like to thank all the current and past members of the Mayor group. A great thank goes to the lab 04 for being excellent lab mates and good friends outside of work.

A special thank goes to Tom Eaton for proofreading my thesis, for co-publishing a review article and for having fruitful discussions apart from chemistry.

I also thank Michel Rickhaus for teaching me how to do the artworks which are presented in this thesis.

I thank Hong Wang and Prof. Lifeng Chi from the University of Muenster for their fruitful collaboration providing excellent STM images and surface analysis. I would also like to thank Prof. Dr. Michel Calame and Jan Brunner from the physics department at the University of Basel for the break junction measurements and Dr. Markus Neuburger for the X-ray analysis.

I also thank Heiko Gsellinger and Dr. Daniel Häusinger for their help with the 2D NMR measurements and Dr. Heinz Nadig for measuring FAB- and EI-mass spectrometry.

Special thanks go to the technical staff: Markus Hauri, Andreas Koller, Alois Schäuble and Roy Lipps.

A big thank goes to my family and friends. A special thank goes to my girlfriend Nina who supported me with her patience and love during the past four years.

Abstract

Molecular electronics is an interdisciplinary field where chemists, physicists and biologists come together to investigate electronic phenomena at the molecular level. From the chemists point of view the design and synthesis of new model compounds which have a controllable function is very much in the foreground. In this work we focus on the synthetic aspect towards such new compounds especially on the incorporation of ferrocene into macrocycles which can act as molecular wires. The fascinating property of ferrocene is its switchable redox-state which has a direct influence on the molecular energy levels and thus the electronic properties including conductivity.

Chapter 1 provides an introduction to the field of molecular electronics. First, the integration techniques of single molecules into electric circuits are described. The structure-property relationships of molecules are then discussed and illustrated with a few examples. Then, the work which has been done with ferrocene and macrocycles is described followed by a collection of synthetic strategies which are useful to assemble complex structures such as ferrocene-macrocycles. Chapter 1 is then completed with a description of the individual projects.

Chapter 2 describes the synthesis of halogen end-capped oligo-phenylene-ethynylenes to study the interactions at the solid/liquid interface and in crystal structures. In addition the possibility of contacting halogen-end groups with gold electrodes is discussed.

Chapter 3 describes the synthesis of a molecular switch where a ferrocene was incorporated into an oligo-phenylene-vinylene structure. Electrochemical-, spectroelectrochemical- and break junction-experiments are discussed.

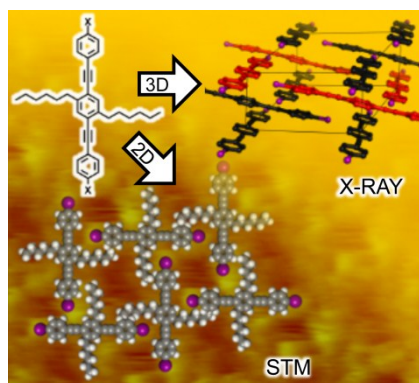
Chapter 4 describes the synthesis of two macrocycles which incorporate a ferrocene unit. The focus lies on the synthetic strategy to develop a route which allows control of the shape of the macrocycle at a very late stage of the synthetic sequence by introducing different linker molecules.

Chapter 5 describes the synthesis towards a macrocycle comprising two ferrocene units.

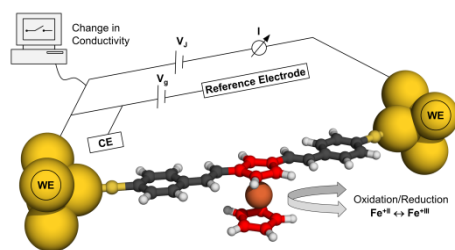
Chapter 6 summarizes the work and provides an outlook.

Chapter 7 provides the experimental details including the characterization of all compounds described throughout the thesis.

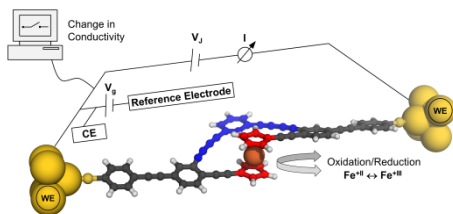
Individual Projects



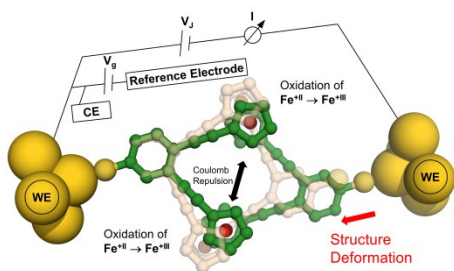
We have synthesized a series of halogen end-capped oligo-phenylene-ethynylenes to study the interactions at the solid/liquid interface and in crystal structures. The range of halogen based interactions and the diversity of intermolecular forces along different crystal axes makes the investigation of such structures particular interesting and challenging. Here we probe the interplay of halide end-groups and the backbone of an OPE to investigate the intermolecular interactions by comparing solution depositions (2D) to x-ray crystal structures (3D). The comparison of the STM images and the crystal structures revealed a striking complementarity in each case.



A 1,3-disubstituted ferrocene wire was successfully synthesized in 14 steps. The cyclic voltammetry experiments on our model compound revealed a fully reversible redox system. The spectroelectrochemical investigation showed that our system can be reversibly switched between Fe^{+II} and Fe^{+III} . The final break junction experiments showed a low plateau yield of 12 % which was too low for a proper statistical analysis.



Two macrocyclic structures comprising a ferrocene unit have been synthesized in 18 steps. The synthesis was developed to change the structural conformation by changing the linker molecule at a very late stage of the synthetic sequence. Such ferrocene structures are envisaged to mimic transistor-like behavior when they are integrated into a three terminal device (electrochemical gating).



The synthesis towards a ferroceneophane comprising two ferrocene joints was envisaged to observe distortion of a rigid macrocycle upon oxidation. The final cyclization failed due to competitive homo-coupling reactions. These findings lead to the synthesis of a new model compound for future break junction experiments.

Table of Content

1	Introduction.....	1
1.1	Molecular Electronics.....	4
1.1.1	Contacting the Molecule	4
1.1.1.1	Mechanically controllable break junctions	4
1.1.1.2	Scanning probe techniques	7
1.1.1.3	Electromigration induced break junction.....	9
1.1.1.4	Three terminal devices	10
1.1.2	Structure-Property Relationship.....	12
1.1.2.1	Anchor groups.....	12
1.1.2.1	Length dependence	13
1.1.2.2	Influence of the conjugation	15
1.1.2.3	Torsion angle dependence.....	16
1.2	Ferrocene compounds.....	19
1.2.1	Electrochemistry.....	19
1.2.2	Ferrocene in functional molecules	20
1.3	Functional Macrocycles.....	27
1.4	Phenyl-Acetylene Bond Formation	29
1.4.1	Synthetic Strategy: where to make the disconnection.....	31
1.4.2	Reactivity and Chemoselectivity of Phenyls.....	37
1.4.3	Masking: using functional group interconversions to control reactivity.....	41
1.4.4	Acetylene Protecting Groups (PGs)	44
1.4.5	Breaking the Symmetry – I: statistical coupling	49
1.4.6	Breaking the Symmetry – II: statistical deprotection.....	50
1.4.7	In Situ Generation of Free Acetylene.....	52
1.4.8	Concepts Applied to Representative Syntheses	54
2	Oligo-Phenylene-Ethynylene Structures with Halide End-Groups	61
2.1	Concept.....	61

Table of Content

2.2	Synthetic Strategy.....	63
2.3	Synthesis.....	64
2.4	Solid-state Investigations.....	68
2.4.1	Dichloro-OPE and dibromo-OPE:	69
2.4.2	Diiodo-OPE:.....	71
2.5	Conclusions of the Solid State Investigations	74
2.6	Break Junction Experiments.....	75
3	Ferrocene Oligo-Phenylene-Vinylene Structures	79
3.1	Concept.....	79
3.2	Synthetic Strategy.....	81
3.3	Synthesis.....	82
3.3.1	Synthesis of 1,3-ferrocenedicarbaldehyde	82
3.3.2	Phosphonate synthesis.....	84
3.3.3	Synthesis of 1,3-bis(vinylene-phenylene)ferrocene	85
3.3.4	Approach with a different protecting group.....	87
3.4	UV-Deprotection Experiments	88
3.5	Synthesis of further ferrocene compounds	90
3.6	Electrochemical investigations	93
3.6.1	Cyclic Voltammetry experiments.....	95
3.7	Spectro-electrochemistry	97
3.8	Break Junction Experiments.....	99
3.9	Conclusion.....	101
4	Synthesis of Interlinked Molecular Wires	103
4.1	Concept.....	103
4.1.1	Synthetic Strategy	105
4.1.2	Structure Calculation.....	108
4.2	Synthesis.....	109

Table of Content

4.2.1	Synthesis of the asymmetric acetylene building block	109
4.2.2	Assembly of the ferrocene wire	111
4.2.3	Synthesis of various linkers.....	113
4.2.4	Cyclization via S _N 2 reaction.....	115
4.2.5	Cyclization via Cadiot-Chodkiewicz coupling	121
4.2.6	Synthesis.....	123
4.3	Conclusion.....	129
5	Car-jack molecule comprising two ferrocene joins	131
5.1	Concept.....	131
5.2	Strategic considerations	132
5.3	Synthesis.....	133
5.3.1	Outlook.....	140
5.4	Conclusion.....	141
6	Summary.....	143
7	Experimental Part.....	147
7.1	General Remarks	147
7.2	Synthesis of oligo-phenylene-ethynylenes	149
7.3	Synthesis of Ferrocene Derivatives	167
7.4	Synthesis of a Interlinked Molecular Wire.....	186
7.5	Synthesis of a Car-jack Molecule.....	210
8	Bibliography	223
9	Appendix.....	235
9.1	Abbreviations.....	235
9.2	Contributions	237
9.3	Spectra of target structures	238

1 Introduction

The technical development of mankind is based on two principles. The first principle is to invent new machines which give access to new functionalities. The second principle is to develop the already existing technology in terms of production costs, efficiency of the actual function, life time and of course reducing the size of the device. A nice example of such a development is the mobile phone. In the beginning, about 20 years ago, mobile phones were very expensive, big and heavy, had an operation time of a few hours and on top of that were only able to make and receive phone calls and text messages. Nowadays, the mobile phone device still has the same purpose but much more additional functions such as internet access, integrated digital cameras, colored touchscreens and many more. The phones are also smaller, cheaper in their production costs and they have an operational time up to a week (depending on the battery used).

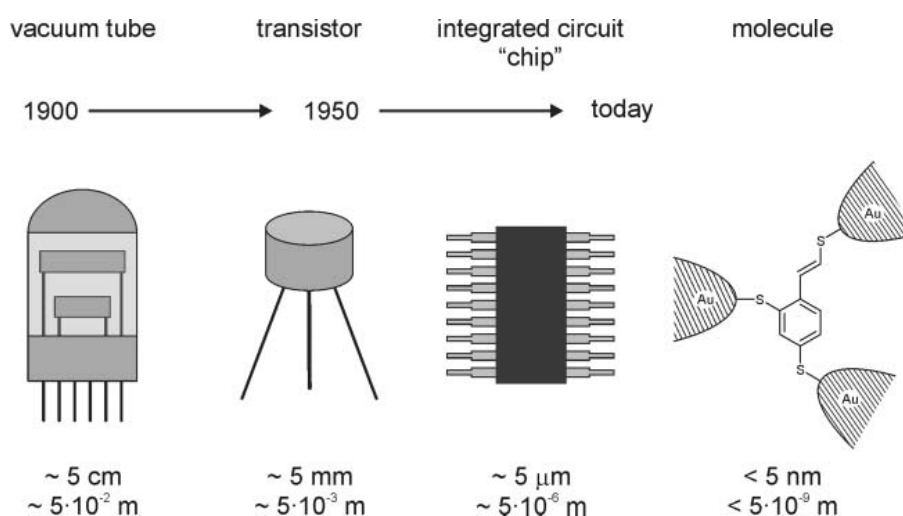


Figure 1. Miniaturization from modular building blocks to molecular junctions. Reprinted from Weibel et al.^[1]

A large influence in such a development is the miniaturization of existing technologies (figure 1). Computer chips have become much smaller and are therefore capable of processing more tasks at the same time. Of course the size of a computer chip does not increase the speed of the initial process (it usually relates to the clock rate which is determined by the frequency of an oscillator crystal) but the fact that much more transistors can be placed in the same

surface area results in an increase in the calculating capacity. This miniaturization trend could especially be observed in the computer industry. The method to reduce the size of a computer chip is called a top-down approach. This process involves techniques such as imaging, deposition and etching which are usually achieved by photolithography.

The lithography technique itself is limited to the wavelength available, which on the other hand limits the possible resolution on the silicon waver. As a result, the top-down miniaturization has reached its limit since one cannot go much further down as 32 nm (i7 core from Intel).

Since the scientific community has realized that the top-down approach is at its limit, a new strategy was elaborated. The idea was to use smaller building blocks and assemble them to larger functional machines which are still smaller in size compared to the ones fabricated by a top-down approach. The idea of the so called bottom up approach was presented by Richard Feynman during his famous talk at *Caltec* in 1959 saying: “There’s plenty of room at the bottom.”^[2] Even though his ideas were very visionary at the time, the computer chips produced today are actually based on the same approach (IC, CMOS, etc.).

The smallest building blocks which still have the structural variety to address functions are molecules. However, the molecules still have to be arranged in the desired direction and their overall functionality has to be explored. That is where the term of molecular electronics sets in.

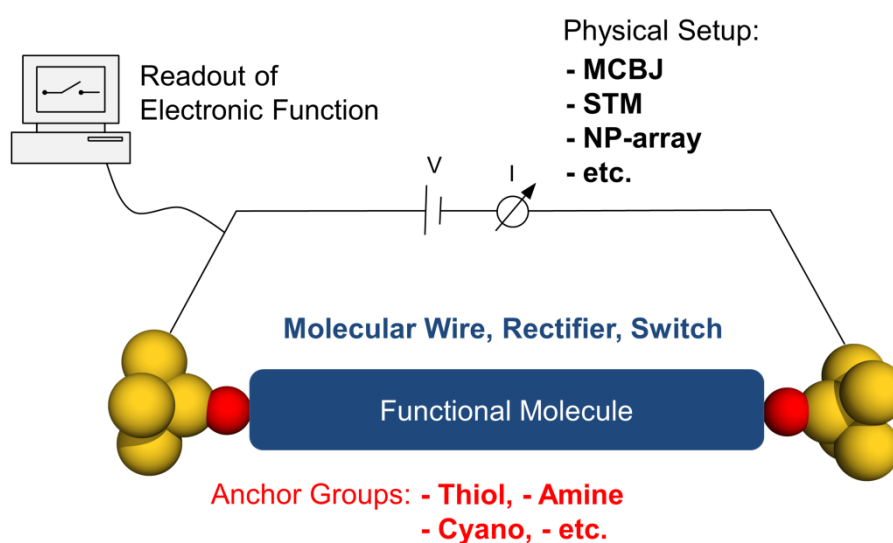


Figure 2. Schematic illustration of a molecular junction.

The basic research focuses on single molecule events, which can be divided into two main research fields. The first research area looks at the actual function provided by a molecule (illustrated in blue, figure 2). The individual properties are usually connected to the structure. By changing the structure systematically one can investigate correlations in the resulting properties such as conduction, rectification and switching.

The second topic usually focuses on the integration of such a molecule into an electrical circuit. The integration can be divided into two individual topics. The first one addresses the connection of a molecule to a larger setup and the second one addresses the measurement technique itself. The anchor group (illustrated in red, figure 2) of an organic molecule is the part which connects the functional molecule to electrodes or other molecules. The nature of the anchor group has a large influence on the overall property of the molecular junction, thus, the systematic investigation of such anchor groups is of great interest. The second one addresses the actual physical setup. This includes the formation of a suitable junction, the reading of the molecular signature and the manipulation of the molecular junction. There are several techniques which provide reproducible results to investigate a small number of molecules.

In the first section of the introduction the physical approach to contact and manipulate molecules and the structure-property relationship of individual molecules is discussed. In the second section, ferrocene compounds as potential functional building blocks are discussed. Rigid Macrocycles with an integrated functionality are addressed in section three. At the end of the introduction a collection of synthetic strategies to assemble phenyl-acetylene bonds is presented.

1.1 Molecular Electronics

1.1.1 Contacting the Molecule

To introduce the field of molecular electronics it is usually easier to discuss the integration of a single molecule into a circuit. There are three main techniques which have seen great improvement over the past years. Each technique has its advantages and disadvantages which are discussed below.

1.1.1.1 Mechanically controllable break junctions

The mechanically controllable break junction (MCBJ) was developed in the early nineties.^[3] This technique was applied to form molecular junctions.^[4] The molecular junction is defined by a molecule which lies between two atomic-scale electrodes. The MCBJ can be compared to a drawbridge which can be opened and closed. An atomic wire with a constriction in the middle is prepared on a flexible polyimide substrate using electron-beam lithography (figure 3A).

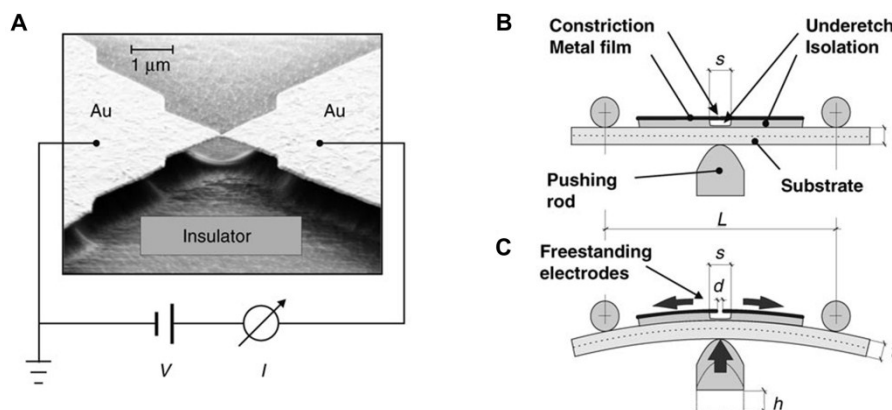


Figure 3. Principle of a MCBJ: A) Scanning electron microscope image of a microfabricated MCBJ sample. B) The MCBJ sample is mounted onto a three-point bending mechanism. C) The substrate is bent until it breaks. Reprinted from Lörtscher et al.^[6]

The substrate is then placed between a pushrod and two counter supports (figure 3B). The rod slowly pushes upwards, thus bending the flexible substrate. During this process the wire becomes stretched. Due to the elongation the diameter of the wire will further reduce until it

finally breaks leaving two atomic-scale metallic contacts which form a tunnel junction (figure 3C). The distance between the contacts is only a few Angstroms and can be adjusted by moving the pushrod up and down.^[5]

The junction distance can not only be adjusted it can also be closed again to form a new metal wire. Since the lifetime of a molecular junction at room temperature is only a few minutes and several measurements have to be performed to obtain a statistical data set, the junction is always opened and closed to form several hundreds of molecular junctions each measured individually. Since all measured conductance traces vary from each other, a statistical analysis in order to quantify the conductance value of a particular molecular junction is needed. The combined conductance traces are usually represented in logarithmic histograms (shown in figure 6) to identify the molecular signals more easily. In atomic sized contacts the classical Ohm's law ($G = I/V$) is no longer applicable since we enter the quantum regime. In the quantum regime the current flows as a transmission process and is described for a single conductance channel by the *Landauer* formula ($G_0 = 2e^2/h = 77.5\mu\text{S}$). In this formula e is the electron charge and h is Plank's constant. The conductance of a single gold atom is therefore limited and characterized as $G_0 = 1$. As a result, the conductance of a small molecule is always less than G_0 .

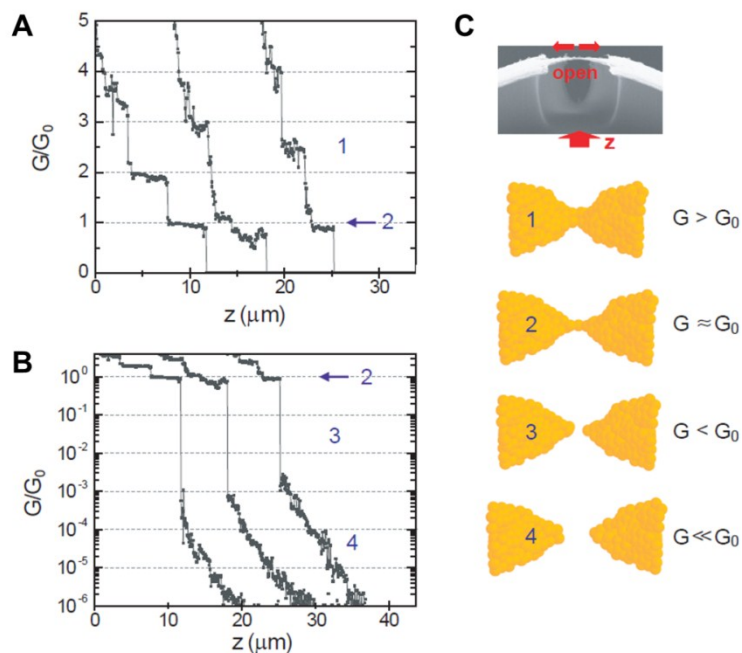


Figure 4. A and B) Three typical opening curves in pure solvent displaying the different event points on the conductance trace which occur during the break of a metal junction. C) Schematic drawing of the individual events. Reprinted from Wu et al.^[6]

In figure 4 a stepwise breaking of a gold wire in pure solvent is displayed. In the beginning (figure 4A and 4C, step 1) the gold wire has a width of about 150 nm and its conductance value G is much higher than G_0 . In the second step the substrate is bent and the metal wire is stretched resulting in a decrease of $G(z)$. Just before the metal wire breaks the conductance G equals G_0 with a value of 1 (step 2). When the junction is further elongated the atomic wire breaks and a sudden decrease of the conductance is observed (step 3). This sudden decay is caused by a contraction and rearrangement of the gold atoms, reshaping the front of the two electrodes. The conductance drop usually stops at $G \approx 10^{-3} G_0$, when electrons start to tunnel between the two electrodes (step 4). This tunneling current decays exponentially with the gap distance d (figure 4C).

These events occur when only solvent molecules are present. If a conducting molecule, functionalized with terminal anchor groups is present, the typical conductance traces change evidently. Anchor groups such as thiols form stable covalent bonds with the gold atoms from the electrodes. In the case of the thiol anchor group the resulting sulfur-gold bond is much stronger than the gold-gold bond. As a consequence, the gold atoms migrate to the binding side to form elongated tips when the electrodes are pulled apart (figure 5A, red arrows). The bridging event (electrode | molecule | electrode) takes place between the previously described steps 3 and 4 (Figure 4). During this bridging-event the electrodes are pulled further apart. However, the expected conductance decay does not occur but a plateau-trace appears instead (figure 5B, red arrow). This plateau represents the conductance G of the molecular junction. Upon further elongation the molecule-gold contacts break again and the conductance signal decreases to zero.

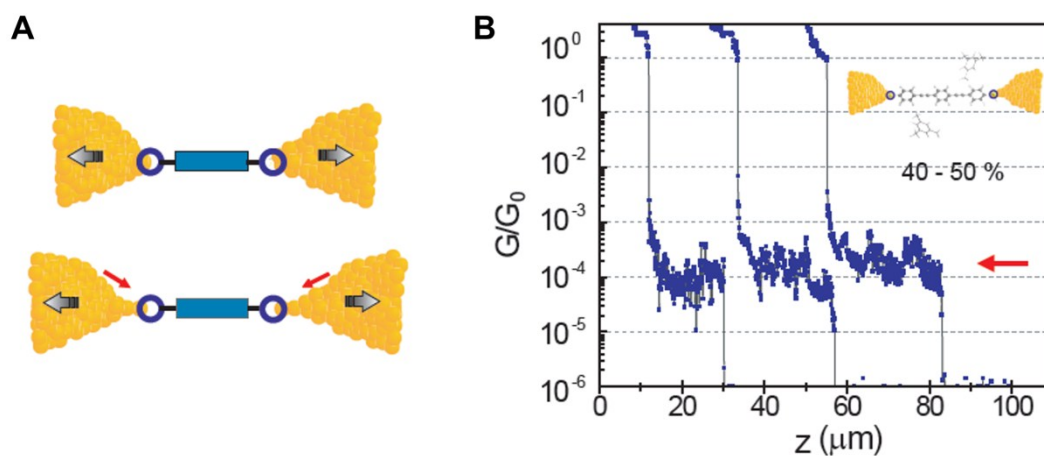


Figure 5. The breaking process containing a solution of a dithiol-OPE after in situ deprotection. A) Schematic illustration of the formation of a molecular junction. B) Three typical single $\log G(z)$ curves showing clear plateaus at $1 \times 10^{-4} G_0$.

Since the conductance traces vary between each measurement and additional fluctuations can be observed a statistical analysis has to be implemented. Usually several combined conductance traces are represented in logarithmic histograms as displayed in figure 6. The example shown represents the data for a dithiol-OPE with a conductance of $1 \times 10^{-4} G_0$.

The big advantage of the MCBJ technique is that the size of the junction can be adjusted and that several hundreds of molecular junctions can be formed providing enough data for a statistical analysis. The MCBJ technique is an excellent instrument for the lab but it is not suited for large area productions and the combination with a third gate electrode remains challenging.

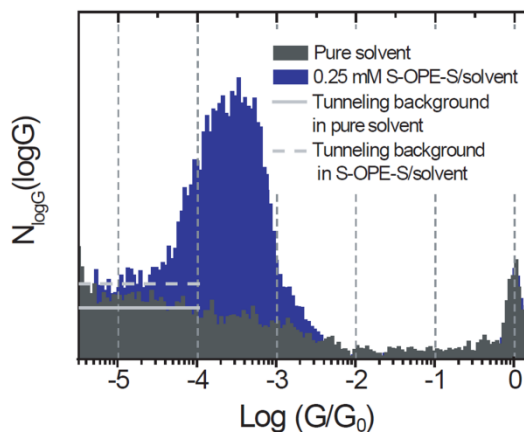


Figure 6. Logarithmic histogram $N_{\log G}(\log G)$ showing a tunneling background in the case of pure solvent and a solution containing OPE molecules. In contrast with the pure solvent, a distinct peak appears for the dithiol-OPE, indicating the signal of the molecular junction.

1.1.1.2 Scanning probe techniques

Soon after the first scanning probe techniques were developed in the 1980s^[7,8] the first organic molecules were investigated using such techniques.^[9,10] The scanning tunneling microscopy (STM) is a similar method to the MCBJ technique described in the chapter above. In general, an atomically flat gold surface, which was previously covered with organic molecules, is prepared as one electrode and a sharpened atomically gold tip is used as the second electrode. The tip is then repeatedly indented into the metallic substrate. After the gold-gold contact is formed the tip is retracted again where in some cases a molecular junction can be formed between the metallic substrate, the molecule and the STM tip. Once the molecular junction is formed a plateau occurs in the conductance trace similar to the above described MCBJ measurement. Upon further retraction of the gold tip the junction breaks and the current trace drops down.^[11] This process of indentation and retraction is then repeated several times to collect enough data for a statistical analysis. However, the

indentation of the STM tip into the gold surface often results in modification or even destruction of the surface. Therefore, the technique has been further developed to pick up the molecule without indentation of the tip. These techniques are called $I(s)$ or $I(t)$ methods and were developed by the group of Richard J. Nichols.^[12] The stepwise formation of a molecular junction is schematically displayed in figure 7.

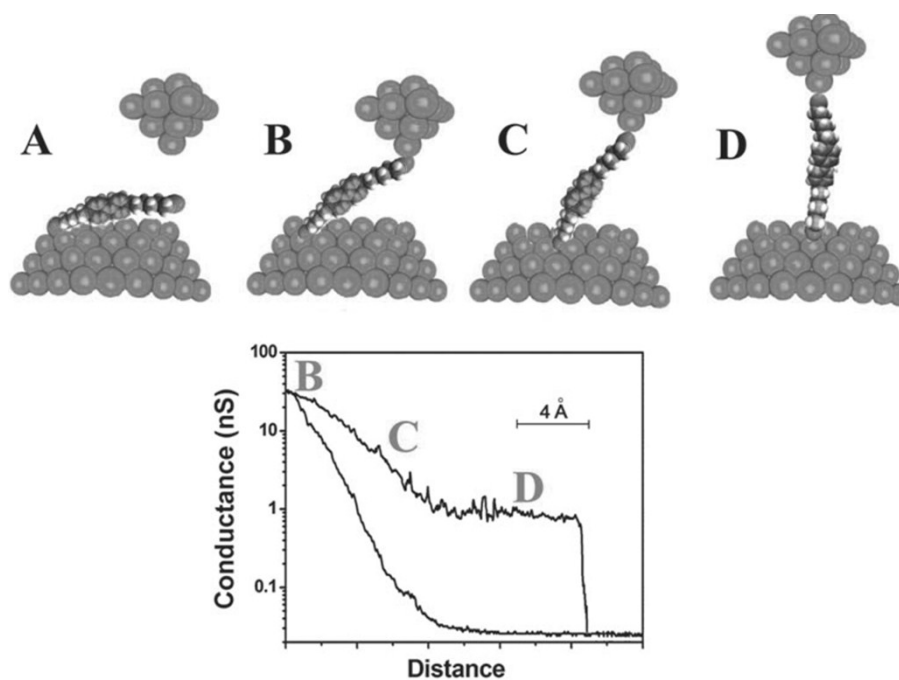


Figure 7. Formation of a molecular junction using STM $I(s)$ technique. Reprinted from Nichols et al.^[12]

Due to its scanning possibilities, the STM technique can also be used to image molecules which are deposited on the surface. The obtained picture represents the wave function of the molecules which allows surface scientists to see how the molecules behave and interact with each other on the surface.^[13,14] A perfect example of different assembly behavior was demonstrated by Kampschulte et al. where different solvent systems led to different arrangements (figure 8).^[15]

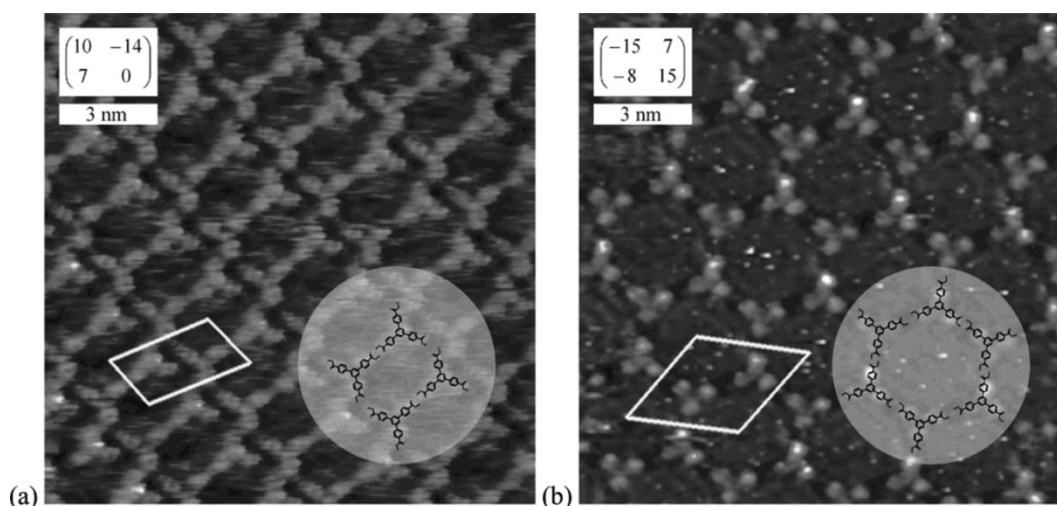


Figure 8. STM surface image showing the assembly of 1,3,5-benzenetribenzoic acid on an HOPG surface. a) shows the modification with the oblique unit cell as obtained in butanoic through heptanoic acid, 1-octanol, 1-nonanol, and 1-decanol, and b) shows the hexagonal chicken-wire modification obtained in nonanoic acid and 1-phenyloctane. For octanoic acid and dodecane both modifications were observed. Reprinted from Kampschulte et al.^[15]

The big advantage of the scanning probe technique is that the gap size can also be adjusted as in the MCBJ. In addition, the STM can image a functionalized surface which makes it a very important tool for the field of surface material science. The drawback is again its limited application to the lab.

1.1.1.3 Electromigration induced break junction

The electromigration induced break junction (EIBJ) is another method to produce nanometer gaps within a metal wire. The breaking process itself can be attributed to the diffusion of atoms due to large current density in a wire. This effect is actually a downside in all electronic circuits since it leads to undesired defects. However, when the electromigration process can be controlled it is possible to open a nanometer gap and therefore produce the junction (figure 9).

In principle there are two ways to integrate a molecule into the junction. One approach is to deposit the molecule on the metal wire prior to the formation of the junction. The junction is then produced by applying a very large bias to induce the electromigration which, in some cases, leads to a breaking underneath the deposited molecule. Another approach is to produce the nanometer gap first and then deposit the molecules. This method avoids that molecules are

exposed to high temperatures which arise during the electromigration process. Both approaches lead to a very low numbers of molecular junctions.

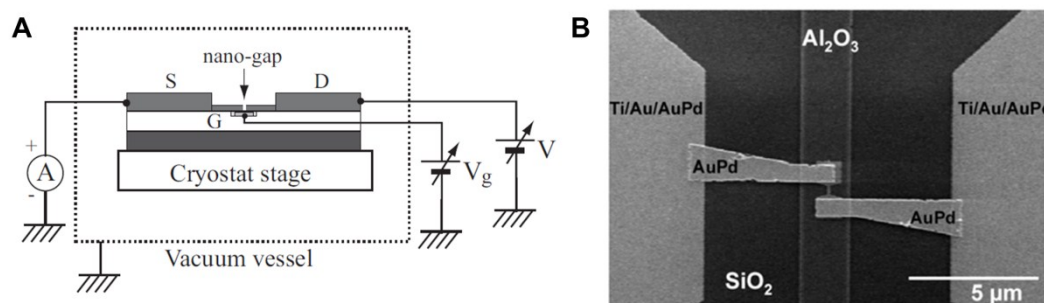


Figure 9. A) Schematic illustration of a gated electromigration induced break junction. Reprinted from Noguchi et al.^[16] B) Device structure fabricated by e-beam techniques prior to breaking of the small wire in the middle. The wire is 50 nm wide and has a thickness of 10 nm. Reprinted from Van der Zant et al.^[17]

The biggest advantage of this technique is the large area fabrication and the introduction of a gate electrode. The gate electrode can be used to manipulate the molecular energy levels which gives control over the function of the device. The gating mechanism will be further discussed in the next section.

The drawbacks of this technique are that the gaps produced can only be adjusted once in the beginning compared to STM and MCBJ techniques where the gap size can be changed during the experiment and that the molecules are exposed to local heating during the breaking process.

1.1.1.4 Three terminal devices

The previously discussed two terminal devices are well suited to measure and investigate single molecules. However, the gate electrode in three terminal devices allows manipulation of the energy levels of the molecules relative to the Fermi levels. This makes it particularly interesting to study different transport mechanisms especially in intermediate and weak coupling regimes.^[18,19] The gate electrode can increase or decrease the molecular energy levels to bring them into or out of resonance with the Fermi-energy levels of the electrodes

allowing access to different charge states such as vibrational states,^[20,21] electronic states^[22] and spin transitions.^[23,24]

Currently the EIBJ is still the easiest way to produce a three terminal device since the gate electrode can be placed very close to the actual junction (figure 10A).^[25,26] However, the drawback of not being able to adjust the gap size of the junction during the experiment led to the development of other three terminal devices. For example the evaporation-deposition of gold electrodes, on top of a gate electrode, using a shadow-mask technique. This technique includes all the advantages of the EIBJ, plus the gap size can be better controlled according to the authors (figure 10B).^[27,28]

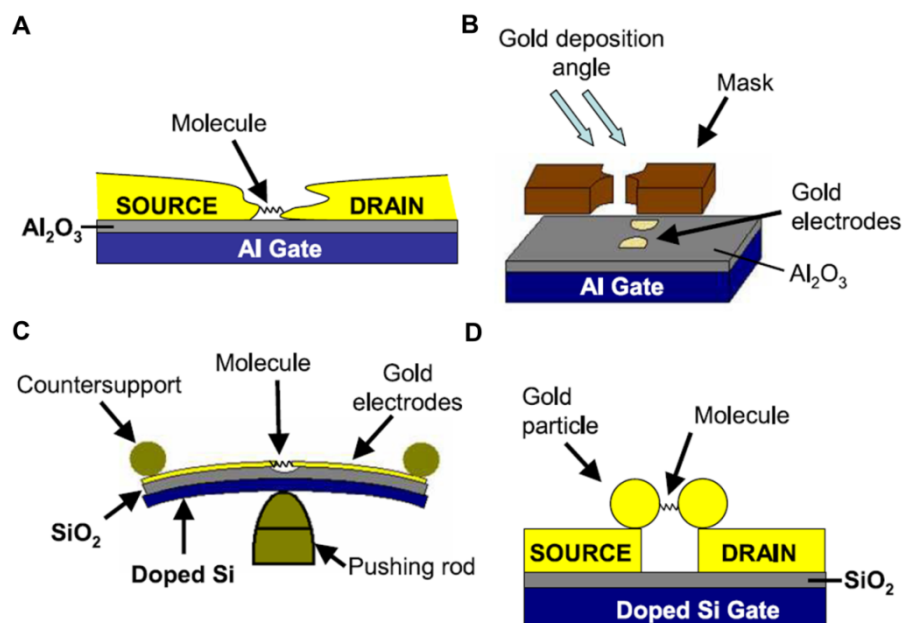


Figure 10. Contact techniques including a gate electrode. Reprinted from Osorio et al.^[18]

Recently a gate electrode was installed in a MCBJ (figure 10C).^[29] However, the gate coupling was rather low. Thus, electrochemical gating became much more interesting which provides the same advantages as “regular” gating. In the electrochemical gating (or electrolyte gating) the potential drop of the individual working electrodes (contact electrodes) and the additionally installed reference electrode can be used to modulate the tunneling current between the source electrode and the drain electrode.^[30,31] Another method for three terminal device gating was demonstrated by Dadosh et al.^[32] The investigated molecule was trapped between two nano particles forming a dumbbell structure. This particle was electrostatically trapped between two gold electrodes deposited on top of a gate electrode (figure 10D).

1.1.2 Structure-Property Relationship

In the previous section the integration techniques and the possibility of manipulation were discussed. In this chapter we look at the electrical properties coming from the molecule itself.

1.1.2.1 Anchor groups

First, we have a look at the anchoring groups. At first glance one would probably say: “*The stronger the binding to the electrodes the better the outcome of the experiment.*” However, when we have a closer look on the electronic coupling between a molecule and the electrodes and what the actual experiment wants to show the details are a bit different.

When the electronic coupling between the electrons in the electrodes and those in the molecule is weak, it is possible to probe absolute values of the molecular energy levels in a solid state device by applying a gate voltage (figure 11, bottom).^[19] Thus, it is possible to measure the addition energy (U_{Add}) of an electron to the molecule. The addition energy is usually determined by electrochemistry or absorption spectroscopy. A good approximation is $U_{\text{Add}} \approx 2E_C + \Delta$, where E_C is the electrostatic charging energy and Δ is the quantum mechanical level spacing of the system. However, this approximation is not always valid in molecular junctions.

If the coupling between the electrodes and the molecule is strong the energy levels in the molecule become significantly broader (illustrated on the top, figure 11). This broadening defines the coupling parameter Γ the value of which is much higher in the strong coupling regime ($\Gamma \gg U_{\text{Add}}$) and much lower in the weak coupling regime ($\Gamma \ll U_{\text{Add}}$).

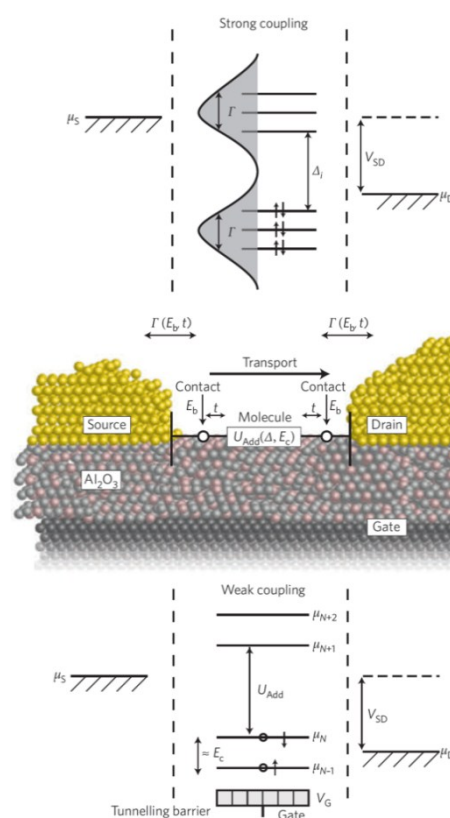


Figure 11. Schematic illustration of a strong (top) and weak (bottom) electronic coupling between the electrons of the electrodes and the electrons of the integrated molecule.

In the intermediate coupling regime phenomena such as the Kondo effect or co-tunneling can be observed. It is also possible to observe or make an asymmetric coupling (strong and weak) between the electrodes and the molecule. This effect often occurs in STM-experiments.

The coupling parameter Γ is usually defined by E_b and t . E_b is the strength of the bond between the electrode and the molecule. This bond strength varies from the strong covalent bond ($E_b = 0.1-5$ eV) which is typical for thiol-gold bonds to the weak van-der-Waals forces (0.001-0.1 eV).^[33,34] However, when a strong covalent bond is formed it does not necessarily mean that the electronic coupling between the electrodes and the molecule is strong. If for example, the sulfur atom is connected via a methylene bridge to the rest of the molecule the overall electronic coupling Γ is still low.^[35] Another significant aspect is the contact geometry which also has a large influence on the electron transport.^[36] These differences in the contact geometry lead to the broad distribution of conductance values which were obtained experimentally over the past years. Thus, it is of great importance to systematically investigate new anchor groups and study their electronic coupling with the molecule of interest.

So far, many anchoring groups such as thiols,^[37,38] amines and phosphines,^[39] pyridines,^[40] selenium,^[41-43] fullerenes,^[44] isocyanides,^[45] nitriles,^[46] carbamates,^[47] and carboxylic acids^[48] have been investigated and used to form electronic devices.^[49] The most well-known and commonly used anchoring groups are thiols and amines as they have a strong binding affinity to gold and provide efficient electronic coupling to the electrodes. In order to gain more insights into the transport mechanism, investigations towards new, stable and efficient anchoring groups are required.

1.1.2.1 Length dependence

Previously we discussed how to contact a single molecule and how the molecule is connected to the electrodes. The possibility to integrate a single molecule opens the door to investigate the correlation between the structure of the molecule and the observed properties. The conductance G of a single molecule can be defined by the Landauer formula;

$$G = A \cdot e^{-\beta d}$$

where A characterizes the contact conductance and β represents the details of the tunneling through the molecule with a distance d .

The most investigated molecules are alkane-dithiols which were suitable candidates to investigate the length dependence on the conductance of a molecule. It was shown that the conductance decays exponentially with increasing length of the molecular backbone.^[50] As illustrated in figure 12 the obtained conductance values are shown for dithiol-alkanes (red), oligopeptides (black), oligothiophene (green) and caotenoids (blue).

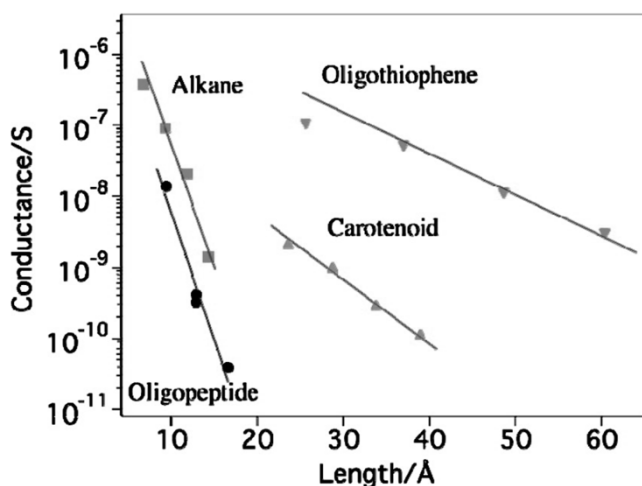


Figure 12. Length dependence on the conductance value of different molecular backbones. Reprinted from Chen et al.^[50]

Similar trends were found for fully π -conjugated molecular wires such as oligo-phenylene-vinylenes (OPVs) and oligo-phenylene-ethynylenes (OPEs).^[51,52] This unique family of molecular wires usually have rigid rod-like structure and small HOMO-LUMO gaps of about 3 eV. The properties of such wires can easily be tuned by changing the substituents on the wire affecting the molecular energy levels.

The general rule of the length dependencies is that the increase of the molecular length or an increase of the HOMO-LUMO gap results in a decrease of the conductance (figure 13). Wandlowski and co-workers systematically investigated the conductance of a series of OPE-type structures by varying their length and by changing their HOMO-LUMO gap keeping the length constant. They also compared their findings to cross-conjugated (or disrupted) systems of similar length.^[52]

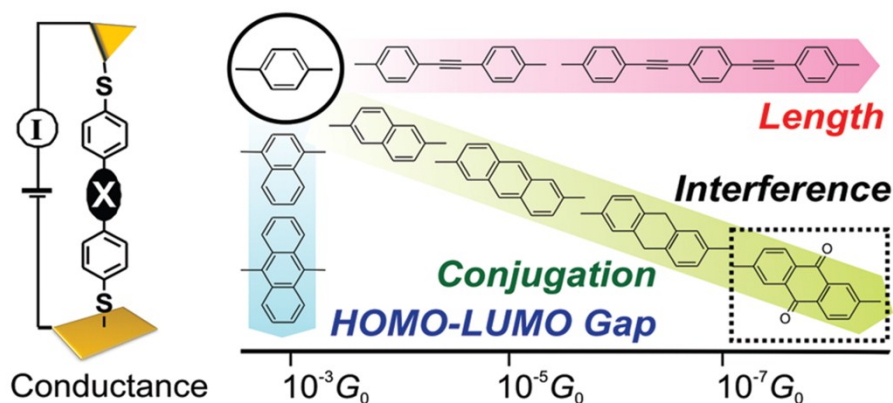


Figure 13. The structural correlation of OPE type structures was systematically investigated by Kaliginedi et al.^[52]

1.1.2.2 Influence of the conjugation

As discussed above the length of a molecular wire has a large influence on the conductance of the molecule. However, if a molecule consists of a conjugated system such as an OPE the topological connection (*ortho*, *meta* or *para*) and the torsion angle (see next section) between those units is also important. It is known that the conjugation through a benzene unit via *para*- or *ortho*-connection unit is much better than through a *meta*-connection which has been demonstrated electrochemically^[53] and theoretically.^[54] This useful property has been successfully applied to a molecular wire with the intention to decouple the molecule from the gold electrodes by changing the connection of the sulfur anchor group from the *para*-position (figure 14, molecule **1**) to the *meta*-position (molecule **2**).^[55] It was shown that conductance through the *para*-substituted benzene in **1** was ten times higher than through the *meta*-substituted benzene in **2**. The reduced current through the *meta*-functionalized rod **2** allowed for formation of more stable molecular junctions which was underlined by measurements at 30 K.

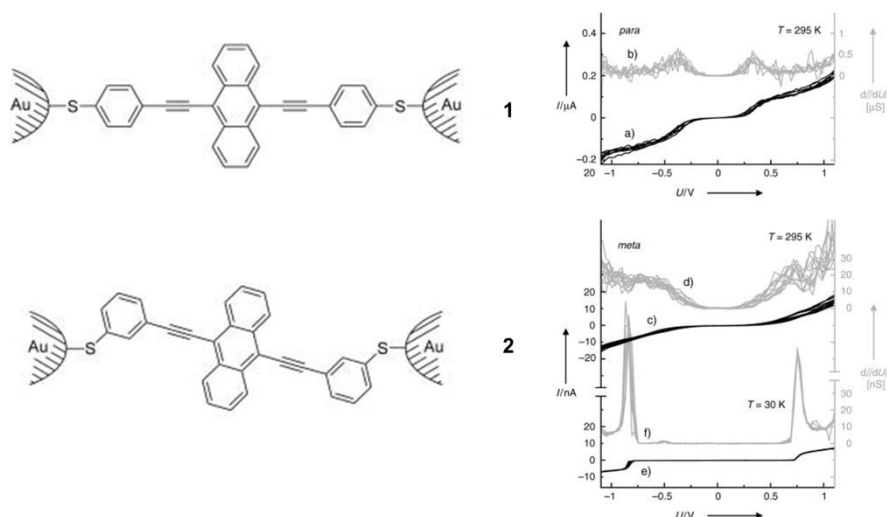


Figure 14. Left: Schematic illustration of molecular junctions of **1** and **2**. Right-top: a) I/U . b) dI/dU for **1**. Right-bottom: c) I/U . d) dI/dU for **2** at room temperature. e) I/U . f) dI/dU at 30 K. Reprinted from Mayor et al.^[53]

1.1.2.3 Torsion angle dependence

Conjugated molecules have been investigated extensively over the past years. Usually, conjugated molecules consist of a rigid structure which makes it easier to predict which actual conformation is being investigated.^[56] However, the conjugation itself depends on the overlap of the π -orbitals which can directly be correlated with the torsion angle Φ between the individual π -systems. The first correlation between the conjugation and the conductance was demonstrated by Venkataraman et al.^[57] The compounds investigated were limited in their rotation around the biphenyl sigma bond which led to the observation of a trend (figure 15A). When the torsion angle Φ was about 90° low conductance was observed and when the torsion angle Φ was about 0° high conductance was observed (figure 15B). The observed conductance correlated linearly to the \cos^2 of the torsion angle Φ between the two phenyl rings (figure 15C) which was interpreted as an increased decoupling of the individual π -systems of both phenyl rings with increasing torsion angle Φ in the molecule. The $\cos^2(\Phi)$ relationship arises from the π -orbital overlap integral A_{RS} which is proportional to the resonance integral β_{RS} (R and S are decoupled chromophores). The interaction between the two orbitals across the sigma bond is defined by the resonance energy E_{RS} which is known to correlate approximately with $\cos^2(\Phi)$.^[58,59]

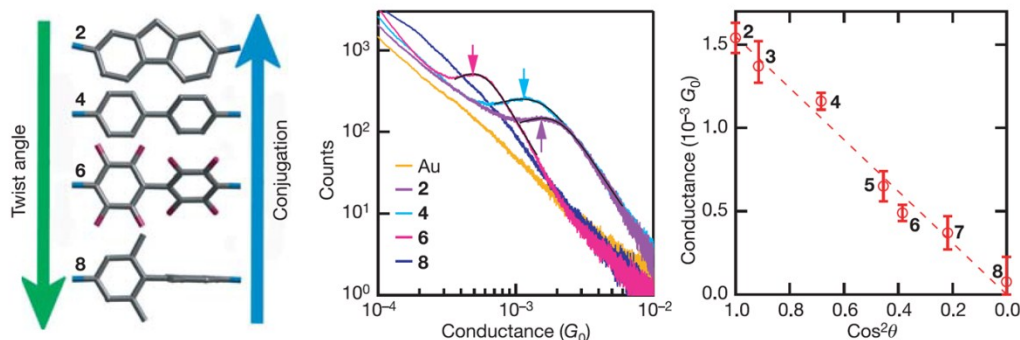


Figure 15. a) Investigated molecules with restricted rotation. b) Measured conductance with STM. c) Correlation between the torsion angle and the conductance. Reprinted from Venkataraman et al.^[57]

The experimental approach to investigate this correlation was later improved by Vonlanthen et al.^[60] They synthesized a series of biphenyl derivatives which were restricted in their rotation around the central sigma bond by bridging alkanes (figure 16).

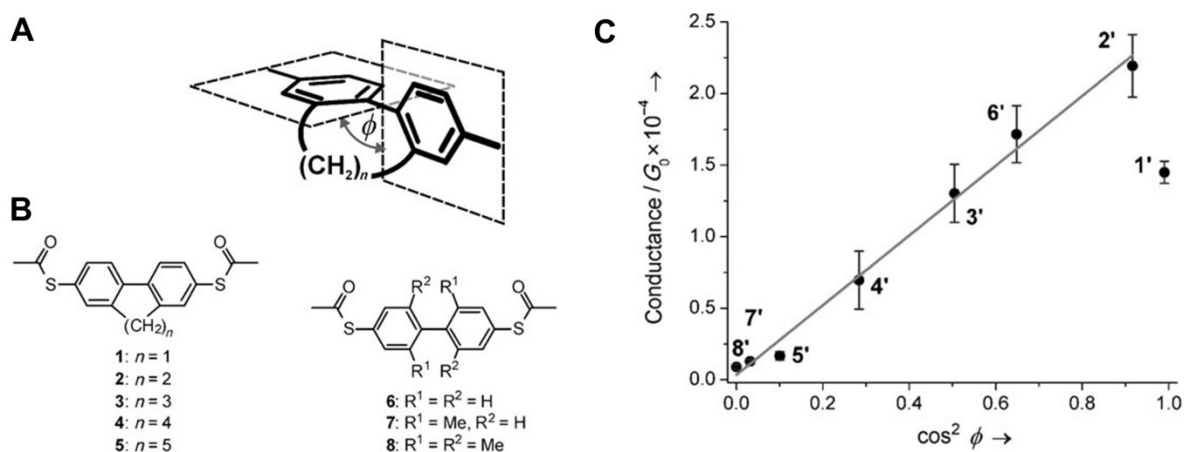


Figure 16. A) Schematic illustration of a torsion angle adjusted biphenyl. B) Synthesized biphenyl series with terminal protected sulfur anchor groups. C) Correlation between the torsion angle Φ and the conductance G_0 . Reprinted from Vonlanthen et al.^[60]

The discussed influence of the torsion angle on the conductance is not only applicable to small biphenyl systems but also to larger structures like OPE type wires.^[61,62] It is known that the planarization of conjugated π -system leads to a reduction of the HOMO-LUMO gap which can easily be observed by a red-shift in the absorption spectrum.^[63] The correlation between the torsion angle and the conductance has motivated many research groups to design

and synthesize a molecular switch where a single benzene unit could be triggered to rotate in- and out- of plane.^[64-67]

The effect of low conjugation through a twisted biphenyl was used to decouple an electron rich from an electron poor system generating a so called donor-bridge-acceptor (D- σ -A) molecule.^[68] If such asymmetric molecules can be integrated into an electric circuit they are more conducting in one direction compared to the other.^[69,70] This effect is called rectification which mimics a diode device. However, the proposed rectifier **1'** contained an electron poor fluorinated benzene unit (left), an electron rich benzene unit (right) and a central biphenyl with two additional methyl substituents forcing the two phenyl rings out of plane (figure 17A). When the bias voltage was continuously increased, the energy levels of both units shifted relative to each other. Whenever an unoccupied level passed by an occupied one, an additional transport channel opened up and the current increased (figure 17B). This is an excellent example of the influence of the torsion angle Φ on the conjugation. The twist between the biphenyl rings was already sufficient enough to decouple the donor from the acceptor part to create a rectifier.

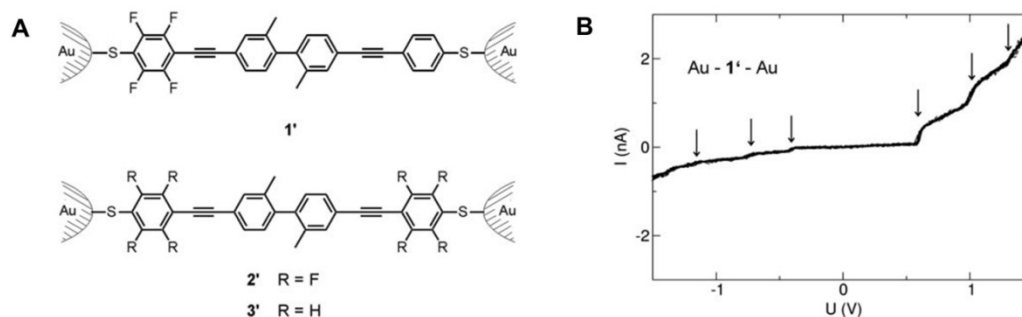


Figure 17. A) Molecular diode (**1'**). The donor and acceptor are separated by a biphenyl which is hindered to rotate freely and thus decouples the two systems. B) Sweeping of the bias voltage results in an increase of the current.

In chapter 1.1.2 the structure-property relationship was discussed for:

- Anchor groups
- Length of the molecular wire
- Conjugation (topological, torsion angle)

All these factors have to be considered in the design of new functional molecules.

1.2 Ferrocene compounds

In the sections above we discussed how to integrate a functional molecule into an electric circuit and how the observed properties correlate with the structure of the investigated molecule. Now we look at ferrocene compounds and their interesting features. But first we have to look at ferrocene itself.

Ferrocene was first discovered by Peter L. Pauson and Thomas J. Kealy in 1951 during their attempt to synthesize fulvalene.^[71] However, at the time the proposed structure of the bis(cyclopentadienyl) iron was wrong. One year later the sandwich-type structure was discovered by Geoffrey Wilkinson and R. B. Woodward and independently by Otto Fischer.^[72] These findings initiated a “*renaissance of inorganic chemistry*” resulting in the synthesis of many metallocene complexes for which Otto Fischer and Geoffrey Wilkinson received the Nobel Prize in 1973.

Today we know that ferrocene is a metalorganic complex with the chemical formula $\text{Fe}(\text{C}_5\text{H}_5)_2$ where an iron (+2) atom is sandwiched by two cyclopentadienyl (*Cp*) rings which are each negatively charged. The twelve π -electrons of the two *Cp*-rings are shared with the iron atom (6 *d*-electrons) via haptic covalent bonding resulting in an 18 electron configuration. The two *Cp*-rings can freely rotate around the central axis which can be observed by NMR and STM.^[73]

1.2.1 Electrochemistry

A great feature of ferrocene is the fully reversible redox system. The iron atom can be oxidized from iron (+2) to iron (+3) resulting in a ferrocenium with the charge of (+1). The ferrocenium can be reduced again to ferrocene. This one electron redox process is fully reversible which makes ferrocene especially interesting as an internal reference for electrochemical investigations. However, the oxidation potential can be determined by cyclic voltammetry and usually depends on the solvent and on the electrolyte concentration.^[74] If the ferrocene bears any substituents the oxidation potential changes in correlation with the electronic nature of the substituent. If for example a *Cp*-ring has an electron withdrawing substituent the oxidation potential shifts to a higher potential. The reason for this shift can be attributed to the increased positive charge on the $\text{Fe}^{+\text{II}}$ which makes it more difficult to remove a further electron. Therefore, cyclic voltammetry is an excellent tool to characterize ferrocene compounds.

The voltammogram determines the oxidation potential of a compound and if its redox process is reversible or not. In addition the number of electrons involved can be calculated. As shown in figure 18 the half-wave potential can be calculated by dividing the sum of the oxidation and reduction potential by two. However, this is only applicable when the following criteria are met: The difference between E_{pa} and E_{pc} is about 59 mV, the ratio between I_{pa} and I_{pc} is 1 and the root of the scan rate should be proportional to i_p .

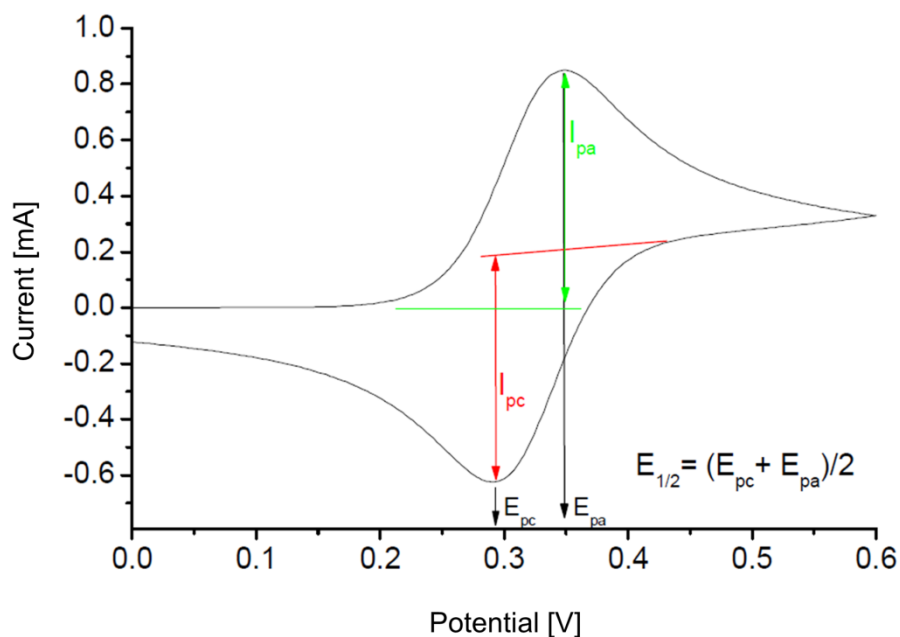


Figure 18. Typical cyclic voltammogram with a potential sweep from 0 V to 0.6 V and back to 0 V.

1.2.2 Ferrocene in functional molecules

In the late nineties *Yamamoto* and *Morikita* synthesized polymers which incorporated ferrocene units (figure 19).^[75,76] Their electrochemical investigations revealed a strong influence of the substituents (on the ferrocene) on the oxidation potential of the ferrocene. The shift to a higher oxidation potential was attributed to the electron withdrawing effect coming from the acetylenes. They also suggested an electron transfer between the ferrocene units within the polymer.

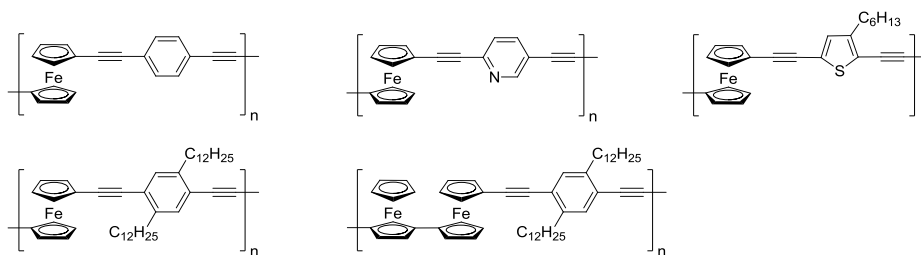


Figure 19. Ferrocene polymers synthesized in 1997.^[75]

Ferrocene was also used to investigate the electron transfer rate through an OPE wire which was immobilized on a gold electrode in an electrochemical setup (figure 20).^[77,61] The OPE had a thiol anchor group on one side and a ferrocene on the other. The OPE was incorporated into a non-conductive SAM. The groups of *John Smalley* and *Marshall Newton* used an indirect laser-induced temperature jump technique (ILIT) to measure the transfer rate through the OPE. They could show that the large conformational dispersion of an OPE (due to free rotation of the benzene units) has an enormous influence on the electron transfer rate.

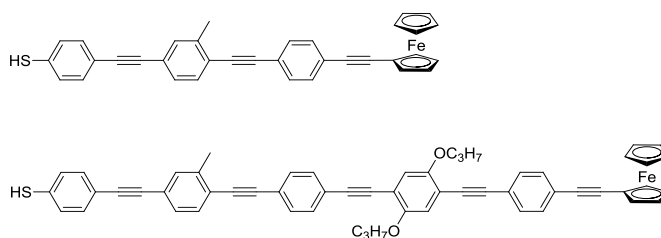


Figure 20. The electron transfer rate through OPEs of different length was investigated by Smalley et al.^[61]

Lawrence Sita and coworkers proposed a molecular wire **3** containing a central ferrocene with a conductance of $0.7 G_0$ (figure 21).^[78] The authors suggested the presence of a low-lying, high-transmission molecular energy level in the ferrocene-wire which matches the Fermi levels of the electrodes. The molecule was integrated into a gold junction produced by electromigration. The observed conductance seems to be unusually high for an organic molecule^[79] raising two big question marks during the study of this paper. The first one concerns the electromigration technique. Even though the technique is suitable to include a gating electrode, but the formation of the nano gap could not be well controlled at the time this work was published. In addition local coulomb heating as well as the creation of artifacts due to the junction formation cannot be ignored.

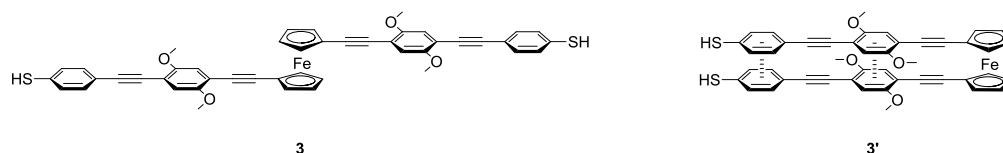


Figure 21. Left) Molecular wire **3** containing a central ferrocene with an observed conductance G_0 of 0.7. Right) Possible conformation of **3'** stabilized by π - π interactions.

The second concern is about the structure itself. The two OPE arms can freely rotate around the ferrocene joint forming a double wire **3'** which can be stabilized by π - π interactions (figure 21, right). One cannot rule out the presence of such a double wire **3'** during the EIBJ experiment. The actual measurement of two OPE rods could explain the observed conductance of $0.7 G_0$.

The group of *Lawrence Sita* and the group of *Holger Butenschön* synthesized other flexible molecular wires which contained two ferrocene joints.^[80,81] However, they have not been able to integrate these wires into any junction which can probably be attributed to the strong flexibility and therefore to the formation of multiple possible conformations (figure 22).

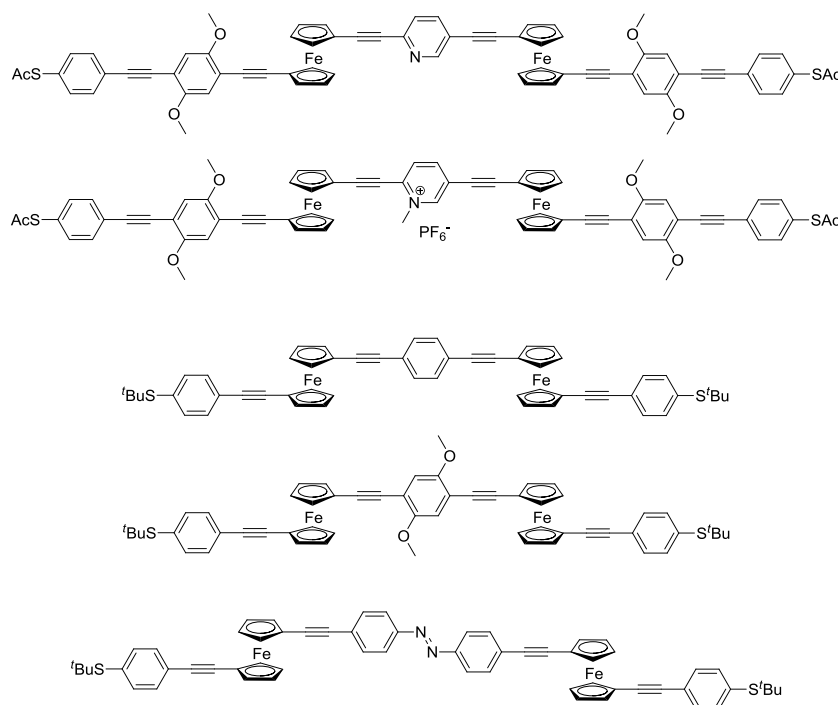


Figure 22. Synthesized molecular wires. The top two have been synthesized by Engtrakul et al.^[80] The lower three have been synthesized by Ma et al.^[81]

The group of *Nongjian Tao* reported the electrochemical gating of a ferrocene compound incorporated in a STM break junction.^[82] They measured two model compounds (figure 23A) and observed an increase in conduction upon electrochemical oxidation of the ferrocene (B). Although, the constructed conductance histograms showed broad rather than distinct peaks (D) the trend to an increase in conductance could nicely be demonstrated (B). The fluctuations in the conductance were attributed to the possibility that the oxidized ferrocene could again be reduced which they believed is possible at low gate voltage.

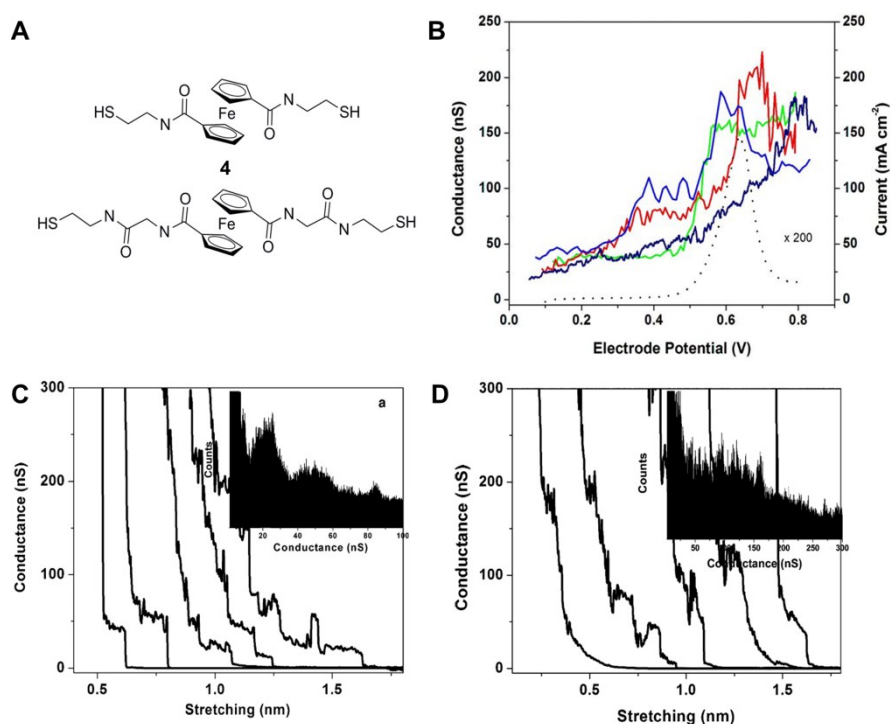


Figure 23. A) Model compound for electrochemical gating. B) The increase in conductance is shown upon oxidation of the ferrocene unit. C) Conductance traces of the top molecule in its reduced state. D) Conductance traces of molecule **4** at a gate voltage of 0.7 V.

The conductance increase associated with the oxidation of the ferrocene was 8-10 times higher compared to its reduced form. This work demonstrated for the first time the electrochemical gating of an integrated ferrocene compound.

Another concept of an electrochemical gated ferrocene switch was introduced by Davis et al.^[83] They embedded an OPV type structure **5** terminated with a ferrocene into a SAM of dodecanthiol (figure 24). The dodecanthiols were chosen because they have the similar length compared to the OPV molecule **5**. Event though, the molecules have the same length, the ferrocene compound appears to be $4.5 \pm 0.8 \text{ \AA}$ higher than the dodecanthiols. The observed height-change can directly be correlated with the difference in conductance. They observed that the tunneling current sensitively dependent on the underlying substrate potential. The relative conductance (on/off state) was topographically estimated. They calculated a conductance ratio of about three orders of magnitude.

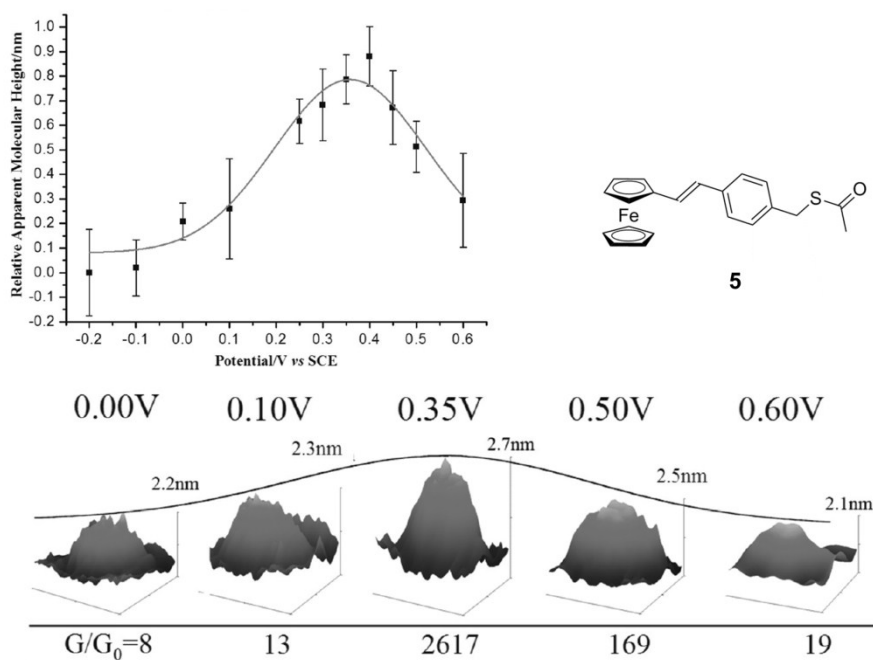


Figure 24. Top) Ferrocene-wire **5** apparent electrochemical STM (EC-STM) height modulation (black squares with a Gaussian best fit) at varying substrate potential, obtained in 10 mM phosphate buffer, pH 7.0; current set-point 0.2 nA, tip-substrate bias 0.2 V. Normalized molecular conductance is tuned by applied potential, reaching a maximum near the half-wave potential. Bottom) 3D representation of the conductance gating of a single molecule of **5**. The tunneling current increases to a maximum close to the electrochemical midpoint potential ($E_{1/2}$), falling off at potentials either side of this. These contrast changes can be used to calculate the relative conductance (G) of states compared to the “off-resonance” height observed at potentials far from $E_{1/2}$. In defining the latter as G_0 , G/G_0 then corresponds to the magnitude of conductance switching (values here generated by averaging over 37 single molecules).

This was a nice demonstration to gate a ferrocene molecule electrochemically. However, the previously discussed ferrocene wires **4** and **5** were the only ferrocene compounds which have ever been successfully gated between two electrodes and their molecular backbones were rather low conducting. All these facts motivated our group to synthesize a molecular switch which consisted of a redox active ferrocene integrated into a highly conductive OPV structure. Sergio Grunder synthesized in his PhD work a ferrocene compound which was connected to two sulfur terminated styrene units (figure 25, left).^[84] Compound **6** was measured by Songmei Wu within her PhD work at the University of Basel.^[6] They built a MCBJ in a liquid cell containing a reference electrode and a counter electrode. In this setup the source and drain electrodes become the working electrode (also called working electrode 1 and 2). The potential drop between the working electrode and the reference electrode can be used to gate the electrochemical cell (or electrolyte). The gating is controlled by a potentiostat (Figure 25, right).

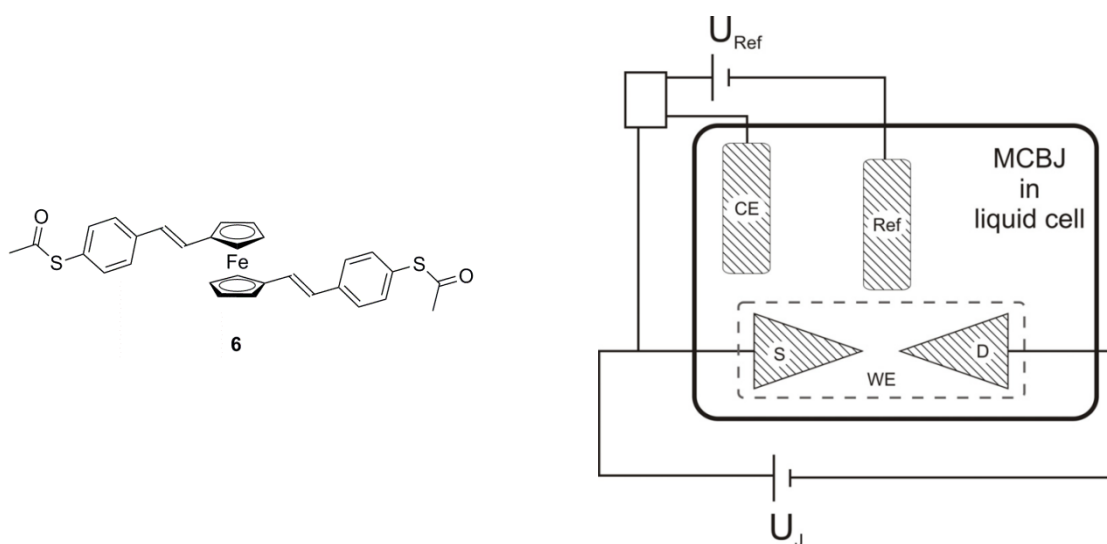


Figure 25. Left) Proposed molecular switch **6**. Synthesized by Sergio Grunder. Schematic drawing of MCBJ combined with an electrochemical cell. Reprinted from Sergio Grnder.^[84]

The conductance was first measured with the reduced form of molecule **6** (figure 27, left). The conductance was about one order of magnitude lower compared to an OPV of similar length.^[38] A reasonable explanation was that the current needed to pass through the ferrocene itself, thus resulting in a lower conductance. On the other hand Seferos et al. demonstrated with their cyclophane OPV **8** (figure 26) that the conductance through space (due to π - π interactions) can be just as good as a fully conjugated OPV **7**.^[85]

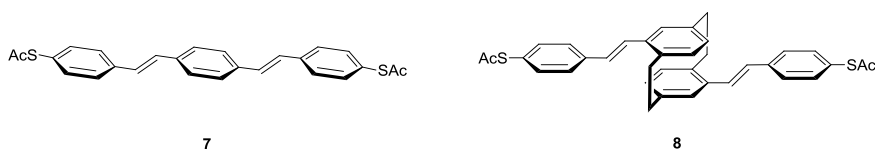


Figure 26. Similar conductivities have been observed either through the fully conjugated OPV **7** (left) or through space as in molecule **8** (right).

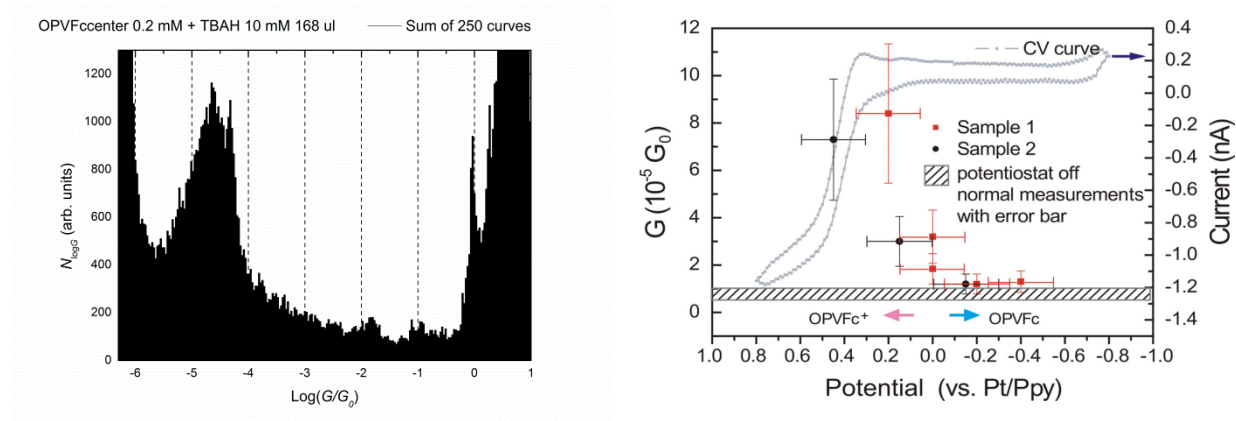


Figure 27. Left) Conductance histogram of compound **6** showing a conductance peak at $3.72 \cdot 10^{-5} G_0$. Right) Electrochemical gating of OPV **6**. The conductance increased upon oxidation to $1.29 \cdot 10^{-4} G_0$.

Figure 27 shows the conductance histogram of compound **6** measured in MCBJ using an electrochemical cell.^[6] The conductance peak of the neutral molecule occurred at $3.7 \cdot 10^{-5} G_0$ with 250 consecutive curves. The potential was then slowly swept to a positive potential (+0.6 V). During this oxidation the conductance increased up to $1.29 \cdot 10^{-4} G_0$ almost one order of magnitude higher compared to the neutral state. This experiment showed that the concept of electrochemical gating works on a redox active molecule which is electronically rather strongly coupled to the electrodes. All the molecules investigated in previous studies had a weak electronic coupling which should have made gating much easier.^[19]

As seen in the discussed examples above, ferrocene is a very interesting molecular building block. In this thesis we wanted to explore new synthetic strategies to incorporate the redox active ferrocene into conducting molecular wires. The individual concepts are discussed below.

1.3 Functional Macrocycles

So far functions of small molecules integrated between two metal junctions have been discussed. Such small functional molecules are ideal candidates to investigate the structure-property relationship, however, when we think about applications these molecules are already too small. When larger molecules are considered as functional components the syntheses become more and more challenging. Currently when electrical functions are mimicked it is usually done by an interplay between different molecules also known as supramolecular architectures. Excellent examples for such structures are rotaxanes and catenanes.^[86,87] For example, rotaxanes are mechanically interlocked systems and consist of a molecular rod threaded through a macrocycle. The rod usually bears large stoppers to prevent the macrocycle from leaving the system (figure 28, left). Catenanes are mechanically interlocked macrocycles consisting of at least two macrocycles (right). In these supramolecular structures the macrocycles (and the molecular rods) are often equipped with functional groups which can be externally triggered to change their property. This often leads to a translation in case of rotaxanes or a rotation in the case of catenanes. The systems are usually bistable which enables switching from one state to the other. Many functional groups have been integrated in such systems to trigger the motions chemically, electrochemically or by light.^[88-90] In figure 28 (left) the principle of a translational movement is illustrated schematically.

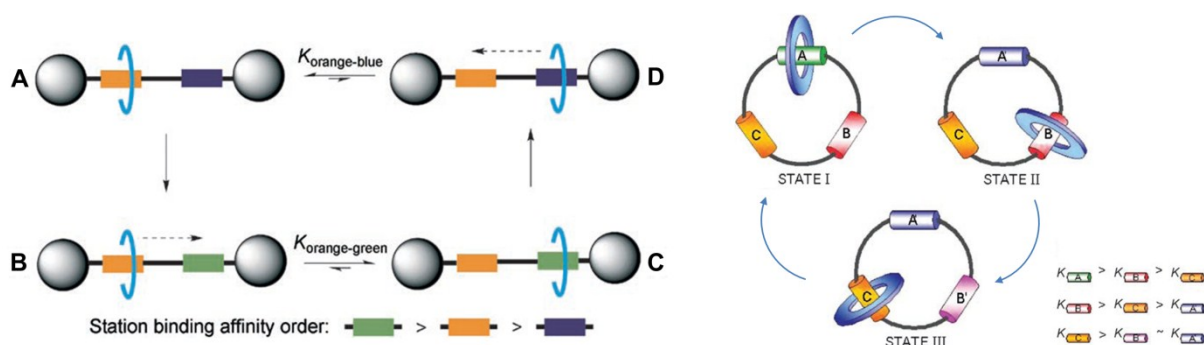


Figure 28. Left) Illustration of a rotaxane where the macrocycle shuttles from one state to the other. Right) Illustration of a catenane where the macrocycle itself can be triggered to rotate around another macrocycle.

Initially the macrocycle sits on the preferred station (A, orange). The blue station then reacts thus changing its affinity towards the macrocycle (B, blue \rightarrow green). The macrocycle then

shuttles to the now-preferred station (C, green). If the reverse reaction on the green station (green \rightarrow blue) occurs the macrocycle shuttles back to its original position. The same principle can be applied to catenanes where the macrocycle can be addressed directly as illustrated in figure 28 (right). All these systems profit from intermolecular interactions and that the functional groups are covalently integrated into the macrocycles or into the threads.

The synthesis towards such functional macrocycles remains challenging especially when more rigid systems are envisaged which give a direction to the functionality.^[91,92,90] Two examples of such rigid macrocycles are shown in figure 29. Macrocycle **9** has two integrated azo-joints which isomerize upon irradiation of UV-light and therefore change the conformation of the macrocycle. The shape of the macrocycle can be switched several times between the *E*- and *Z*- conformation.^[93] Macrocycle **10** consists of an OPE-wire and an electronically passive bridge. The nitrogroup on the revolving central benzene ring can interact with the hydrogen from the opposite benzene ring. These interactions could be controlled electrochemically which would allow the ring to lie in plane with the other benzene rings (more conductive) or be rotated out of plane (less conductive).^[94]

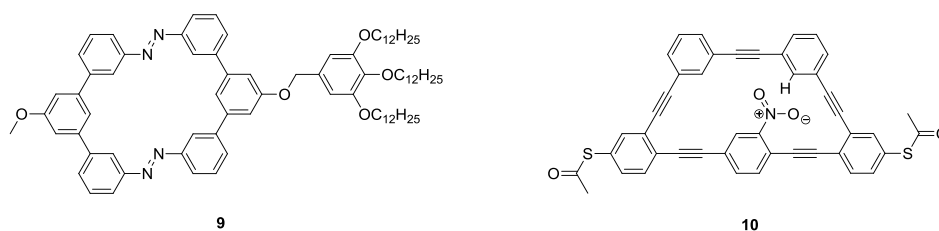


Figure 29. Two rigid macrocycles which have an integrated functionality.

Both macrocyclic structures required a well-planned multi step synthesis. Since one goal of this work was the development of a synthetic route towards an electrochemically switchable macrocycle, we summarized all synthetic concepts and strategies of phenyl-acetylene scaffolding and published the results as a micro-review in the *European Journal of Organic Chemistry*.^[95] This collection is presented in the next chapter and has been written together with Tom Eaton and Marcel Mayor.

1.4 Phenyl-Acetylene Bond Formation

Structure-property relationships are at the heart of a scientists' interaction with nature. From peptides to molecules, the spatial arrangement of functional groups in a substance plays a dominant role on its properties and function.^[96] Defining the structural architecture of a molecule in order to systematically investigate the effect this has on its physical properties requires the synthesis of complex organic molecules from much smaller, simpler building blocks. Palladium-catalysed coupling chemistry has provided a fast and efficient method for the formation of new C–C bonds^[97,98] and has revolutionized the synthesis of macromolecular structures. The importance of cross-couplings to synthetic organic chemistry has finally been recognised at the highest levels, the topic being awarded the 2010 Nobel Prize in Chemistry.^[98,99] To our surprise, sp^1 – sp^2 cross-couplings were not mentioned by the Committee in their announcement, despite the importance of this coupling reaction.

The acetylene functional group in particular provides its own advantages over other C–C bonds providing both enhanced rigidity and conjugation.^[100] *Sonogashira* couplings are a facile way to introduce acetylenes,^[101,102] classically involving the coupling of an acetylene to an aryl halogen centre^[103] allowing for conjugated π -systems to be formed from suitable building blocks. This micro-review describes synthetic strategies for the formation of suitable building blocks geared towards the assembly of larger molecular architectures. The structural motif of phenyl-acetylene bonds finds use in applications as diverse as; molecular electronics,^[104] nano-sensors,^[105] liquid crystals,^[106] natural products,^[107,108] optoelectronics,^[109] organic-inorganic hybrid structures^[110,111], surface functionalisation^[112] and cell imaging^[113] amongst many others. In many instances acetylene couplings are preferred over *Suzuki*^[114] or *Stille*^[115] direct sp^2 – sp^2 couplings as they can be essential to achieve coplanarity, increasing the π -conjugation length and decreasing the HOMO–LUMO gap. This has been shown for various chromophores including NDIs,^[116] oligophenylethylenes (OPEs),^[117,118] BODIPYs^[119] and substituted porphyrins^[120] which show a marked bathochromic shift in absorption.

Phenyl-acetylene scaffolds became very popular through the 90's as a facile method to assemble large organic molecular architectures focusing on the synthetic challenge, function being a secondary consideration.^[100,121] Since then the function of molecules has displaced structure as an objective, as has been demonstrated with bottom-up approaches towards functional graphene sheets.^[122] Acetylenes in shape-persistent macrocycles^[123] have been shown to display liquid crystalline behaviour^[106] and self-organisation on a surface.^[124] These

properties require precise control over functional group orientation within the building blocks prior to macrocyclisation. With the correct spatial orientation π - π aggregation can also be induced.^[125,126]

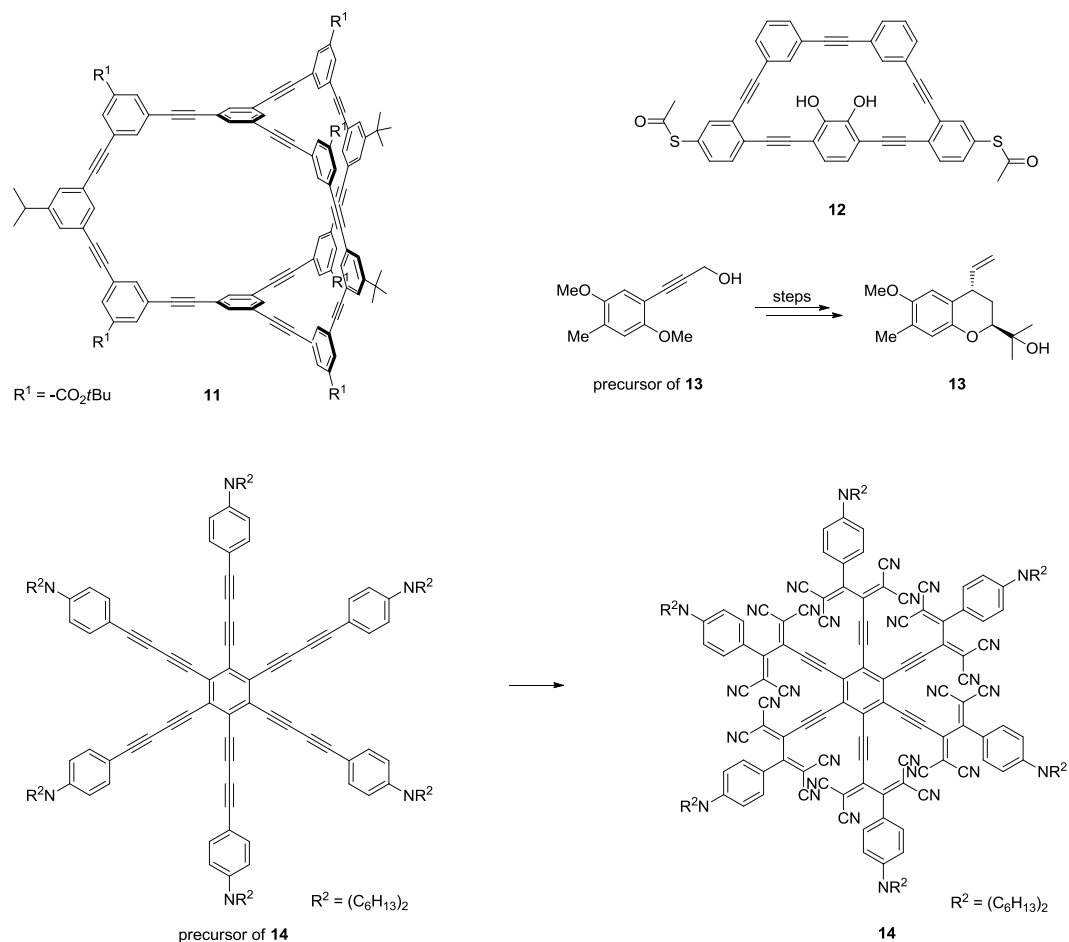


Figure 30. Examples of phenyl-acetylene structures.

In figure 30 four typical examples from different areas of synthetic chemistry illustrate the breadth of systems in which phenyl-acetylene bonds are found. Three dimensional (3D) structures in particular represent another level of complexity in structure-property relationships. Protein folding and DNA helices are naturally occurring examples of the bearing structure can have on function at the molecular level. Chemical approaches to mimic the controlled assembly of such massive biological systems are very difficult to replicate. As synthetic organic chemists we can try to imitate this complexity, using a bottom up approach by combining suitable building blocks. Pioneering work by Jeffery Moore and co-workers^[127] on 3D cages required precise control over the substitution patterns of their building blocks in

order to achieve 3D architectures such as compound **11**. The context of this micro-review is to cover the relevant synthetic toolkit required to imitate such syntheses.

In the field of molecular electronics, structure-property relationships of single molecules can be investigated using phenyl-acetylenes. Structure **12** was designed around the macrocyclic turnstile from Jeffery Moore^[128] in order to study switching behaviour by molecular rotation.^[129] The synthesis of such a complex structure with the substitution pattern found in **12** is a challenge, requiring a well-planned strategy involving the correct choice of disconnections and suitable protecting groups in order to overcome issues of reactivity and stability.^[130] The successful synthesis of **12** made extensive use of the strategies discussed in this micro-review.

In natural product synthesis phenyl-acetylenes are found both in synthetic intermediates and in target compounds, often introduced by *Sonogashira* reactions.^[107] A phenyl-acetylene bond was introduced to a precursor en route to (–)-Heliannuol E (**13**)^[131] a natural product found in sunflowers.

In materials chemistry dendrimer-like structures such as **14** have shown very large intramolecular charge transfer interactions, and therefore a very high uptake of electrons. This allows for the possibility of making a molecular battery. François Diederich and co-workers^[132] required the formation of an electron rich acetylene moiety in order to facilitate a [2+2] cycloaddition reaction to form molecule **14**. This demonstrates the tunability of acetylene reactivity possible by changing the local electronic environment. The enhanced reactivity of acetylenes has recently been popularised with the advent of “click” chemistry.^[133] The scope of this micro-review is limited to the most important tools and strategies required for the assembly of acetylene-phenyl building blocks, with a view towards the formation of larger nanoscale architectures, as acetylene scaffolds and the formation of substituted 1,4-butadienes is well reviewed elsewhere.^[100,134]

1.4.1 Synthetic Strategy: where to make the disconnection

The first step in any synthesis is to settle upon a target structure, this will depend upon the required mechanical, optical, or binding properties of the compound in question. Once a target has been decided upon, retrosynthetic analysis, as reviewed by Elias Corey^[135] represents a powerful tool in the design of a successful synthesis. When making a retrosynthetic analysis of sp^1 and sp^2 hybridised carbon systems, with the intention of performing palladium

catalysed cross-coupling reactions, there are a few important generalisations to bear in mind (figure 31). The principle consideration is which phenyl group contains the halogen (acceptor) component and which contains the acetylene (donor) component.

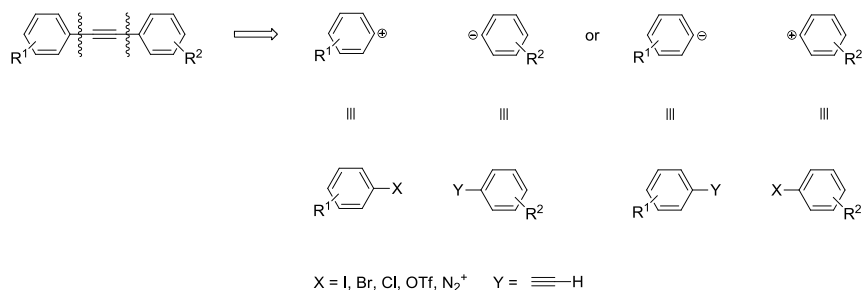
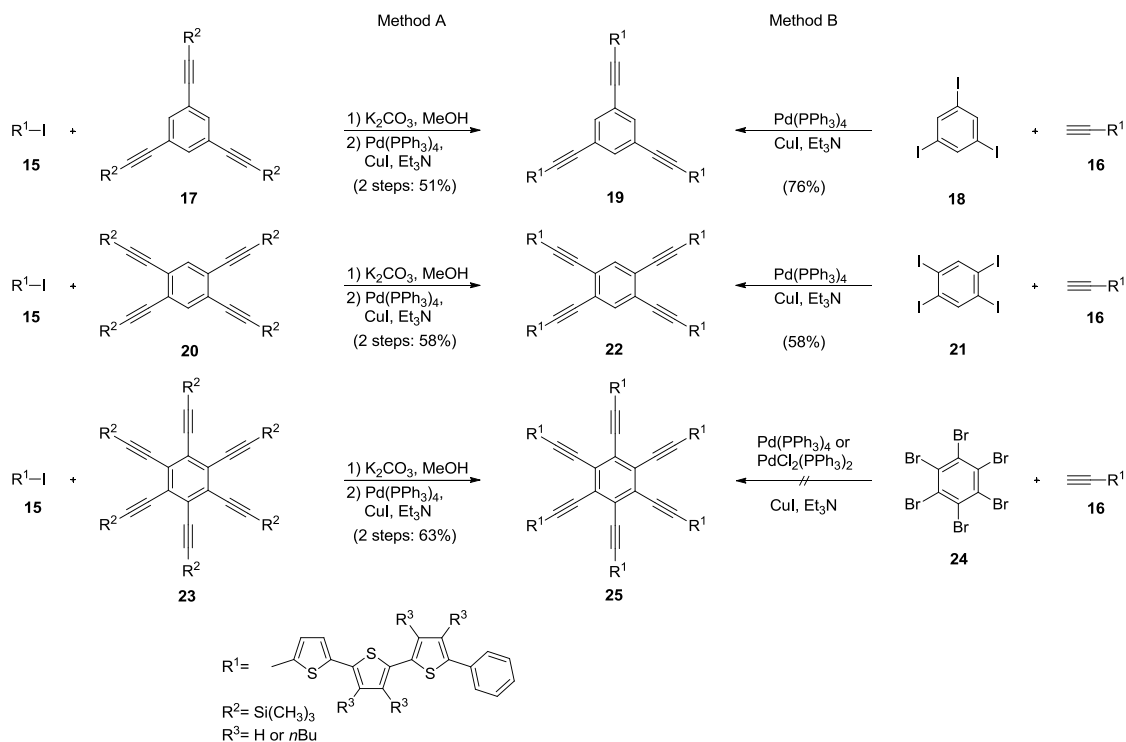


Figure 31. Retrosynthesis of the phenyl-acetylene bond.

This seemingly arbitrary decision about where to place a disconnection and which side should be a1 (acceptor) and which d1 (donor), can make the difference between success and failure in the elucidation of the target compound. Most syntheses can be classified as either following the principles of convergence or divergence,^[136] where the building blocks are assembled together before attachment to a central unit (convergent) or building blocks are assembled directly onto a core substituent (divergent). Narita et al.^[137] have employed the use of just such a change in disconnection in their convergent synthesis of star-shaped oligothiophenes (scheme 1). Under the same coupling conditions of Pd(PPh₃)₄, CuI and NEt₃ but by changing which building block was the acceptor and which was the donor, they were able to obtain their target stars. Method A involves the coupling of iodo-polythiophene **15** (acting as a1) to acetylene functionalised benzene rings **17**, **20** and **23** (acting as d1). Method B exchanges the position of the acetylene onto the acetylene-functionalised polythiophene **16** (acting as d1) and the halogen benzenes **18**, **21** and **24** (acting as a1). For the tri-functionalised star **19** method B afforded a higher yield. For **22** both approaches are comparable and for **25** only method A formed the product. This could be due to the switch to hexabromobenzene (**24**) in place of hexaiodobenzene for method B, possibly required due to the very low solubility of hexaiodobenzene. This example illustrates the bearing which the choice of disconnection can have on the outcome of a synthetic strategy.



Scheme 1. The effect of changing the acetylene disconnection.

After proposing which disconnections should be made, and which mode of assembly, either convergent or divergent, shall be employed one can then turn to the formation of these proposed building blocks. In section 1.4.2 on chemoselectivity we will discuss the tuning of the acceptor (halogen, triflate, N_2^+) and how the insertion of more than one of these components allows for selective couplings providing a great deal of control over building block assembly. When it becomes difficult to obtain this precise control one can employ the technique of masking which we discuss in section 1.4.3. Masking deals with the transformation of one functional group into another, presenting the best in reaction control. It differs from a protecting group (PG) in that direct cleavage of the masking group is not possible. A functional group interconversion (FGI) is first required before the site would become active to the reaction conditions. This allows for greater functional group tolerances to be achieved with the same building block. Differing electronic properties and subsequent reactivity can also be achieved through masking, for example in the conversion from a nitro to an amine and finally into an iodine.

Addition of an acetylene moiety to any building block usually requires a PG unless one uses molecular acetylene. The range of available PGs is discussed in section 1.4.4 where the relative advantages of processability, solubility, ease of deprotection and the matching of different PGs to achieve orthogonality are explained. Then we turn to the special case of

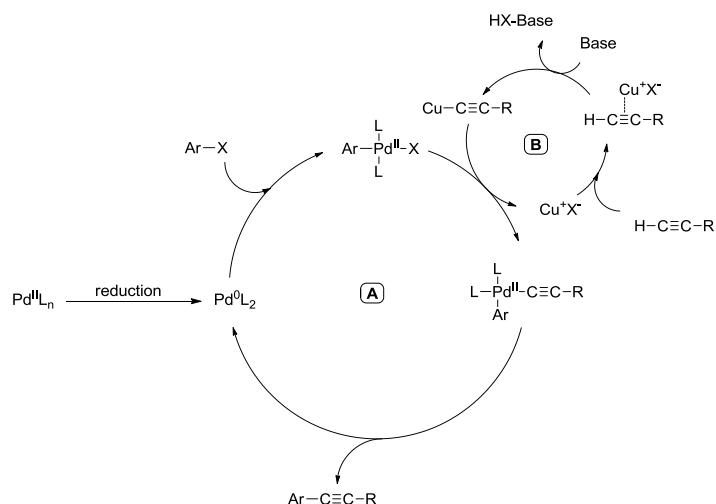
statistical coupling and deprotection reactions which allow for the introduction of asymmetry to an otherwise symmetric (for example containing the ideal symmetry elements C_2 or σ_v) building block. By this, we mean performing a ‘statistical reaction’ on only one reactive site where two identical ones are present, thereby introducing ‘asymmetry’ to the molecule. This asymmetry can be introduced either by manipulation of functional groups prior to application of cross-coupling reactions, an idea expanded upon in section 1.4.2, or by performing a statistical cross-coupling as discussed in section 1.4.5 + 1.4.6 below. A third option is to perform a statistical deprotection of protected acetylenes bearing the same protecting groups. Oligomer and macrocyclic syntheses often contain examples of these strategies^[138,139] as a library of functionalized compounds are desired and it can be easier to use the same building blocks which can be statistically functionalised to introduce diversification in the number of target structures.

When side-products, including diacetylenes or polymerisations in a macrocycle forming reaction are an issue, in situ deprotection of the acetylene moiety in the presence of the *Sonogashira* coupling agents can lead to improved yields or even elicit an otherwise unattainable compound. These in situ reaction strategies are discussed in section 1.4.7 followed by examples in section 1.4.8 bringing all the concepts we have mentioned together, but first we turn to the role of palladium and copper in *Sonogashira* cross-couplings.

Mechanism of the Sonogashira Reaction

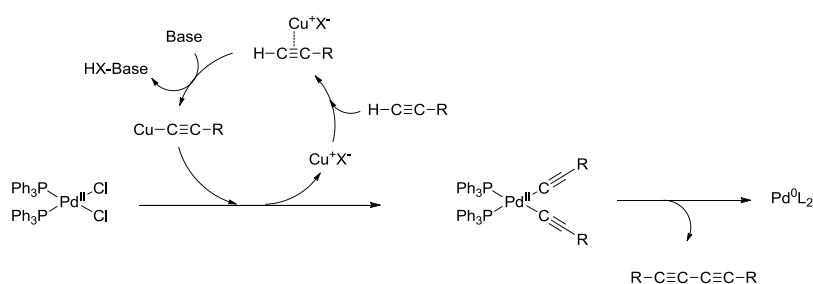
Below we briefly summarise the currently accepted mechanism of the *Sonogashira* reaction, with a focus on gaining a better understanding of the problems which can occur and how to avoid the formation of side-products, such as di-acetylene homocoupled product or conjugated enynes.^[140] The generally accepted catalytic cycle^[101,103] for the copper co-catalyzed cross-coupling reaction is believed to take place through two independent catalytic cycles (scheme 2). The palladium catalysed reaction (cycle A) starts with a fast oxidative addition of the aryl acceptor (Ar-X; where X = I, Br, Cl, OTf, N_2^+) to the active catalyst generated from the initial palladium complex.

It is known that electron donors such as phosphanes, amines and ethers, used as ligands and solvents can reduce palladium(II) species, to the palladium(0) complex.^[141] The electronic nature of the substrate which adds to the palladium(0) is very important. Electron withdrawing groups on the substrate reduce the electronic density of the Ar-X bond and therefore facilitate the oxidative addition.^[142,143]



Scheme 2. Catalytic cycle of the palladium/copper co-catalysed *Sonogashira* cross-coupling reaction.

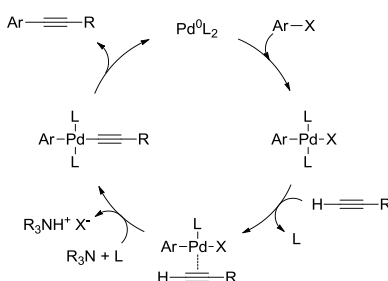
The second step is a transmetalation with a copper acetylide generated in cycle B (scheme 2). This is usually the rate determining step. After a *cis/trans* isomerization and a reductive elimination the cross-coupled product is formed and the catalyst is regenerated. The copper cycle (cycle B) is still poorly understood. It is believed that the base abstracts the acetylenic proton of the terminal alkyne, thus forming a copper acetylide in the presence of the copper(I) salt, but the amines used are usually not basic enough to deprotonate the alkyne to make the anionic nucleophile that should form the copper acetylide. Therefore, a π -alkyne-Cu complex could be formed. The coordination of the copper would make the proton much more acidic and therefore easier to abstract by a weaker base. These copper acetylides could also be involved in the formation of the active Pd^0L_2 complex (scheme 3).^[101]



Scheme 3. Possible formation step of the active catalytic species.

Some questions still remain about the nature of the real active catalyst. Some results indicate that an anionic palladium complex would be the active species if anions or halides are present.^[144] The mechanism of the copper free *Sonogashira* cross-coupling reaction is also not

very well understood (scheme 4). It should be noted that the absence of trace copper in otherwise ‘pure’ metals such as palladium is an area of contention. Traces of copper below current detection limits may still be present which could influence the reaction mechanism. In any case the first step must be the same oxidative addition of an Ar-X to a Pd^0L_2 complex as in the copper co-catalyzed cycle discussed previously (scheme 2). It is commonly accepted that the alkyne coordinates via a ligand exchange process to the palladium(II) complex. This complexation increases the acidic nature of the proton which is then abstracted from the base to form the new complex $\text{ArPd}(\text{C}\equiv\text{CR})\text{L}_2$, which affords the coupling product by reductive elimination.



Scheme 4. Proposed mechanism of a copper-free *Sonogashira* cross-coupling reaction.

Terminal acetylenes can also play an important role in the palladium cycle. It is possible that the terminal alkynes coordinate the palladium(0) complex prior to the oxidative addition step, thereby producing a decelerating effect by formation of unreactive or slow-reacting ($\eta^2\text{-RC}\equiv\text{CH}$) Pd^0L_2 complexes.^[145] The stationary regime of a catalytic cycle is more easily reached if the reaction rates of all the elemental steps are as close as possible to each other. This can be achieved by accelerating the rate-determining step or decelerating the fast reactions by stabilizing high-energy species.^[146] If the oxidative addition step is faster than the transmetallation step, the decelerating effect of the alkynes provides a better efficiency for the catalytic cycle, bringing the rates of the two steps closer together. This can be enhanced by increasing the reaction temperature. However, if the oxidative addition step is slower than the transmetallation step, as is the case for arylbromides or arylchlorides, it becomes even slower in the presence of the nucleophilic alkynes and the catalytic reaction would become less efficient.

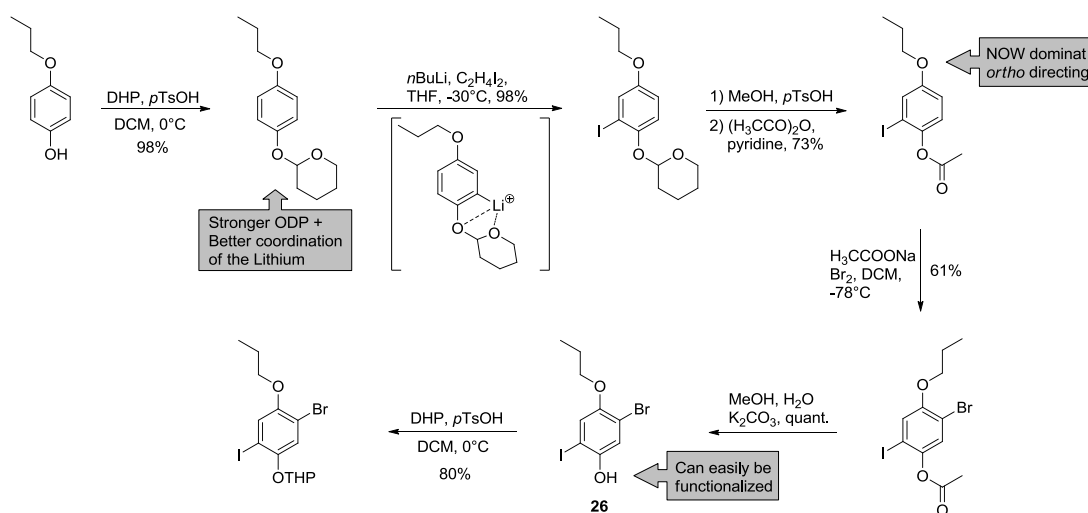
To improve the yield of a *Sonogashira* cross-coupling reaction one should screen a few standard palladium catalysts such as; $\text{Pd}(\text{PPh}_3)_4$, $\text{PdCl}_2(\text{PPh}_3)_2$, $\text{Pd}(\text{OAc})_2$ and $\text{Pd}(\text{dba})_2$

combined with different bases at different temperatures. If the yields are still not satisfactory the design of new ligands for the palladium complex should be considered or a change in the retro synthetic strategy is required. In this review we want to focus on the strategic approach and not on the optimization of the palladium catalyst as this has already been extensively covered in other reviews.^[141,147,148]

1.4.2 Reactivity and Chemoselectivity of Phenyls

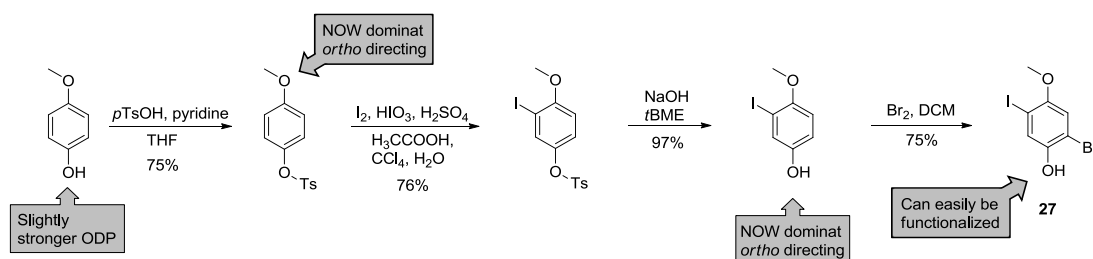
While symmetric systems are more easily assembled than asymmetric ones there are many applications where an inherent asymmetry is required, such as push-pull systems and molecules for use in the field of molecular electronics.^[149,104,150] Building blocks for *Sonogashira* cross-coupling reactions require the presence of acceptor groups to undergo oxidative addition. The order of reactivity of halobenzenes towards oxidative addition to Pd(PPh₃)₄ was found by Fitton et al.^[142,143] to be Ar-I > Ar-Br > Ar-Cl with large enough a difference in reaction rates to allow for high chemoselectivity. Over the past decades, many research groups have developed catalytic systems which promote the oxidative addition of arylbromides^[151,152] and arylchlorides.^[153,154] Besides arylhalides, aryltriflates^[155] and aryldiazo-compounds^[156,157] have drawn a lot of attention over the past few years. The use of these functional groups as acceptors will be discussed later.

The order of reactivity of the arylhalides can be used to sequentially introduce acetylenes bearing orthogonal protecting groups onto a multi-functionalized building block. This method stands in contrast to a statistical approach, which works well as long as the central parts of the desired building blocks are symmetric^[158,159] and as long as chemical waste is not an issue. However, if the building block is asymmetric a statistical approach leads to more side products and the purification can become difficult and time consuming. On the other hand, designing an asymmetric iodo-bromo-benzene compound which has an extra functionality in a preferred position can also be difficult. Sigurd Höger^[160] demonstrated a nice approach to control the chemoselectivity to form such an asymmetric iodo-bromo-benzene building block (scheme 5).



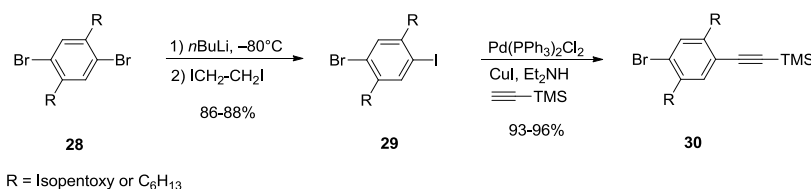
Scheme 5. Chemoselective introduction of halides using substituent control.

He reported two strategies for the synthesis of monoalkylated hydroquinones **26** and **27** containing a bromine and an iodine in the 2- and 5-positions (schemes 5 and 6). The difference in reactivity of the halogens in **26** and **27** towards palladium(0) species allows for selective transformations to orthogonally protected acetylenes. This allows these positions, as well as the phenolic groups present, to be further functionalized.^[161] The different *ortho*-directing-powers^[162] (ODP) of the substituents on the benzene ring were used to selectively introduce an electrophile such as iodine or bromine.



Scheme 6. Chemoselective introduction of halides using substituent control.

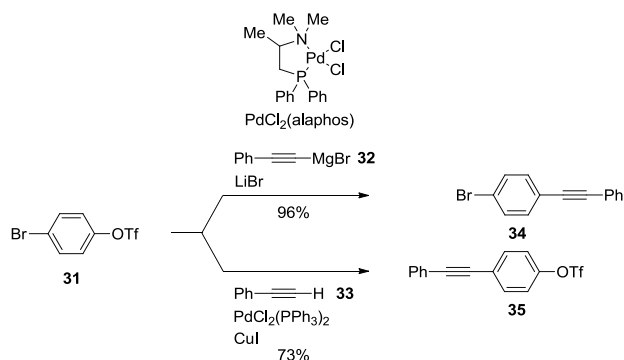
The fastest route to an asymmetric molecule can often be to start with a symmetric compound, and introduce the asymmetry by controlling the equivalents of reagent added. Manipulation of functional groups, such as halogen exchange or -OH protection^[163] are good examples. Statistical couplings and deprotections are further expanded upon in sections 5 and 6.



Scheme 7. Halide exchange to allow selective introduction of TMS-acetylene.

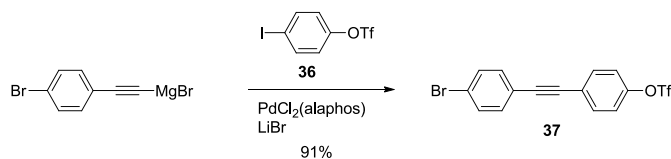
In order to avoid a statistical coupling to make **30**, Adelheid Godt and co-workers^[164] found conditions for a selective halogen exchange in their synthesis of monodispersed OPEs (scheme 7). Using *n*BuLi at -80°C was necessary in order for a clean transformation from **28** to **29** after quenching the lithium salt with I-CH₂-CH₂-I. Chemoselective palladium catalysed coupling of TMS-acetylene with the iodine of **29** afforded the asymmetric building block **30**. This was then used in a successful coupling sequence, eventually forming an octomeric OPE.

The use of alternative acceptor groups for performing the oxidative addition in palladium catalysed reactions are becoming more prevalent. A triflate (–OTf) leaving group is not as reactive as iodine but has a similar reactivity to that of bromine. The biggest advantage of a triflate-strategy is the possibility to have a hydroxy group present on a building block which can be transformed into a triflate at any time. The hydroxy group can be protected if other reaction sequences do not tolerate the presence of a free alcohol. Many protection/deprotection protocols for hydroxy groups are known^[165] and a suitable strategy can be chosen for a longer reaction sequence. A selective alkynylation of bromo-aryl-triflate **31** (scheme 8) was reported by Tamio Hayashi and co-workers^[166] They showed that aromatic compounds bearing both bromine and triflate can undergo a selective replacement of either bromine or triflate by an acetylene group. It was found that the triflate group was selectively replaced by the acetylene group to give **34** in 96% yield when PdCl₂(alaphos) and phenylethynylmagnesium bromide (**32**) were used. On the other hand, under standard *Sonogashira* conditions, preferential substitution of bromine to give **35** was observed, although the selectivity was lower, with a purified yield of 73%.



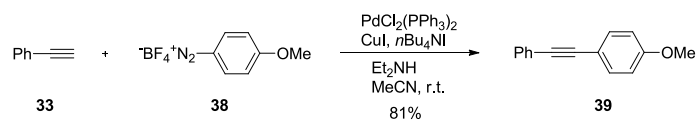
Scheme 8. Control of acceptor group substitution by changing the donor and active catalyst species.

To compare the order of reactivity towards the $\text{PdCl}_2(\text{alaphos})$ catalyst an iodoaryl triflate derivative **36** was used instead of the bromoaryl triflate **31** to make **37** (scheme 9). It was shown that the order of reactivity of the leaving groups on an aromatic ring is iodine > triflate > bromine in the *Grignard* cross-coupling reaction catalyzed by $\text{PdCl}_2(\text{alaphos})$.



Scheme 9. *Grignard* cross-coupling reaction.

Aryldiazonium salts, such as **38**, represent an attractive alternative to aryl-halides or triflates because of their higher reactivity,^[157] their formation under milder conditions, their availability from inexpensive anilines, and because additional base is not required in several applications (scheme 10). The reaction of **33** and **38** occurs under mild conditions in the presence of $n\text{Bu}_4\text{NI}$ and proceeds through a domino iododediazoniatio/*Sonogashira* cross-coupling sequence to give **39**. Good to excellent yields are usually obtained. A variety of alkyl, aryl, and heteroaryl substituents on the alkyne substrate can be used and many useful functionalities including bromo-, chloro-, keto-, ester-, ether-, cyano-, and nitro-substituents on the aryldiazonium salt are tolerated. The entire aryldiazonium salt synthesis/iododediazoniatio/cross-coupling sequence can also be performed as a one-pot domino process, omitting the isolation of the arenediazonium salt.^[157]



Scheme 10. Diazonium salt as acceptor in a Sonogashira cross-coupling reaction.

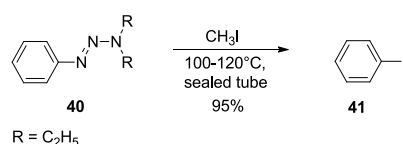
While the use of different acceptor groups to enable selective couplings to a building block may be more aesthetically pleasing, in some instances a statistical approach incorporating orthogonal protecting groups can afford target structures in fewer transformations. It is often possible to obtain a higher yield of product from a single step statistical reaction than the overall yield from a series of non-statistical reactions. These possibilities of breaking the symmetry of a building block are discussed in section 5 and we hope that by using a combination of these approaches a best fit to any synthetic route can be made.

1.4.3 Masking: using functional group interconversions to control reactivity

With increasing demand for enhanced functionalities of macromolecules, the design and the retrosynthetic strategies have become more and more challenging. Multiple aromatic substitutions of arylhalides do not always work with a statistical approach. Reasons for this can be ecological (additional waste), economical (increased costs) or simply isolation problems in the lab. Therefore a more selective and efficient strategy must be chosen. As described above, the different reactivity of aryl halides towards oxidative addition to the palladium(0) species could be a useful tool. This strategy is limited to building blocks, which can survive harsher coupling conditions such as high temperatures or long reaction times owing to the reduced reactivity of arylbromides and arylchlorides.^[142,143] If the nature of the building block does not allow for these harsher conditions, one is limited to the more reactive aryl iodides. This again raises the issue of the selectivity when more than one iodine coupling site is required.

To avoid a statistical coupling approach, masking of the halide should be considered. The ideal masking group should be readily available, stable to a variety of chemical conversions and conveniently transformed under mild conditions in a high yield to the desired aryl halide. A useful masking group for an iodine is an amine, which has additional advantages and disadvantages for further functionalization on the benzene core by means of activation or deactivation^[130]. The reactivity of the aromatic system can be tuned by the introduction of a

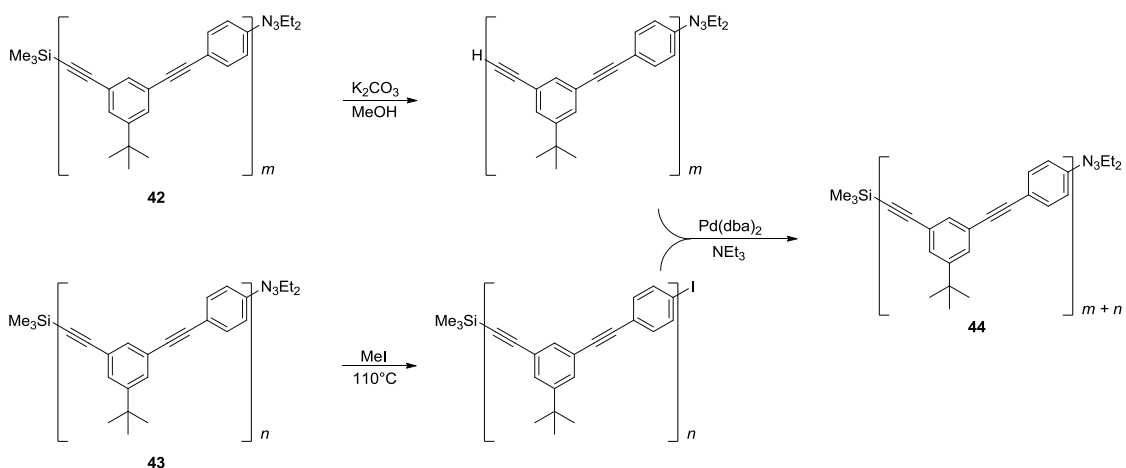
nitro group as a precursor to the amine, switching from an electron rich to an electron poor system. The transformation from an amine to an iodine is well known and was first reported by *Traugott Sandmeyer* in 1884.^[167] However a free amine can also act as a di coupling partner, known as a *Hartwig-Buchwald* reaction,^[168,169] leading to side products. As a consequence the amine may need to be protected in order to increase its stability towards the reaction conditions and yet it should still be labile enough to be deprotected and subsequently transformed into an iodine. Jorge Barrio has reported on the conversion of 1-aryl-3,3-dialkyltriazene **40** to aryl iodides using either trimethylsilyl iodide^[170] or sodium iodate.^[171] This protocol was later improved by Moore et al.^[172] using methyl iodide as the iodine source to make **41** (scheme 11).



Scheme 11. Functional group interconversion of triazine into iodine.

The triazine **40** can easily be made from the amine derivative^[170] (see scheme 13) and the reaction can be performed with equal success using various N,N-dialkyl substituents. In fact, it was found that pyrrolidine triazenes have a greater tendency to form crystalline solids than the corresponding N,N-dialkyl derivatives. Thus, the pyrrolidine triazenes can easily be purified by recrystallization.

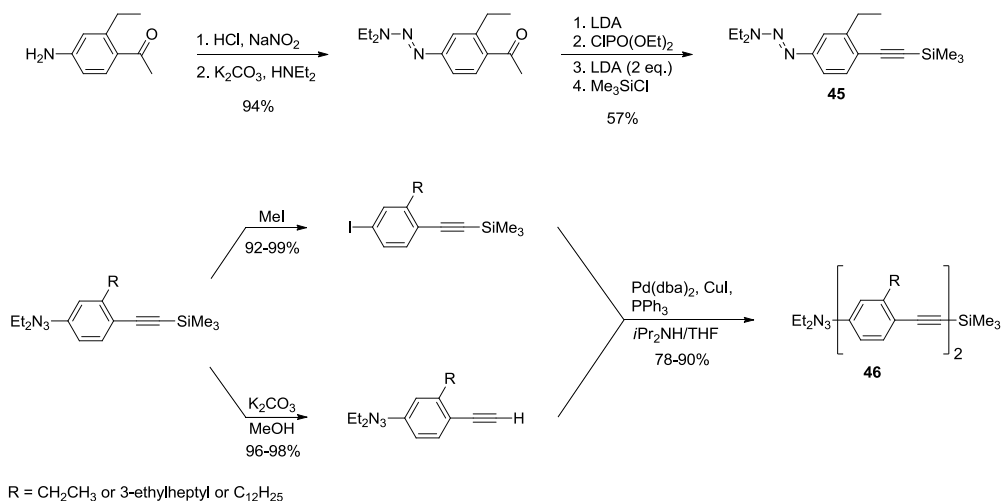
A very nice example was shown by Jeffrey Moore and co workers.^[173] They used a divergent-convergent approach to synthesize an oligo-phenylene-ethynyne (OPE) structure **44** (scheme 12).



Scheme 12. The final convergent step in the divergent-convergent OPE synthesis.

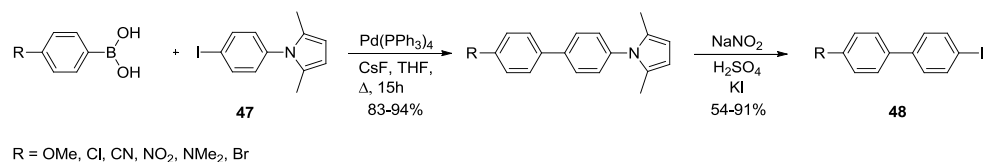
The diethyltriazenyl/trimethylsilyl functionalised structures **42** and **43** are the parent compounds. Desilylation and exchange of the triazenyl substituent for an iodo substituent are the two divergent steps, followed by the alkynyl–aryl coupling, the convergent step.

Another interesting strategy is masking the acetylene itself. This requires having a functional group in place which can later be transformed into an acetylene. There are several methods described in the literature of how to convert a carbonyl into an acetylene (*Corey-Fuchs*^[174], *Seyferth-Gilbert*^[175]). The problem with such an approach is the reactivity of the carbonyl towards a nucleophile. An extra protection/deprotection step would be necessary. A very nice alternative was reported from Ei-ichi Negishi and James Tour.^[176] They used an acetyl group to mask the acetylene (scheme 13). First an enolate was formed using LDA, which was then trapped with diethyl chlorophosphate to afford an enol intermediate. After elimination to form an acetylene, a further equivalent of LDA formed an acetylide anion. This was then quenched with trimethylsilyl chloride to afford the TMS-protected acetylene **45**. Tour et al.^[177] (scheme 13) nicely showed the synthetic power of these two masking strategies to synthesize **46** using an iterative approach.



Scheme 13. Masking of both the donor and acceptor.

Another Masking group was used by Arne Lützen and co-workers.^[178,179] They introduced a dimethylpyrrole moiety to protect the amine in **47**. This masking group is suitable for cross-coupling reactions followed by a diazo formation and iodine substitution to form **48** (scheme 14).



Scheme 14. Functional group interconversion of dimethylpyrrole into an iodine.

This method is an alternative to the triazene strategy introduced above. The advantage of the pyrrole masking group is its fast transformation into an iodine at room temperature. It typically leads to fewer side products during a coupling reaction compared to a free amine.

1.4.4 Acetylene Protecting Groups (PGs)

During the design of a successful synthetic route disconnections must be made which correspond to viable building blocks. Consideration should be given to which moiety should act as the acceptor and which as the donor, as was discussed in section 1.4.1. At the same time suitable PGs should also be considered. In order to aid this process below is a selection of

known acetylene PGs. Each is discussed in turn, listing the relative advantages, disadvantages and the conditions under which the acetylene-H will be revealed and therefore made active to coupling conditions.

Protecting groups currently play a vital role in organic synthesis allowing very complex structures to be assembled by careful choice of the PG and the order of assembly.^[163] In most syntheses PGs are required due to a lack of reaction selectivity. In acetylene based molecular structures PGs are used to enable the introduction of acetylene units. The use of acetylene gas would simply give rise to the di-coupled product,^[180] leaving aside the obvious difficulty of using such a reagent. In this section we will focus on the most common acetylene protecting groups representing the donor moiety of the cross-coupling cycle. See section 1.4.2 for a discussion of the acceptor moiety.

The choice of acetylene PG should consider its functional group tolerance and ease of removal, however these are not the only considerations. The PG may also engender other favourable properties to a synthesis including, orthogonality (expanded upon below), increased polarity to aid in purification on silica gel, increased solubility, stability, and the possibility of statistical or in situ deprotection.

Acetylene Protecting Groups

Silyl based protecting groups have been particularly popular due to their early adoption and ease of removal, either under mild basic conditions or using fluoride ions (F⁻) in protic solvents. Increasing bulk around the silicon centre engenders increased stability which can be used for selective removal of less bulky silyls faster than bulkier ones.^[181] This range of stabilities to basic conditions can be employed, culminating in the use of an F⁻ source, which will cleave all silyl PGs. Thus when multiple silyl protecting groups are present, sequential lability can be employed to deprotect specific acetylenes and after further coupling build up larger structures with a specified substitution pattern. They are most often formed by the reaction of a chlorine substituted silicon centre with ethynlmagnesiumbromide. There are many possible acetylene PGs^[165] however we shall only summarise the most popular ones here as, in practise, most researches stick to the following easily accessible acetylenes (figure 30).

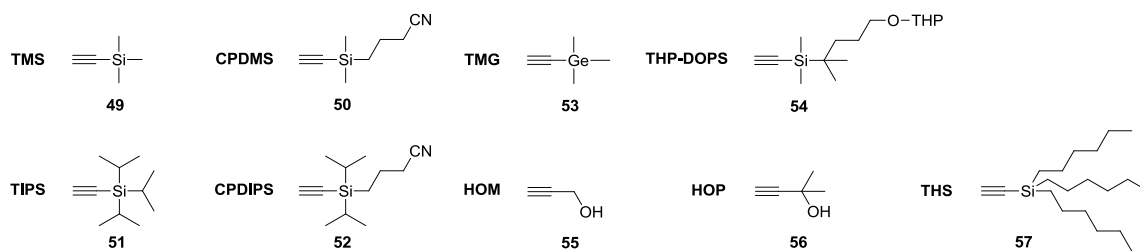


Figure 30. Commonly used acetylene protecting groups.

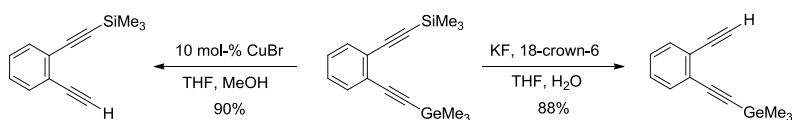
Trimethylsilyl acetylene 49 (TMS) is one of the most common acetylene protecting groups. It was employed by *Kenkichi Sonogashira* in the early days of cross-coupling synthesis,^[180] and was also used as a PG in *Cadiot-Chodkiewicz* cross-coupling reactions.^[181] The TMS PG is best used when all that is required is insertion of an acetylene, and where no other properties are sought from the PG itself. Easy removal of TMS is made by application of mild basic conditions; usually K_2CO_3 in the presence of a protic solvent. TMS will also be cleaved readily in the presence of an F^- source such as KF with 18-crown-6 as a chelator or TBAF (see TIPS for details). The addition of silver salts (Ag^+) can also be used to deprotect TMS,^[182] and is usually preferable to the in situ use of alkali metal hydroxides,^[183] owing to its greater functional group tolerance.

(3-Cyanopropyl)dimethylsilyl acetylene 50 (CPDMS) was introduced by Sigurd Höger to develop a polar analogue of the popular TMS PG using a CN alkyl chain bonded to the silicon centre.^[184] The CPDMS adds polarity to the acetylene moiety making purification on silica gel much easier, but is still as easily removed as TMS under the same mild alkali conditions in the presence of a protic solvent. It will also be removed by an F^- source.

Triisopropylsilyl acetylene 51 (TIPS) is another very popular PG used for its increased stability to acidic and basic conditions owing to the steric bulk of the three isopropyl groups around the silyl centre. It is easily removed in the presence of an F^- source making it a very tolerant PG to most other functional groups, while still maintaining a facile deprotection.^[185,186] It has been reported that the yield of the deprotection can be increased in the presence of small quantities of water, moderating the reactivity of the fluoride anion.^[187] Commercial TBAF is sold as a 1M solution in THF containing wt.-5% water, which is usually sufficient. Deprotection using AgF offers an alternative to TBAF, and in the presence of a bromine source it can be used to insert a halogen en route towards the formation of 1,4-butadienes.^[188]

(3-Cyanopropyl)diisopropylsilyl acetylene 52 (CPDIPS) was also introduced by the group of Sigurd Höger^[189] as a more stable version of the CPDMS PG which behaves as a polar analogue of the popular TIPS PG requiring an F⁻ source for deprotection but still engendering the increased polarity of the CPDMS, but also added stability to temperature, acidic and basic conditions.

Trimethylgermanium 53 (TMG) is a relatively old PG^[181,185] which has not seen wide adoption. It can be cleaved with catalytic CuBr in MeOH and has been used as an orthogonal protecting group to TMS in the synthesis of acetylene interlinked oligosaccharides (scheme 15).^[190]



Scheme 15. Orthogonal deprotection of TMS and TMG groups.

The acetylene-GeMe₃ is made by reacting ClGeMe₃ with ethynylmagnesiumbromide. Recently TMG has been employed in an in situ deprotection and subsequent azide click reaction by washing a functionalised surface with Cu(I) to act as both the deprotecting agent and as catalyst of the click reaction.^[191]

Dimethyl[1,1-dimethyl-3-(tetrahydro-2H-pyran-2-yloxy)propylsilylalkyne] 54 (DOPS). Chengzhi Cai and Andrea Vasella^[192] introduced a new application of silyl protecting groups to acetylene chemistry with their use of DOPS. This group is orthogonal to TMS and sequentially labile to other silyl PGs. The deprotection of the THP PG under acidic conditions reveals a free alcohol. Then treatment of the compound with a suitable base (eg LiDBB lithium 4',4'-ditert-butylbiphenylide) in a dry aprotic solvent deprotonates this alcohol and leads to intramolecular attack of the silicon centre, thereby revealing the free acetylide. These conditions would leave a TMS protected acetylene intact.

Hydroxymethyl acetylene 55 (HOM) as a PG was introduced by Bumagin et al.^[193] and has the advantage of affording polarity and orthogonality to the silyl PGs. It is cleaved within 20 minutes after treatment with MnO₂ and KOH to afford the free acetylene upon workup and has been used in the successful synthesis of long-chain oligomers, where the effectiveness of the HOM as a polar tag steadily decreased with increasing chain length.^[159]

2-Hydroxypropyl acetylene 56 (HOP) This polar PG is most useful when the purification of reaction products will be a problem. This can be especially useful when more than one HOP group is statistically added or removed on a building block and requires isolation. It can be removed by heating with alkali metal hydroxides or hydrides, usually in refluxing toluene^[194] via a retro-*Favorskii* reaction.^[195] This treatment does mean that this PG may be incompatible with base sensitive functional groups, but as long as dry toluene is used it can be removed selectively in the presence of silyl PGs including TMS.^[196]

Trihexylsilyl acetylene 57 (THS) adds long alkyl chains allowing for increased solubility of the unit to which it is attached. This can allow for easier processability of a building block prior to its removal and subsequent coupling to another, hopefully soluble, partner. It was successfully used by Reeve et al.^[113] in the synthesis of a series of push-pull porphyrin molecules, which without the increased solubility of the alkyl chains, would be too difficult to purify. Using a statistical deprotection of the THS with TBAF they were able to introduce the push-pull units after *Sonogashira* coupling from their initial symmetric diprotected porphyrin.

Orthogonality of PGs

Orthogonality is a desirable trait in PG strategies where one PG can be selectively removed in the presence of another PG in any order (figure 31). The conditions for cleaving one PG must be tolerated by the other, and vice versa. (X off, Y stays, or Y off and X stays).

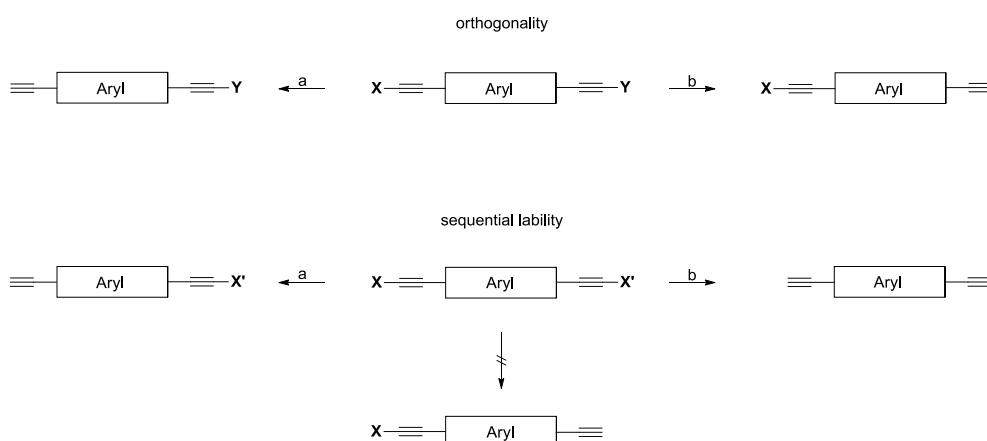
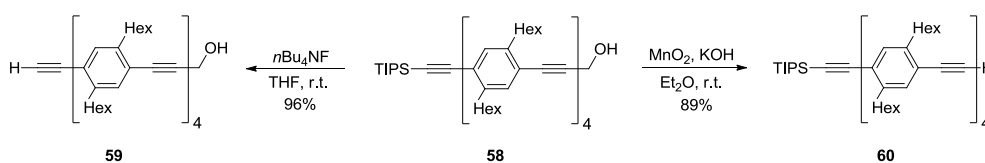


Figure 31. Concept of orthogonal and sequentially labile acetylene protecting groups.

True orthogonality is very difficult to achieve using a combination of silyl PGs as addition of an F^- source will cleave all, with the rate determined by the degree of steric bulk around the silyl centre. This can be seen in the case of the DOPS PG. So only sequential removal is

practical (X off, then X'), but the order of deprotection is limited as the 'least stable' group must be removed first. (e.g. the TMS in a TIPS/TMS combination). Sequential removal of silyl groups is therefore possible, but this places severe limitations on the sequence in which reactions can be performed.

Adelheid Godt and co-workers^[159] were able to use a combination of the HOM and TIPS PGs in their synthesis of OPE rods (see scheme 16) where removal of TIPS from **58** using TBAF gave **59** in 96% yield without affecting the HOM group and removal of HOM from **58** to afford **60** was possible in 89% yield.



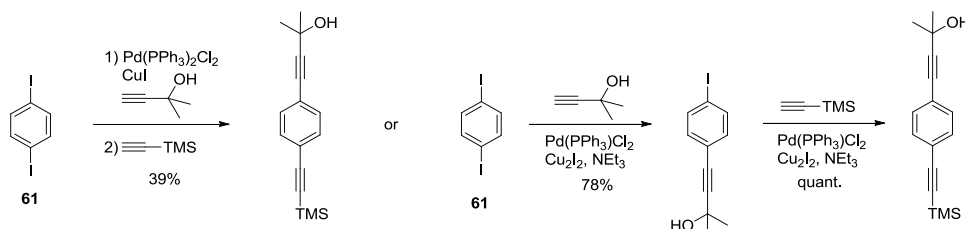
Scheme 16. Orthogonal deprotection of HOM and TIPS groups.

This work has recently been expanded upon by Sahoo et al.^[158] using the same orthogonal PGs and also incorporating ether linkers as polar tags on their OPE rods.

1.4.5 Breaking the Symmetry – I: statistical coupling

So far we have discussed how to use the selectivity of different Ar-X to introduce acetylenes bearing different protecting groups. This approach is especially helpful if an asymmetric building block is required. Whenever the al coupling component is symmetrically arranged with respect to any other R-groups (usually containing a C_2 or σ_v ideal symmetry element) in a building block, statistical reactions can be employed. A statistical reaction usually leads to a mixture of starting material, mono-substituted product and di-substituted product. These mixtures are not always easy to separate, especially when apolar protecting groups such as TIPS or TMS are used, or if the molecules are already very large. To overcome this problem one should introduce more polar protecting groups such as the HOM/HOP^[158] or the CPDMS^[184] and CPDIPS,^[189] developed by Sigurd Höger for this purpose. These building blocks can now be used to build up larger asymmetric molecules or can be used in a divergent synthesis towards a macro molecular structure.^[159] Yields of the mono-functionalized species can be increased by using an excess of the acceptor component **61** relative to the equivalents

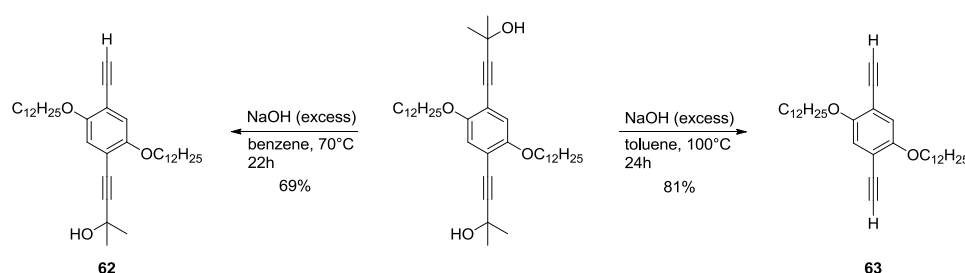
of acetylene used. Yields as high as 80% have been achieved this way.^[197] It is possible to introduce orthogonal protecting groups in a one-pot reaction^[198] or stepwise^[199] (scheme 17). Even though the stepwise approach includes an extra purification step, it usually provides higher overall yields.



Scheme 17. Statistical coupling: one-pot versus a step-wise introduction of acetylene.

1.4.6 Breaking the Symmetry – II: statistical deprotection

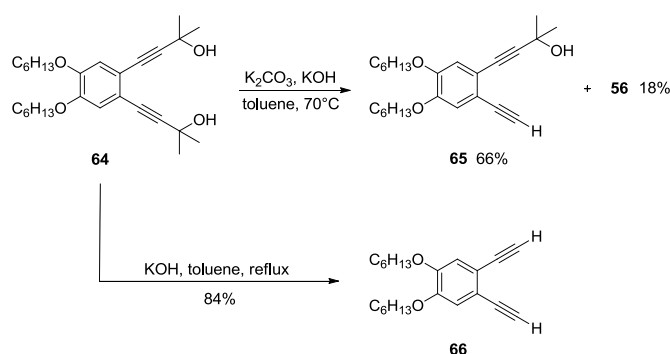
When two or more identically protected acetylenes are present in a molecule, then a statistical deprotection procedure may be employed (scheme 18). The HOP PG is particularly well suited to this approach as the polarity it engenders to a compound allows for easy purification on silica gel of the fully-protected, mono-deprotected and fully-deprotected derivatives. By varying the strength of the base, temperature and reaction time used for the deprotection one can reliably optimize the formation of the required component. However it is often difficult to determine which of these variables is predominant for each particular deprotection.



Scheme 18. Statistical and complete deprotection depending upon the conditions applied.

Abderrahim Khatyr and Raymond Ziessel^[200] showed that an excess of NaOH in benzene at 70°C for 22 h gave **62** in 69% yield. However, at 100°C in toluene for the same time **63** was obtained in 81% yield. The Raymond Ziessel group performed the same transformation under

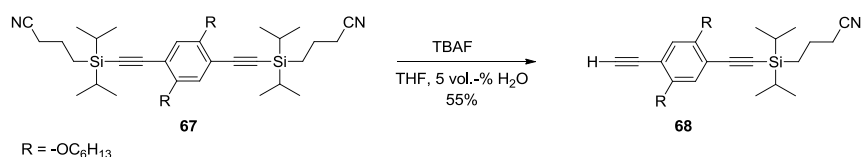
similar conditions (NaOH in benzene at 70°C) for 14 h. They only obtained a 45% yield with the majority of starting material re-isolated^[201] indicating the relative difficulty in reproducing this statistical deprotection. Luo et al.^[202,203] have recently shown that by monitoring the deprotection more closely by TLC the monodeprotected product can be obtained within 20 min. By dissolving **64** in toluene in the presence of 4.4 equiv. of K₂CO₃ and then adding 0.9 equiv. of KOH at 70°C and monitoring the reaction by TLC every 5 min for the observation of fully deprotected **66**, and after about 20 min, on the first appearance of **66** the reaction was worked up yielding **65** in 66-69% yield after column chromatography on silica gel.



Scheme 19. Statistical and complete deprotection depending upon the conditions applied.

Using only KOH, **66** was obtained in 84% yield after 2 h (scheme 19).^[202]

Statistical deprotection of the TIPS PG can be achieved in a similar manner. Slow addition of TBAF as an F⁻ source followed by close monitoring by TLC can afford the mono-deprotected product in good yield. This method is exemplified by Sigurd Höger and co-workers^[189] in their seminal work on CPDIPS where the polar TIPS analogue is proven to be efficiently deprotected with TBAF in the presence of 5 vol.-% water as shown in the reaction of **67** to **68** in a yield of 55% after stirring for six hours (scheme 20). Owing to the polarity endowed by the CN group a large difference in R_f allows facile separation on silica.



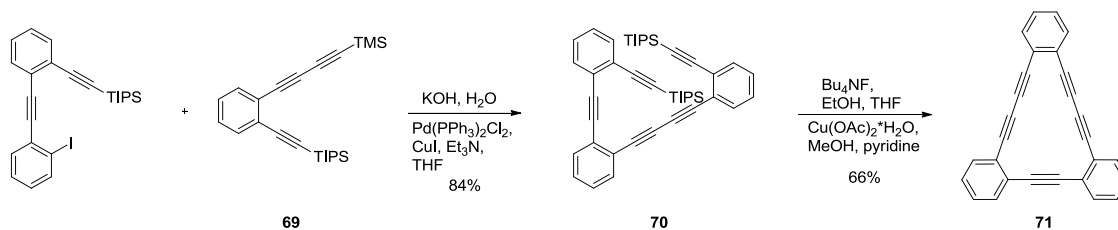
Scheme 20. Statistical deprotection of CPDIPS-acetylene.

This approach is not limited to the TIPS or CPDIPS group. Under acidic conditions of 1.5 equiv. acetic acid in wet THF, a thiophenyl substituted benzene with two TBDMS protected acetylenes was mono-deprotected using TBAF to afford the monosilylated product in a yield of 48%.^[138]

1.4.7 In Situ Generation of Free Acetylene

After talking about the order of reactivity of arylhalides towards oxidative addition to palladium(0) complexes we should also mention the oxidative addition of acetylenes to palladium(0) complexes. If the oxidative addition of the acetylene is much faster than the oxidative addition of the arylhalide then formation of the homo-coupled product can be favoured. This process can also be promoted in the presence of trace quantities of oxygen, facilitating a *Hay*-type coupling. The exact origin of 1,4-butadiene side-products is often ambiguous, as the precise oxygen content is usually not investigated. To prevent the formation of the homo-coupled product one could accelerate the oxidative addition step of the arylhalide. It often helps to change the ligands of the palladium(0) complex.^[147] Bulkier and more electron-donating ligands usually accelerate the oxidative addition of the arylhalide which leads to the intended cross-coupled product. An alternative would be to slow down the oxidative addition of the acetylene by reducing the amount of free acetylene in the reaction. To do so, one could slowly add the free acetylene to the reaction mixture or one could slowly generate the free acetylene in the reaction. The second approach is called in situ generation or in situ deprotection.

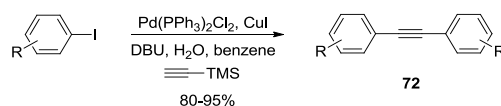
A useful method is the deprotection of TMS-acetylene with small amounts of hydroxide ions. Haley et al.^[204] used this method for the synthesis of benzannelated dehydroannulene **71** (Scheme 21). By reducing the amount of free acetylene coming from **69** in the first step they favoured the cross-coupled product over the homo-coupled product. The small amount of hydroxide ions slowly deprotected the TMS-acetylene but not the TIPS-acetylene. Once the TMS acetylene was deprotected it reacted with the excess aryl iodide.



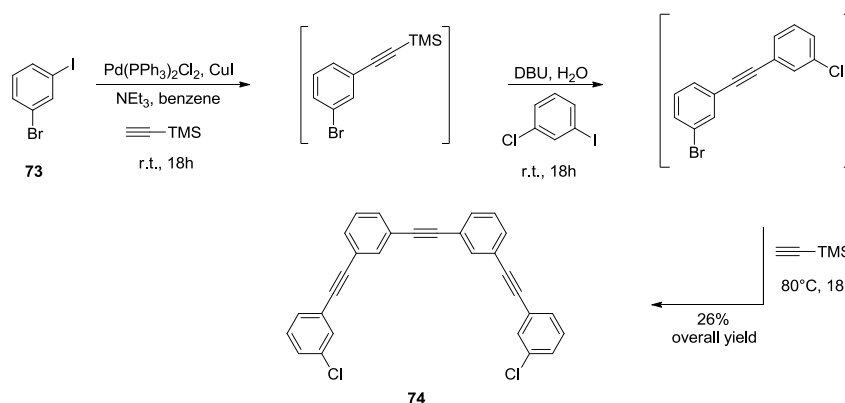
Scheme 21. Demonstration of in situ deprotection coupling reactions.

Applying the same strategy for the second step an intramolecular ring closing reaction was favoured over the intermolecular polymerization reaction. In this case, a large excess of TBAF was used to deprotect the TIPS-acetylene **70** and a highly diluted reaction mixture helped to favour the intramolecular homo-coupling reaction to form **71**.

Another example using in situ deprotection was reported by Mio et al.^[205] They demonstrated a divergent approach to generate symmetric and asymmetric tolanses **72** in a one-pot reaction (scheme 22). In addition, a convergent strategy was applied to synthesize triarylethynylene and tetraarylethynylene **74** from **73** (scheme 23).



Scheme 22. Formation of symmetric tolanses using an in situ deprotection.



Scheme 23. Four sequential *Sonogashira* reactions in one pot controlled by in situ deprotection.

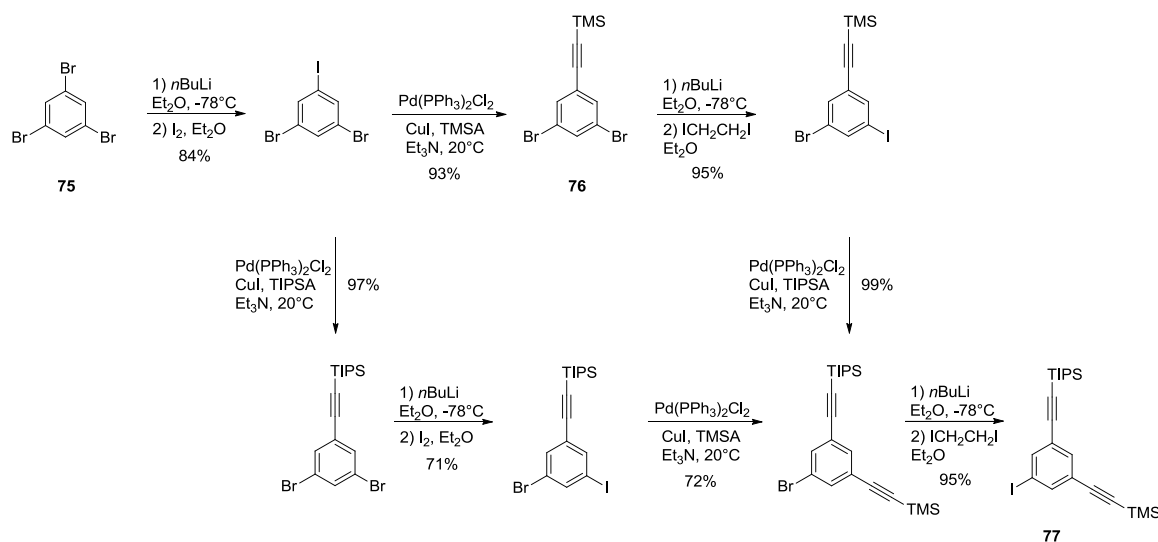
These examples show nice methodologies for in situ deprotection of TMS acetylenes and TIPS acetylenes. If very high reaction temperatures and reaction times are necessary, control

over the in situ removal of TMS is not very effective. Chow et al.^[206] reported in 2001 on another modified *Sonogashira* cross-coupling reaction. HOP was used as the protection group and it was in situ deprotected using sodium hydroxide in a water/toluene mixture.

1.4.8 Concepts Applied to Representative Syntheses

Below is a collection of examples which brings together all of the strategic tools we have described in this review. By using the right combination of retrosynthesis, catalyst, masking and protecting groups it should be possible to elicit any plausible phenyl-acetylene structure.

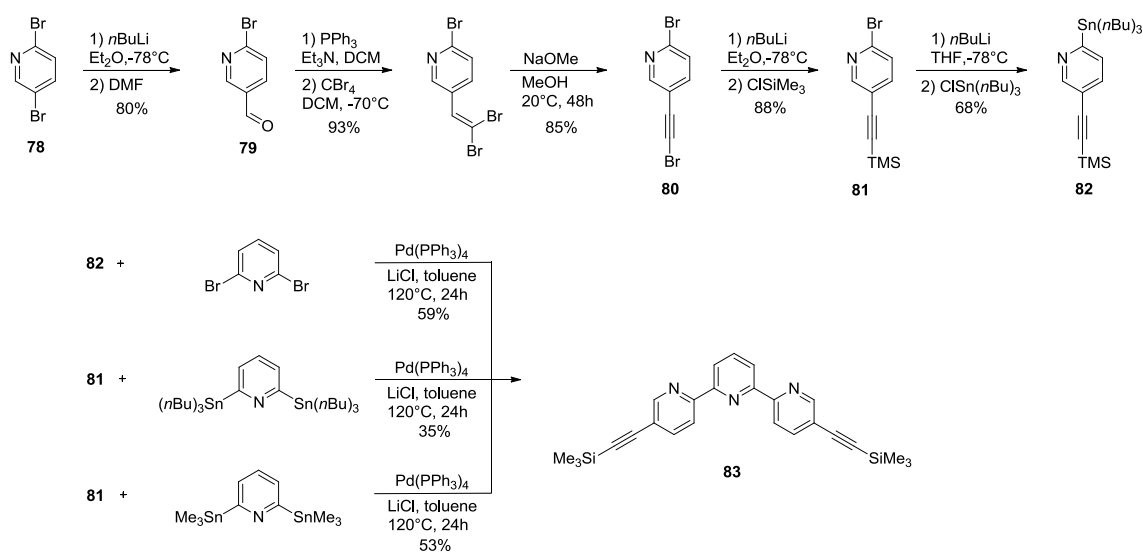
Paul Baxter^[207] in his synthesis of a hexagonal macrocycle used a selective halogen exchange followed by a chemoselective cross-coupling of an acetylene (see section 2). Initially statistical introduction of TMS-acetylene from **75** to **76** yielded a mixture of mono, di and tri substituted aryls which could not be easily separated. But the stepwise introduction of an iodine gave control over assembly of the asymmetric building block **77** in high yields (scheme 24).



Scheme 24. Use of chemoselective control in the formation of phenyl-acetylene building blocks.

Paul Baxter^[207] also illustrates an example of a selective assembly using the tools of chemoselectivity (see section 1.4.2) and masking (see section 1.4.3) (scheme 25). Initially a bromine in **78** was replaced with an aldehyde using *n*butyl-lithium and DMF to form **79**. Aldehyde **79** was transformed into acetylene derivative **80** via a *Croey-Fuchs* reaction^[174] and

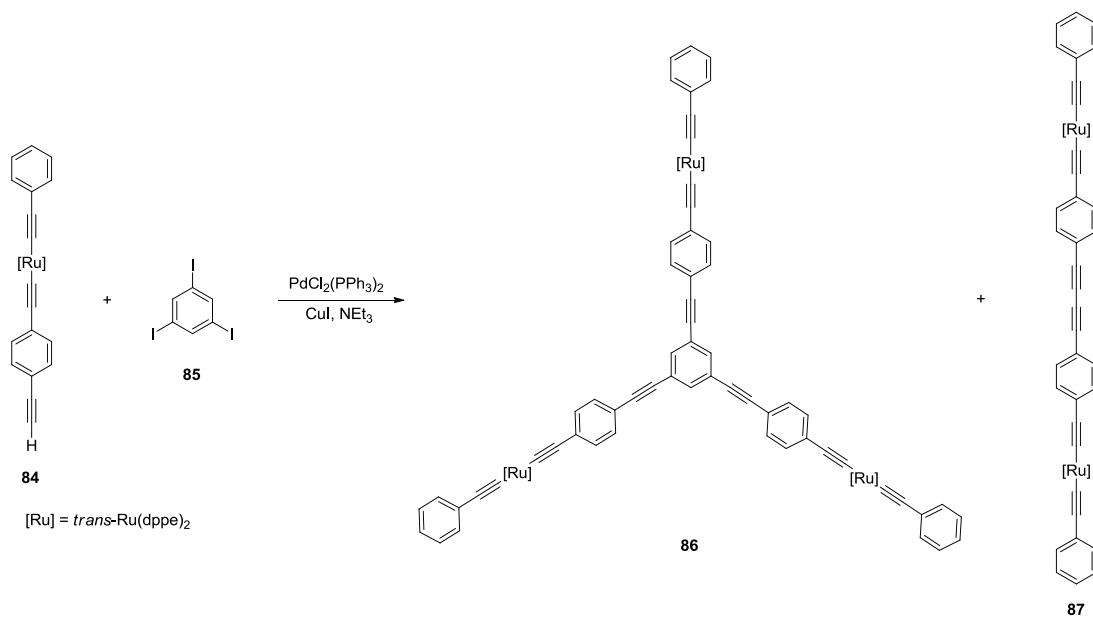
then protected with TMS to afford **81**. Using this strategic approach they could selectively introduce the acetylene and the tin functional group in **82**. The yields of the *Stille* coupling to form **83** were further improved by changing the disconnection for the last cross-coupling reaction by exchanging the acceptor and donor moieties (see section 1.4.1). This reaction sequence demonstrates that the tools discussed in this review are not restricted to *Sonogashira* couplings, but can be applied more generally to other reaction types in the assembly of larger structures from their constituent parts.



Scheme 25. Functional group interconversions and change of disconnection to form a terpyridine.

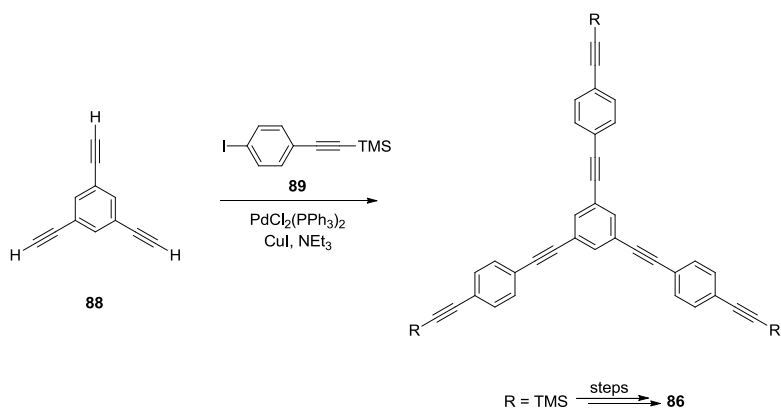
The synthesis of star shaped or branched molecules present their own particular challenge. It is usually possible to form the desired product as part of a reaction mixture but purification of the target can be very troublesome. As a consequence this can mean that a synthetic route becomes unviable. The synthesis of such compounds are usually described as following the principles of convergence, where an OPE is coupled to the central motif forming the star in the final step, or divergence, where the star is built up by iterative couplings using protection/deprotection procedures (see section 1).

McDonagh et al.^[208] attempted a convergent route towards organic/inorganic hybrid star **86** (scheme 26) starting from OPE **84** coupling with triiodobenzene (**85**) but were unable to separate it from the diacetylene linear rod **87**, even after rigorous de-oxygenation of the reaction mixture in an attempt to hinder its formation.



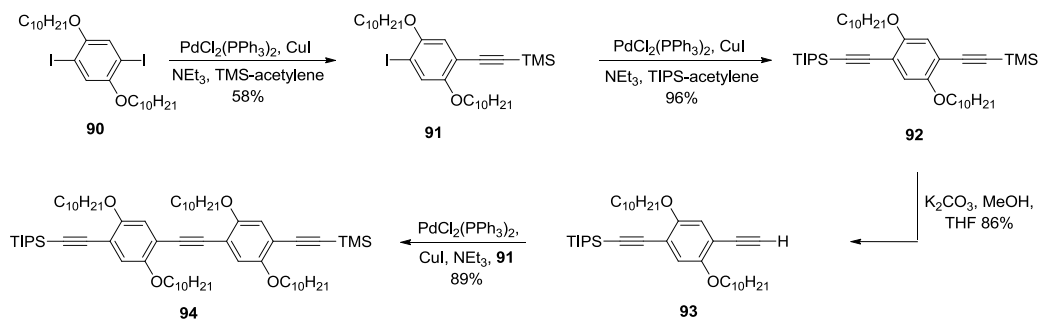
Scheme 26. Difficulty of a convergent approach to star synthesis due to the formation of 1,4-butadiynes.

Instead they decided to use a divergent synthetic route building up the star from triethynylbenzene (**88**) and sequential coupling of **89** (scheme 27). After insertion of Ruthenium and a final divergent coupling they were able to obtain **86** avoiding any inseparable reaction mixtures.



Scheme 27. Divergent approach to star synthesis.

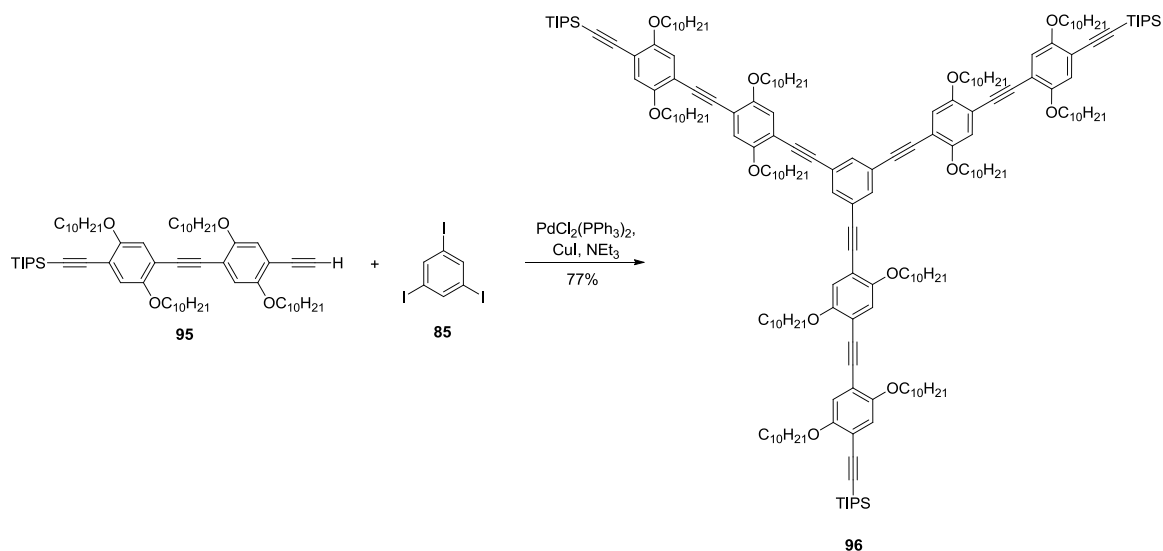
However the presence of substituents at the 2- and 5-positions appears to allow for a successful convergent approach as shown in the coupling of **95** to **85** as the side chains appear to shift the balance in the formation of diacetylene side products. James Tour and co-workers^[209] comment specifically on this effect, further expanded upon in their work towards the synthesis of C₆₀ terminated star OPEs^[210] (scheme 28).



Scheme 28. Asymmetric OPE synthesis using orthogonal protecting groups.

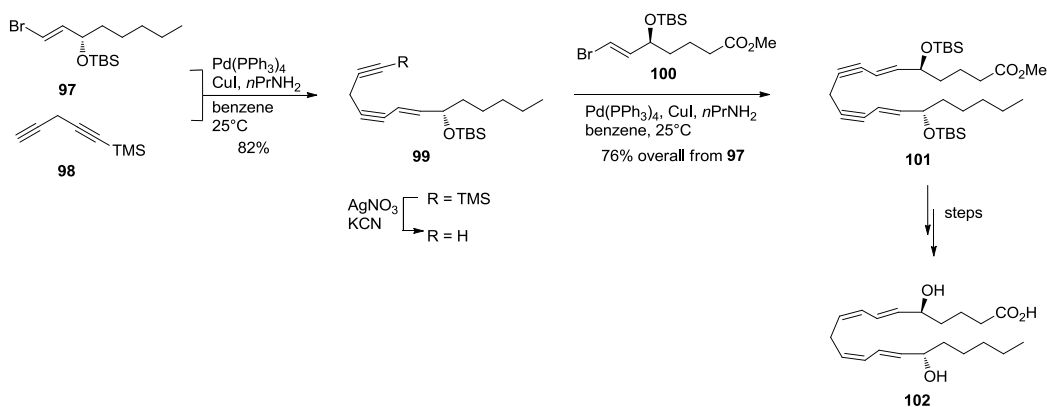
They formed the asymmetric OPE **94** via a statistical coupling procedure (see section 5) in order to introduce two sequentially labile PGs (see section 4). Statistical coupling of TMS acetylene to **90** broke the inversion centre present in this molecule. This was followed by subsequent coupling with TIPS-acetylene, to afford the asymmetric building block **92** containing the sequentially labile PGs TMS and TIPS. Selective removal of TMS using standard conditions afforded **93** which could be extended with a further cross-coupling with **91**. After removal of TMS they were able to couple OPE **95** to tri-iodobenzene **85** constituting a successful convergent synthesis of star **96** (scheme 29). The authors describe an easier

purification of this product from its reaction mixture than expected as there was less diacetylene homocoupled product than they had observed in other OPE syntheses. They attribute this to the steric hinderance of the $-\text{OC}_{10}\text{H}_{21}$ chains on the aryl monomers.^[210]



Scheme 29. Convergent approach to the synthesis of a branched OPE.

The strategies described in this micro-review are also applicable to natural product synthesis.^[107] (*5S,15S*)-dihydroxy-6,13-*trans*-8,11-*cis*-eicosatetraenoic acid (**102**) was synthesized starting from a *Sonogashira* coupling of **97** with mono-protected bis-acetylene **98** as a masked *Z*-alkene (see section 3).^[211] This structural geometry would be very difficult to form via other methods. Deprotection of the TMS protecting group on **99** followed by a second *Sonogashira* coupling with **100** allows for the formation of the asymmetric compound **101**. After further functional group interconversions the final target **102** was obtained (scheme 30).



Scheme 30. Part of a natural product synthesis where *Sonogashira* cross-coupling reactions were applied.

We have chosen this particular example to show that the *Sonogashira* reactions are not limited to arylhalides as the $\alpha 1$ moiety. Vinylhalides such as **97** or heteroaromatic halides can also be successfully coupled with acetylenes.^[103]

Summary

In this chapter, synthetic tools including retrosynthetic analysis, chemoselectivity, masking, choice of protecting group and statistical approaches towards the formation of phenyl-acetylene building blocks were discussed. Gaining control of the substitution pattern of smaller building blocks was shown to be a method for guiding the interlinking of phenyl-acetylenes to build larger architectures. Taking into account the relative advantages and disadvantages of each synthetic technique may reduce the time spent synthesizing molecules so that one may focus on applications, discovering what role structure plays in function. The emerging inter-disciplinary fields including; molecular electronics, photovoltaics, energy storage, and medicinal chemistry among many others strongly depend on the bottom-up assembly of molecular building blocks and therefore on classical organic chemistry.

We hope that using this collection of synthetic tools young researches will find it easier to synthesize even larger macromolecular structures expanding the art of synthesis by design. It is hard to predict what new application may be found for molecular systems, but what is certain is that being able to control the spatial arrangement of functional groups will always be important.

2 Oligo-Phenylene-Ethynylene Structures with Halide End-Groups

2.1 Concept

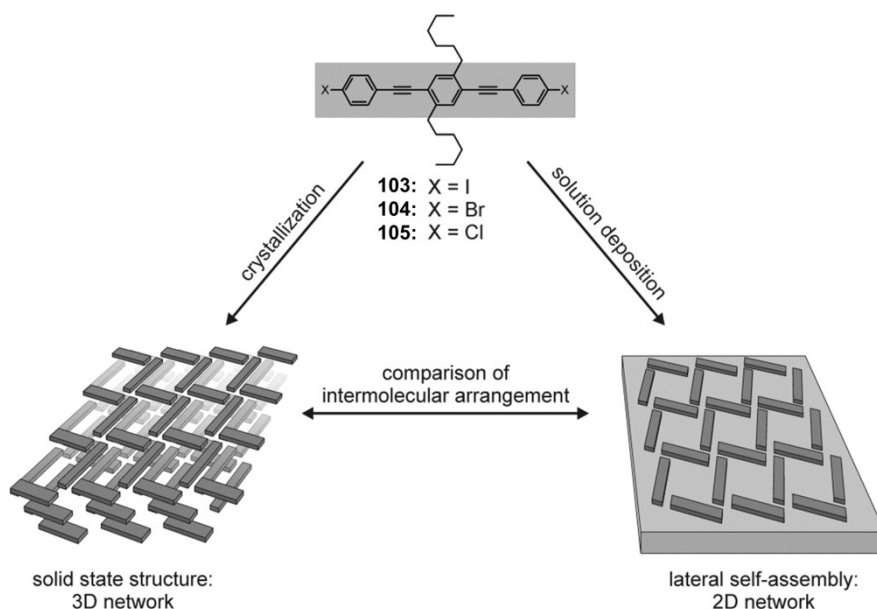


Figure 32. The model compounds were assembled at the solid/liquid interface and crystallized in order to compare the lateral arrangement of the molecules at the surface with planar sheets in the solid state structure.

In the field of material science, the functionalization of metal and graphite surfaces with organic molecules is of increasing interest. Being able to control the electrochemical and physical properties of surfaces such as conductivity, resistance and hydrophilic/hydrophobic properties has made many new applications possible.^[212,213] To alter the properties of an entire surface homogeneously the molecules must be arranged in a periodic manner. The easiest way to achieve this is by solution deposition with molecules able to control their orientations with respect to their neighbors. This so called self-assembly process depends on intermolecular interactions including hydrogen bonding,^[214] hydrogen-halogen or halogen-halogen interactions,^[215] Van-der-Waals interactions^[216] and dipole-dipole (molecule/substrate) interactions.^[217] The self-assembly of organic molecules at the solid/liquid interface leads to large organized molecular patterns on surfaces. These laterally controlled supramolecular architectures can provide surface properties which can be used in new strategies for bottom-

up approaches to assemble macromolecular structures.^[13] Of particular interest are self-assembled systems yielding porous networks, providing a well-defined two-dimensional pattern as templates for functional guests.^[218-223] Mu et al. reported on the self-assembly of fluorinated rods^[224] and branched fluorinated stars^[225] where the fluorine/hydrogen- as well as molecule/substrate-interactions dictated the assembly of a lateral network. Inspired by these large area self-assembled patterns we became interested in the organizing power of halide/hydrogen interactions. To explore the influence of various halides for lateral self-assembly on a flat substrate and for three dimensional arrangement in single crystals, we designed the molecular rods **103-105** (figure 32). These rods consist of flat and rigid oligo-phenylene-ethynylene (OPE) backbones favoring their molecule/substrate interactions.^[224,226] Terminal halides (-Cl, -Br, -I) are expected to direct the lateral assembly by a wide variety of intermolecular interactions^[215,227,228] such as C-X \cdots H, C-X \cdots X-C and C-X \cdots π -orbital. The differences in electrostatic potentials and sizes of the halides are expected to vary the strength of the intermolecular interactions and might thus be reflected in the resulting self-assembled structures. As halides have both, positive and negative electrostatic potentials, they can be attracted by both negative halides (or π -orbitals) or electro positive hydrogens.^[215,227,229] Two hexyl substituents at the central phenyl units of the OPE rods are required to provide processability of the molecular building blocks. These alkyl substituents are expected to reduce the molecular density of the rod on the substrate but should be small enough to still allow a tight packing directed by the terminal halogens. The spontaneous formation of laterally ordered flat sheets of densely packed molecules is of particular interest as a potential motif for a tightly packed 3D molecular assembly. The stacking of such sheets might result in a crystal like 3D order providing a perfect interface between a flat substrate material and the molecules crystalline state.

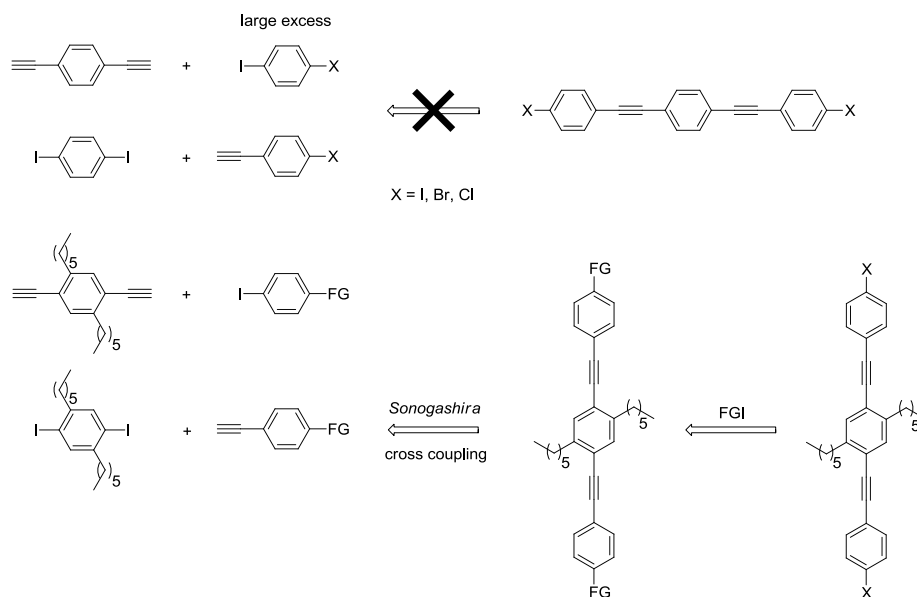
In the field of crystal engineering various intermolecular interactions have been studied extensively.^[230] In particular strong and directional hydrogen bonds (e.g. O-H \cdots O or N-H \cdots O) were investigated in detail.^[231] Particularly interesting are halogen bonds because of the twofold role of the halogen atom. On one hand the halide substituent can interact with a lone-pair provided by a heteroatom in proximity and thus act as the hydrogen does in a H-bond.^[232] On the other hand the halide can also provide lone-pairs for electron deficient atoms of neighboring molecules. Thus various interactions (e.g. C-X \cdots X-C and C-X \cdots Y-C) can be observed with halogen substituents.^[233-235] This diversity of possible interactions increases the complexity in controlling the crystal growth by the molecules design. In a crystal engineering approach the strength of intermolecular interactions is tuned by controlling the spatial

arrangement of various substituents by the molecules backbone structure.^[236,237] A major design challenge in engineering crystals comprising exclusively organic molecules, is that molecules with functional groups pointing in all three dimensions are required.^[238] Variation of modular functionalities along one axis and maintaining equally weak intermolecular interactions in all three directions in the crystal at the same time is a very difficult task. Alternative organic building blocks are aromatic structures.^[239,240] Two-dimensional structural control is easily achieved in the planes of the aromatic rings, while the packing of the obtained sheets in the third dimension is less controlled. The aromatic rings impart some interactions of their own ($\pi\cdots\pi$, C-H \cdots O) which may contribute to ordered staples. However, such crystals differ considerably in the strength of the interactions between the molecules within and between the sheets. The combination of the diversities of halogen based interactions and of the intermolecular forces along different crystal axis makes crystal engineering with such structures particular interesting and challenging.

Following these considerations we systematically investigated halide based interactions by comparing the self-assembly of terminally halogen substituted OPE-rods **103-105** at the solid/liquid interface (2D) and in a single crystal (3D). A particular focus is set on the extent of similarity of the patterns obtained by intermolecular interactions.

2.2 Synthetic Strategy

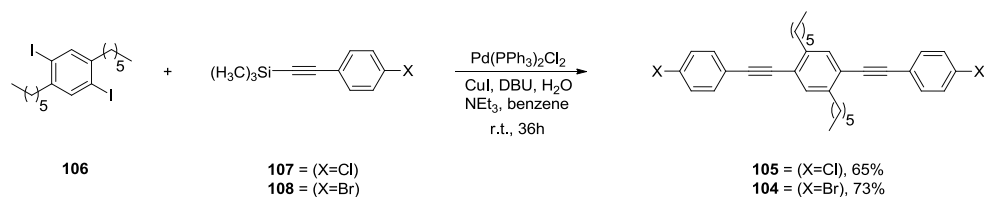
The OPE target structures consist of a π -conjugated backbone and either chlorine, bromine or iodine end groups. The target structures were synthesized by either a convergent or divergent approach.^[95] Any attempts to build up these structures directly failed (scheme 31) due to polymerization, homo-coupling and poor solubility of the target structures. In case of the diiodo-OPE XY a masking strategy was proposed. To overcome the problem of side reactions an inert functional group can be introduced and converted into the desired functional group at a later stage. Hexyl-chains were introduced to the central unit of the OPE structure to increase both, solubility and processability of the target structures.



Scheme 31. A direct approach to terminally halogen functionalized OPE-rods is not possible due to selectivity problems. To avoid such problems a FGI was proposed.

2.3 Synthesis

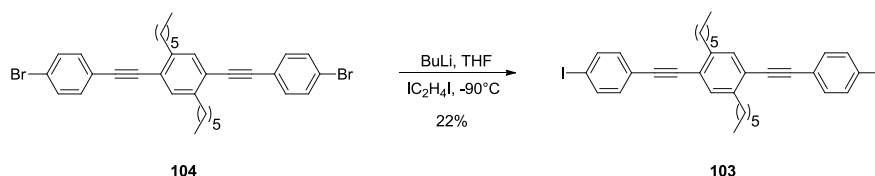
The assembly of the dichloro-OPE **105** and of the dibromo-OPE **104** is displayed in scheme 32. Both rods were assembled using a pseudo high-dilution strategy profiting from the considerably increased reactivity of aryl-iodides compared with other aryl-halides in Sonogashira coupling chemistry.^[241] First 1,4-diiodo-2,5-dihexylbenzene (**106**) was synthesized following literature precedent.^[242] Having building block **106** and the commercially available compounds (4-chlorophenylethynyl)trimethylsilane (**107**) and (4-bromophenylethynyl)trimethylsilane (**108**) in hand, the final assembly of target structures **105** and **104** were achieved by Sonogashira cross coupling reactions (scheme 32). An in situ deprotection method^[241] was chosen to minimize the amount of free acetylene in the reaction to prevent homo-coupling. Therefore, DBU as a non nucleophilic base and small traces of water were used to slowly deprotect the TMS-acetylenes **107** and **108**. The low concentration of free acetylene favored its reaction with the Pd-activated aryl-iodide and provided the desired rods **105** and **104** in reasonable yields. The dichloro-OPE **105** and the dibromo-OPE **104** were isolated in 65% and 73% yield respectively.



Scheme 32. Synthesis of dichloro-OPE **105** and dibromo-OPE **104**.

For the assembly of the diiodo-OPE derivative **103** various different synthetic strategies have been explored. The synthetic strategy described for **105** and **104** was based on the increased reactivity of iodine as a leaving group in Sonogashira cross coupling reactions^[243,244] and its application for the assembly of **103** gave polymeric products instead of the desired rod. The same problem occurred when the disconnection was changed and the acetylenes were on the central core as in **113** (scheme 35). Even if a large excess of 1,4-diiodobenzene was used the formation of polymeric products was still observed. Thus, we had to change the strategy to a functional group interconversion (FGI).

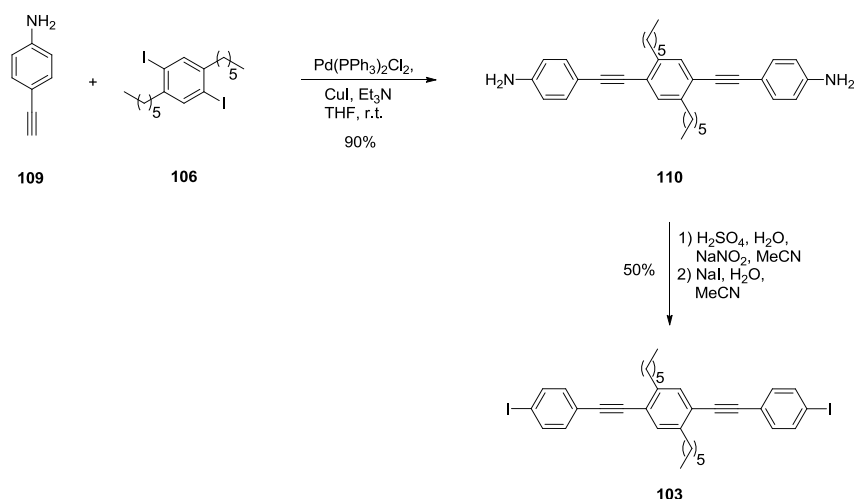
Having the dibromo-OPE **104** already in hand, a halide exchange reaction was the first synthetic choice (scheme 33).^[245,246] Treatment of **104** with butyl-lithium and 1,2-diiodoethane lead to a mixture of products. The isolation of the desired diiodo-OPE **103** turned out to be challenging due to very comparable polarities of the dibromo-OPE **104** and the iodo-bromo-OPE. However, the target structure **103** was isolated in a low yield of 22% as an off-white solid by column chromatography.



Scheme 33. Halide exchange reaction to introduce the iodine end group.

Alternatively masking strategies were considered in order to improve the yield and purity of the target structure. An ideal masking group would be readily available, stable to a variety of chemical conversions, and conveniently transformed under mild conditions and in a high yield to form the desired aryl-iodide.^[95]

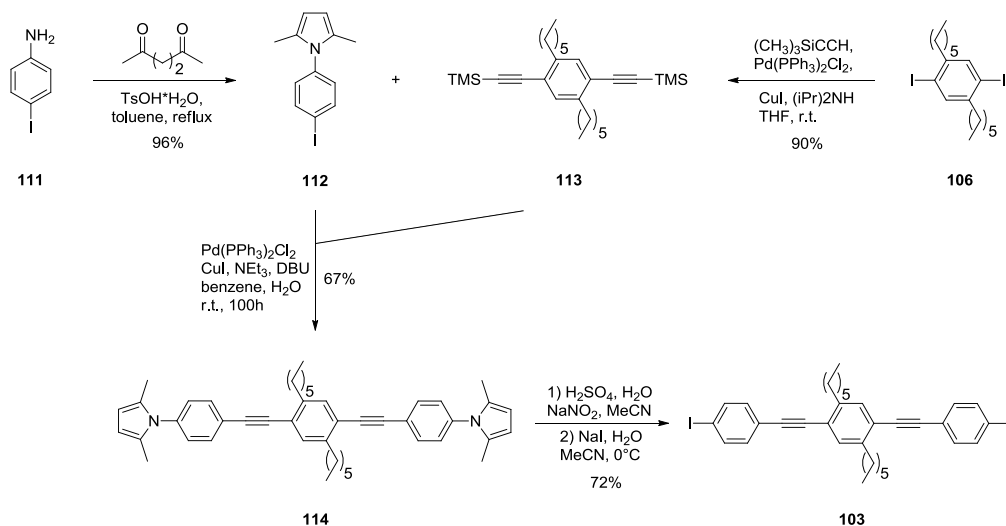
An amine is suitable for such a functional group interconversion (FGI), therefore a diamino-OPE **110** was synthesized to subsequently convert it into the diiodo-OPE **103** (scheme 34).^[67] The idea was to profit from the polarity differences between the starting material **110** and product **103**. This FGI was first reported by Sandmeyer^[247] and was improved over the course of the last century.^[67,248] The diamino-OPE **110** was synthesized with a Sonogashira coupling reaction in a yield of 90% using building blocks **109** and **106**.^[249,250] OPE **110** was then converted into a diazonium salt using sulfuric acid and sodium nitrite in acetonitrile at 0°C. After 24h the reaction was quenched with sodium iodide to afford the diiodo-OPE **103** in an improved yield of 50%.^[248] However, during the reaction, considerable amounts of partially dehalogenated OPEs were formed which again made the isolation of **103** challenging.



Scheme 34. Synthesis of compound **103** via Sandmeyer type reaction.

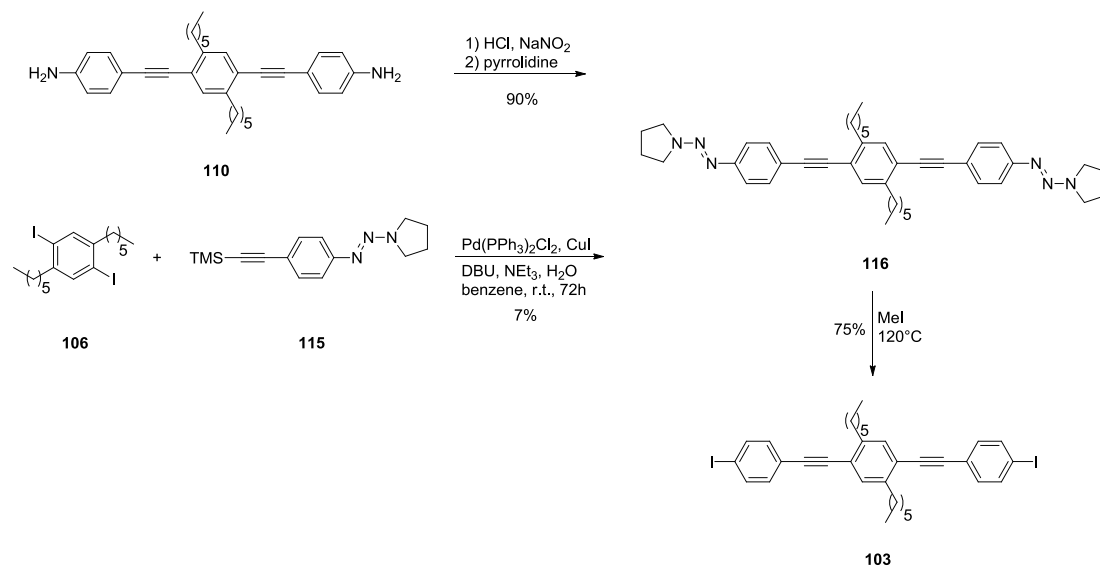
Dimethylpyrroles were suggested as base-stable masking groups which can be transformed to iodines under Sandmeyer-type conditions (scheme 35).^[251,248] The required building block **112** for the OPE synthesis was obtained according to literature precedent starting from 4-iodoaniline (**111**).^[252] The second diacetylene building block **113** was obtained in 90% yield with standard cross-coupling conditions.^[253] To assemble the masked OPE **114** a divergent approach gave an overall yield of 58%. The final Sandmeyer-type reaction using a water/acetonitrile mixture as a solvent gave the desired diiodo-OPE **103** in a yield of 72%. A simple filtration over a short silica plug, using a hexane:*tert*-butylmethylether mixture (40:1) as solvent was performed to isolate the pure product **103** in an overall yield of 41% as a white crystalline solid. Interestingly, side products with comparable polarities were not observed. The increased solubility of the dimethylpyrrole-OPE **114** in the water/acetonitrile mixture

may have improved the formation of the diazonium-salt during the Sandmeyer reaction. As in the case of the diamino-OPE **110** (scheme 34) the slow formation of the diazonium salt in the heterogenous dispersion is assumed to be responsible for the large quantity of side products.



Scheme 35. Synthesis of compound **103** using dimethylpyrroles as masking groups.

Finally, alkylated triazenes were explored as masking groups for iodines (scheme 36).^[254,255] They can be directly substituted with iodine using methyl iodide in a sealed tube at 120°C. Alkylated triazenes are stable towards strong bases and high temperatures. Pyrrolidine-triazenes are known for favorable crystallization properties and we hoped for improved isolation features of these intermediates. The required triazene building block **115** was synthesized following a procedure reported by Godt.^[256] The ditriazene-OPE **116** was synthesized with a cross-coupling reaction in very poor yields of 7%. Even changing the disconnection and putting the acetylenes on the central unit did not improve the yield. Instead the diamino-OPE **110** was transformed into the ditriazene-OPE **116**, which was isolated by crystallization in a yield of 80%. OPE **116** was subsequently transformed into the diiodo-OPE **103** in a yield of 75%. A simple filtration over silica using cyclohexane as solvent afforded the pure product. The overall yield for the triazene strategy was with 54% slightly increased over the pyrrole strategy (41%). However, the considerably increased temperature required during the triazine strategy might be a drawback when additional functional groups are present.



Scheme 36. Synthesis of compound **103** using a triazene-masking strategy.

2.4 Solid-state Investigations

The crystals for x-ray analysis were either grown by slow cooling of a saturated cyclohexane solution to 4°C or by slow evaporation of cyclohexane at room temperature. All three compounds crystallize in the centro-symmetric space group P-1. While the unit cell of OPE **105** and OPE **104** contains one molecule each, the unit cell of OPE **103** contains two molecules and a cyclohexane molecule. In all three structures, the molecules are located on an inversion center of the space group P-1. Thus, in the case of OPE **105** and OPE **104** the molecules are arranged parallel to each other. In the case of OPE **103** the two molecules and the solvent molecule are located on different inversion centers of the space group P-1 permitting formation of a fishbone like arrangement with the direction iodine \cdots iodine of the two different orientations forming an angle of about 90°.

All the STM measurements were conducted using a Nanoscope IIIa Scanning tunneling microscope (STM), and the STM tip was prepared by mechanically cutting Pt/Ir wire (90:10). The molecules were dissolved in 1-phenyloctane (purchased from Sigma with the purity of 98.0%) to make saturated solutions. The solution was subsequently dropped on a freshly cleaved highly oriented pyrolytic graphite (HOPG) surface. The HOPG/1-phenyloctane interface was investigated by STM. All STM images were performed in constant current mode.

2.4.1 Dichloro-OPE and dibromo-OPE:

The crystal structures of both OPEs **105** and **104** show a parallel arrangement of the rods (figure 33A and 34A) forming several layers which are slightly shifted by 5.2 Å and 5.7 Å respectively. By looking at a planar cut through the crystal structures similar chlorine···chlorine (figure 33B, 5.0 Å and 4.8 Å) and bromine···bromine (figure 34B, 4.8 Å and 5.1 Å) distances could be observed. Chlorine···hydrogen as well as bromine···hydrogen interactions could be observed where the terminal halogen interacted with two hydrogens coming from two different rods. The area of the unit cell (in a plane) comprising a single OPE molecule is about 1.84 nm² for the dichloro-OPE **105** and about 1.93 nm² for the dibromo-OPE **104** (see chapter 7).

Figures 33C and 34C show the STM images of a monolayer of OPE **105** and OPE **104** on a HOPG surface. A lamellar structure where the rods lie parallel to each other was observed in each case. The unit cell for the dichloro-OPE **105** was determined with $a=2.0\pm 0.1$ nm, $b=1.0\pm 0.1$ nm and $\alpha=76\pm 2^\circ$ whereas the unit cell for the dibromo-OPE **104** was determined with $a=2.0\pm 0.1$ nm, $b=1.0\pm 0.1$ nm and $\alpha=75\pm 4^\circ$. The unit cells which contain one molecule have a surface area of about 1.94 nm² (OPE **105**) and 1.93 nm² (OPE **104**) (see additional information in the experimental part).

By comparing the individual molecular arrangements of a planar cut through the crystal structure (figure 33B and 34B) with the molecular arrangements at the solid liquid interface (figures 33C and 34C) an exact match of the parallel crystal arrangement was observed. The same zig-zag arrangement of the chlorines and the bromines was found. Halogen···hydrogen interactions as well as alkyl-chain interdigitations could be observed on the surface. Eight halogen···hydrogen interactions per molecule were observed (figure 33B and 34B, indicated in green) in the crystal structure and at the solid liquid interface.

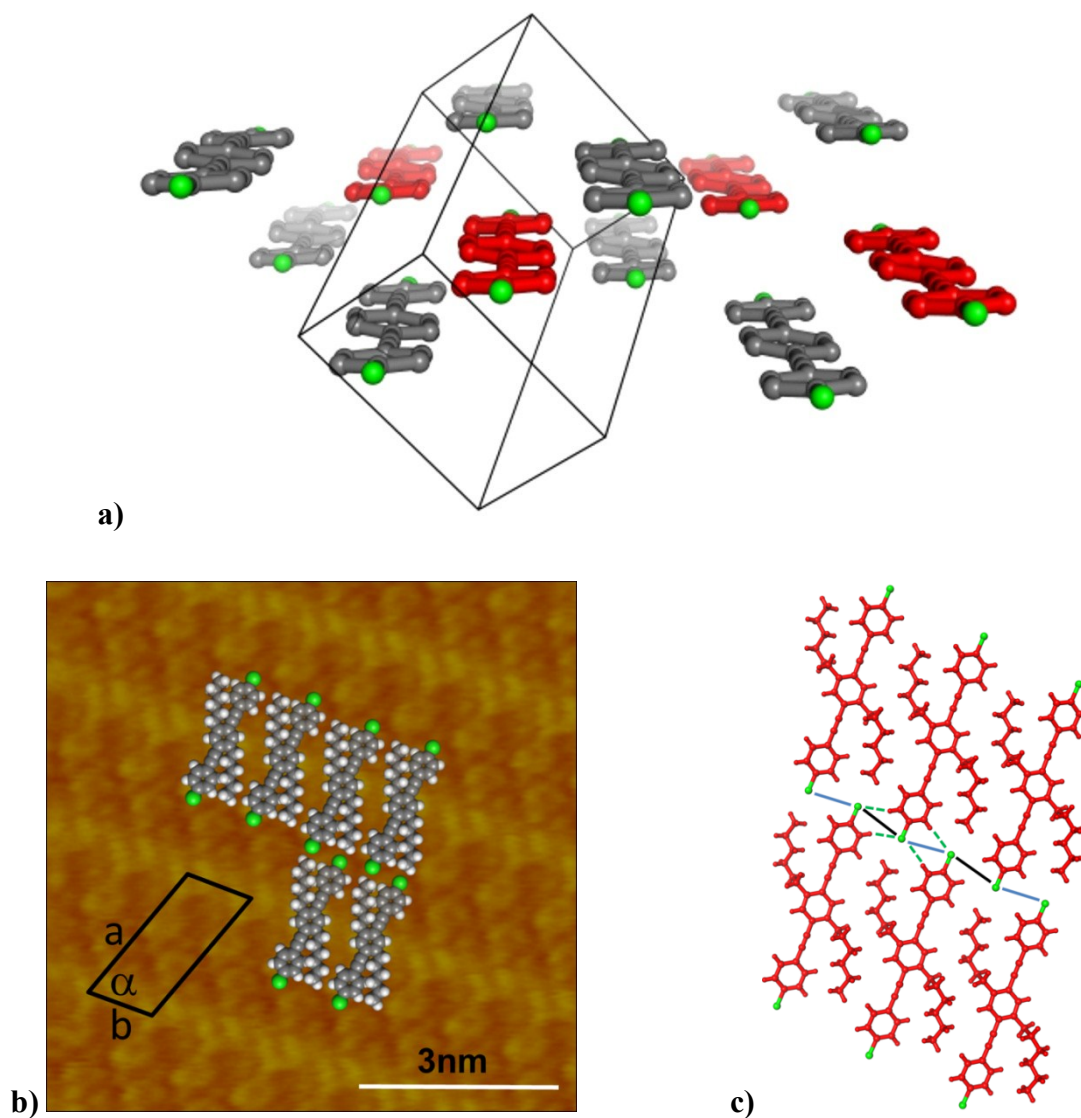


Figure 33. a) The crystal structure (hexyl chains and hydrogens were removed for clarity) of the dichloro-OPE **105** reveals a parallel arrangement of the rods. b) Planar cut through the crystal structure of **105**. The slightly larger distance of 5.0 Å is shown in blue and the slightly shorter distance of 4.8 Å is shown in black. The chlorine...hydrogen interactions (3.4 Å) are shown in green. c) STM image of a dichloro-OPE **105** covered HOPG surface.

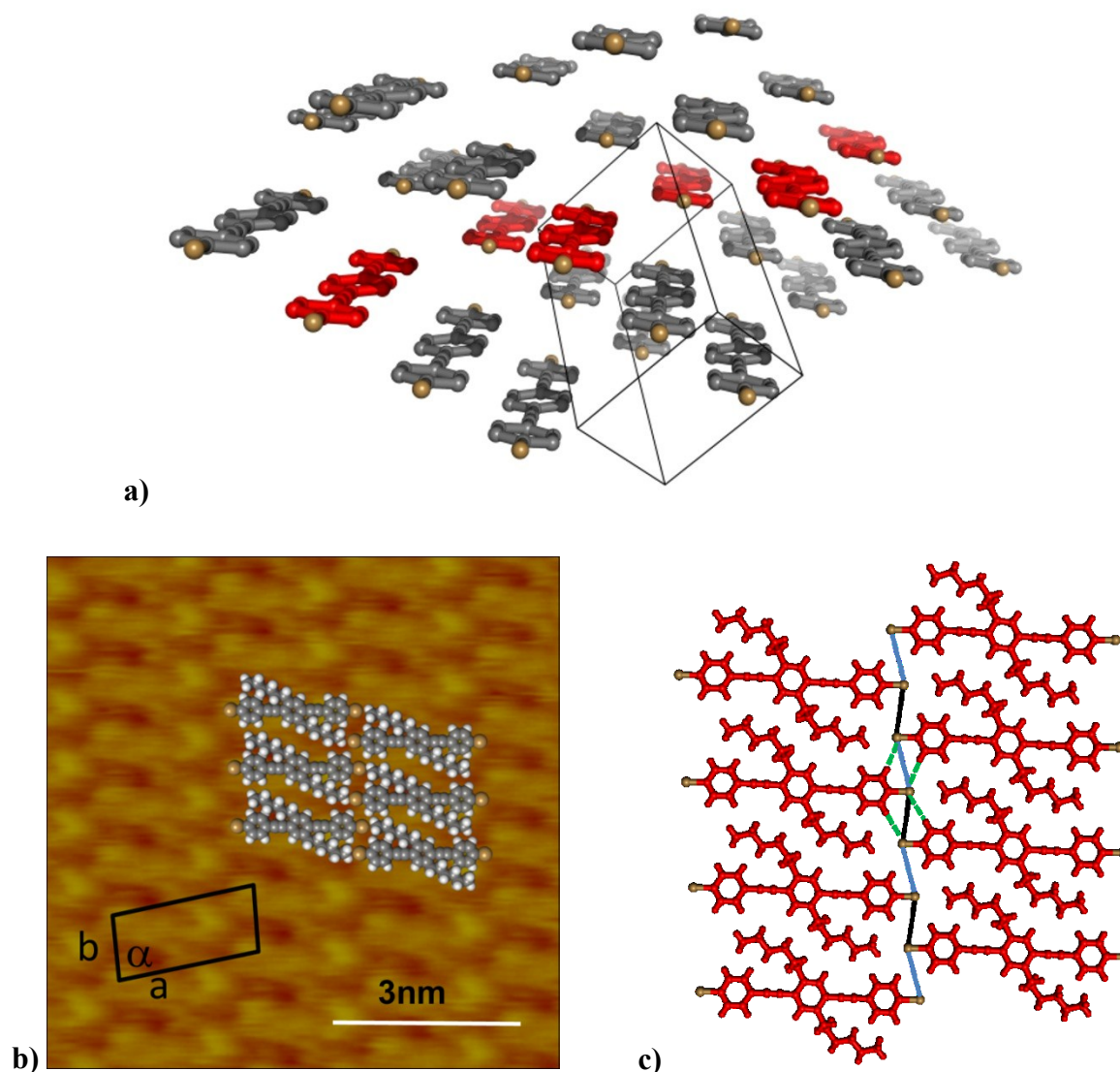


Figure 34. a) The crystal structure (hexyl chains and hydrogens were removed for clarity) of the dibromo-OPE **104** reveals a parallel arrangement of the rods. b) Crystal structure of the dibromo-OPE **104** showing the parallel ordering. The larger distance of 5.1 Å is shown in blue and the shorter distance of 4.8 Å is shown in black. The bromine \cdots hydrogen interactions (3.3 Å) are shown in green. c) STM image of a dibromo-OPE **104** covered HOPG surface.

2.4.2 Diiodo-OPE:

The packing order of the crystal structure reveals several layers of molecules (figure 35A). Looking at the unit cell three planar sheets can be observed having a total height of 7.3 Å. When looking at a planar cut through the crystal (figure 35B) a perpendicular arrangement of the rods can be observed. This arrangement leads to the formation of two cavities. The distance between the iodines within these cavities is 14.2 Å and 8.3 Å respectively. The

angles of the perpendicular rods are between 92.3° and 93.7° . The central benzene units of the rods are placed in the corners of the unit cell and they have a distance of 15.0 \AA and 15.3 \AA to one another. The area of the unit cell (in a plane) comprising two OPE molecules and a cyclohexane is about 4.54 nm^2 (see additional information in the experimental part).

The terminal iodine has a strong positive electrostatic potential along the molecular axis and a negative electrostatic potential off the axis forming a “belt” around the iodine.^[215] Therefore, it can interact with electron donors such as other halogens and π -orbitals as well as electron acceptors including hydrogens.^[227] The perpendicular arrangement of the rods comes from a strong iodine $\cdots\pi$ -orbital interaction where the electro positive potential of the iodine interacts with an electro negative π -orbital of a second rod (figure 4a). The central benzene unit is able to undergo π - π stacking with another OPE-rod which is alternated perpendicular. This crystal structure reveals that the functional groups (-I, -H, $\text{C}\equiv\text{C}$) within the molecule clearly dictate the two dimensional arrangement. The three dimensional arrangement was controlled by the central benzene unit.

Figure 35C shows the STM image of a monolayer of the diiodo-OPE **103** at the solid/liquid interface. The molecules form a highly ordered network with large and small pores. The unit cell was determined with $a=2.1\pm 0.1 \text{ nm}$, $b=2.0\pm 0.1 \text{ nm}$ and $\alpha=90\pm 4^\circ$. The unit cell contains two OPE **103** molecules with a surface area of about 4.2 nm^2 . By looking at the molecular arrangement on the surface it can be observed that the rods lie perpendicular to each other thus forming large and small cavities.

By comparing the molecular arrangement in a planar cut through the crystal (figure 35B) with the arrangement at the solid/liquid interface (figure 35C) an almost perfect match was observed. The area of two molecules in the crystal structure is about 4.5 nm^2 which is comparable to the surface coverage at the solid/liquid interface (4.2 nm^2). The same interactions where one terminal iodine interacts with one π -orbital and two hydrogens could be identified. These observed interactions clearly dictate the two-dimensional assembly in both, the crystal structure and at the solid-liquid interface. Alkylchain interdigitations^[226] play a smaller part. This could be due to the eight iodine \cdots hydrogen and four iodine $\cdots\pi$ -orbital interactions per molecule.

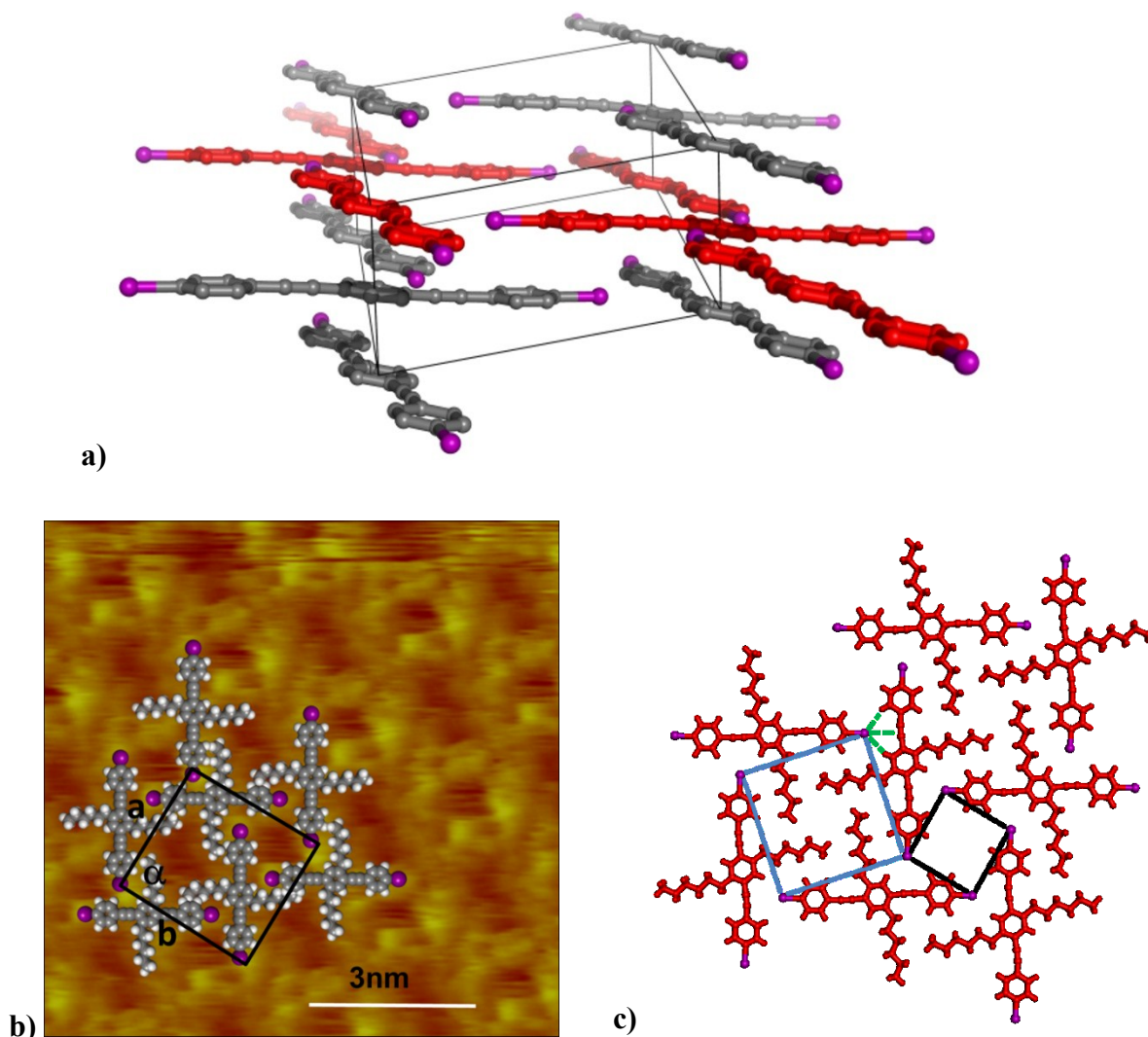


Figure 35. a) The crystal structure (solvent, hexyl chains and hydrogens were removed for clarity) of the diiodo-OPE **103** reveals a perpendicular arrangement of the rods forming large and small cavities. b) Planar cut of the diiodo-OPE crystal showing the squared cavities. The larger iodine-iodine distance of 14.2 Å is shown in blue and the shorter iodine-iodine distance of 8.3 Å is shown in black. The iodine···hydrogen (3.2 Å and 3.3 Å) and the iodine··· π -orbital (4.1 Å) interactions are shown in green. c) STM image of a diiodo-OPE **103** covered HOPG surface.

We have compared a plane through the crystal structures with the assembly at the solid/liquid interface and found a remarkable similarity for each OPE **103-105**. However, when we compare the OPEs to each other we find considerable variations of their arrangement induced by the terminal halide.

Similar arrangements were found for the dichloro-OPE **105** and the dibromo-OPE **104**. The halides show a zig-zag line coming from halide···hydrogen interactions and alkylchain

interdigitations (figure 33 and 34). It seems that these are the only interactions which control the arrangement. We were able to measure that the dichloro-OPE rods **105** are not commensurable with the graphite sheet and therefore we can assume that the assembly was mainly controlled by intermolecular interactions. The dibromo-OPE **104** monolayers and the diiodo-OPE **103** monolayers were not stable enough to determine their commensurability. This also indicates that intermolecular interactions dominate the assembly.

For the diiodo-OPE **103** a quite different arrangement was observed compared to the OPEs **104** and **105**. The halides do not only interact with electro positive hydrogens from neighboring rods but also with an electronegative π -orbital. These interactions lead to a perpendicular arrangement (figure 35). Presumably the larger size of the iodine together with the larger electropositive potential is responsible for this alteration in molecular packing. In particular the latter is assumed to form an interaction with the acetylene π -system resulting in the perpendicular arrangement of the molecular rods.

The comparison of the three molecular packings suggests $X\cdots H$ bonds as the dominating intermolecular interaction which becomes weaker with increasing size and decreasing electronegativity of the halogen atom ($Cl > Br > I$).^[257] In the case of **103** the $I\cdots H$ bonds are weak enough that the $I\cdots\pi$ -system interaction begins to compete.

2.5 Conclusions of the Solid State Investigations

A series of halide end-functionalized OPEs **103-105** were synthesized in order to investigate their packing properties in single crystals as well as on atomically flat graphite substrates. In spite of their structural simplicity and similarity the synthesis of the target structures **103-105** was more challenging than expected. OPE **105** and **104** were synthesized in good yields using an in situ deprotection method to prevent the formation of side products. Various synthetic strategies to OPE **103** were investigated and functional group interconversion (FGI) turned out to be superior in yield and isolation properties of the target structure. Efficient syntheses of OPE **103** with respect to yield, purity and reaction steps were found. While the triazene-masking strategy gave the highest overall yield and a very pure product, the dimethylpyrrole masking group worked considerably better than the free amine FGI and requires lower reaction temperatures.

A comparison of STM images and crystal structures for OPEs **105**, **104** and **103** revealed a structural similarity for each rod. In their crystal structures a planar slice with an arrangement

of the molecules resembling their two dimensional packing on the flat surface was found for each case. These results support the hypothesis of a slice by slice crystal growth and suggest flat surfaces as ideal interfaces to promote crystal growth. Of particular interest was the arrangement of the diiodo-OPE **103**. The STM image as well as the crystal structure revealed a porous network of alternating pore sizes. The assembly can be rationalized by iodine···hydrogen and iodine··· π -orbital interactions. This perpendicular arrangement might pave the way to porous crystals grown on flat substrates.

In summary the large influence of halides on the packing of OPE rods was shown. This is rationalized by their differences in electrostatic potentials. The comprehension of these interactions will enable controlled surface functionalization and opens the door to controlled crystal growth on flat substrates.

2.6 Break Junction Experiments

The investigation of structure-property relationships^[258,259] in complex molecules has been facilitated by break junction techniques, such as mechanically controlled break junctions (MCBJ)^[260,261] and scanning tunneling microscopy (STM),^[37,262] allowing for the rational design of functional molecules. To measure and investigate electron transport through a single molecule one must not only synthesize molecules which mimic traditional electrical components, but also design efficient molecule-electrode contacts, so called anchoring groups. These anchoring groups should bind to the electrodes and provide efficient electronic coupling between the molecule and the electrode.^[263,264] In principle, there are mainly two ways to contact molecules to electrodes. The first one is achieved by a strong covalent binding between the metal electrode and for example thiols^[37,38] or amines.^[39] The second one can be achieved by coordination where for example pyridines^[40] or isocyanides^[45] coordinate to the metal electrode. Those contact events have been extensively studied and reviewed.^[37,19]

Another, yet less explored, possibility to contact a molecule with an electrode can be achieved by Van-der-Waals interactions. So far, there are only a few reported studies which use Van-der-Waals interaction to contact molecules with metal or carbon electrodes. Björnholm and coworkers^[265,266] used C₆₀ as anchor groups where they profited from a strong hybridization between the fullerene and the gold atoms resulting in an excellent charge injection from the electrode onto the fullerene. Polyaromatic hydrocarbons (PAH) were successfully used by Grunder et al. to contact the molecule with carbon nanotubes (CNT).^[267]

These studies showed that Van-der-Waals interactions can be used to form a contact between electrodes and organic molecules. Therefore we envisaged our own model compounds **117** and **103** (figure 37), which are terminally functionalized with halides, to be ideal candidates to form electrode-molecule-electrode contacts. As discussed above, terminal halides have an extended electron cloud and thus provide an ideal surface area to interact via Van-der-Waals forces with gold electrodes. The weaker but still efficient electronic coupling between the electrodes and the molecule could lead to deeper insights into the coupling mechanism since the broadening of the energy levels is reduced.^[19]

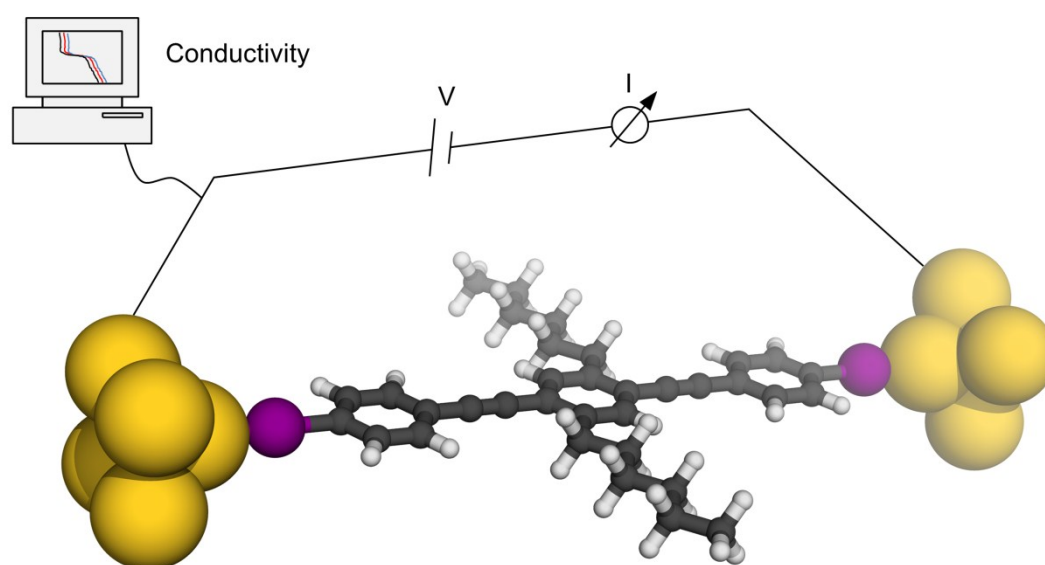


Figure 36. Schematic illustration of a contacted diiodo-OPE between two gold electrodes.

We proposed that halides can act as anchoring groups due to their large size and diffuse electron distribution. The dibromo-OPE **117** without any hexylchains and the diiodo-OPE **103** were investigated by the group of Christian Schönenberger and Michel Calame at the University of Basel (figure 36).

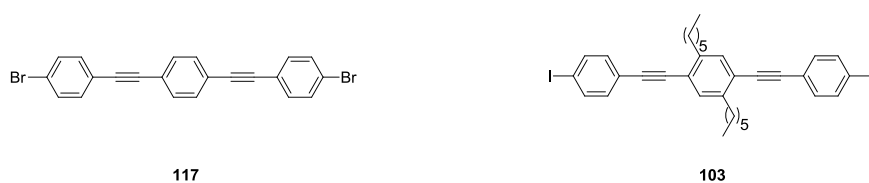


Figure 37. Halide end-capped OPE's investigated by MCBJ-experiments.

The measurements were performed with a bias voltage of 0.1 V and a pushrod speed of 31.2 $\mu\text{m/s}$. The first molecule **117** which was investigated consisted of an OPE backbone and two bromide-end groups. Two different concentrations in different solvents were investigated (1 mM in ethyl benzoate and 0.25 mM in THF/mesitylene). As displayed in the histograms in figure 38 no conductance peak could be observed.

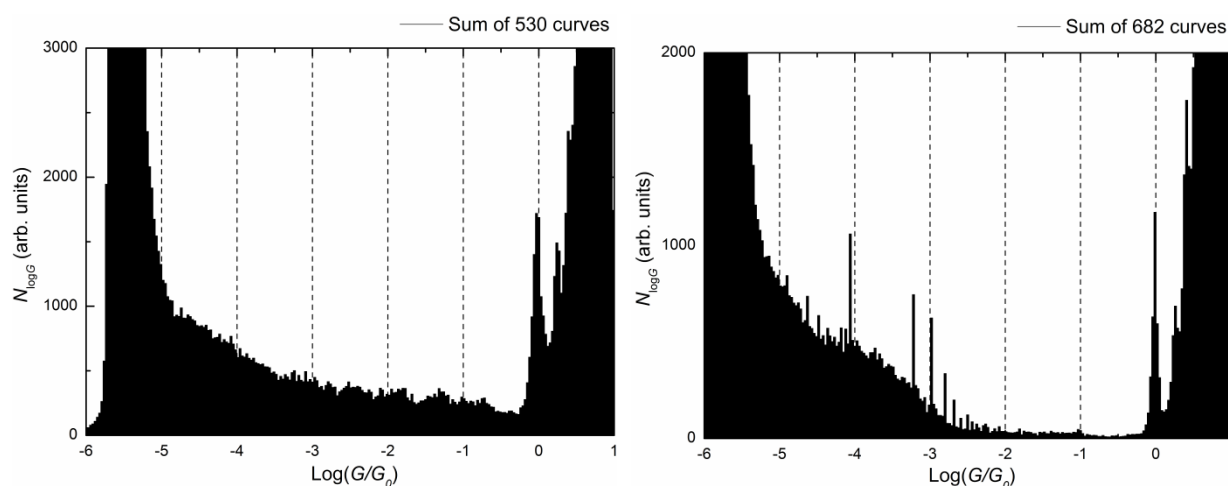


Figure 38. Logarithmic histograms of molecule **117**. The left histogram contains the sum of 530 opening curves and the right histogram contains the sum of 682 opening curves.

This result was attributed to the very low solubility and therefore very low concentration of compound **117** in the investigated solution. In the next experiment the diiodo-OPE **103** bearing two alkyl chains was investigated. The additional alkyl chains increased the solubility enormously in a mixture of THF and mesitylene (1:4).

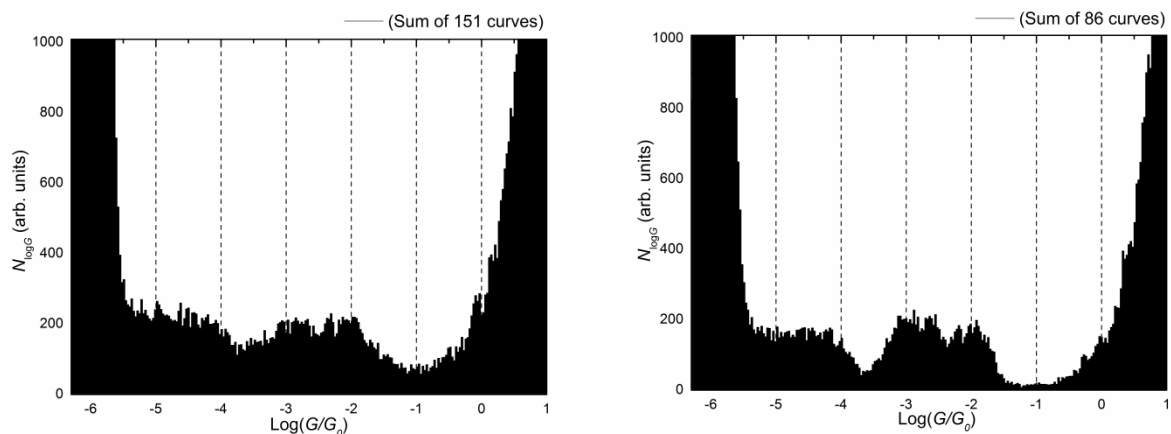


Figure 39. Logarithmic histograms of diiodo-OPE **103**. The left histogram contains the sum of 151 opening curves and the right histogram contains the sum of 86 opening curves.

On the left histogram the sum of all curves is shown (figure 39). One can see two small peaks at 10^{-2} and $10^{-3} G_0$. On the right histogram only curves showing a plateau are summarized. The peaks appear clearer but are still very small. It is rather difficult to compare and rationalize these findings with known literature data.^[38] For example OPE molecules bearing sulfur as anchoring groups show conductance values of $10^{-4} G_0$ which is lower of about two orders of magnitude. It is known that a weaker electronic coupling between the anchor group (molecule) and the gold electrodes results in higher conductivity due to a lower injection (or tunneling) barrier for an electron.^[268,264] Therefore we conclude that the iodine anchor groups did not bind well to the gold electrodes to form a stable molecular junction. This weak coupling could lead to the “observed” high conductance values. However, the number of bridging events is not good enough to have convincing statistical data.

3 Ferrocene Oligo-Phenylene-Vinylene Structures

3.1 Concept

It has been reported that ferrocene compounds are excellent candidates for highly conductive molecules.^[78] The group of Lawrence Sita reported a conductance of $0.7 G_0$ which is extremely high for an organic molecule (e.g. sulfur terminated OPEs have a conductance around $1 \cdot 10^{-4} - 10^{-3} G_0$).^[38] They integrated an OPE-wire **3** (scheme 21) comprising a central ferrocene unit, which connected the two arms in the 1,1'-position, into an electromigration induced break junction. The conductance of single molecules is usually much smaller ($\ll 2e^2/h$) because the HOMO and LUMO are typically not aligned with the Fermi energy level of the electrodes. However, the issue of the possible free rotation around the central ferrocene axis resulting in a possible double wire is addressed below in chapter 4.

Another interesting feature of such ferrocene compounds is their reversible oxidation state. The iron of the ferrocene complex can be reversibly oxidized between Fe^{+II} and Fe^{+III} . This property makes such ferrocene derivatives particularly interesting for investigations towards three terminal devices. Three terminal devices usually consist of source- and drain-electrodes and an additional gate electrode (or a reference electrode for electrochemical gating). If the electrode is placed close enough the gate electrode can reduce or oxidize a molecule between two electrodes.^[18] Until now, only a few examples have been reported where gating controlled the conductivity upon reduction^[269-271] or oxidation.^[272]

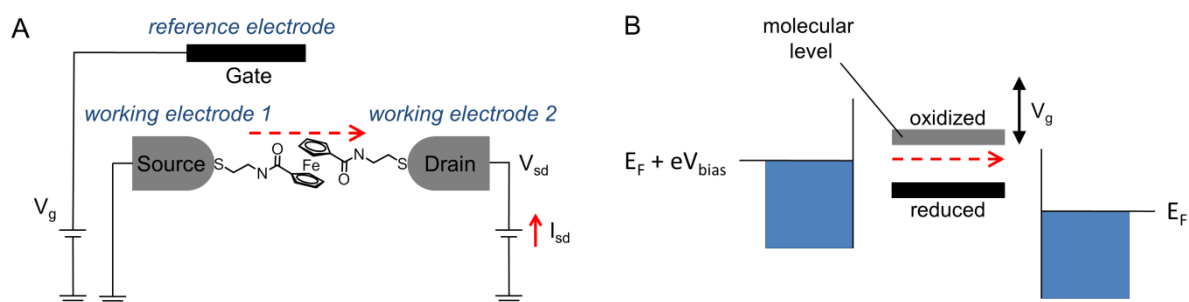


Figure 40. A) Schematic illustration of an integrated ferrocene wire in an electrochemically gated STM setup. B) The influence of the gating effect on the molecular levels is shown. The energy levels can be lowered (upon reduction) or increased (upon oxidation) to match the Fermi energy level. Reprinted from Chen et al.^[50]

The electrochemical gate shifts the energy levels of the molecule up and down relative to the Fermi energy levels of the electrodes (Figure 40, B). If for example, the LUMO is lowered upon reduction to the Fermi energy level of the electrode, resonant tunneling can occur.

In the case of a ferrocene molecule the HOMO can be raised to the Fermi energy level upon oxidation. As a result of the alignment resonant tunneling occurs and the conductance is increased.^[273,274,272] A similar behavior was observed for the ferrocene derivative **6** synthesized by Sergio Grunder.^[84] Compound **6** was integrated in a MCBJ setup with a reference electrode (gate electrode) to oxidize and reduce the molecule. The first experiments showed an increase in conductance upon oxidation which supports the proposed mechanism.^[274] The molecule itself was substituted in the 1,1'-position which means that the two arms can rotate freely around the central axis. The x-ray structure showed that the molecule indeed forms a stacked structure in the solid state (figure 41, right). The actual structure which is measured in the junction remains unclear since the ferrocene itself can also act as an anchor group.^[83]

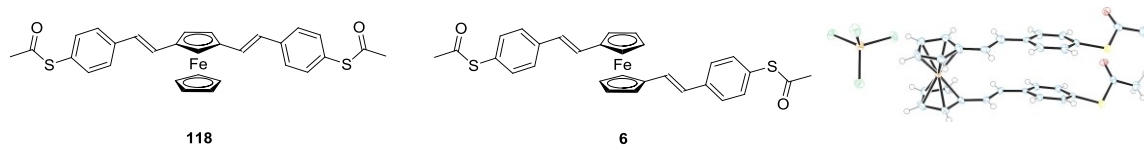


Figure 41. Left: 1,3-disubstituted ferrocene **118**. Right: 1,1'-disubstituted ferrocene **6** synthesized by Sergio Grunder including the obtained crystal structure.^[84]

Here we propose a molecular switch **118** by introducing an electrochemically addressable ferrocene into a conducting organic molecule. The proposed molecule consists of a central ferrocene unit which is substituted by two styrene side-units in the 1,3-position. The benzene units bear sulfur groups to form stable contacts to gold electrodes (figure 41).^[262,37] The sulfur anchor groups are protected with an acetyl-protecting group which can be removed in situ prior to the experiment.^[275] The 1,3-substitution pattern provides a rigid conjugated backbone compared to the previously discussed compound **6**. This molecule should be contacted by two gold electrodes as illustrated in figure 42. Once the bridge is formed the ferrocene **118** can be oxidized by applying a positive voltage on the gate electrode (reference electrode).

The MCBJ-technique is a very suitable method for such an investigation since it is possible to install counter and reference electrodes and to perform the experiment in an electrolyte solution.

Of particular interest is the difference in conductivity between a 1,1'-disubstituted ferrocene **6** and a 1,3-disubstituted ferrocene **118**. Since the 1,3-disubstituted ferrocene has a more rigid structure and the conjugation is not disrupted by a metal complex we expect to observe a different conductivity in the neutral state. We envisage that the conductivity can be tuned by the electrochemical gate and that the switching process is reversible. The reversibility of the switch can further be supported by spectro-electrochemical (SEC) investigations.

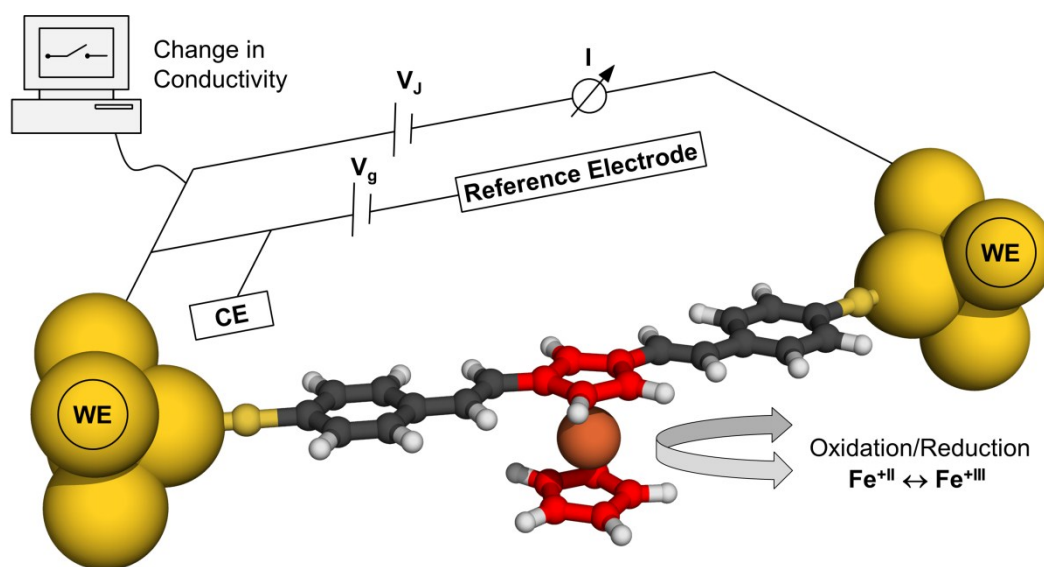
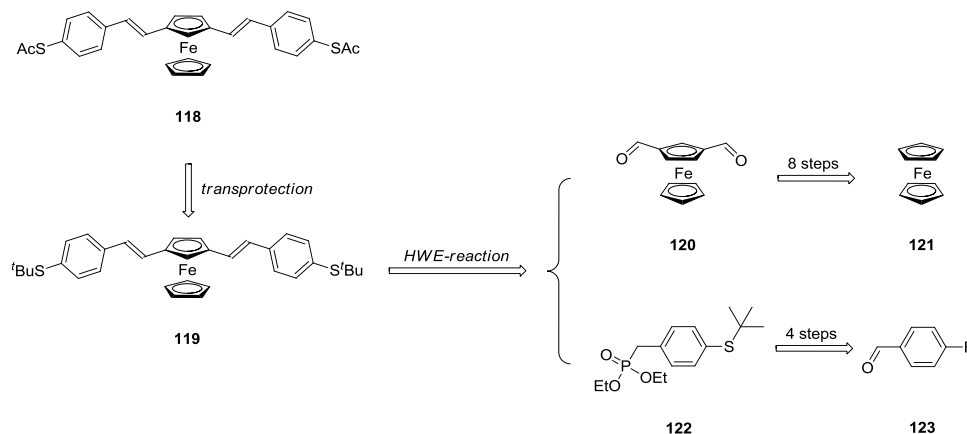


Figure 42. Schematic illustration of a contacted molecule which can change its conductivity upon oxidation or reduction of the ferrocene unit.

3.2 Synthetic Strategy

The first disconnection was made at the two double bonds on the target structure **118** (scheme 37). To form a double bond a *Horner-Wadsworth-Emmons* (HWE) reaction seems to be an excellent choice.^[276] The conditions are relatively mild and the reaction of aldehydes with stabilized ylides leads to olefins with excellent *E*-selectivity. Even though the reaction conditions are quite mild an acetyl protected sulfur group does not survive the basic conditions used to deprotonate the benzylic protons of phosphonate **122**. Therefore, a more stable protecting group such as the *tert*-butyl-PG as in molecule **119** was envisaged. Once the

molecule **119** is assembled a deprotection-protection sequence gives the desired compound **118**.



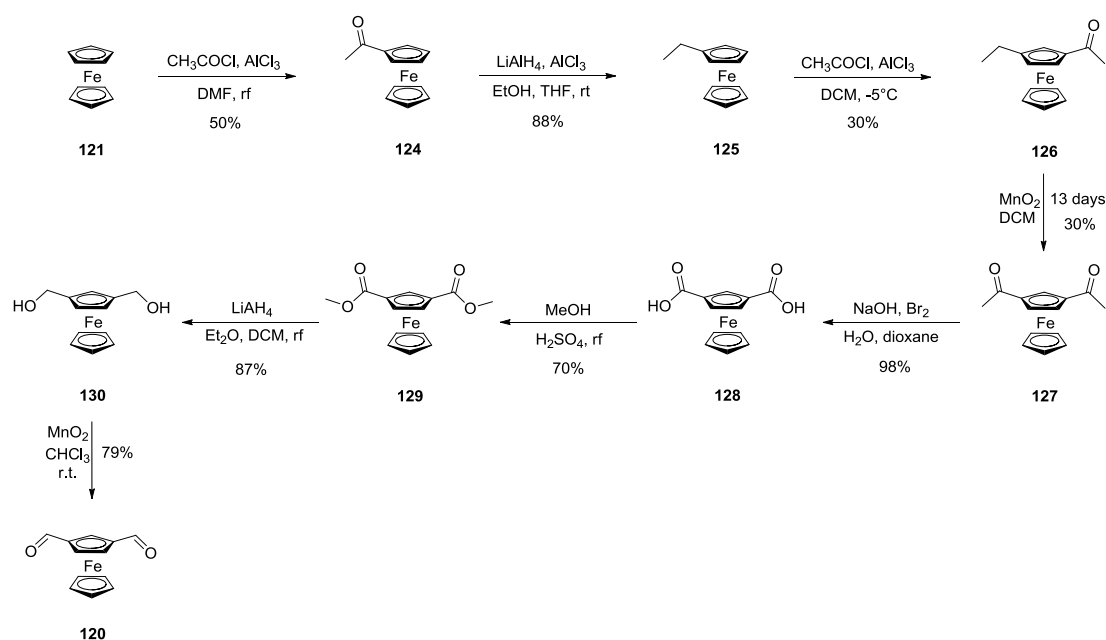
Scheme 37. Synthetic approach for compound **118**.

The 1,3-ferrocenedicarbaldehyde (**120**) can be synthesized within 8 steps starting from ferrocene **121**.^[277-279] This procedure ensures a 1,3-substitution pattern as shown in scheme 38. Another approach could also be used to synthesize a 1,3-disubstituted ferrocene using a chiral auxiliary.^[280] However, the starting materials and the reagents used are so expensive that the initially mentioned approach was favored. The phosphonate **122** can be synthesized within four steps from 4-fluorobenzaldehyde (**123**).^[281,282]

3.3 Synthesis

3.3.1 Synthesis of 1,3-ferrocenedicarbaldehyde

The acetylferrocene (**124**) was synthesized by a classical *Friedel-Crafts* acetylation. Therefore, ferrocene (**121**) was added to a solution of methylene chloride (DCM) containing acetyl chloride and aluminium chloride. The problem of this reaction was over substitution. It is almost impossible to introduce only one acetyl group to the molecule. Sub-stoichiometric amounts of the acetyl chloride or inverse addition did not improve the yield. Once the acetylferrocene (**124**) was formed it became much more reactive by stabilizing the transition state of a second and third substitution. Nevertheless, purification by column chromatography led to the pure acetylferrocene (**124**) in a yield of 50 % (scheme 38).



Scheme 38. Reaction sequence for the formation of 1,3-ferrocenedicarbaldehyde (**120**).

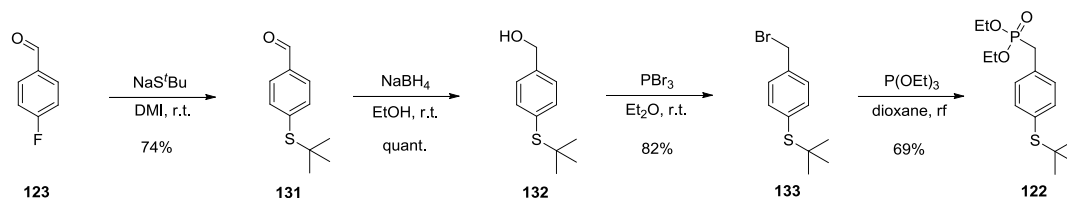
The next reaction step was necessary to control the 1,3-substitution pattern. A direct second acetylation of acetylferrocene (**124**) at the third position seems to be the first choice. However, it is not possible to substitute at the third position when an acetyl group is already present in the molecule which slightly deactivates the cyclopentadienyl (*Cp*) ring. Therefore the acetyl group had to be reduced to an ethyl group to activate the system. The ethyl group directed the second acetylation to the 3-position. To make the ethylferrocene (**125**) the acetylferrocene (**124**) had to be reduced using lithium aluminium hydride and aluminium chloride in diethylether. The crude product was purified by column chromatography to afford the desired ethylferrocene (**125**) in a yield of 88 %. 1-Acetyl-3-ethylferrocene (**126**) was then synthesized by another *Friedel-Crafts* reaction. Therefore, a solution of acetyl chloride and aluminium chloride in DCM was added to a solution of ethylferrocene (**125**) in DCM at room temperature. After quenching the reaction with water and extraction, the crude product was purified twice by column chromatography to afford the desired compound **126** (30 %) as a red oil. The purity of compound **126** was essential for the next reaction step since it had to be re-isolated and used again. The ethyl substituent in molecule **126** had to be oxidized to an acetyl group. This could be achieved by adding activated manganese(IV) oxide to a solution of 1-acetyl-3-ethylferrocene (**126**) in DCM. The reaction was stirred at 50°C for 13 days and every day two equivalents of manganese(IV) oxide were added. The reaction was very slow and the

conversion was 30 %. The product **127** could easily be crystallized by removing the DCM and adding hexane. The soluble starting material **126** was completely re-isolated to repeat the reaction. Once we had the 1,3-diacetylferrocene (**127**) in hand we could further oxidize it to the di-carboxylic acid **128**. This reaction is usually used in industry to make chloroform or bromoform. The 1,3-diacetylferrocene (**127**) was added portion wise to a mixture of sodium hydroxide and bromine in dioxane at 0°C. After one hour the reaction was complete and the desired 1,3-ferrocenedicarboxylate (**128**) was isolated by extraction in a yield of 89 %. We then tried to reduce compound **128** to the 1,3-bis(hydroxymethyl)ferrocene **130** using DiBAL-H in THF. Instead of the desired compound **130** we made 1,3-dimethylferrocene. The DiBAL-H was too reactive and reduced the acid all the way to the methyl group. Therefore we changed the approach by making first the dimethylester out of the carboxylate and then reduced it to an alcohol in a second step. The dimethyl-1,3-ferrocenedicarboxylate (**129**) was synthesized by heating a mixture of compound **128** and sulfuric acid in methanol for 48 hours. The di-methylester **129** was isolated by filtration over a short silica plug eluting with benzene and DCM to give a yield of 70 %. The next reduction using four equivalents of lithium aluminium hydride in diethylether was successful and gave the desired bis(hydroxymethyl)ferrocene (**130**) in a yield of 87 %. Having the bis(hydroxymethyl)ferrocene (**130**) in hand a simple oxidation using manganese(IV) dioxide in chloroform gave the desired 1,3-ferrocenedicarbaldehyde **120** in a yield of 79 %. The manganese(IV) dioxide can oxidize an alcohol effectively to an aldehyde without any over oxidation to carboxylic acids.^[283] The 1,3-ferrocenedicarbaldehyde **120** could be synthesized in a overall yield of 1.9 % and in a quantity up to 300 mg. This rather low yield is a little misleading since the oxidation of compound **126** (step 4) with manganese(IV) dioxide could be repeated several times.

3.3.2 Phosphonate synthesis

The phosphonate **122** was synthesized within four steps starting from the commercially available 4-fluorobenzaldehyde (**123**). The 4-fluorobenzaldehyde is suitable for nucleophilic substitution reactions because the intermediate is strongly stabilized by the aldehyde in the para-position and the fluoride has a polarization effect on the carbon at the reaction centre. Therefore, 4-(*tert*-butylthio)benzaldehyde (**131**) was synthesized by adding 4-fluorobenzaldehyde to a solution of sodium 2-methyl-2-propanethiolate in DMI (scheme 39).

The crude product was purified by distillation to afford the desired compound **131** in a yield of 74 %.



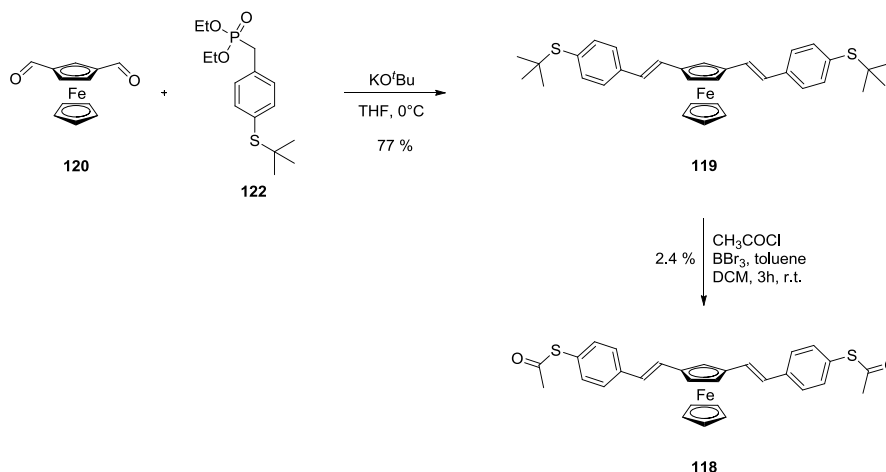
Scheme 39. Synthesis of phosphonate **122**.

The aldehyde **131** was then reduced to the alcohol **132** in a yield of 92 % using sodium borohydride in ethanol. In the next step the hydroxy group had to be replaced by bromine. A good reagent for such a substitution is phosphorus tribromide (PBr_3). In the first reaction step the PBr_3 activates the oxygen from the alcohol and generates the bromide. In the second reaction step the nucleophile attacks the carbon centre to replace the activated hydroxy group. The (4-(bromomethyl)phenyl)(*tert*-butyl)sulfane (**133**) was synthesized by adding PBr_3 at 0°C to a solution of (4-*tert*-butylthio)phenyl)methanol **132** in diethyl ether. The crude compound was purified by recrystallization from hexane/ethyl acetate to afford the desired product **133** as a white solid in a yield of 82 %. The diethyl 4-(*tert*-butylthio) benzylphosphonate **122** was synthesized by an *Arbuzov* reaction.^[284,285] Therefore, a solution of the benzylbromide **133** and triethyl phosphite in dioxane was heated to reflux for 12 hours. The crude product was distilled to give the 4-(*tert*-butylthio)benzylphosphonate **122** as a colorless oil in a yield of 69 %. The second building block **122** could be synthesized in an overall yield of 41 % within four steps.

3.3.3 Synthesis of 1,3-bis(vinylene-phenylene)ferrocene

Once the two building blocks **120** and **122** were synthesized the assembly of molecule **119** was investigated (scheme 40). Thus, potassium *tert*-butoxide dissolved in THF was added to a mixture of compounds **120**, **122** and THF at 0°C . The mixture was allowed to warm to room temperature and was stirred for another 3 hours. After the reaction was complete the reaction mixture was extracted and the crude product was purified by column chromatography eluting with hexane and DCM (2:1) to afford the desired compound **119** as a red solid in a yield of

77 %. This reaction worked very well and very little formation of mono-reacted product was observed. The use of potassium *tert*-butoxide turned out to be an excellent choice since it did not react with the ferrocene compound **120**. In an attempt to use *n*-butyl lithium as a base the starting material **120** started to decompose rapidly.



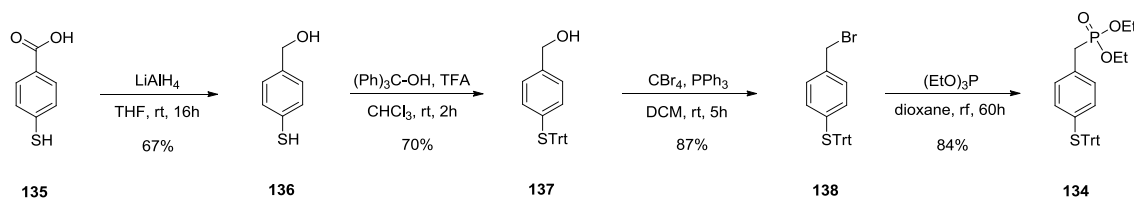
Scheme 40. Final assembly followed by trans-protection to the target structure **118**.

The next step was rather troublesome. The sulfur needed to be transprotected by removing the *tert*-butyl-PG and directly introduce the acetyl-PG. The *tert*-butyl-PG was necessary for the *HWE*-reaction but it is useless for MCBJ-experiments since the reagents to remove this PG are too aggressive. On the other hand, an acetyl-PG can easily be removed with tetra-butyl ammonium hydroxide prior to the experiment. The transprotection was carried out by dissolving compound **119** in acetyl chloride (excess of 630 equiv.) and toluene. A boron tribromide (BBr₃) solution was slowly added to the mixture at room temperature. After aqueous workup the crude compound was purified twice by column chromatography (silica, 1st column: hexane/ethyl acetate 5:1, RF: 0.24; 2nd column: DCM, RF 0.9) to afford the desired target molecule **118** as a red solid in a yield of 2.4 %.

This low yield on the very last step was very disappointing and changing the reaction parameters did not improve the yield as it was already reported in Sergio Grunder's thesis.^[84] Consequently we tried to change the strategy by introducing another protecting group at an earlier stage. The protecting group should be base stable and easily removed under mild non-oxidative conditions. The free thiol (or sulfur anion) tends to form sulfur-sulfur dimers under oxidative conditions. The protecting group of choice was the triphenylmethyl-PG (trityl-PG). It is base stable and can be removed under acidic conditions. Therefore, a trityl-protected

phosphonate **134** was synthesized starting from the commercially available 4-mercaptobenzoic acid (**135**) within 4 steps (scheme 41).

3.3.4 Approach with a different protecting group

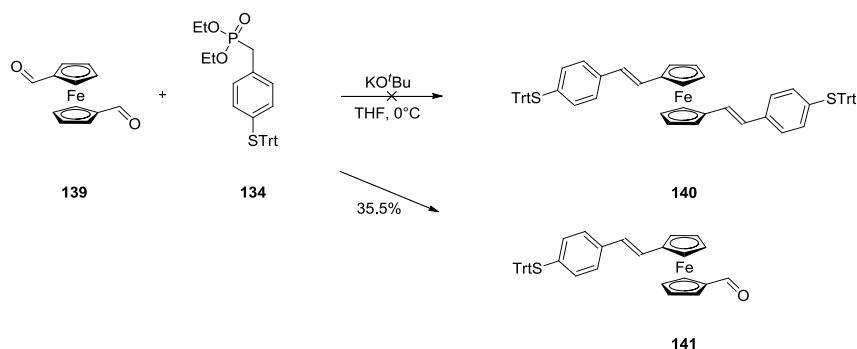


Scheme 41. Synthesis of a trityl protected phosphonate **134**.

(4-Mercaptophenyl)methanol (**136**) was synthesized by adding a solution of 4-mercaptobenzoic acid (**135**) in THF to a solution of lithium aluminium hydride at room temperature. After aqueous workup and recrystallization from ethanol the pure compound was isolated in a yield of 67 %. In the next step the thiol group was protected with the trityl-PG. Therefore, triphenylmethanol and TFA were added to a solution of (4-mercaptophenyl)methanol (**136**) in chloroform at room temperature. After the reaction was complete sodium bicarbonate was added to quench the reaction. After aqueous workup the crude product was purified by column chromatography eluting with hexane/*t*BME (2:1) to afford the desired compound **137** as a colorless oil in a yield of 70 %. In the next step the hydroxy group had to be replaced by bromine. Using the same conditions as above (scheme 39, step 3) with PBr₃ as reagent did not work very well yielding too many side products. Instead an *Appel* reaction was performed to substitute the hydroxy group by a bromine.^[286] Thus, triphenylphosphine was added to a solution of compound **137** and carbon tetrabromide in dry DCM at 0°C. The reaction was allowed to reach room temperature and was stirred for 5 hours. After aqueous workup the crude product was purified by column chromatography to afford the desired (4-(bromomethyl)phenyl)(trityl)sulfane (**138**) as a white solid in a yield of 87 %. The phosphonate **134** was finally synthesized by applying the same protocol as discussed above (scheme 39). The desired diethyl 4-(tritylthio)benzylphosphonate **134** was isolated in a yield of 84 %.

The phosphonate **134** together with the commercially available 1,1'-ferrocenedicarbaldehyde (**139**) was then used to screen reaction conditions for a *HWE*-reaction (scheme 42). The reaction did not work as expected. In any attempt an insoluble precipitate was formed. We expected that the sulfur was deprotected and then polymerized to sulfur-sulfur oligomers. The

attempt to reduce a possible sulfur-sulfur bond did not work. Only a mono-substituted ferrocene compound **141** could be isolated in a yield of 35 % by using potassium *tert*-butoxide as base and little THF as solvent. Since the reaction could not be developed for the 1,1'-ferrocenedicarbaldehyde (**139**) to a certain satisfaction we did not pursue a trial on the valuable 1,3-ferrocenedicalbaldehyde (**120**).



Scheme 42. HWE-reaction leading to a mono-substituted ferrocene derivative **141**.

3.4 UV-Deprotection Experiments

The binding event of a sulfur anchor group to a gold electrode remains unclear. Usually a weak base such as tetrabutylammonium hydroxide (TBAH) is used to remove the acetyl-PG in the MCBJ-cell prior to the experiment. Whether the acetyl-PG is removed in a first step and the resulting free sulfur anion binds to the gold or if the sulfur-acetyl group binds to the gold in the first place before the PG is removed has been investigated by Valkenier et al.^[275] The conclusion of their work was that the binding event can be controlled by the base which was used for deprotection. However, the necessary amount of base depends on the electronic properties of the molecule itself. For this reason we tried to investigate the deprotection process by monitoring the reaction progress with UV measurements. To apply the findings of the UV measurements to the MCBJ-experiments the same conditions were used. Therefore, a stock solution (0.03 mM) of 1,1'-disubstituted ferrocene **6** in mesitylene/THF (3:1) was prepared. The deprotection reagent (TBAH) was diluted to a concentration of 0.05 M in THF. We tested two different reagents. One contained 30 equivalents of water per TBAH molecule and the other one contained no water but was dissolved in methanol/*iso*-propanol instead of pure THF. A quartz UV cuvette was filled with 3 ml of ferrocene solution and two equivalents (3.6 μ l) of TBAH*30 H₂O solution (0.05 M) were added. The mixture was stirred

for 1 minute and a UV spectrum was recorded between 900 nm and 290 nm every minute for 30 minutes. As displayed in figure 43 almost no change was observed in the spectra.

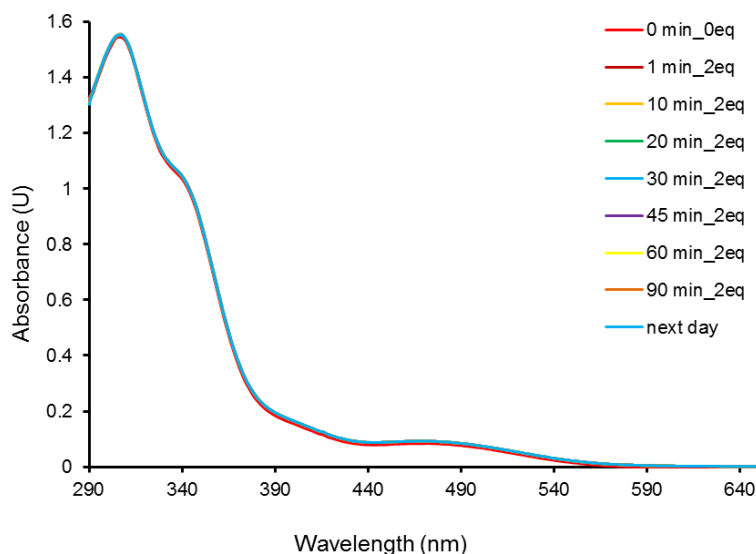


Figure 43. Deprotection experiment using two equivalents of TBAH.

The same experiment was repeated with four equivalents of deprotection reagent instead of two. In this case, a change of the UV spectrum was observed (figure 44). A decrease in intensity was observed at 304 nm. The shoulder at 340 nm disappeared and a smaller decrease of intensity was observed at 470 nm. It seemed that the reaction was complete after 30 min using four equivalents of deprotection reagent. The experiment was also done using 8 equivalents of TBAH but a faster deprotection could not be observed. Also the presence or absence of water did not have an influence on the deprotection rate. On the other hand, a water-free deprotection should be considered when working with water sensitive compounds.

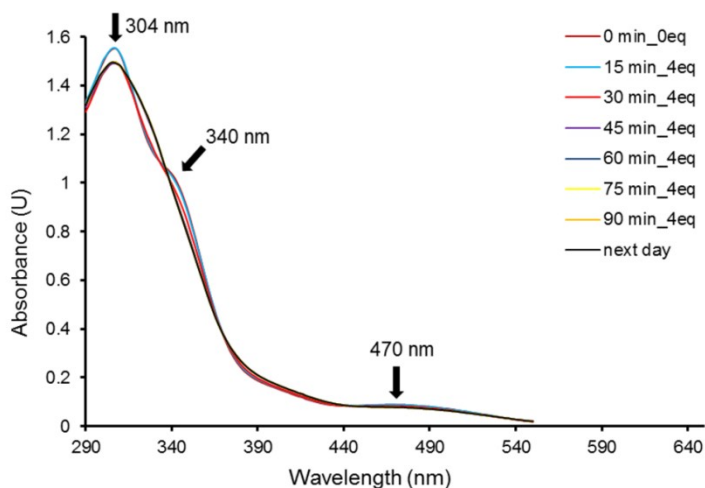


Figure 44. Deprotection experiment using four equivalents of TBAH.

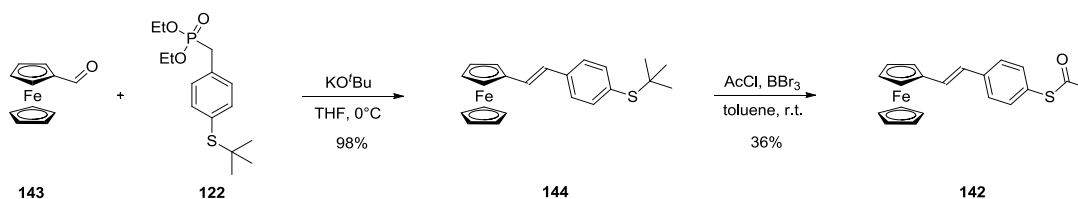
3.5 Synthesis of further ferrocene compounds

To conclude the MCBJ-experiments another ferrocene compound **142** was synthesized (figure 45). This compound consists of a ferrocene and only one vinyl-phenylene substituent which bears an acetyl protected sulfur group. The idea was to preclude the hypothesis that the ferrocene itself could bind to gold as it could happen to the 1,1'-distyreneferrocene **6** upon π - π stacking with itself (figure 45, right).



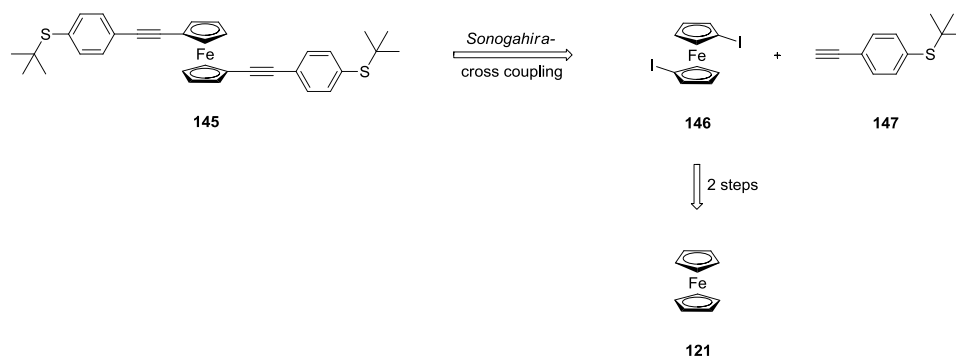
Figure 45. Left: Mono-substituted ferrocene derivative **142**. Right: Possible structure of compound **6**.

In the first step potassium *tert*-butoxide was added to a mixture of a commercially available ferrocenecarbaldehyde (**143**) and phosphonate **122** in dry THF at 0°C (scheme 43). The compound was isolated by extraction and purified by column chromatography eluting with hexane/DCM (2:1) to afford the desired ferrocene derivative **144** in a yield of 98%. Compared to the reaction described above (scheme 40) a much better yield was observed. For the next step acetylchloride and BBr₃ were used to deprotect and in situ protect the sulfur end group to make **142**. This reaction yielded in 36% which was much higher compared to the di-substituted ferrocene compounds (scheme 40). A possible explanation could be the better solubility of the smaller molecule **144**. When two sulfur end groups within one molecule **119** are deprotected at the same time a very low solubility is expected and therefore the formation of side-products is favoured.



Scheme 43. Synthesis of mono-substituted ferrocene **142**.

To complete our series of ferrocene compounds an ethynylene-substituted ferrocene **145** was envisaged. The molecule consists of a central ferrocene unit which is substituted at the 1,1'-position with an ethynylene-phenylene unit. The phenylene bears again a protected sulfur end group (scheme 44).

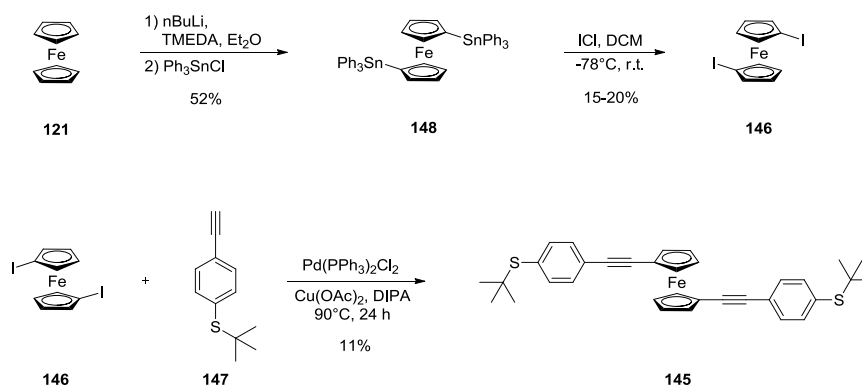


Scheme 44. Strategic considerations for a 1,1'-disubstituted ferrocene **145**.

The disconnection was made between the ferrocene and the acetylene group. This could be achieved by a Sonogashira cross coupling reaction between 1,1'-diiodoferrocene (**146**) and *tert*-butyl(4-ethynylphenyl)sulfane (**147**). It was essential to have iodine on the ferrocene as leaving groups because the commercially available 1,1'-dibromoferrocene was not reactive. The 1,1'-diiodoferrocene (**146**) could be synthesized within two steps starting from ferrocene (**121**). The *tert*-butyl(4-ethynylphenyl)sulfane (**147**) was previously synthesized in our group according to a literature procedure.^[287]

The 1,1'-diiodoferrocene **146** had to be synthesized via 1,1'-bis(triphenylstannyl)ferrocene. A direct iodination of ferrocene (**121**) via lithiation or a halide exchange reaction of 1,1'-dibromoferrocene did not work. Every attempt yielded in multiple substitution and polymerisation. The problem of a multiple substitution is the purification and isolation since the physical properties are almost identical between every possible isomer. The introduction of the iodine had to be fast and selective. Tin substituents are excellent leaving groups for such a purpose. The problem is its toxicity. The introduction of tributylstannyl into ferrocene followed by an iodination was reported by Butler et al.^[288] The alkylated tin compounds gave excellent yields but also showed the highest toxicity. Therefore, the procedure was very extensive due to a workup of every single waste solution. For this reason triphenylstannyl was introduced to ferrocene. Triphenyltin compounds are 1000 times less toxic than alkylated tin compounds^[289] and they are not soluble in polar solvents which makes it much easier for

proper handling. Therefore, ferrocene (**121**) dissolved in ethylether was added to a solution of *n*butyl lithium and tetramethylethylenediamine (TMEDA) in diethylether. The resulting mixture was stirred at room temperature for 12 hours. Triphenyltin chloride was then added and the reaction mixture was stirred for another 6 hours. The reaction was quenched with water and diluted with *t*BME and toluene (5:1). After an aqueous workup the compound **148** was adsorbed onto basic aluminium oxide and then chromatographed over silica eluting with cyclohexane/DCM (5:1) to afford the desired compound **148** as an orange solid in a yield of 52 % (scheme 45). All waste solutions were collected and properly disposed. This compound is expected to be less toxic than triphenyltin chloride since the molecule is much bigger and non-volatile. Nevertheless, extra precaution should be considered at any time when this compound is used.



Scheme 45. Synthesis of 1,1'-disubstituted ferrocene **145**.

In the next step a solution of iodine monochloride in DCM was added quickly to a solution of compound **148** in DCM at -78°C. After the addition was complete the reaction mixture was allowed to reach room temperature and was stirred for 12 hours. The reaction mixture was then concentrated under reduced pressure and the residue was dissolved in cyclohexane and filtered over silica to remove the triphenyltin chloride. The filtrate was again concentrated and the residue was purified twice by column chromatography (figure 46) (1st column: silica, cyclohexane/*t*BME 40:1; 2nd column: RP18-silica, acetonitrile/water 5:1). The second purification step was never described in literature, hence the reported yields could never be reproduced. This reaction was done almost 20 times and the isolated yields varied between 15-20 %.

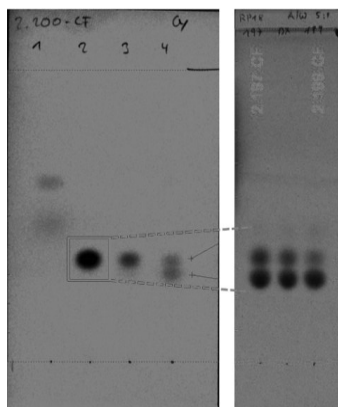


Figure 46. TLC plates visualized by 254 nm. Left: silica-plate, cyclohexane as eluent. Right: RP18-silica plate, acetonitrile:water (5:1).

Once we had the 1,1'-diiodoferrocene (**146**) and compound **147** in hand a twofold Sonogashira cross coupling reaction was performed using bis(triphenylphosphine)palladium (II) chloride and copper acetate as catalysts and diisopropylamine as base and solvent (scheme 45). The reaction was stirred for 24 hours at 90°C. The reaction mixture was concentrated under reduced pressure and the residue was purified by column chromatography eluting with cyclohexane/DCM (2:1) to afford the desired compound **145** in a yield of 11 %. Any attempt to do this cross coupling reaction with 1,1'-dibromoferrocene was not successful and the starting material was always reisolated. Even for the 1,1'-diiodoferrocene (**146**), elevated temperatures and pure bases as solvents were necessary to insert the palladium species into the ferrocene-iodine bond.

3.6 Electrochemical investigations

Cyclic voltammetry has become a very efficient tool to characterize the properties of redox active molecules. Depending on the electronic nature around the redox center the oxidation potential changes and can therefore be characterized. We measured the ferrocene compounds **119**, **149**, **144**, and **145** in an all-glass electrochemical cell using a glassy carbon as working electrode, a silver net as counter electrode and a Ag/AgCl reference electrode. The glassy carbon electrode was necessary to prevent early decomposition of the investigated compounds. For the same reason, the compounds were measured with the *tert*-butyl-PGs since they are much more stable in the supporting electrolyte compared to ones bearing an acetyl-PG.

The solvent and the electrolyte concentration have an enormous effect on the redox potentials. The dependence of the redox potentials on the concentration of the supporting electrolyte is much more pronounced for solutions composed of relatively nonpolar solvents than for solutions of relatively polar solvents.^[74] For this reason a 100 mM solution of tetrabutylammonium tetrafluoroborate (TBABF₄) in acetonitrile was used to conduct the measurements. The electrolyte should be absolutely redox inert within the investigated voltage range.^[74]

The first characterization of the compounds **119**, **149**, **144**, and **145** was to check whether these systems are reversible or not. A reversible system meets the following criteria:

- The difference between E_{pc} and E_{pa} should be 59 mV.
- The ratio of i_{pc} and i_{pa} should be 1.
- i_p should be proportional to the square root of the scan rate.

It is almost impossible to meet these criteria to a 100 % but one should get close.

To measure the ferrocene derivatives **119**, **149**, **144**, and **145** a 1 mM solution (+100 mM electrolyte) was prepared. The glassy carbon electrode was polished^[290,291] and the platinum net counter electrode was cauterized. The solution was degassed with nitrogen prior to the experiment. In a first step all the molecules were reduced by sweeping to a negative voltage of about -1V. Then different scan rates were run to determine the redox potentials and the amount of electrons involved.

3.6.1 Cyclic Voltammetry experiments

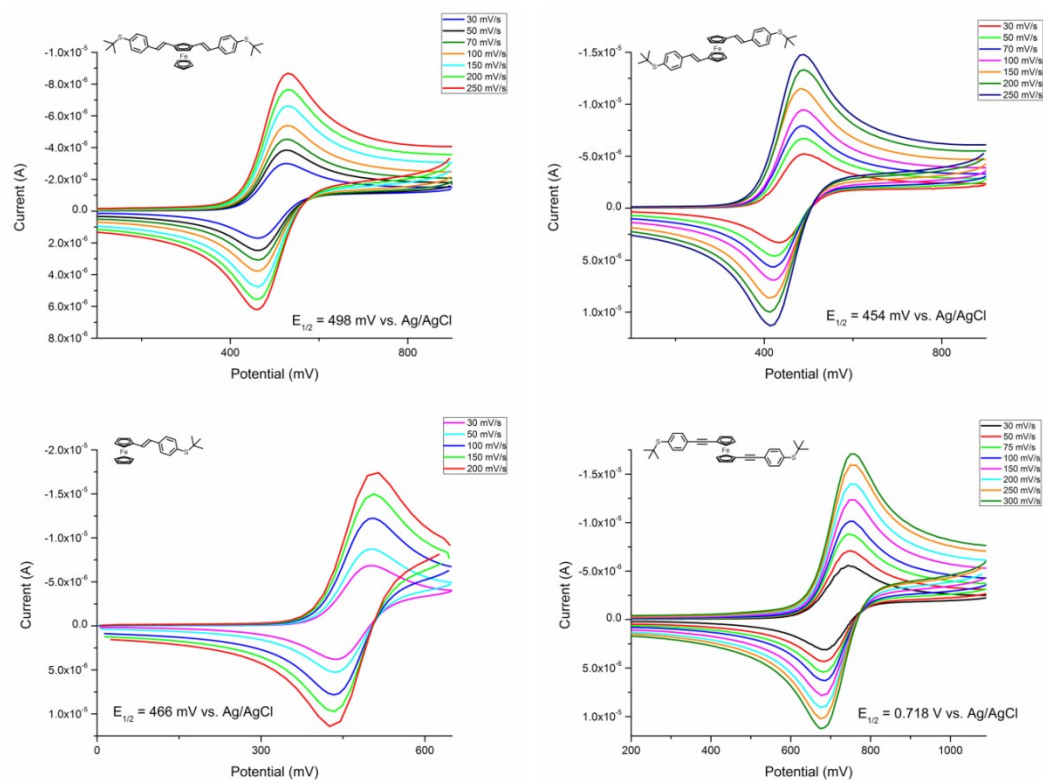


Figure 47. CV's of ferrocene derivatives **119**, **149**, **144**, and **145**. Measured in acetonitrile using a glassy carbon working electrode and TBABF₄ as electrolyte.

Derivative	E_{pc} (mV)	E_{pa} (mV)	ΔE_p (mV)	$E_{1/2}$ (mV)	i_{pc}/i_{pa} (A)	n	
	119	528	467	61	498	1.01	0.96
	149	485	423	62	454	1.00	0.95
	144	495	437	58	466	1.04	1.02
	145	748	687	61	718	1.03	0.97

Table 1. Electrochemical data of compound **119**, **149**, **144**, and **145**.

All ferrocene derivatives have a fully reversible redox system. The current ratio between i_{pc} and i_{pa} is about 1. The difference between the potentials E_{pc} and E_{pa} is about 59 mV and the current correlates to the square root of the scan rate (table 1).

As we can see in table 1 the half wave potentials of 1,3-disubstituted ferrocene **119** and 1,1'-disubstituted ferrocene **149** are almost the same, yet they are higher compared to ferrocene (452 mV) This means that the electron withdrawing effect coming from the substituents is dominant and steric effects due to shielding of the iron atom can be ignored.^[292] The mono-substituted ferrocene **144** was rather difficult to measure since decomposition started after 650 mV. However, a reversible redox system was observed with a half wave potential at 466 mV. This is higher compared to ferrocene and to 1,1'-disubstituted ferrocene **149** but lower compared to 1,3-disubstituted ferrocene **119**. A big change of the half wave potential was observed when the vinylene groups were replaced by ethynylene groups as in compound **145** (table 1). The half wave potential of this 1,1'-disubstituted-ethynylene ferrocene **145** was 718 mV which is about 260 mV higher compared to the 1,1'-disubstituted-vinylene ferrocene **149**. A reasonable explanation could be a better conjugation between the phenylene unit and the cyclopentadienyl ring through the acetylene group. This leads to a stronger electron withdrawing effect which results in an increase of the positive charge on the iron atom and its oxidation becomes more difficult.

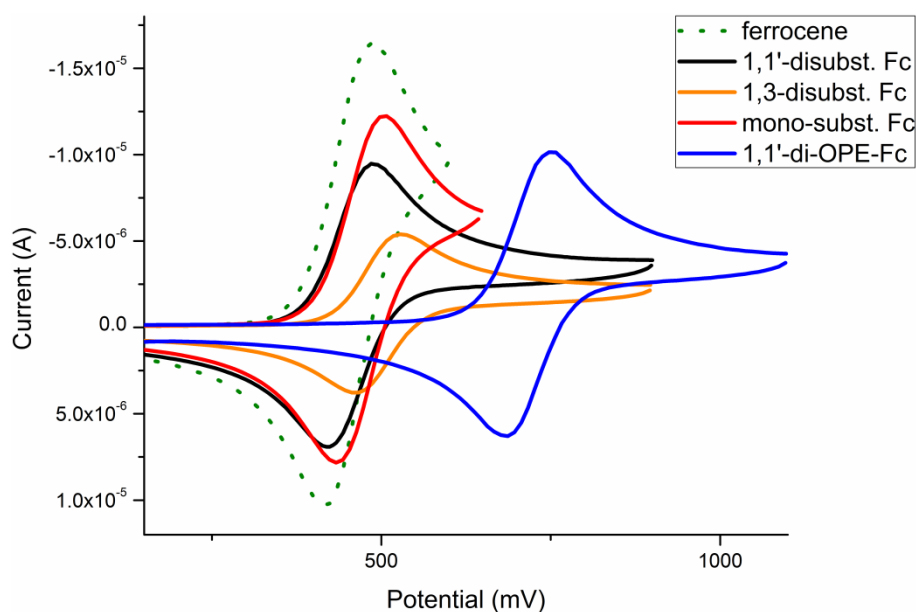


Figure 48. CV's of compound **119**, **149**, **144**, and **145**. A clear shift to a higher potential of compound **145** can be observed.

3.7 Spectro-electrochemistry

To correlate the oxidation state with the UV-absorbance spectroelectrochemical (SEC) experiments were performed to investigate their switching behavior. Therefore, a 1 mm quartz cuvette equipped with a gold net counter electrode, a silver working electrode and a Ag/AgNO₃-reference electrode (in MeCN) were used to conduct the experiment. In the beginning the potential was swept to -1.0 V to make sure that the entire ferrocene derivative **119** in solution was in its reduced state (neutral molecule).

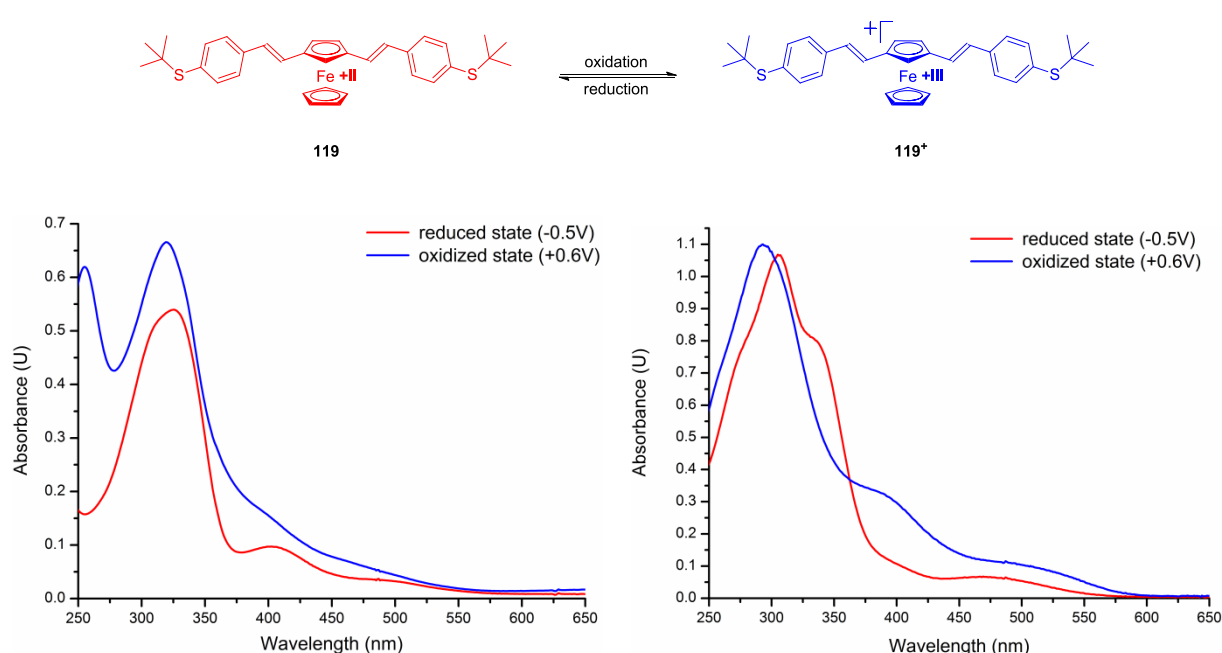


Figure 49. Left) Spectroelectrochemical plot of 1,3-disubstituted ferrocene **119**. Right) Spectroelectrochemical plot of 1,1'-disubstituted ferrocene **6** (reprinted from Grunder et al.^[84]).

The first UV was measured at -0.5 V (figure 49, left, red curve) which was also the starting point of the experiment. The solution was then slowly oxidized (~ 1 mV/s) to +0.6 V and a UV spectrum was recorded every minute until no change in the UV spectrum was observed (figure 49, left, blue curve). The UV spectrum of the reduced form (red) shows an absorption maximum at 325 nm with a possible shoulder at 310 nm. In addition two smaller very broad peaks are located at 402 nm and 500 nm. The bands of the absorption spectrum were not assigned to their transitions. Thus it is difficult to interpret the changes observed upon oxidation of the ferrocene derivative **119**. At 325 nm an increase in intensity and a small hypsochromic shift to 319 nm could be observed. The shoulder at 310 nm in the reduced form

seems to shift to 255 nm. The broad peaks at 402 nm and 500 nm show an increase in intensity and a small hypsochromic shift. The observed changes upon oxidation are rather small and by comparing these results with the SEC-investigations of compound **149** (figure 49, right) we can see that the changes are of similar value.

The reversibility of the redox system was investigated by running three sweeps using the same setup as discussed above. The starting point (figure 50, blue curve) was again at -0.5 mV and the solution was slowly oxidized (2 mV/s) to +0.6 mV (black curve). A negative potential was applied and the solution was slowly reduced to -0.5 mV. Since almost an identical UV/vis spectrum (purple curve) was recorded it was assumed that the entire ferrocene derivative **119** was again in the reduced form. The solution was again oxidized to +0.6 mV (red curve) until no change in the UV/vis spectrum could be observed.

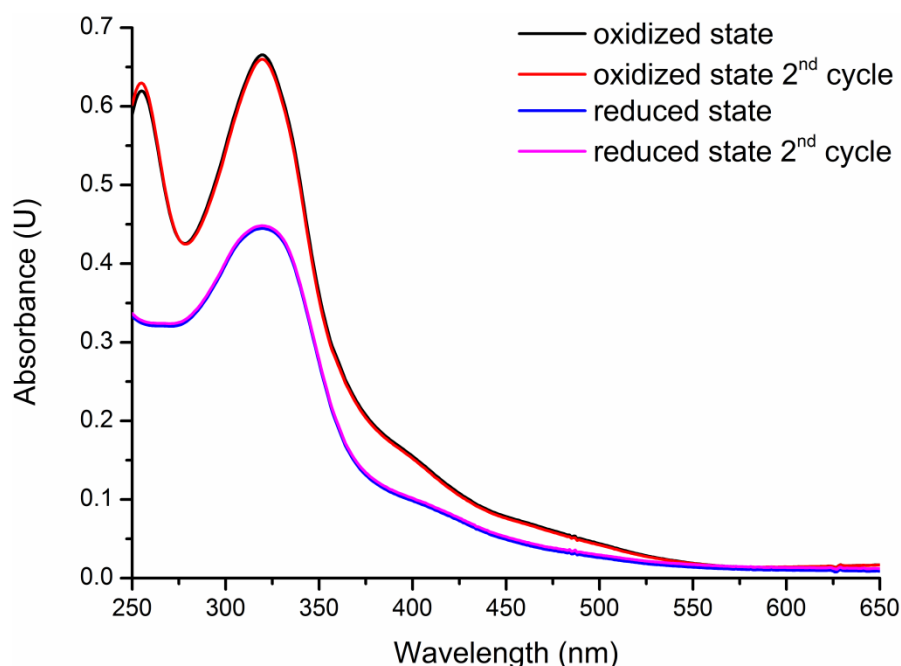


Figure 50. Reversibility of the central redox system.

It was shown that we can switch between the neutral (or reduced form) and the oxidized form. Even though the changes in the UV/vis spectra are rather small, a change of the HOMO-LUMO gap should still be detectable by conductance experiments.

3.8 Break Junction Experiments

To investigate if this molecular switch **118** was also applicable to a molecular junction MCBJ experiments were performed by the group of Christian Schönenberger and Michel Calame at the University of Basel. The concept of the electrochemical setup was discussed in the introduction section 1.2.2.

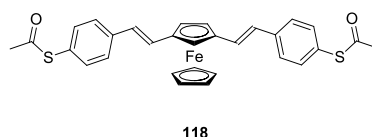


Figure 51. Molecule **118** was investigated in a MCBJ-experiment.

A 0.1 mM solution of 1,3-disubstituted ferrocene derivative **118** in DCM was prepared. Then 3 ml of this stock solution were treated with 20 μ l of a solution of tetrabutylammonium hydroxide (TBAH) in DCM (10 mM) to deprotect the sulfur groups. The first experiment was carried out to control if a stable molecular junction could be formed (figure 52).

As displayed in figure 52 (left) a few plateaus (red circle) were observed during the MCBJ measurement. On the other hand, the plateau yield is only 12 %. On the right picture the logarithmic histograms are shown where a small peak between 10^{-5} and $10^{-4}G_0$ occurs.

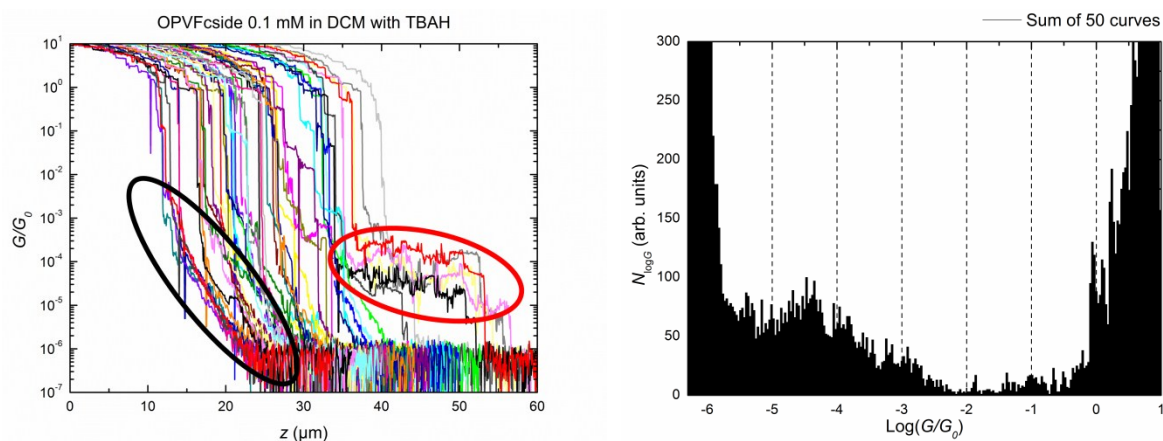


Figure 52. Left: Conductance traces of molecule **118** in DCM. Black circle shows the exponential decay of the solvent system. The red circle shows a few plateaus formed during the experiment. Right: Logarithmic histograms of the conductance traces are displayed.

Since no strong signal was measured more TBAH (10 μ l in THF) was added to the solution. However, no improvement of the signal could be observed. In total, one equivalent of deprotecting reagent (TBAH) was added. Our UV-experiments revealed that at least two equivalents of deprotecting reagent per sulfur group were necessary to deprotect both sulfur atoms. In contrast to an all organic OPE bearing sulfur anchoring groups, sub-stoichiometric amounts of TBAH are sufficient to deprotect enough molecules, necessary for a successful experiment.^[260]

Our collaborators successfully reproduced the first obtained results which were reported in the Thesis of Sergio Grunder^[84] by using three equivalents of TBAH to deprotect molecule **6**. They then observed a plateau yield between 32 and 60 %. However, the 12 % plateau yield from molecule **118** is not high enough to collect a statistical data set to properly demonstrate a gating effect. The problem seems to be the amount of deprotecting reagent. If too much of TBAH is used in the electrochemical MCBJ-cell the leakage current becomes too strong and the experiment cannot be performed.

If we compare the obtained results of the two ferrocene derivatives **118** and **6** with each other we can see that both conductance peaks appear at about $10^{-5} G_0$. The current pathway, either through a *Cp*-ring (molecule **118**) or through the ferrocene (molecule **6**), has no influence on the conductance of such OPV-type wires (figure 53).

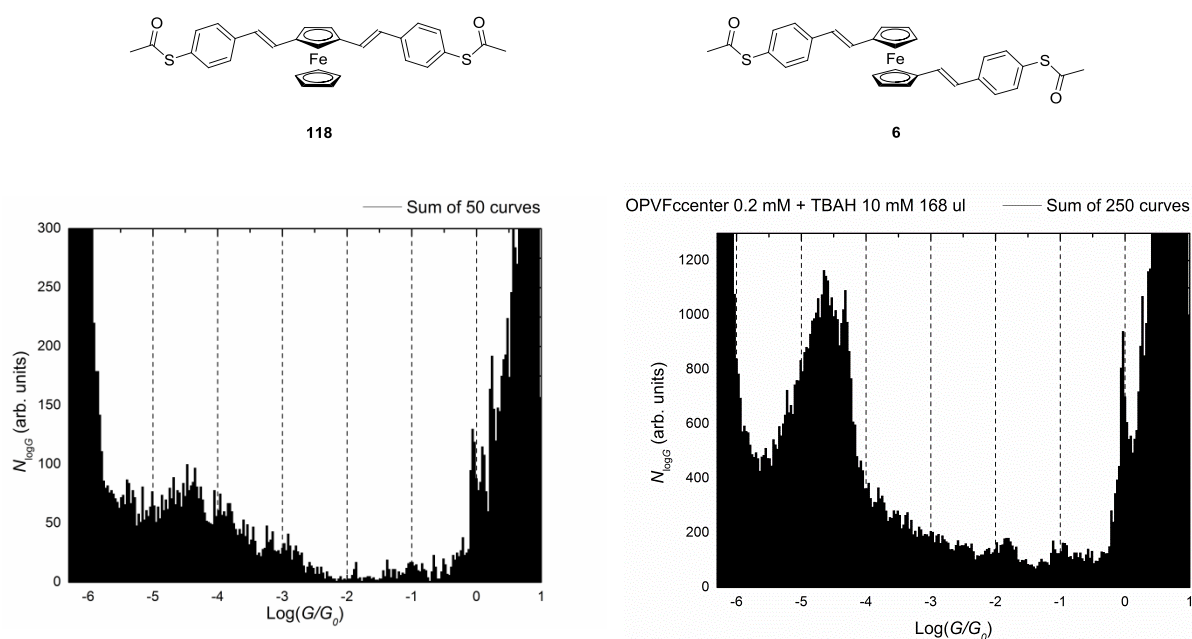


Figure 53. Comparison of conductance histograms between compounds **118** and **6**.

3.9 Conclusion

The 1,3-disubstituted ferrocene derivative **118** was successfully synthesized in 14 steps. The most troublesome step was the last transprotection from the *tert*-butyl-PG to the acetyl-PG. This reaction step could not be further optimized since the reagents which are necessary to remove the *tert*-butyl-PG are too aggressive towards ferrocene and double bonds, low yields are always expected. A replacement of the *tert*-butyl-PG by a trityl-PG failed due to stability and solubility issues on the *HWE*-reaction step. Replacing the protecting group will remain the key to improve the overall yield. A sulfur protecting group needs to be found which is stable towards basic conditions and can easily be removed under mild conditions. To complete the series of small ferrocene compounds two additional compounds have been synthesized. A mono-substituted ferrocene derivative **142** was synthesized within 6 steps to have a control molecule for the MCBJ experiments. A 1,1'-disubstituted ferrocene ethynylene derivative **145** was synthesized in three steps.

The deprotection of the acetyl-PG with TBAH was investigated by UV/vis experiments. It was shown that at least two equivalents of deprotection reagent per protecting group were necessary to deprotect the sulfur group. Since the deprotection reaction itself was very slow and the deprotection reagent did not affect the molecule, four equivalents of TBAH per acetyl-PG should be considered.

Cyclovoltammetry experiments on our four model compounds **119**, **149**, **144**, and **145** revealed a fully reversible redox system for all compounds investigated. It was vital to use a glassy carbon working electrode instead of a gold electrode to prevent early decomposition. It was shown that the electronic nature of the substituents has a large effect on the oxidation potentials of the ferrocene derivatives **119**, **149**, **144**, and **145**. The more electron-withdrawing the substituent was, the more difficult it was to remove an electron from the iron atom, hence shifting the redox potential to a higher voltage. Having both vinyl-substituents on the same *Cp*-ring of the ferrocene as in molecule **119** the observed shift to a higher voltage was slightly larger compared to its counterpart **149** which has only one substituent per *Cp*-ring. By replacing the vinylenes with etynylenes as in molecule **145** a large change of the redox potential was observed. The conjugation through the acetylenes was much better, therefore the electron-withdrawing effect coming from the benzene unit was much bigger.

The spectroelectrochemical investigations of compound **119** showed a slight hypsochromic shift and an increase in intensity upon oxidation. The observed changes in the UV/vis

spectrum were not very large, however, the change of the HOMO-LUMO gap should be detectable by conductance experiments. It was also shown that the switching of compound **119** is reversible. We oxidized and reduced the system twice and the obtained UV/vis spectra matched the previous ones. With these experiments we were able to show that we synthesized a reversible switch upon oxidation and reduction.

The attempt to contact the molecule **118** with two gold electrodes in the MCBJ experiment was unsuccessful as revealed by low yield of plateau formation (12 %). We believe that the amount of deprotecting reagent used (0.7-1 equiv.) was not enough to deprotect enough molecules for sufficient junction formation. However if too much deprotecting reagent is used a tremendous increase of the background current is observed which makes a conductance measurement impossible. One possibility to overcome that problem is to use an aliphatic amine as deprotecting reagent instead of TBAH which is a salt. Although, the exact amount which would be necessary to deprotect enough molecules has to be investigated by UV/vis-measurements.

Both ferrocene derivatives show similar conductance values around $10^{-5} G_0$. Therefore, we can conclude that the current pathway, which is either through a *Cp*-ring (**118**) or through the ferrocene (**6**), has no big influence on the conductance.

4 Synthesis of Interlinked Molecular Wires

4.1 Concept

In the preceding chapter we investigated the concept of molecular switching upon oxidation and reduction of an organic molecule containing a ferrocene unit. The spectroelectrochemical investigations supported our theory that the HOMO-LUMO gap and therefore the conductance of a redox active molecule can be controlled by manipulating its oxidation state.^[273] However, the final contacting experiments could not be reproduced to a certain statistical satisfaction. We believe that the conformational freedom of these vinylene structures increased the difficulty of forming a stable sulfur-gold bond. Based on these findings and the reported conductivities of ferrocene compounds by Getty et al.^[78] we envisaged a new molecular switch (figure 54) comprising a central ferrocene unit (red), two conducting rigid arms (black), sulfur anchor groups (yellow) and a linker (blue) which controls the shape of the molecule. Once we have such a molecular wire in hand, MCBJ experiments combined with electrochemical experiments should allow us to obtain more detailed information about the structure-property relationships of such compounds.

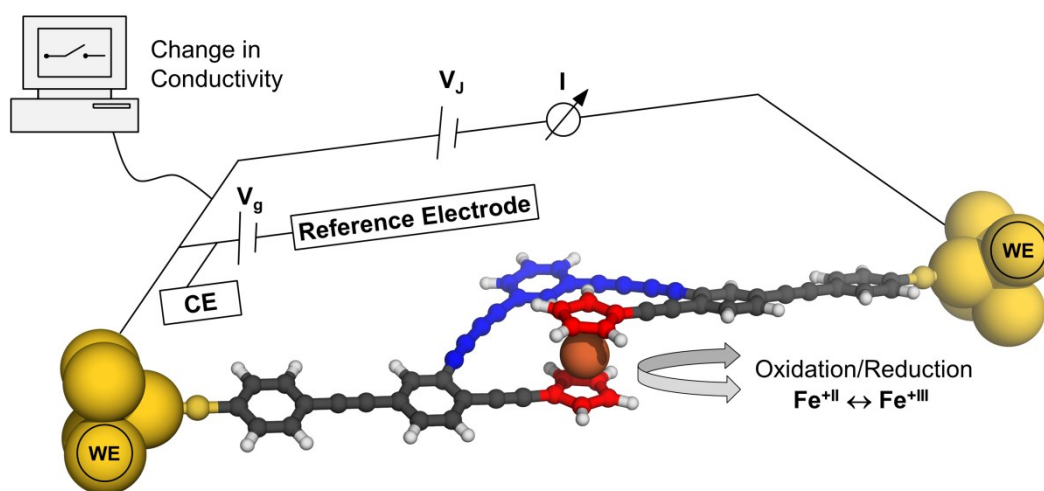


Figure 54. Proposed concept of a switching molecule between two gold electrodes.

The drawback of the presented molecule **3** by Getty et al.^[78] (figure 55) is the rotational freedom of the central ferrocene which allows the molecule to adopt several different conformations, thus leading to different properties. By looking at the observed conductivities of $0.7 G_0$, which is rather unusual for an organic molecule, a “sandwich-form” where both arms are aligned and stabilized by π - π interactions can be assumed. This structural change could have an enormous effect on the conductivity since two wires are measured in the junction at the same time.

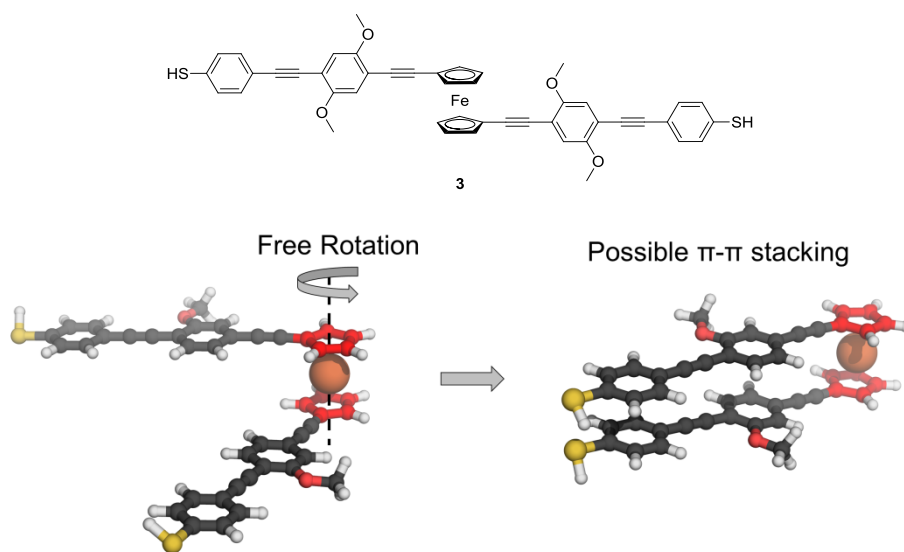


Figure 55. Molecular wire **3** with a conductance of $0.7 G_0$ was reported by S. Getty et al. The issue of a freely rotatable wire leading to the formation of a double wire is illustrated below.

In order to control this possible rotation we designed a similar molecule which is fixed by a rigid linker (figure 56). The linker itself should be as low conducting as possible.

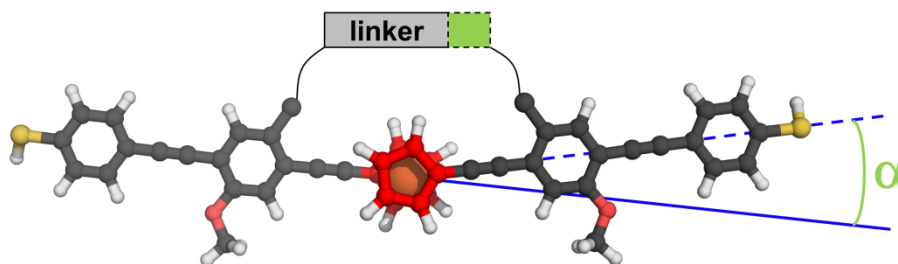
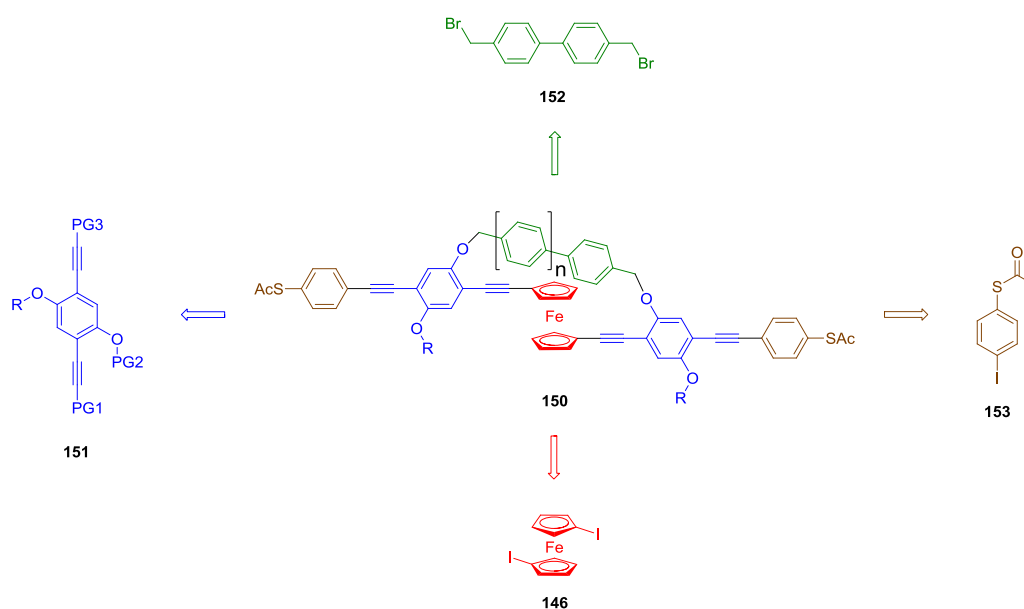


Figure 56. Solution: Top-view of a locked ferrocene derivative. The rigid linker controls the shape of the entire molecule.

4.1.1 Synthetic Strategy

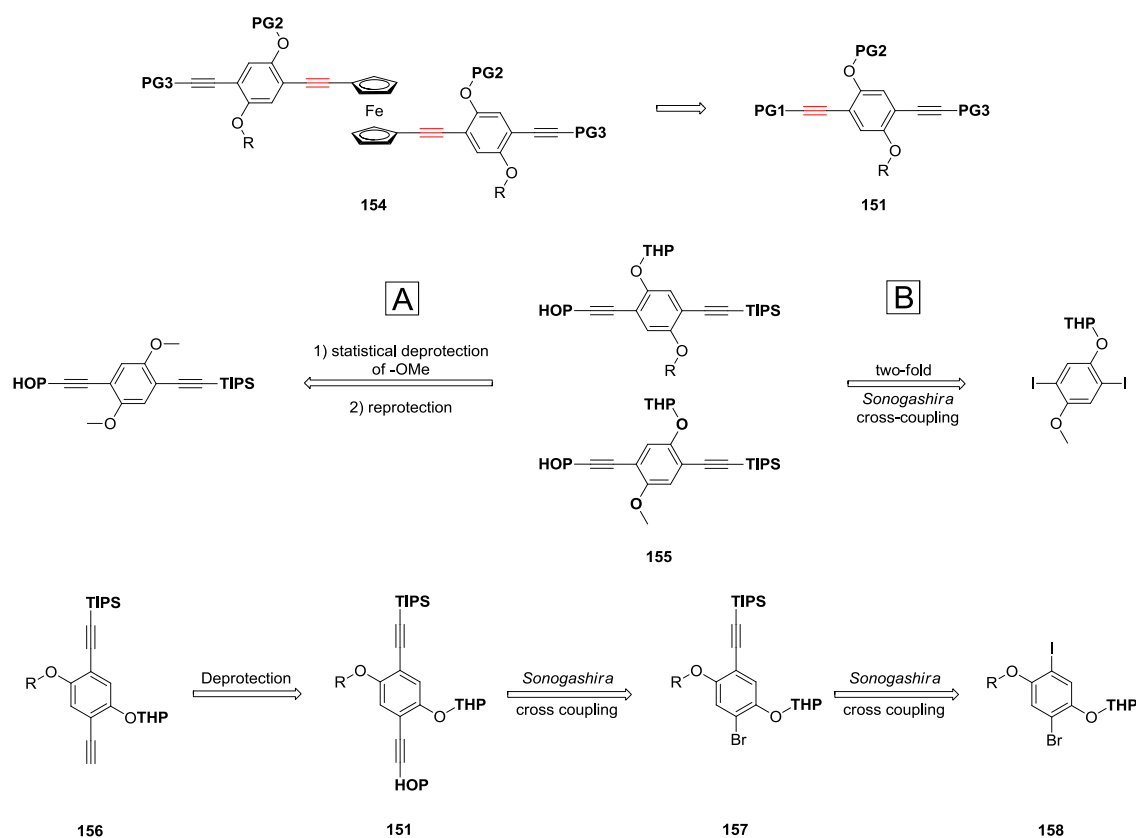
The retro synthetic analysis of a possible target molecule **150** gave us four major building blocks. The central ferrocene unit is substituted in a 1,1'-position. The first disconnection is made between the ferrocene and the acetylene bond. The obvious synthetic approach to form such a bond is a *Sonogashira* cross coupling reaction.^[103,141] The necessary 1,1'-diiodoferrocene can be synthesized within two steps as it is discussed in chapter 3. The introduction of a protected acetylene to the ferrocene followed by a deprotection leaving the free acetylenes is not possible due to fast cyclization to a ferrocenophane.^[293] Therefore, the acetylene had to be on the di-acetylene building block **151** (blue).



Scheme 46. Retro synthetic analysis.

The di-acetylene building block **151** (blue) bears three orthogonal protecting groups to control the assembly of the wire and to avoid the formation of side products. It is important that PG1 can be removed prior to the *Sonogashira* coupling reaction and that PG2 as well as PG3 remain intact. They also need to be stable towards organic bases and higher temperatures. Therefore we envisaged building block **151** as the key intermediate bearing a HOP-PG, a TIPS-PG and on the alcohol a THP-PG (scheme 46).

In addition, it is absolutely essential that the functional group O-PG2 is next to the acetylenes connected to the ferrocene (indicated in red in scheme 47). A statistical approach to make **154** is extremely difficult due to inseparable mixtures (scheme 47, isomers **158**). Regardless which route is applied (A or B) one always ends up with a mixture of regio-isomers **155** which are difficult to isolate since they have similar physical properties. Even if possible to enrich the desired isomer, using an impure compound in the next reaction step would lead to mixtures of higher complexity. Therefore, building block **158** was chosen as key intermediate to introduce the acetylenes stepwise. Building block **158** can be synthesized in 5 steps.^[294] The strategic considerations regarding this building block **158** were discussed in chapter 1.4.

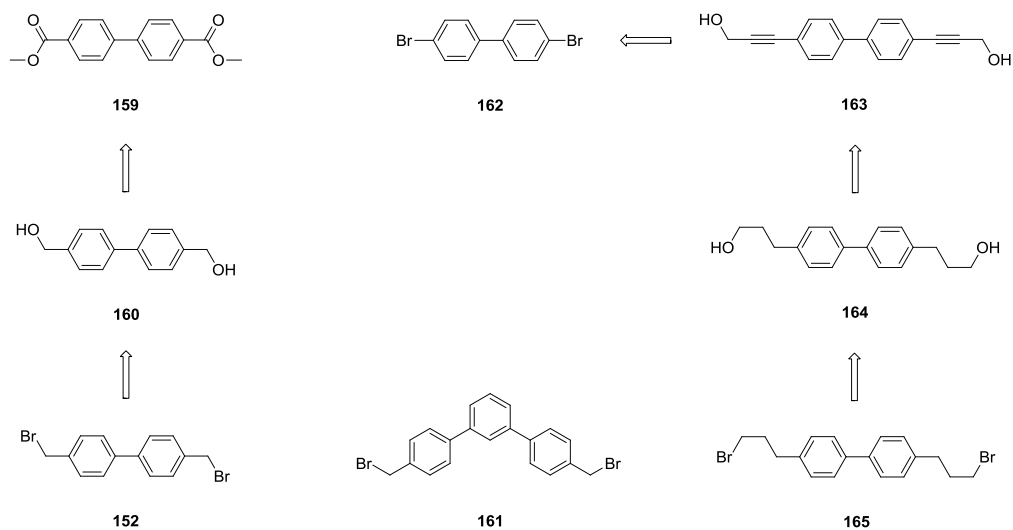


Scheme 47. Strategies for the assembly of building block **154**.

After the first assembly and removal of the THP-PG (red-blue, scheme 46) the free hydroxy groups are in *ortho*-position to the acetylenes which are connected to the ferrocene. We intended to cyclize the molecule via a nucleophilic substitution reaction. Therefore, we proposed a linker bearing two benzylic or aliphatic bromines which are known as excellent leaving groups in S_N2 reactions. The biphenyl linker **152** can be synthesized in two steps whereas the biphenyl linker **165** can be synthesized in three steps. The terphenyl linker **161** is

commercially available. All these target structures were modeled using MMFF (Merck molecular force field) calculations (see next chapter).

Compound **153** (scheme 46) can be synthesized in two steps starting from the commercially available benzenesulfonyl chloride (**191**).^[295]



Scheme 48. Synthetic strategies for linkers **152** and **165**. Linker **161** is commercially available.

4.1.2 Structure Calculation

The choice of the linker was essential to the outcome of the final structure and its rigidity. The possible target structures have been calculated using Spartan 08 (V 1.2.0) with molecular mechanics: MMFF (Merck molecular force field).^[296-299] The idea was to obtain a rigid system which allows the molecule to form a “straight” wire. The first biphenyl-methylene linker (figure 57, top row) shows a kinked rod structure. The terphenyl-methylene linker (middle row) showed a more rod like structure. To increase the probability of a nucleophilic attack at the carbon center more flexible chains were introduced to a biphenyl linker. This biphenyl-propylene linker (bottom row) is not as rigid as the two linkers discussed above but the cyclization should be much easier to achieve. All linkers have been tested in the cyclization reaction.

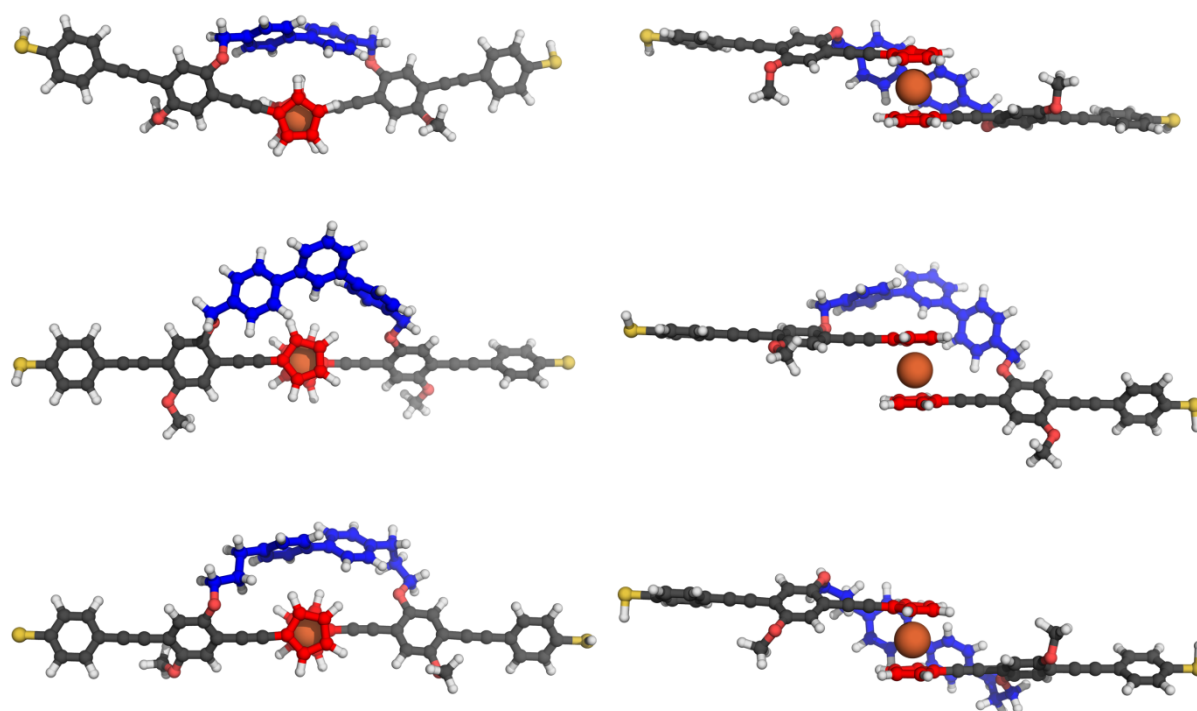
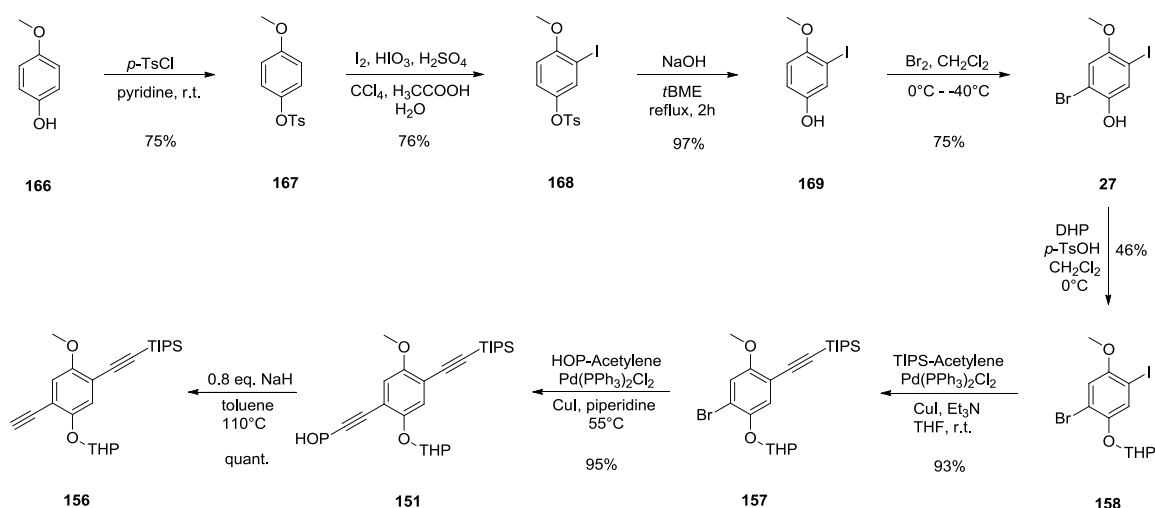


Figure 57. Calculated possible target structures. Left: Top-views. Right: Side-views.

4.2 Synthesis

4.2.1 Synthesis of the asymmetric acetylene building block

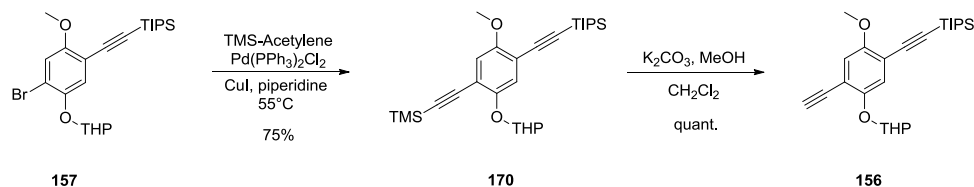
As discussed above building block **156** needs to be synthesized in 8 steps (scheme 49). Starting from the commercially available 4-methoxyphenol (**166**), 4-methoxyphenyl *p*-toluenesulfonate (**167**) was synthesized by treating **166** with pyridine and *p*-toluenesulfonyl chloride at room temperature. Simple recrystallization from methanol gave compound **167** in a yield of 75 %. Compound **167** was then iodinated by using a mixture of iodine, iodic acid, sulfuric acid, chloroform, acetic acid and water. The crude product could again be crystallized from methanol to afford the desired 3-iodo-4-methoxyphenyl-*p*-toluenesulfonate (**168**) in a yield of 76 %. The next deprotection step to **169** was necessary to change the electronic properties of the molecule, thus enabling a substitution *ortho* to the free hydroxy group in the subsequent step. Therefore, compound **168** was dissolved in *t*BME, heated to 55°C and treated with sodium hydroxide. After aqueous workup, compound **169** was isolated in a yield of 97 %. 2-Bromo-5-iodo-4-methoxyphenol **27** was then synthesized by adding bromine to a solution of **169** in methylene chloride at 0°C. After aqueous workup, followed by a recrystallization from heptane the desired compound **27** was isolated in a yield of 75 %.



Scheme 49. 8 step synthesis towards building block **156**.

In the next reaction step, dihydropyran was added to a solution of **27** and *p*-toluenesulfonic acid in methylene chloride to protect the hydroxy group. Compound **158** was isolated in a

yield of 46 % as a white solid. Compound **158** could now be further functionalized in high yields without losing control over selectivity. First a TIPS-acetylene was introduced using standard *Sonogashira* coupling conditions. Thus, compound **158** was added to a mixture of bis(triphenylphosphine)palladium (II) chloride, copper iodide, triethylamine, dry THF and TIPS acetylene. The mixture was stirred at room temperature for 15 hours. The crude product was purified by column chromatography (silica, cyclohexane:ethyl acetate 35:1 + 5% triethylamine) to afford the desired compound **157** in a yield of 93 %. The TIPS-PG was chosen because it is stable in all subsequent reaction conditions and it can be removed under mild conditions once the macrocycle is formed. The second acetylene bearing a HOP-PG was then introduced with another *Sonogashira* coupling reaction. It was found that piperidine as base and solvent leads to excellent yields since the conditions applied for bromine-substitution are usually harsher. Therefore, compound **157** was added to a mixture of bis(triphenylphosphine)palladium (II) chloride, copper iodide, piperidine and HOP-acetylene. The mixture was heated to 55°C and stirred for 17 hours. The desired product **151** was isolated in a yield of 95 % using column chromatography (silica, cyclohexane:*t*BME 5:1 → 1:1 + 5 % triethylamine). The HOP-PG was then removed by dissolving compound **151** in toluene and adding 0.8 equivalents of sodium hydride. The mixture was heated to reflux for 30 minutes. After cooling to room temperature the mixture was filtered over silica to afford the NMR-pure product **156** in “quantitative” yields. The problem of this deprotection is the formation of a side product which is highly fluorescent but is not seen in the NMR-spectrum. The polarity difference of the two compounds is too small to separate the desired product **156** from the side product. Therefore, the product was used as obtained for the next reaction step which resulted in lower yields.



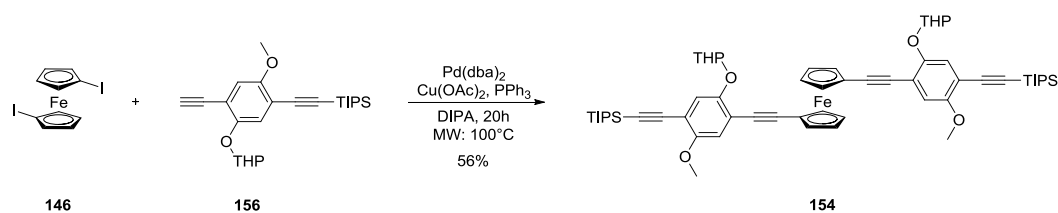
Scheme 50. Synthesis of building block **170** bearing two orthogonal PGs.

To overcome this problem another protecting group was introduced by applying the same reaction conditions as above except TMS-acetylene instead of HOP-acetylene was used (scheme 50). Compound **170** was synthesized and isolated in a yield of 75%. The

deprotection of the TMS-acetylene using methanol and potassium carbonate gave a pure compound **156** in quantitative yields. The drawback of this strategy was the isolation of compound **170** by column chromatography. The polarity differences of starting material **157** and product **170** gave too small R_f difference resulting in a time consuming isolation. By comparing the two protecting groups with each other, the HOP-acetylene was favored over the TMS-acetylene. The advantage of a fast isolation of **151** prior to the deprotection overcame the little yield loss on the next reaction step.

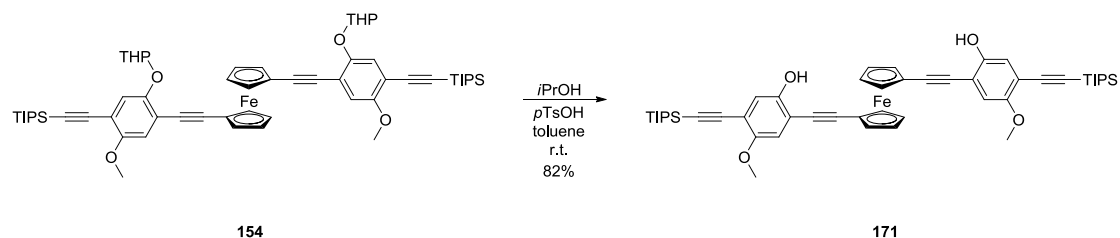
4.2.2 Assembly of the ferrocene wire

The next step in the sequence was the connection of the diacetylene building block **156** with ferrocene **146** by a twofold *Sonogashira* coupling reaction (scheme 51). As already described in the literature the 1,1'-diiodoferrocene (**146**) is not very reactive considering the oxidative addition to a palladium(0) source.^[95] Therefore, cross coupling reactions involving ferrocene derivatives are usually performed in the absence of additional solvents and at higher temperatures. Many catalytic systems and temperatures have been screened to improve yields. Elevated temperature lead to higher yields, however, if the reaction temperature is too high the catalyst decomposes and the homo-coupling reaction is favored. The highest yield was achieved by performing the reaction in a microwave reactor. Compounds **146** and **156** were added to a mixture of bis(dibenzylideneacetone)palladium, triphenylphosphine and copper acetate in pure *iso*-propylamine. The reaction tube was sealed and heated to 100°C for 20 hours. The crude product was purified by column chromatography to afford the desired compound **154** in 56 % yield. The reaction was not complete after 20 hours, however, when the reaction mixture was stirred too long at 100°C, removal of the THP-PG was observed and to some extent dehalogenation of the mono-substituted intermediate also occurred.



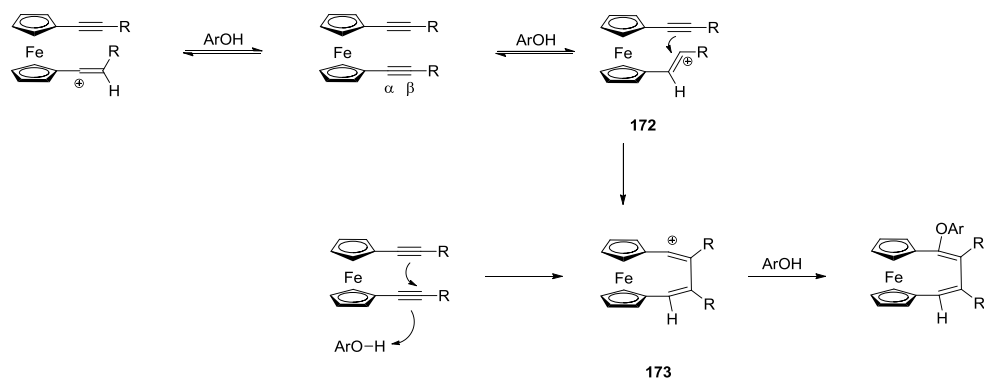
Scheme 51. Sonogashira cross coupling reaction to a 1,1'-disubstituted ferrocene **154**.

Compound **154** was then successfully deprotected by using *iso*-propanol and *p*-toluenesulfonic acid monohydrate to make **171** in a yield of 82 % (scheme 52). It was essential to use the bulky *iso*-propanol to remove the THP-PG since the non-bulky methanol led to the formation of side products.



Scheme 52. Deprotection of the hydroxy group.

Ma et al. reported the formation of undesired ferrocenophane derivatives in their attempt to use 1,1'-di(propynyl)ferrocene in alkyne metathesis (scheme 53).^[300] They extensively investigated acidic as well as basic reaction conditions. It was shown that mildly acidic conditions lead to a reversible protonation at the C_β and, to a lesser extent, at the C_α yielding in a less stabilized carbocation **172** at C_β. This cationic center can now be irreversibly attacked by the other C_β to form a ferrocenyl-stabilized vinyl cation **173**. Alternatively, a concerted reaction path was considered, which avoided the unfavorable β-cationic intermediate by a direct formation of **173**.

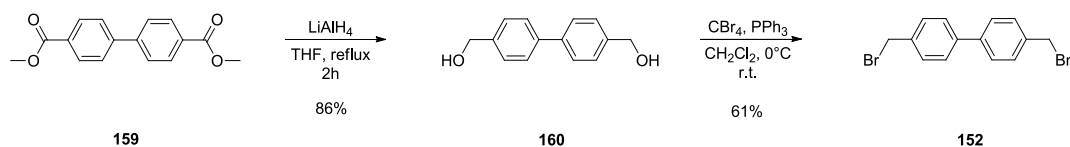


Scheme 53. Mechanism of ring formation as proposed by Ma et al.^[300] showing the formation of a ferrocenophane as a side reaction under acid conditions.

Similar side reactions have also been reported by Pudelski and Callstrom using basic reaction conditions.^[301,302] This issue is discussed in the next chapter.

4.2.3 Synthesis of various linkers

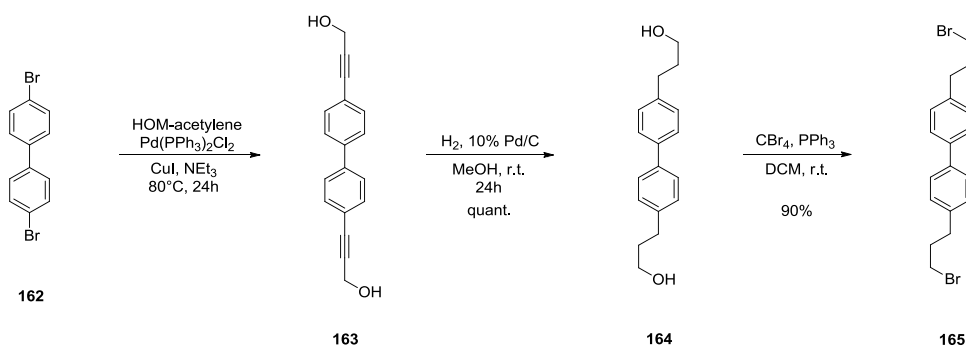
The first linker **152** which was synthesized consisted of a biphenyl-core and two benzylic bromides which can be replaced by nucleophiles (scheme 54). Therefore, the commercially available dimethylbiphenyl-4,4'-dicarboxylate (**159**) was added to a suspension of lithium aluminium hydride and THF. The mixture was allowed to reflux for two hours before it was quenched with water. After an aqueous workup product **160** was isolated in a yield of 86 %.



Scheme 54. Biphenyl-linker synthesis.

An *Appel* reaction was then carried out to replace the hydroxy groups on **160** by bromines. Thus, triphenylphosphine was added to a mixture of compound **160**, carbon tetrabromide and DCM at room temperature. The reaction mixture was stirred for 24 hours followed by a filtration over silica eluting with cyclohexane to afford the desired compound **152** in a yield of 61 %.

The next linker which was synthesized was more flexible due to longer alkyl chains allowing easier access for a $\text{S}_{\text{N}}2$ back-attack for a relatively motion-restricted nucleophile. Starting from the commercially available 4,4'-dibrombiphenyl (**162**) a *Sonogashira* coupling reaction was performed to introduce HOM-acetylene (scheme 55).



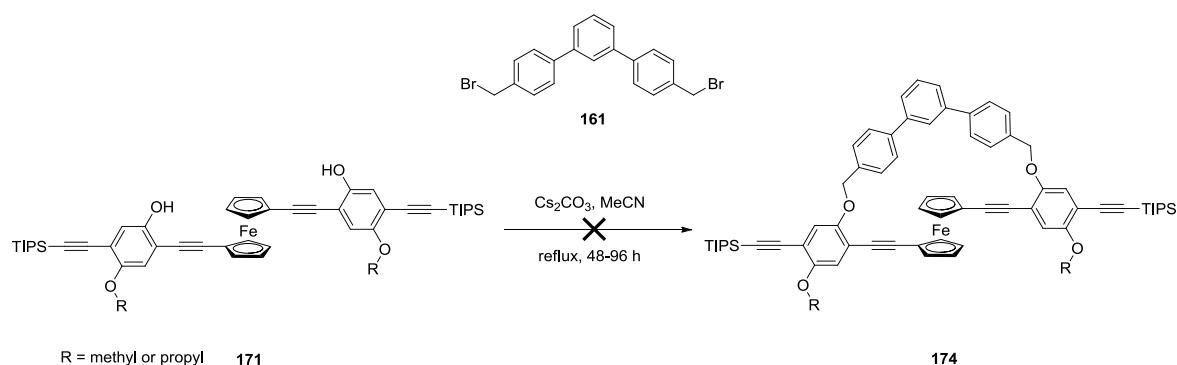
Scheme 55. Biphenyl-linker comprising a more flexible alkyl chain to favor S_N2 reactions.

The acetylene was added to a degassed mixture of compound **162**, bis(triphenylphosphine)palladium(II) chloride, copper iodide and triethylamine at 80°C. The mixture was stirred for 24 hours followed by an aqueous workup. The attempt to purify product **163** by column chromatography failed due to the low solubility of the product. Therefore the crude product was then directly used in the next reaction step.

The reduction of the triple bonds was achieved by applying 4 bar of hydrogen to an autoclave containing compound **163**, 10 % palladium on charcoal and methanol. The starting material was not completely soluble in methanol. Nevertheless, the reaction was stirred for 24 hours at room temperature followed by a filtration through Celite. The crude product was then purified by column chromatography (silica, ethyl acetate: cyclohexane 1:1 → ethyl acetate) to afford the desired product **164** in quantitative yields. At this stage the linker **164** was very soluble due to the increased flexibility of the side chains. The replacement of the hydroxy groups by bromine was again achieved by an *Appel* reaction.^[286] Therefore, triphenylphosphine was added to a mixture of compound **164**, carbon tetrabromide and DCM at room temperature. The crude product was purified by column chromatography eluting with cyclohexane: ethyl acetate (3:1) to afford the desired product in a yield of 90 %.

4.2.4 Cyclization via S_N2 reaction.

In the first cyclization attempt linker **161** was used. This terphenyl linker was relatively rigid and a slightly larger than the biphenyl linker **152** increasing the chance for a S_N2 attack of the phenolate. As displayed in figure 57 in section 4.1.2 the possible macrocycle should form a straight molecular wire. To favor an intra-molecular cyclization over an inter-molecular polymerization a pseudo-high dilution strategy was envisaged. Therefore, compound **171** and compound **161** were each dissolved in 10 ml acetonitrile and taken up by two syringes. These solutions were slowly added with a syringe-pump over 48 hours to a refluxing mixture of cesium carbonate and 20 ml of acetonitrile as shown in scheme 56. Diederich and coworkers have reported that similar cyclization reactions were favored by the use of cesium carbonate over weaker bases such as potassium- or sodium carbonate.



Scheme 56. Cyclization attempt to form macrocycle **174**.

During the reaction the formation of a new main product was observed. The newly formed compound was much more non-polar than the starting material which could make sense consistent with a loss of the polar hydroxy groups. However, NMR-studies did not confirm that a substitution took place. MALDI-MS and ESI-MS studies revealed that the new compound had the same mass as the starting material yet the NMR signals were clearly shifted (figure 58). A second product which could be isolated indicated in the NMR spectrum that a mono-substitution took place. The resulting mass on the other hand could not be identified by MALDI and ESI-MS. It seemed that the substitution took place on one arm of the molecule and another side reaction took place on the other arm.

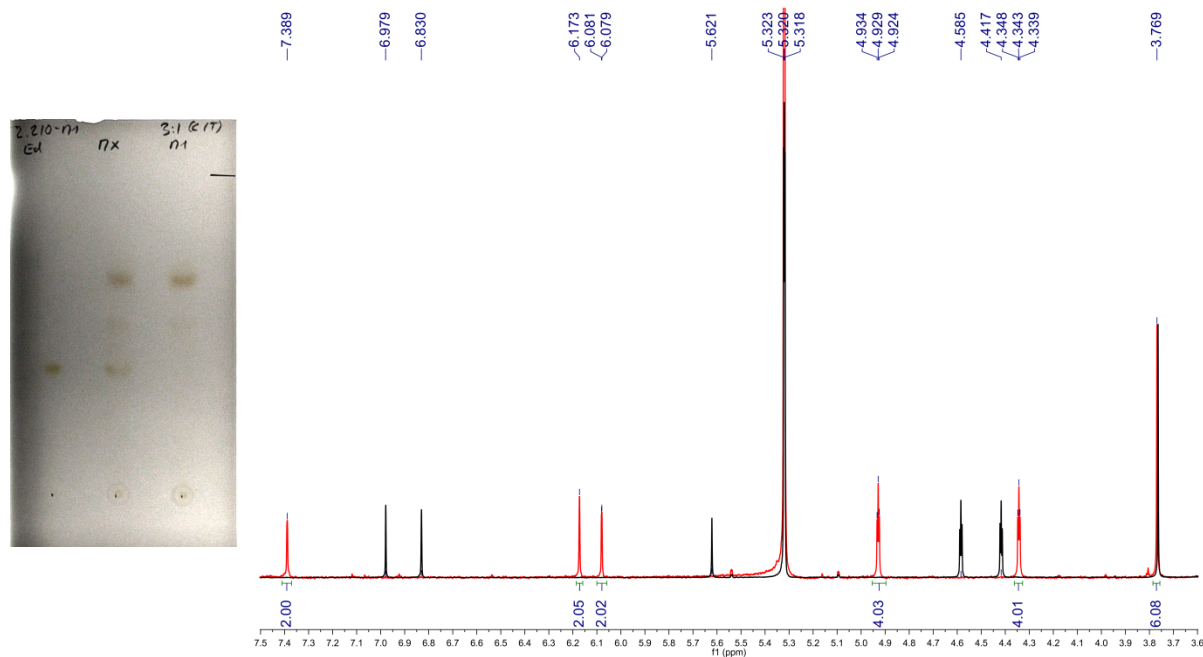
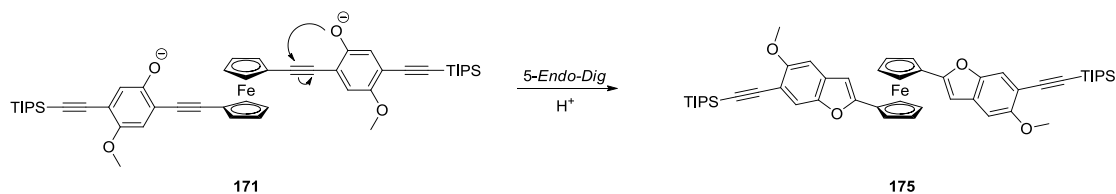


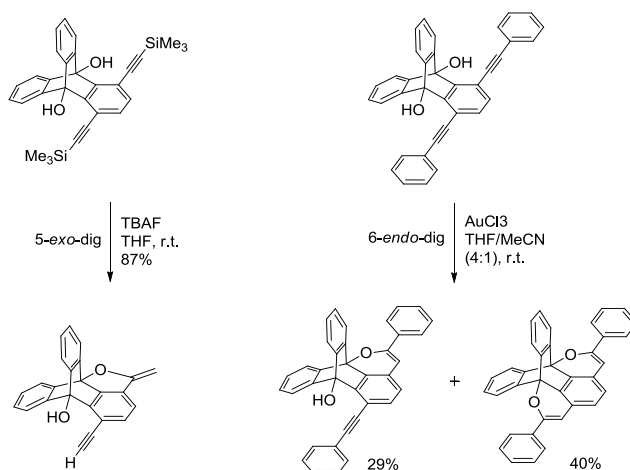
Figure 58. TLC plate showing the starting material **171** on the left side and two new products on the right side. NMR showing traces of the starting material **171** (black) and the formed side product (red).

By looking at the NMR trace of the formed side product (red trace) a clear high field shift of an aromatic proton to 6.15 ppm can be observed and a new proton appears at 6.0 ppm. The proton of the free alcohol (black trace) at 5.6 ppm disappears and the two proton signals of the cyclopentadienyl rings are shifted apart to 4.97 and 4.38 ppm respectively. Taking into account that the mass remains the same and a high field shift of a proton can be observed, a 5-*Endo-Dig* cyclization can be concluded (scheme 57).^[303,304] Such a cyclization could lead to a double bond, hence the appearance of a new proton signal although the mass would remain the same.



Scheme 57. Reasonable mechanism of the side product formation.

Swager and coworkers reported cyclization reactions on similar molecules (scheme 58). Therefore, we have tried to identify our proposed structure by HMBC- and HMQC-experiments (figure 59).



Scheme 58. Similar cyclization reactions reported by VanVeller et al.^[305]

By looking at the full HMBC spectrum (figure 59) we can exclude the presence of a carbonyl group since we have no coupling signals above 190 ppm.

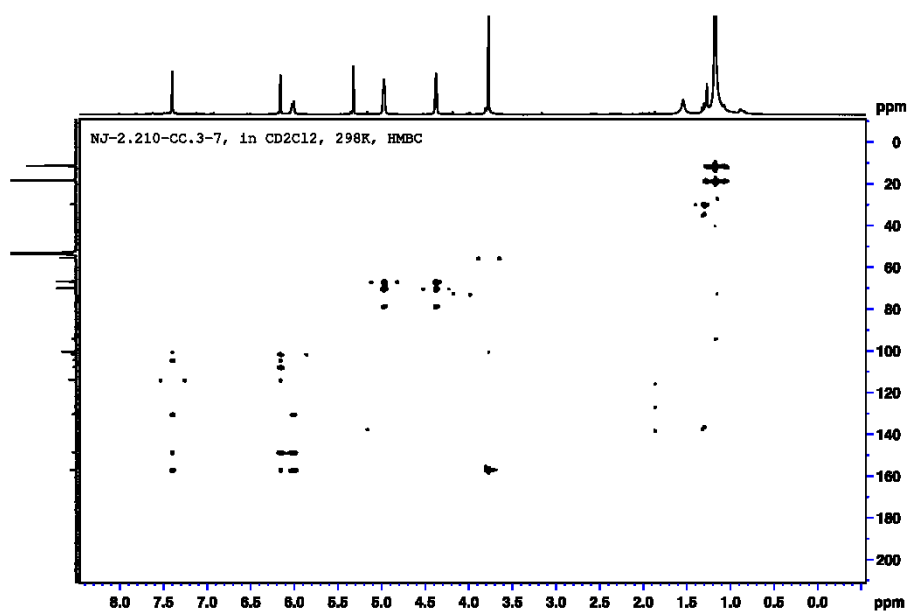
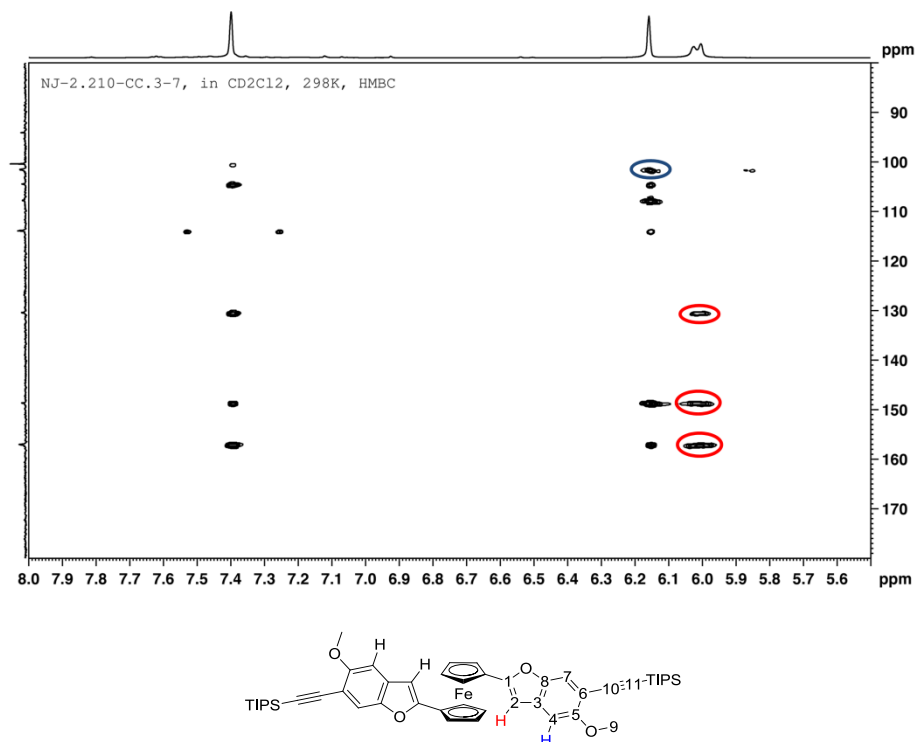


Figure 59. Full HMBC spectrum of compound 175.



When we zoom in we can see a $^3J_{C,H}$ coupling between the blue proton (6.15 ppm) and C-2 (101.5 ppm). We also see two strong $^2J_{C,H}$ couplings between the red proton (6.00 ppm) and C-3 (130.4 ppm) and C-1 (148.7 ppm). In addition, we observe a strong $^4J_{C,H}$ coupling between the red proton and C-5 (157.1 ppm) which is possible due to conjugation. The HMQC reveals the two $^1J_{C,H}$ couplings between the red proton and C-2 (101.5 ppm) as well as the blue proton and C-4 (100.4 ppm).

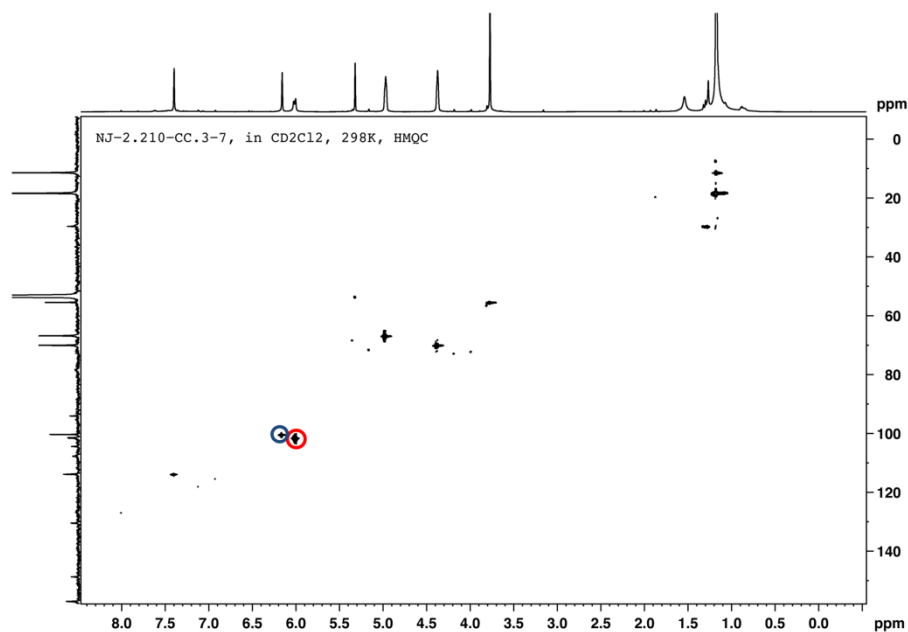
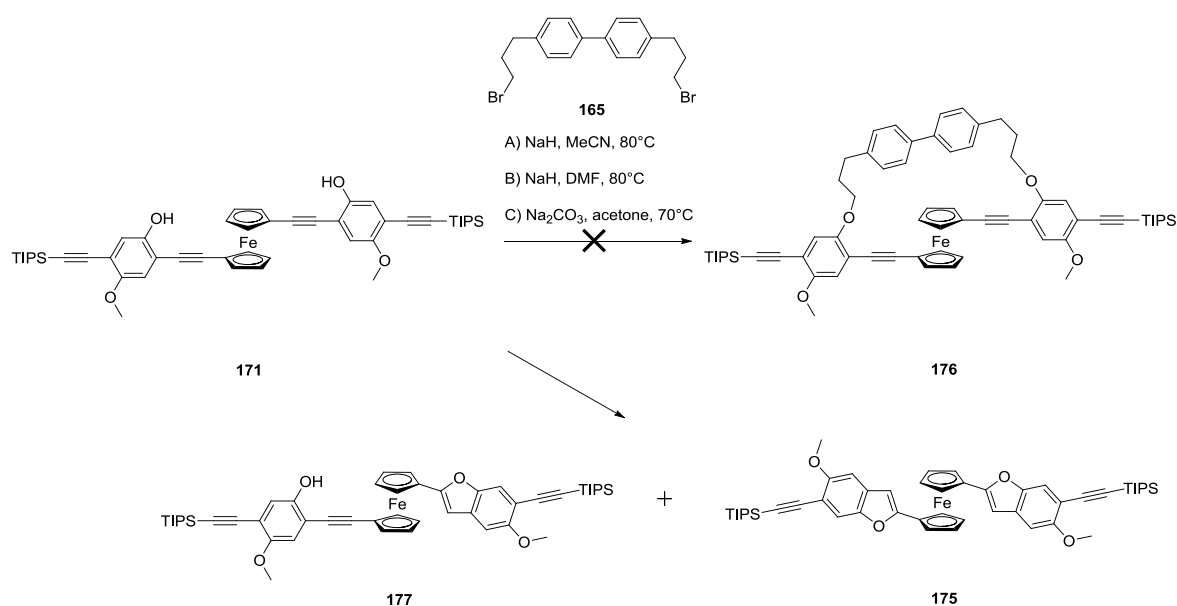


Figure 60. HMBC (top) and HMQC (bottom) of compound 175.

The next idea was to use a weaker base such as sodium carbonate which usually deprotonates the hydroxy after the nucleophilic attack. With this change we expected that the nucleophilic attack at the benzylic position of the linker **161** is faster than a cyclization with the triple bond. Therefore, the same reaction conditions were applied except sodium carbonate was used instead of cesium carbonate. To our disappointment, the same cyclization took place and **175** was formed as the main product. Either the base was too strong or the terphenyl linker **161** was too rigid to find the optimal geometry for a second S_N2 attack.

The previously discussed linker **165** was then used to attempt a cyclization (scheme 59). Linker **165** has a longer carbon chain to provide more flexibility for a second S_N2 attack. The first attempt was carried out using sodium hydride as base in acetonitrile at 80°C. The starting materials **171** and **165** were again slowly added over 48h to create a pseudo high dilution reaction. The reaction again formed undesired side products **175** and **177** which could be identified by NMR- and mass-spectroscopy.



Scheme 59. Cyclization attempt with a more flexible linker **165** using various reaction conditions. The side reaction to **175** and **177** occurred much faster than the nucleophilic attack of the hydroxy group on the linker.

As one can see in the picture of the TLC plate the same non-polar products were formed. The observed masses in MALDI- and ESI-MS measurements indicated that again a *5-Endo-Dig* cyclization took place.

Other polar/aprotic solvents such as DMF and acetone were then investigated. In the first attempt, DMF and sodium hydride as base were used. The formation of the non-polar side product was not observed (figure 61, blue box). However, the prepared solution of starting material in DMF darkened during the addition to the reaction mixture. The NMR revealed that this newly formed slightly less polar product was asymmetric indicating to two different arms on the central ferrocene. The mass which was found was again the same as the starting material. We inferred that only one side of the starting material underwent a *5-Endo-Dig* cyclization and that the other one remained intact.

In the second attempt, acetone as solvent and sodium carbonate as base was used. We observed again the formation of a slightly less polar product (figure 61, left TLC). The TLC shows that the starting material **171** was completely consumed after 48 hours (TLC's on the right) and that the linker **165** was still present (blue circle, right). NMR- and mass-spectroscopy showed again the formation of undesired side product **177** in the black circle and some formation of the double cyclized **175** in the red circle.

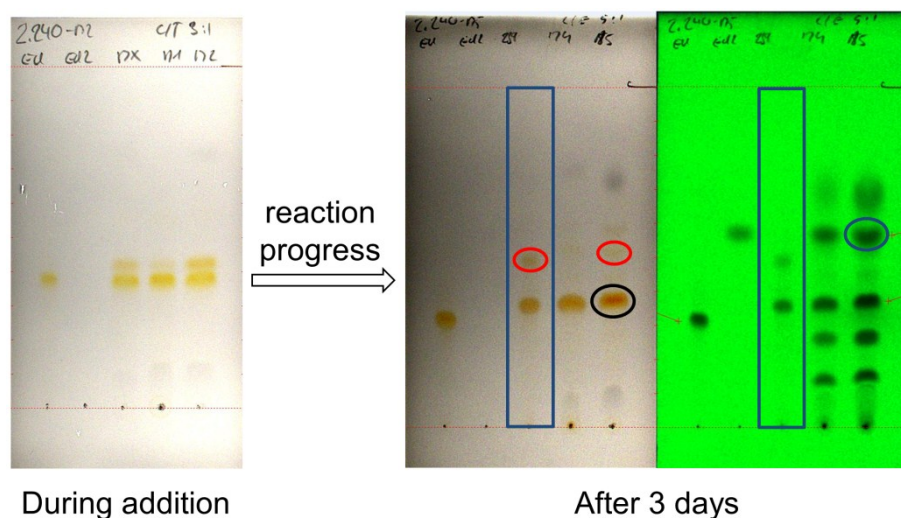


Figure 61. Left: TLC during the addition of starting material **171** and linker **165**. Right: TLC 48h after the addition was complete. The blue box shows the sample obtained from the reaction using DMF as solvent. Red circle) Side product **175**. Black circle) Side product **177**.

Based on these results we had to change our synthetic approach to connect the two arms. As we learned from another project (discussed in the next chapter) homo-coupling cyclization reactions are favored by similar ferrocene compounds. Therefore, we envisaged a cyclization via *Cadiot-Chodkiewicz* type coupling.^[306,307]

4.2.5 Cyclization via Cadiot-Chodkiewicz coupling

As discussed above a new cyclization approach was envisaged using the *Cadiot-Chodkiewicz* coupling to connect the two arms in molecule **171** with each other. The MMFF calculations showed that a simple benzene unit which is meta-substituted by two diacetylenes (blue part) forms a rigid structure as illustrated in figure 62.

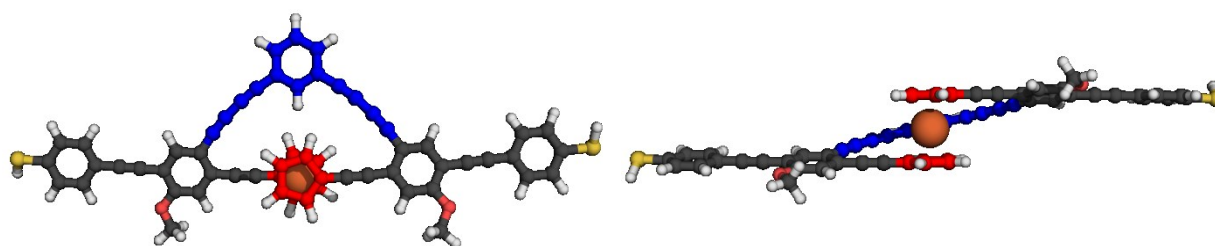
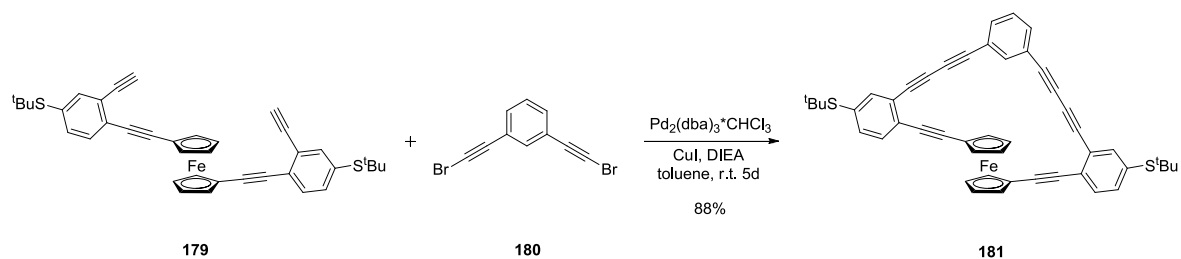


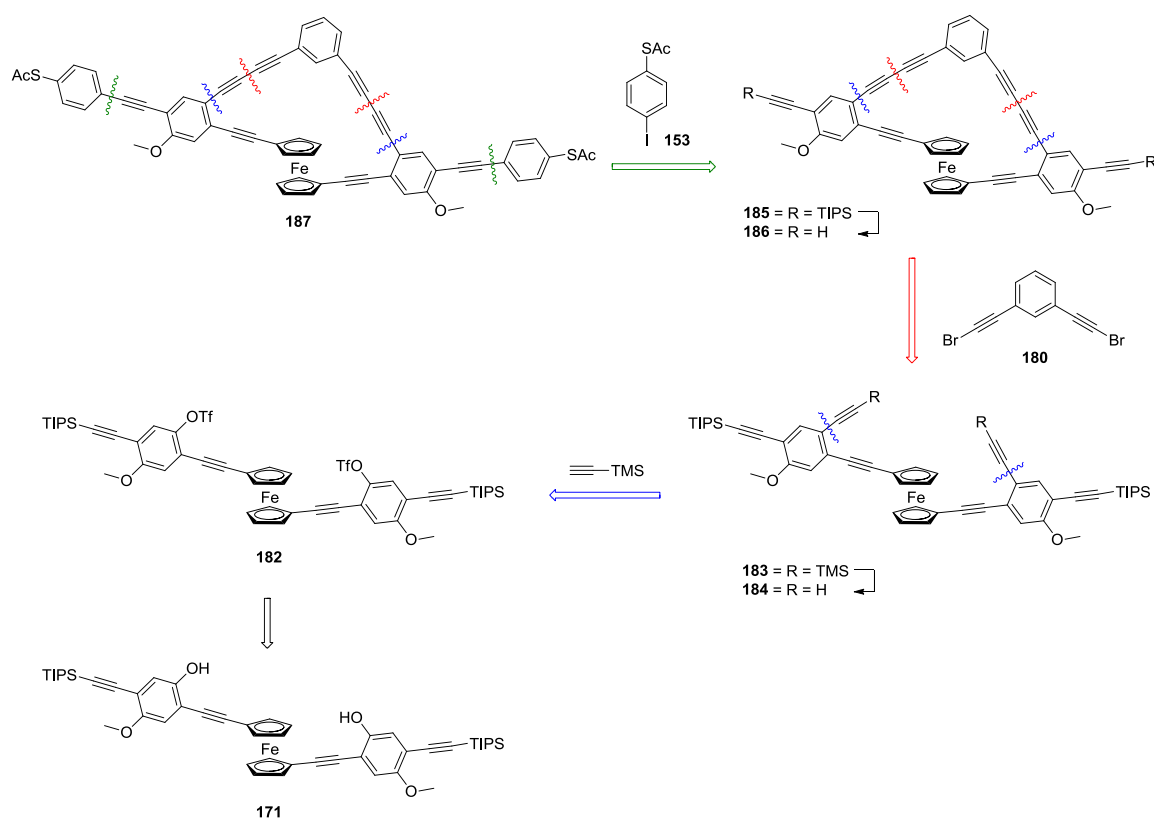
Figure 62. Proposed structure calculated with Spartan using MMFF. Left: Top-view of molecule **178** bearing a rigid diacetylene linker (blue). Right: Side view of molecule **178**.

A test cyclization reaction was carried out to see whether such a cyclization is possible or not. A ferrocene compound **179** which was obtained from another project (chapter 5) was used to interlink the two arms with each other (scheme 60). Therefore, compound **179** and linker **180** were dissolved in toluene and slowly added with a syringe pump to a mixture of tris(dibenzylideneacetone)dipalladium-chloroform, copper iodide, DIEA and toluene. The educts **179** and **180** were added within 24 hours to create pseudo high dilution conditions. After the addition was complete, the reaction mixture was stirred for four days. The crude product was purified by column chromatography eluting with cyclohexane:*t*BME (20:1) to afford the desired product **181** in 88 % yield.



Scheme 60. Cyclization of ferrocene derivative **179** using a *Cadiot-Chodkiewicz* coupling.

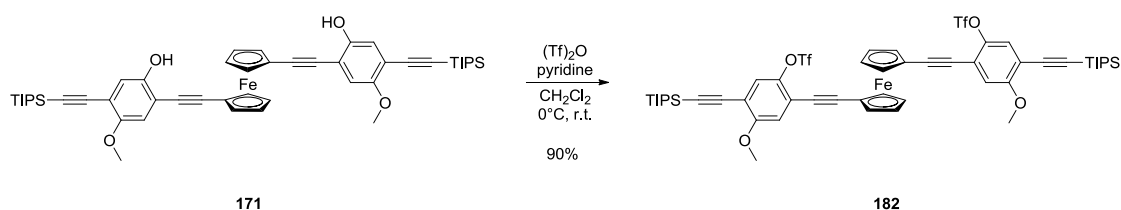
To apply these findings we had to change our molecule (scheme 61). The strategic considerations were based on compound **181** which we had already in hand from our previous synthetic work. In the first step, the hydroxy groups in molecule **171** have to be transformed into triflates which are suitable for oxidative additions to palladium sources. Once we have compound **182** in hand, TMS-acetylene can be introduced to obtain **183** by a *Sonogashira* coupling reaction. The TMS-PG can then be removed to expose the acetylenes. This compound **184** can undergo a two-fold intermolecular *Cadiot-Chodkiewicz* type coupling with linker **180** which can be synthesized according to a literature procedure.^[307] Once the ferrocenophane **185** is assembled a deprotection of the TIPS-acetylenes followed by a *Sonogashira* cross coupling leads to the possible target structure **187**.



Scheme 61. Strategic considerations towards molecule **187**.

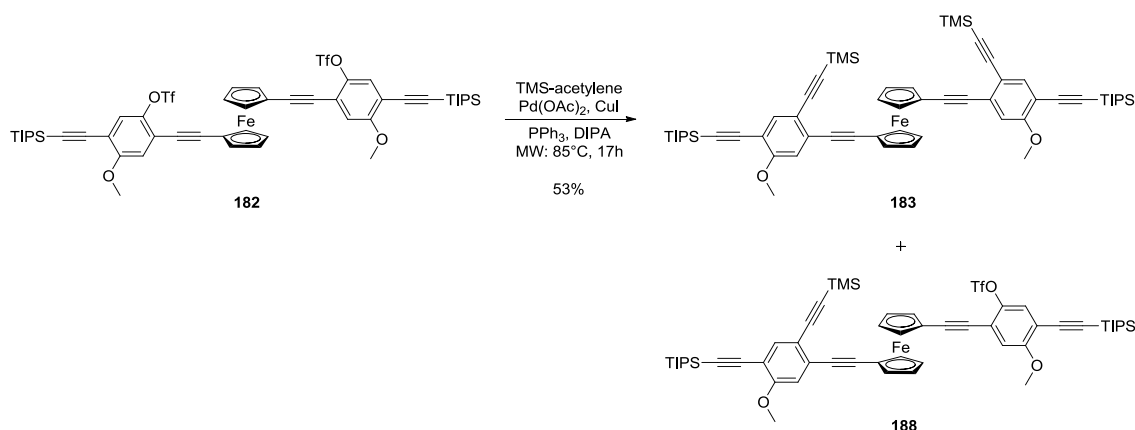
4.2.6 Synthesis

In the first step the hydroxy groups in molecule **171** had to be transformed into triflates. Therefore, compound **171** was dissolved in dry DCM and cooled to 0°C. Then triflic anhydride dissolved in DCM was slowly added. The mixture was allowed to warm to room temperature and was stirred for 1 hour. After aqueous workup the desired compound **182** was obtained in a yield of 90 % (scheme 62).



Scheme 62. Transformation of hydroxy groups into triflates.

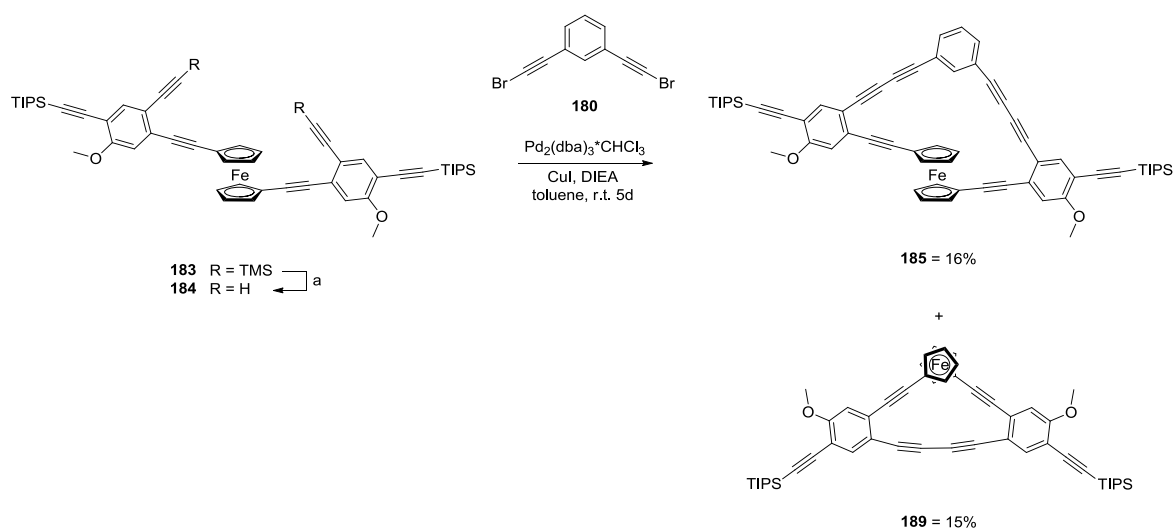
The next reaction step was not as easy as expected. We tried several *Sonogashira* coupling conditions to introduce the TMS-acetylenes into compound **182** (scheme 63). It seemed that the oxidative addition of the palladium was difficult. We tried different catalysts such as bis(triphenylphosphine)palladium(II) chloride, palladium(II) acetate and bis(dibenzylideneacetone)palladium(0). In addition different solvent and bases were screened.



Scheme 63. Introduction of TMS acetylene to make compound **183**.

The best reaction yield was obtained by using palladium(II) acetate and triphenylphosphine (4 equiv. based on catalyst) as catalyst, copper iodide as co-catalyst, diisopropylamine as base and solvent and 40 equivalents of TMS-acetylene. The reaction was carried out in the microwave reactor at 85°C (~62 W) for 17 hours. When the reaction temperature was increased (>90°C), the palladium precipitated as black-palladium. When the temperature was decreased, the reaction was too slow to observe any conversion. After the reaction was complete, the mixture was diluted with *t*BME and filtered over Celite. The filtrate was concentrated and the residue was purified by column chromatography (1st column: silica, cyclohexane: *t*BME 20:1; 2nd column RP18-silica, acetonitrile:THF 3:1) to afford the desired compound **183** in a yield of 53 %. The mono-substituted product **188** had almost the same RF-value as the starting material **182** on the TLC. As a result it was not separated from the starting material and reused to repeat the reaction several times. The 53 % yield of the above described reaction is probably too high since the starting material already contained mono-substituted **188**.

Once we had compound **183** in hand a deprotection of the TMS-acetylene was performed in quantitative yields by using an excess of methanol and 2.2 equivalents of potassium carbonate (scheme 64). The diacetylene **184** was then used in a *Cadiot-Chodkiewicz* cyclization reaction with the previously obtained compound **180**.^[306,307]



Scheme 64. a) MeOH, K₂CO₃, DCM, r.t., quant. *Cadiot-Chodkiewicz* cyclization reaction between compound **184** and **180** to make **185** plus a side product **189**.

Therefore, compounds **184** and **180** were each dissolved in toluene and slowly added over 40 hours to a mixture of tris(dibenzylidene-acetone)dipalladium*chloroform (32.5 mol%), copper iodide (83 mol%) and DIEA in toluene at room temperature. After the addition was complete the reaction was stirred for five days. The final concentration of the reaction mixture was 0.27 mM, however, due to the very slow addition of the starting materials **184** and **180**, an extremely low concentration was maintained to favor an inter-molecular coupling followed by an intra-molecular coupling.

After the reaction was complete, the mixture was extracted and concentrated under reduced pressure and the residue was purified by column chromatography (1st column: silica, cyclohexane: *t*BME 20:1; 2nd column RP18-silica, acetonitrile:THF 2:1) to afford the desired macrocycle **185** in a yield of 16 %. A side product **189**, which was formed due to direct intra-molecular homo-coupling, could also be isolated in a yield of 15 %.

An interesting interchelation effect was observed during the NMR studies of compound **185**. The first recorded NMR (in CD₂Cl₂) showed 4 distinct signals for the central ferrocene structure which is reasonable since the free rotation around the ferrocene axis is blocked. However, when the sample was concentrated again and later dissolved in another solvent (*d*-acetone) only two signals occurred. The cavity of compound **185** probably contained remaining solvent molecules from the column chromatography such as tetrahydrofuran or the less expected acetonitrile. Compound **185** was then again measured in CD₂Cl₂ to see if more than two signals for the ferrocene protons occur, but again only two signals were observed. The signal at 8.6 ppm (blue) disappeared after the first solvent exchange and never appeared again. The NMR traces are shown in figure 63 with the first NMR (blue) being recorded in CD₂Cl₂ after column chromatography, the second one was recorded in *d*-acetone (green) and the third one was again recorded in CD₂Cl₂ (red).

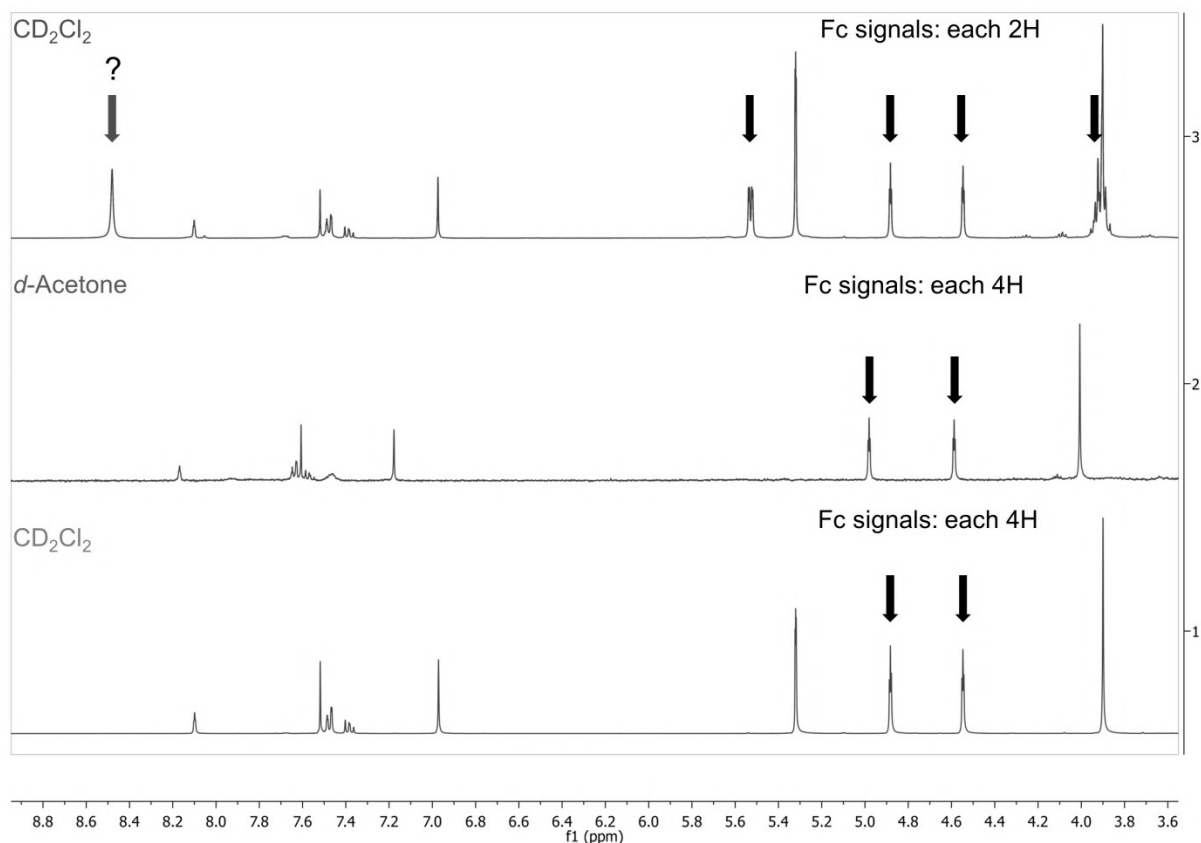


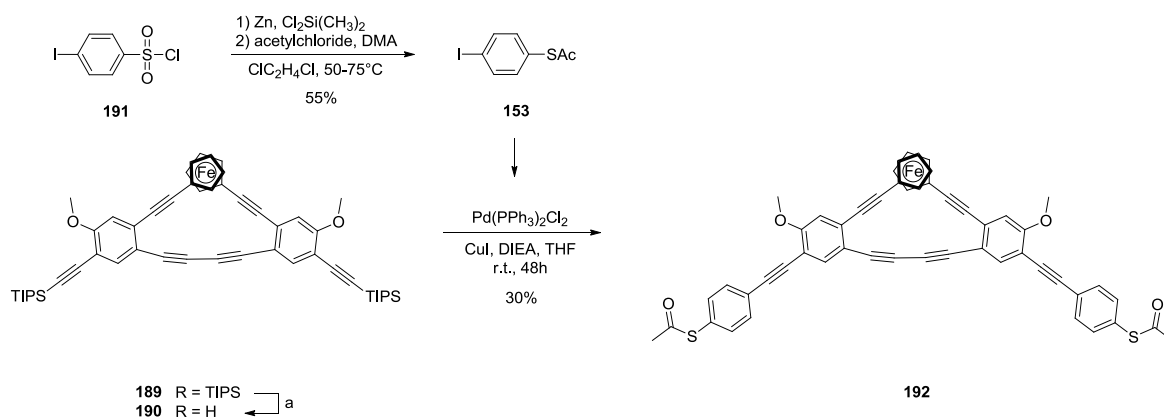
Figure 63. NMR traces of compound **185**. Top) **185** recorded in CD_2Cl_2 after column chromatography. Middle) **185** recorded in *d*-acetone. Bottom) **185** was recorded again in CD_2Cl_2 . The signal at 8.6 ppm (top) disappeared after the first solvent exchange and never appeared again.

The previously obtained side product **189** has an interesting structure as well because the diacetylene-bridge is in meta-position and therefore less conductive. This property could be used to manipulate the conductance via the ferrocene which is still in the para-position to the molecular wire. As a first step, compound **189** was dissolved in dry methylene chloride and treated with 2.5 equivalents of tetrabutylammonium fluoride (TBAF, 1M in THF) at room temperature. After two hours, the reaction was quenched with water and extracted with *t*BME. The organic solution was concentrated under reduced pressure to afford the desired compound **190** in quantitative yield (scheme 65, a).

To finish the assembly towards a molecular wire another coupling building block **153** had to be synthesized first (scheme 65). Therefore, the commercially available pipsyl chloride (**191**) was reduced with zinc and the resulting thiol was trapped with acetyl chloride to afford the acetyl-protected sulfur compound **153** in a yield of 54 %.

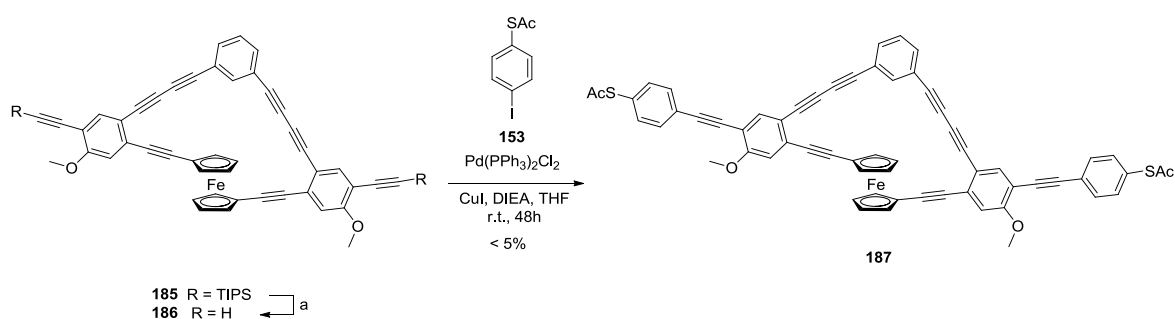
The obtained diacetylene **190** was then coupled with compound **153** using Sonogashira cross coupling conditions. Compound **190** was added to a mixture of 2.3 equivalents of **153**,

bis(triphenylphosphine)palladium(II) chloride (4 mol%), copper iodide (4 mol%) and DIEA in THF. The reaction mixture was stirred for 48 hours at room temperature. After the reaction was complete, the mixture was diluted with *t*BME and filtered over celite. The filtrate was concentrated and the residue was purified by column chromatography (RP18, acetonitrile:THF 4:1) to afford the desired compound **192** in a yield of 30 %.



Scheme 65. a) **189**, TBAF (1M in THF), DCM, r.t. Sonogashira cross coupling reaction between **190** and **153** to obtain **192**.

The same strategy was then applied to the other ferrocene macrocycle **185**. Compound **185** was dissolved in dry methylene chloride and treated with 2.5 equivalents of TBAF (1M in THF) to remove the TIPS-PGs (scheme 66). After two hours the reaction was quenched with water and extracted with *t*BME. The mixture was then concentrated under reduced pressure to afford the desired diacetylene **186** in quantitative yields.



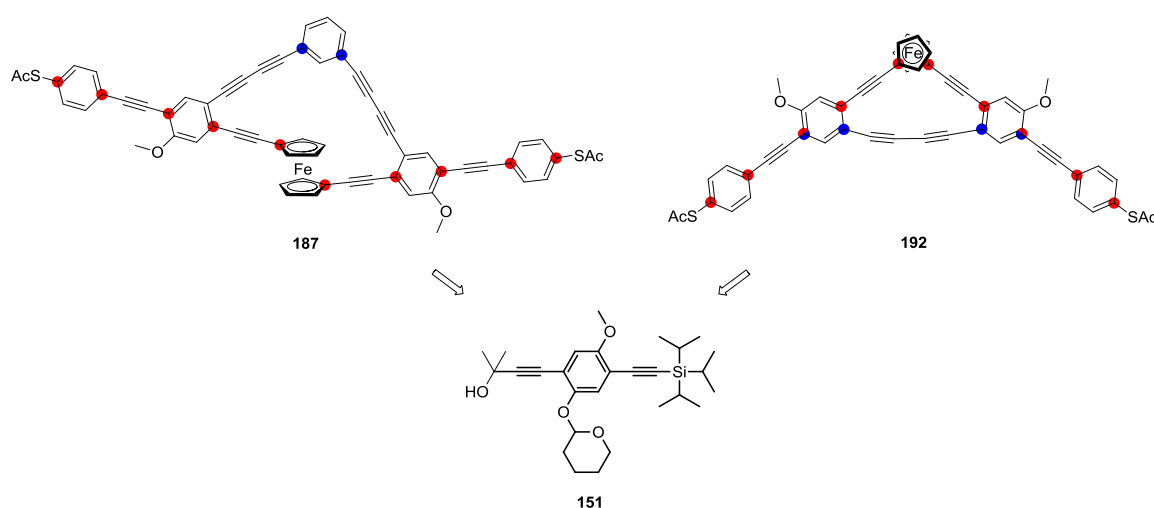
Scheme 66. Synthesis of compound **187** via a Sonogashira cross coupling reaction.

The obtained diacetylene was then added to a mixture of 2.3 equivalents of **153**, bis(triphenylphosphine)palladium(II) chloride (4 mol%), copper iodide (4 mol%) and DIEA in THF. The reaction mixture was stirred for 72 hours at room temperature. After the reaction was complete, the mixture was diluted with THF and filtered over celite. The filtrate was concentrated and the residue was purified by column chromatography (RP18, acetonitrile:THF 4:1). The obtained mixture was less soluble, compared to the previously synthesized compound **192** but still soluble enough to dissolve in the eluent. Once the column was started the product precipitated. The column was eluted with pure THF and chloroform. It was possible to elute some of the product but the majority remained on the RP-silica. The silica was then taken out and washed several times with DMF. The filtrate was concentrated under reduced pressure. The eluted product could be analyzed by MALDI-MS and NMR. The MALDI-MS showed a clear product signal for the charged compound **187** [963 M^+] and an unidentified side product [803 M^+] (see appendix). The mass of the side product could not be assigned to any reasonable fragment of the product. The NMR spectrum revealed that the desired product **187** was present, although not pure (see appendix). Therefore the isolated yield was estimated to be lower than 5 %.

4.3 Conclusion

Two ferroceneophane structures **187** and **192** have been synthesized within 18 steps (scheme 67). The use of building block **151**, which bears three orthogonal protecting groups, was necessary for a successful assembly of these macrocyclic structures. The greatest advantage of building block **151** was the presence of the hydroxy group which could be further functionalized and replaced by an acetylene at a later stage in the project. The developed synthetic strategy allows for a change of the final macrocyclic structure since the cyclization takes place at a very late stage of the synthetic sequence.

Both macrocycles should conduct mainly through the ferrocene unit since their bridging parts are connected in the *meta*-position on the benzene ring (blue dots) which is known to be less conductive than *para*- and *ortho*-substituted benzenes (red dots, scheme 67).^[55]

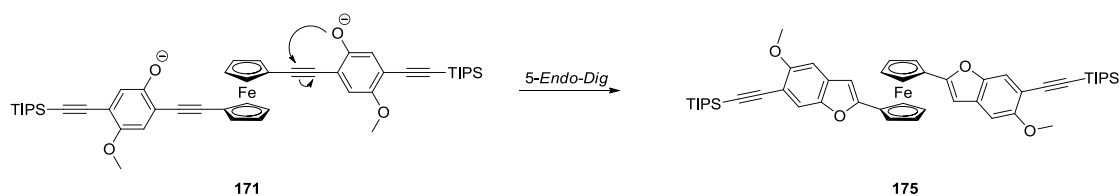


Scheme 67. Synthesized target structures **187** and **192**. The red dots represent the most conjugated pathway. The blue dots represent the less conjugated pathway due to a *meta*-substitution pattern.

The purification at the final step of the synthesis towards compound **187** was very difficult and needs to be improved. As soon as the crude material was loaded onto the column it precipitated. We believe that the acetyl PGs were removed and some sulfur-sulfur dimer formation occurred. These dimers are very insoluble and therefore difficult to analyze and an attempt to reduce the sulfur-sulfur dimer was simply not possible with the amount of material available. However, it was still possible to elute some of the target compound off the column and analyze it with MALDI-MS and NMR. Both techniques showed that the target

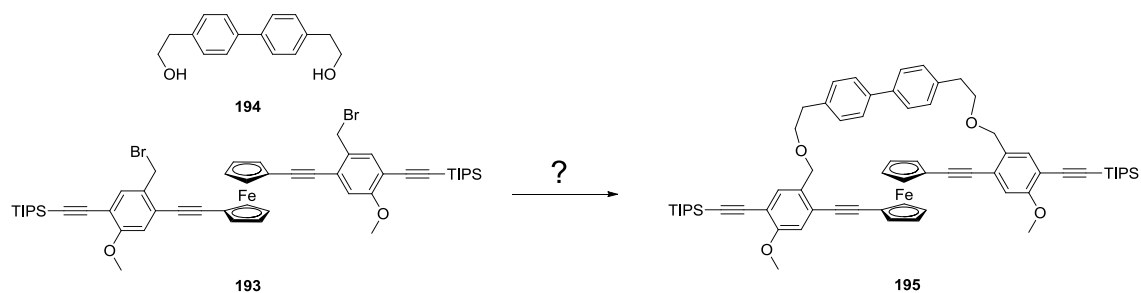
compound **187** was present but not pure. In contrast, compound **192** was very easy to purify by column chromatography. It was possible to completely characterize **192** by 2D NMR and MALDI-MS.

The attempt to cyclize the ferrocene rod **171** with an aliphatic linker failed due to an intramolecular *5-Endo-Dig* cyclization side reaction (scheme 68). This side reaction always occurred in basic media when the OPE-rod was connected to the ferrocene. The basic media was required to deprotonate the hydroxy group to induce the nucleophilic attack on an aliphatic bromide of the linker molecule. The use of sodium carbonate which is a rather weak base and usually deprotonates the hydroxy group after the nucleophilic attack did not favor an intermolecular cyclization.



Scheme 68. The *5-Endo-Dig* cyclization occurred as a side reaction during the attempt to cyclize compound **171** with a linker molecule.

The strategy needs to be changed to overcome this problem. I suggest that the hydroxy groups on **171** should be replaced by benzylic bromides as in **193** and that the hydroxy groups are placed on the aliphatic linker molecule **194** (scheme 69). In such a case we could reduce the presence of a good nucleophile close to the acetylenes avoiding the resulting *5-Endo-Dig* cyclization.



Scheme 69. Proposed change of reaction centers to prevent an intramolecular cyclization.

5 Car-jack molecule comprising two ferrocene joins

5.1 Concept

Another attempt to investigate the influence of a structural deformation on the properties of a molecule can be probed by our proposed molecule **196**. We envisaged a macrocycle with two ferrocene joints. The two ferrocene units are substituted at the 1,1'-positions by flexible acetylenes which are again connected in *ortho*-position to two benzene units. The benzene units bear sulfur anchor groups to contact the molecule with gold electrodes.

As displayed in figure 64 the neutral molecule **196** (green) should have a certain conductivity which can be measured by STM techniques. Once the two ferrocene units are oxidized from Fc^0 to Fc^{+1} , they should push each other apart due to coulomb repulsion. As a consequence of that repulsion the structure should be deformed resulting in a shorter sulfur-sulfur distance (pale red). This change in distance should be detectable by STM measurements. We also expect that the conductivity changes upon oxidation. These features could open the door to new applications such as switches in electronic devices.

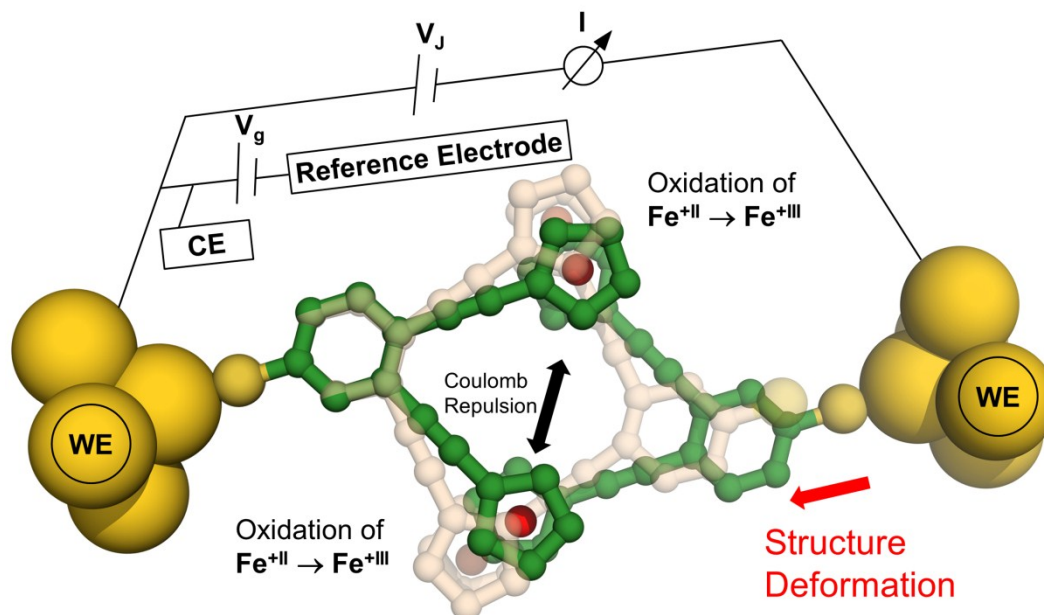
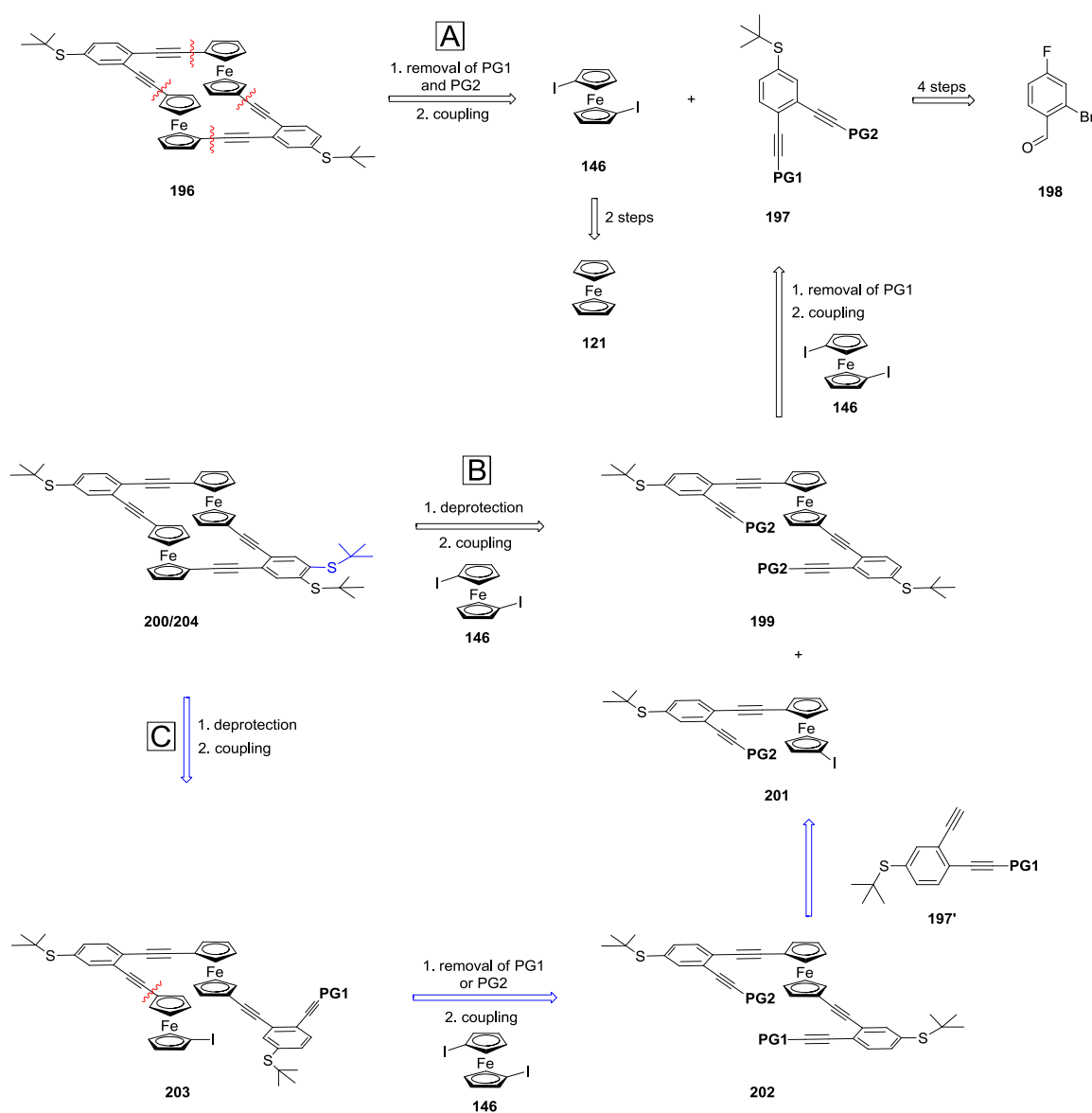


Figure 64. Schematic concept of a structural deformation of a macrocycle upon oxidation. The neutral molecule is displayed in green and the oxidized molecule is displayed in pale red.

5.2 Strategic considerations

This proposed macrocycle **196** can be assembled by three different strategies (A, B and C). The first disconnections are made between the ferrocenes and the acetylenes which gives us the two building blocks **146** and **198** (scheme 70). The easiest way to connect these two building blocks is by a *Sonogashira* coupling reaction.^[95] The synthesis of the diiodo-ferrocene was discussed in chapter 3.5. Building block **197** bears two orthogonal protecting groups and can be synthesized from **198** in four steps.



Scheme 70. Strategic considerations to synthesize molecule **196**.

The most inconvenient route would be if we remove both PG's in **197** and let it react with **146** in a high dilution reaction (strategy A). This would certainly lead to a wild mixture of products which would be impossible to separate. Therefore, strategy A is not favored.

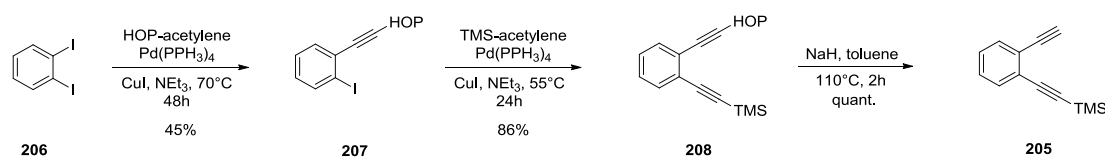
A semi-stepwise approach is displayed as pathway B. In a first step PG1 is removed from compound **197**. The free acetylene is then coupled with diiodo-ferrocene **146** to give **199**. Removing both PG2 in **199** followed by a high dilution coupling reaction with diiodo-ferrocene **146** leads to the target structure **200** (black).

Performing the first coupling reaction between **197** and **146** with sub-stoichiometric amounts of **197**, a mono-substituted ferrocene **201** can be isolated. Now we remove PG2 in **197** instead of PG1 and couple the resulting acetylene **197'** with compound **201** to obtain ferrocene **202**. This ferrocene derivative **202** bears two orthogonal PG's. After we remove only one PG, the resulting free acetylene can be coupled in a statistical reaction with an excess of diiodo-ferrocene **146** to obtain compound **203**. A final deprotection followed by an intermolecular coupling reaction leads to the target structure **204** (blue).

The last proposed strategy C certainly provides the most control over the assembly. However, the two statistical reaction steps usually provide very low yields. Therefore, pathway B is favored over C since the approach is shorter and only the last step should be troublesome due to polymeric side reactions.

5.3 Synthesis

To couple the ferrocene with acetylenes some test reactions were performed to find ideal conditions. Therefore, a benzene derivative **205** bearing two acetylenes ortho to each other was synthesized. The first step was a *Sonogashira* cross coupling reaction to introduce a HOP-acetylene to a 1,2-diiodobenzene (**206**). A statistical approach was chosen to introduce the acetylene only once leaving the second iodine free for further coupling.

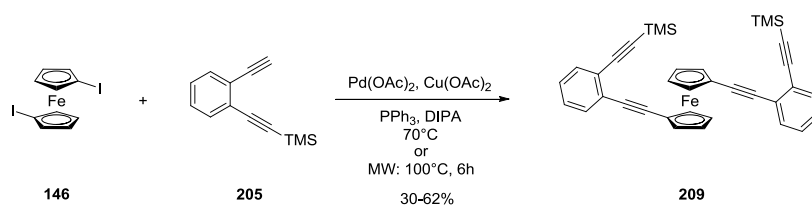


Scheme 71. Synthesis of building block **205**.

These statistical reactions usually give the desired mono-substituted product **207** in a yield of 40-50 %. Since the two iodines in **206** are in *ortho*-position to each other, elevated temperatures were necessary to introduce the acetylenes. Therefore, a mixture of compound **206**, tetrakis(triphenylphosphine)palladium, copper iodide and triethylamine was heated to 70°C for 48 hours. The crude product was then purified by column chromatography, eluting with cyclohexane:EtBME (1:1) to afford the desired product **207** in a yield of 45 %. Due to the increased polarity of the HOP-PG the isolation of **207** from the starting material and the doubly substituted side product was very simple and fast. This would not be the case if, for example, TMS-acetylene or TIPS-acetylene was used in the first step. In the next step, TMS-acetylene was introduced by heating a mixture of compound **207**, TMS-acetylene, tetrakis(triphenylphosphine)palladium, copper iodide and triethylamine at 55°C for 24 hours. The crude product was again purified by column chromatography to afford product **208** in a yield of 86 %.

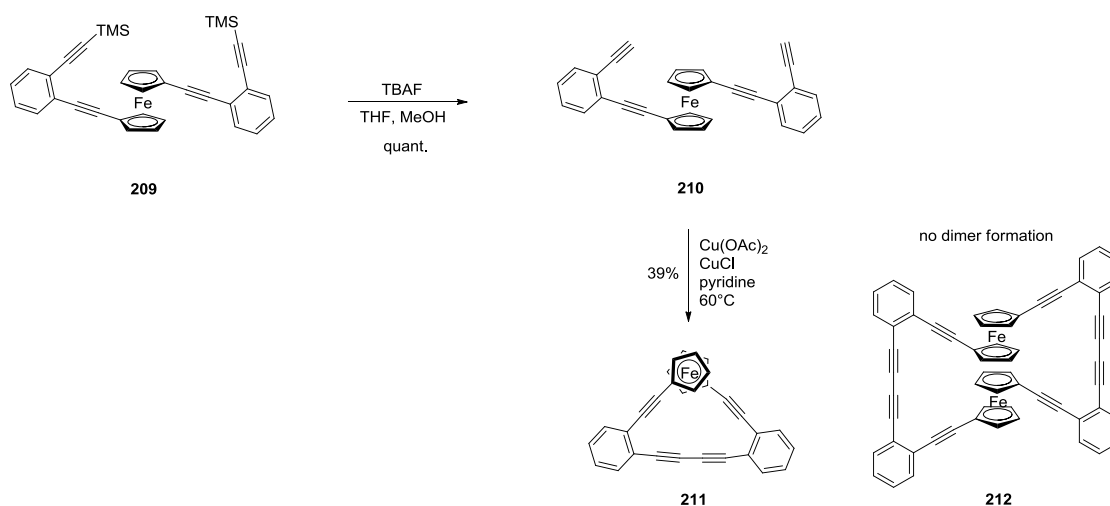
Now, we had compound **208** bearing two orthogonal PG's. The HOP-PG was then removed by heating compound **208** in toluene and sodium hydride to 110°C for 2 hours. The reaction mixture was filtered over a short silica plug and the filtrate was concentrated by reduced pressure to obtain molecule **205** in quantitative yield.

The coupling between **205** and **146** towards **209** was then investigated (scheme 72). As discussed above, such coupling reactions do not always work well. Therefore, many different catalysts, co-catalysts and bases were tested to improve the yield. The best yield of 62 % was achieved by using palladium acetate with four equivalents of triphenylphosphine and copper acetate as co-catalyst in diisopropylamine at 70°C for 42 hours. The reaction time could be shortened to 6 hours by using the microwave reactor at 100°C. Not many catalytic systems were found to be tolerable for elevated temperatures in the microwave reactor. Most of the catalysts decomposed very quickly above 70°C forming black palladium.



Scheme 72. Sonogashira coupling reaction between diiodo-ferrocene **146** and **205**.

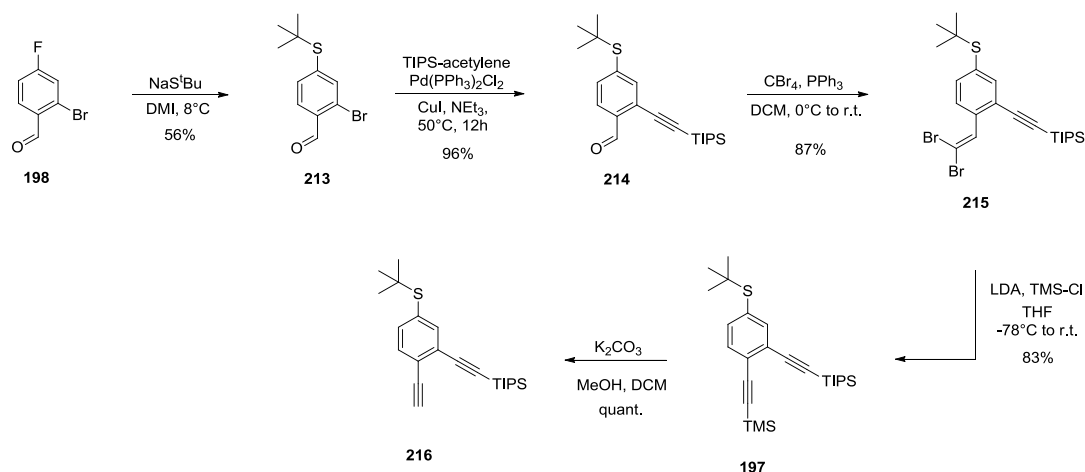
Having compound **209** in hand an oxidative coupling reaction was investigated. We were interested to see if small cycles such as **211** and **212** could be formed. Therefore, we deprotected compound **209** by adding TBAF to a solution of **209** in THF and methanol at room temperature. After filtration over silica the filtrate was concentrated to obtain the deprotected compound **210** in quantitative yield. Compound **210** was then slowly added with a syringe pump to a solution of copper acetate and copper chloride in pyridine at 60°C. The newly formed product was isolated by column chromatography to obtain compound **211** in a yield of 39%. The formation of a dimer **212**, as displayed in scheme 73, was not observed during the reaction or in mass-spectra analysis.



Scheme 73. Homo-coupling of compound **210**.

The next building block **197** was synthesized within four steps starting from the commercially available 2-bromo-4-fluorobenzaldehyde (**198**) (scheme 74). The first step was a nucleophilic substitution on the activated fluoride with a thiolate.^[308,309] This reaction follows an addition-elimination mechanism which means that the nucleophile binds in a first step to a vacant π^* -orbital. In a second step the leaving group eliminates which leads to the overall substitution reaction. Electron-withdrawing groups (EWG) stabilize ortho and para to the position of substitution. Without such an EWG present, nucleophilic aromatic substitution occurs only under extreme conditions. Another important factor is the leaving group. Halides have a polarization effect on the carbon center which increases the overall reaction rate. In our case, the fluoride is more suitable for substitution than the bromide as it is more electronegative and thus has a larger polarization effect. However, when we added the thiolate to the reaction

mixture at room temperature, we observed the formation of doubly substituted side products which were difficult to separate.



Scheme 74. Synthesis of building block **197**.

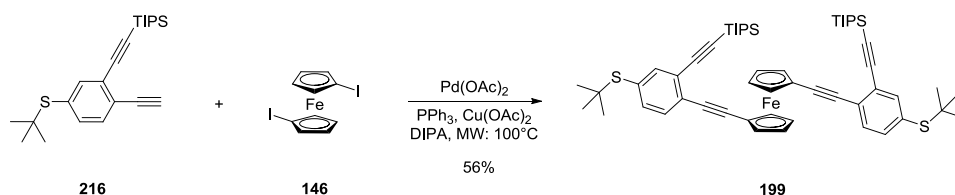
Therefore, we cooled the reaction mixture containing compound **198** and DMI to approximately 8°C (m.p. of DMI) and slowly added 1 equivalent of thiolate. After aqueous workup and column chromatography, product **213** was isolated in 56 % yield. In this case, the formation of a doubly substituted side product was not observed. For the next reaction step a protected acetylene was introduced by a Sonogashira coupling reaction. The first acetylene which was introduced was a TMS-acetylene. This reaction worked in a yield of 84 %, however, the reaction two steps later where the acetylide needs to be trapped with TIPS-chloride did not work. The next acetylene which was introduced was HOP-acetylene to gain more polarity in the molecule. This reaction worked fine but again the formation of the acetylene out of the aldehyde did not work. Then TIPS-acetylene was introduced by adding the acetylene to a mixture of compound **213**, bis(triphenylphosphine)palladium chloride, copper iodide and triethylamine. The reaction mixture was heated to 50°C and stirred for 12 hours. The crude product was purified by column chromatography to obtain the desired product **214** in a yield of 96 %.

The transformation of the aldehyde into a terminal acetylene was made by a *Corey-Fuchs* reaction.^[310] This two-step methodology starts with a *Wittig*-type reaction to form a dibromoalkene **215** by adding triphenylphosphine to a mixture of compound **214** and carbon tetrabromide in DCM. The crude product was isolated by column chromatography eluting with cyclohexane:*t*BME (5:1) to afford product **215** in a yield of 87 %. The dibromoalkene

215 was dissolved in THF and treated with lithium diisopropylamine to generate the bromoalkyne intermediate via dehydrohalogenation. The intermediate underwent a metal-halogen exchange to form the lithium acetylide which was trapped by TMS-chloride to form the TMS-acetylene **197**. The pure product was obtained after column chromatography in a yield of 83 %.

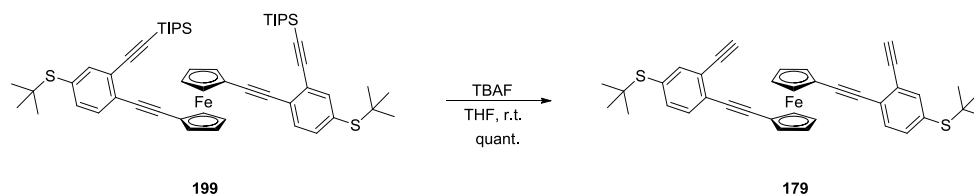
The obtained product **197** had two silyl-PG's which can be sequentially cleaved (TMS before TIPS). The TMS was removed by treating compound **197** with methanol and potassium carbonate generating the free acetylene **216** in quantitative yields (scheme 74).

To assemble molecule **199** the same Sonogashira coupling conditions were applied from the coupling reaction between **146** and **205** (scheme 72). Therefore, a mixture of compound **216**, compound **146**, palladium acetate, triphenylphosphine, copper acetate and diisopropylamine was heated in the microwave reactor at 100°C for 5 hours. The crude product was filtered over celite, concentrated and purified by column chromatography eluting with cyclohexane:DCM (5:1) to obtain the desired product **199** in a yield of 56 % (scheme 75).



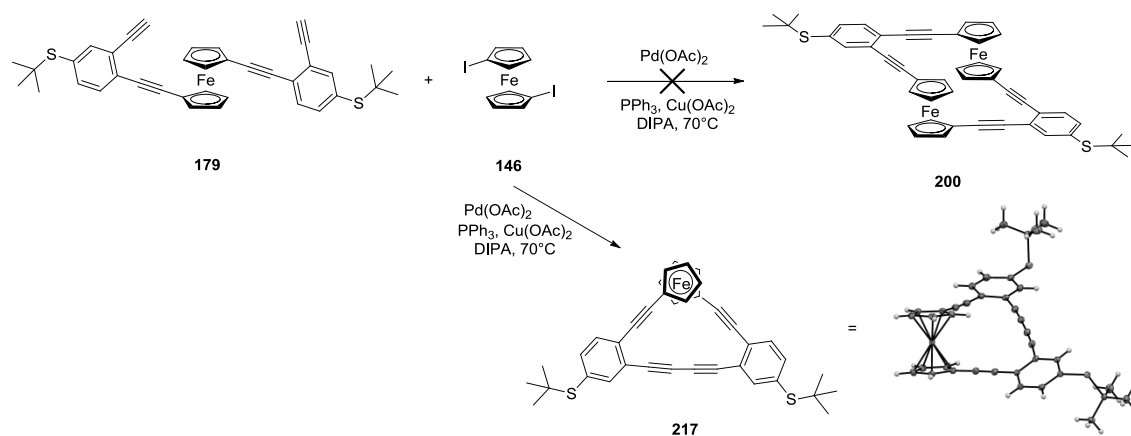
Scheme 75. Sonogashira cross coupling reaction to obtain **199**.

The deprotection of the TIPS-acetylenes in **199** was made by adding a 1M TBAF solution to a solution of compound **199** in THF at room temperature. After 45 minutes the reaction mixture was filtered through a silica pad to afford **179** in 96 % yield.



Scheme 76. Deprotection of **199** using TBAF in THF.

The next step was to cyclize compound **179** with **146** to obtain the target macrocycle **200** (scheme 77). A high dilution reaction was envisaged to favor an intramolecular reaction once the first coupling between the ferrocene **146** and the acetylene **179** was complete. Therefore, compounds **179** and **146** were each dissolved in diisopropylamine and slowly added over 48 hours to a mixture of palladium acetate (5 equiv.), triphenylphosphine (20 equiv.), copper acetate (0.5 equiv.) and diisopropylamine. The low copper acetate concentration was chosen to disfavor a homo-coupling between the acetylenes. However, the formation of the desired macrocycle **200** containing two ferrocene units was never observed.



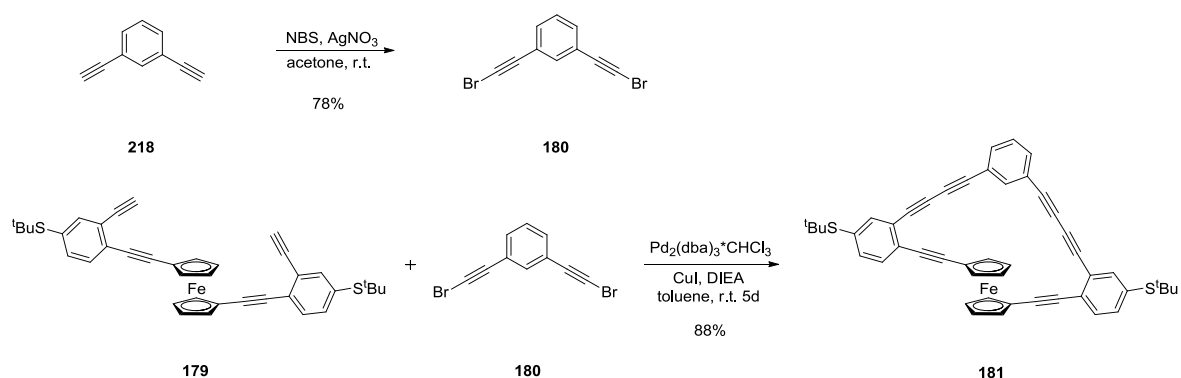
Scheme 77. Cyclization attempt to form compound **200**. Instead compound **217** was isolated.

Instead the formation of the intramolecular homo-coupled product **217** was observed. Even when the reaction was performed without any copper present the side product **217** was formed. We presumed that the oxidative addition of the diiodoferrocene **146** to the palladium source was too slow compared to the intramolecular homo-coupling.

These results inspired us to investigate the observed homo-coupling further and if we might be able to use it to our advantage. A cyclization of **179** with a second diacetylene building block was envisaged as the acetylene homo-coupling worked very well. A suitable reaction to achieve such a cyclization is the *Cadiot-Chodkiewicz* coupling.^[306]

The first step was to synthesize the bromo-acetylene **180** from the commercially available 1,3-diacetylenebenzene (**218**).^[307] Therefore, the benzene derivative **218** was added to a mixture of NBS and silver nitrate in acetone at room temperature. The crude product was isolated by column chromatography eluting with cyclohexane:*t*BME (20:1) to afford the desired building block **180** in a yield of 78 %.

Having building blocks **179** and **180** in hand the cyclization was achieved by slowly adding the educts to a mixture of tris(dibenzylideneacetone)dipalladium-chloroform, copper iodide, DIEA and toluene (scheme 78). The educts **179** and **180** were added within 43 hours to create pseudo high dilution conditions. After the addition was complete, the reaction mixture was stirred for four days. The crude compound **181** was purified by column chromatography eluting with cyclohexane:*t*BME (20:1) to afford the desired product **181** in 88 % yield.

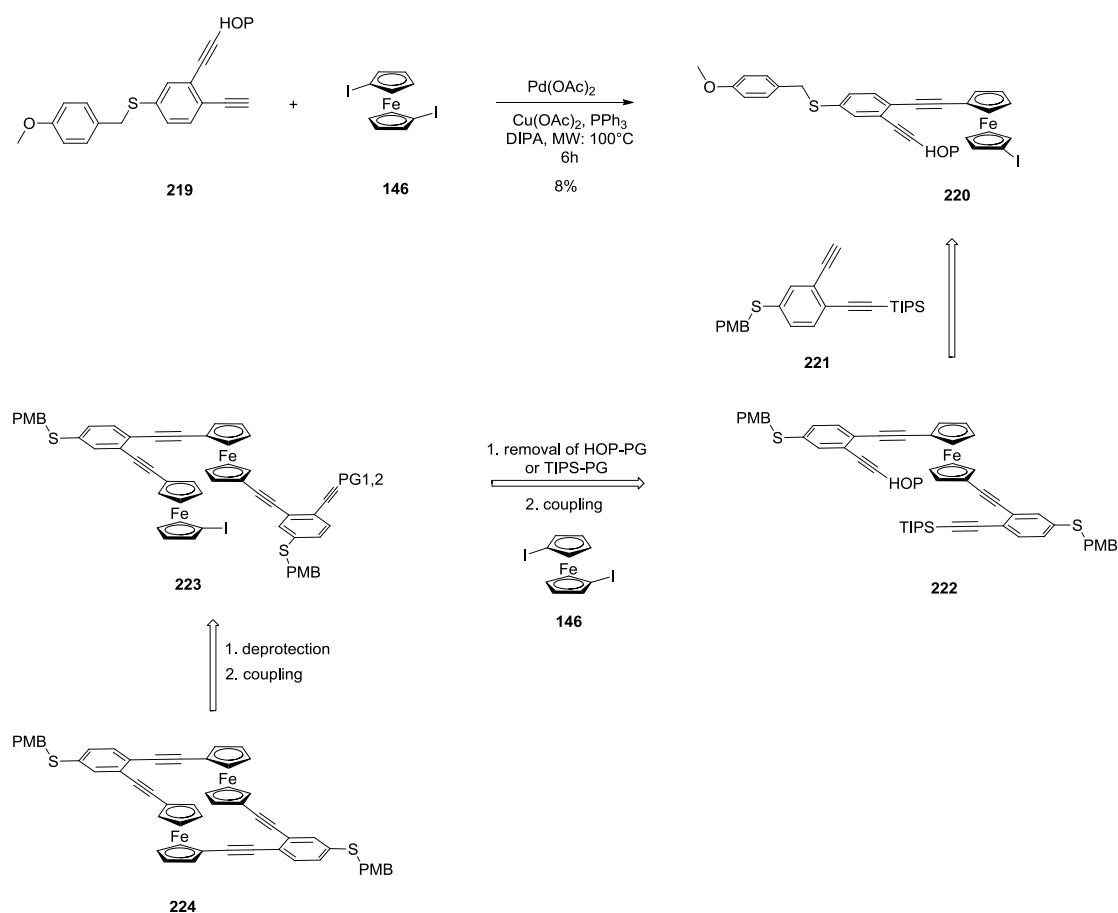


Scheme 78. Cyclization of **179** using a *Cadiot-Chodkiewicz* coupling.

Since this reaction worked so well we applied this strategy to the project which was described in chapter 4.

5.3.1 Outlook

Since the semi-stepwise approach did not work we started on the synthesis of the completely stepwise route (scheme 70, route C). For the first coupling reaction compound **219** was used which was previously synthesized in our group by Loic Lepleux. Compound **219** has a para-methoxybenzyl-PG to protect the sulfur. This PG promises an easier transprotection to the favored acetyl-PG. However, to favor a mono-substitution of the diiodoferrocene (**146**) stoichiometric amounts of **219** were used for the reaction. The conversion was not as good as expected and the isolated yield of mono-substituted **220** was 8 % (scheme 79). This reaction needs to be improved to continue the investigation of a stepwise approach. Different ligands should be explored to improve the oxidative addition of **146** to the palladium source.



Scheme 79. Outlook towards the synthesis of compound **224**.

The obtained compound **220** can now be coupled with compound **221** which needs previous deprotection. The envisaged compound **223** bears two orthogonal protecting groups which

gives better control over the assembly. One PG can be removed and the free acetylene can be coupled with an excess of diiodoferrocene (**146**) to get compound **223**. The remaining PG in compound **223** can be removed and a high dilution intramolecular coupling reaction can be performed to close the macrocycle **224**.

5.4 Conclusion

A semi-stepwise synthetic route was investigated to synthesize compound **200** (scheme 77). However, the final cyclization was not successful due to the competitive intramolecular homo-coupling reaction between the acetylenes forming macrocycle **217** (figure 65). This side reaction inspired us to investigate a cyclization using two diacetylene building blocks. The applied *Cadiot-Chodkiewicz* coupling successfully yielded in macrocycle **181**. These findings changed our strategic approach for the project discussed in chapter 4. When we have a look at the topological connection of the two macrocycles we can assume that the red pathway is higher conductive compared to the blue pathway. An electrochemical manipulation of the current passing through the ferrocene unit can therefore be envisaged.

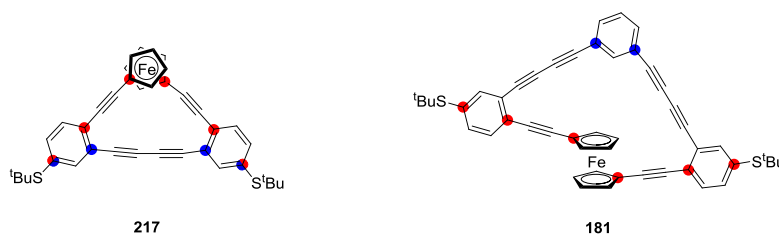


Figure 65. Obtained macrocycles **217** and **181** on the route to synthesize a macrocycle containing two ferrocene joints.

The stepwise approach to assemble macrocycle **224** needs to be further investigated. It was shown that the change of the sulfur PG (from *t*Bu-S to PMB-S) already had a big influence on the coupling yield (scheme 79). Hence, the protecting group strategy has to be reevaluated to improve the stepwise approach.

6 Summary

In the first project three halide end-capped OPEs were successfully synthesized (figure 66). The intermolecular interactions between the terminal halides and hydrogens and π -systems were investigated in their solid state structures. A striking resemblance between a planar cut through the crystal structure and the two dimensional assembly on a HOPG surface was observed for each compound. This finding supports the hypothesis that a sheet by sheet crystal growth on a flat surface should be possible.

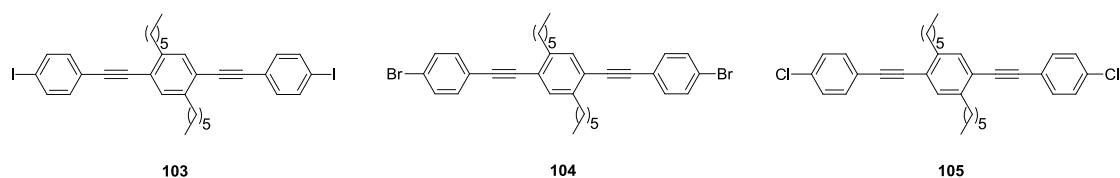
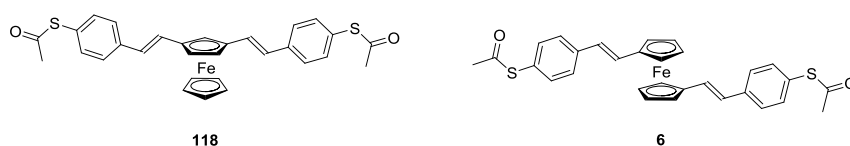


Figure 66. Synthesized OPEs **103-105** with terminal halogen end-groups.

In collaboration with the group of Michel Calame at the University of Basel we tried to integrate molecule **103** into a MCBJ. Due to the extended electron cloud of halogens we envisaged that halide end-groups could act as anchor groups to gold contacts and form stable molecule-electrode contacts. The MCBJ measurements revealed that the formed contacts, based on Van-der-Waals interactions between halides and gold electrodes, were not stable enough to collect sufficient data for a statistically significant analysis.

In the second project, an OPV-type ferrocene derivative **118** was synthesized within 14 steps. We wanted to compare the conductivity of this 1,3-disubstituted derivative with a 1,1'-disubstituted ferrocene **6** which was previously synthesized in the Major group by Sergio Grunder (figure 67).^[84]



Scheme 67. Synthesized target structure **118**.

The MCBJ experiments revealed that the conductance was similar in both cases. We found that the amount of deprotecting reagent which was used to deprotect the sulfur anchor groups was very important. Compared to previous studies where sub-stoichiometric amounts of TBAH were enough to deprotect the investigated molecules we experienced a very low plateau yield. UV/vis-experiments showed that at least two equivalents per sulfur-PG were necessary to deprotect the molecules completely. Since the experiment was carried out in an electrochemical MCBJ-setup, to investigate a possible gating effect, the amount of TBAH was limited due to an increase of background current which makes an investigation impossible.

To overcome this impasse, new deprotecting reagents such as aliphatic amines should be considered. Another option could be to deprotect the molecule in advance and filter the tetrabutylammonium ions off. Although, such an approach would be very difficult to handle since an oxidative sulfur-sulfur dimer formation is almost unavoidable.

In the third project a synthetic route towards two ferrocene macrocycles which can act as molecular wires was developed (figure 68). Both structures **187** and **192** were synthesized within 18 steps. The cyclization step was achieved by a *Cadiot-Chodkiewicz* type coupling. The advantage of this synthetic route is that the cyclization takes place at the end of the sequence which allows bridging the ferrocene wire with different linkers (blue).

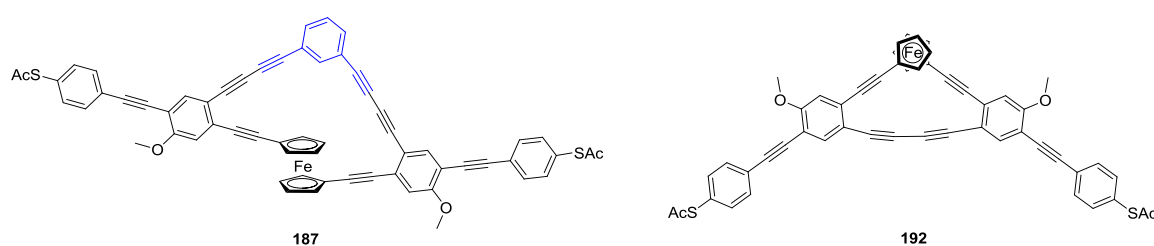


Figure 68. Synthesized target structures **187** and **192**.

Both structures should channel the current through the ferrocene unit which will be determined by MCBJ experiments. We envisage to gate the ferrocene unit electrochemically to observe a transistor like behavior.

The attempt to cyclize the ferrocene wire with an aliphatic linker via S_N2 reaction failed due to a *5-Endo-Dig* side reaction which was unavoidable.

In the fourth project the synthesis towards a ferrocene macrocycle comprising two ferrocene units was envisaged. The final cyclization failed due to a competitive intramolecular homo-coupling yielding in molecule **217** (figure 69). This result inspired us to make macrocycle **181** using a *Cadiot-Chodkiewicz* type coupling. This synthetic strategy was then successfully applied to the project discussed above.

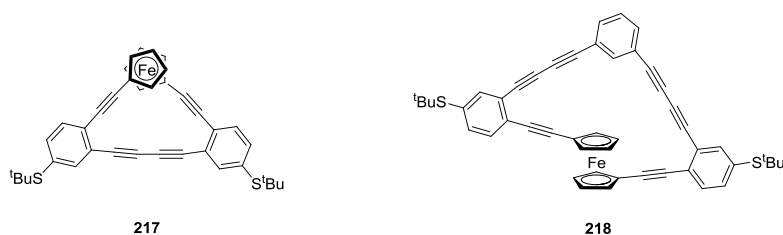


Figure 69. Synthesized macrocycles **217** and **181**.

All in all, synthetic strategies have been developed to synthesize functional molecules which can be addressed electrochemically. This functionality placed on suitable molecular building blocks can be used to influence the conductance of molecular junctions by electrochemical gating.

7 Experimental Part

7.1 General Remarks

All purchased chemicals were directly used for synthesis without further purification. Dry solvents were purchased from Sigma-Aldrich. All oxygen-sensitive reactions were performed under an argon atmosphere. The glass material was pre-heated to 120°C and cooled down under an argon flow.

Silica gel (60 µm) was purchased from Sigma-Aldrich. TLC plates (silica gel 60 F₂₅₄) were purchased from Merck.

Nuclear Magnetic Resonance

All ¹H-Nuclear- (¹H-NMR) and ¹³C-Nuclear- (¹³C-NMR) Magnetic Resonance were recorded on a *Bruker DPX-NMR* (400 MHz/100.6MHz) or on a *Bruker DRX-500* (500 MHz/125 MHz) instrument. Chemical shifts (δ) are reported in parts per million (ppm) relative to residual solvent peaks or trimethylsilane (TMS). NMR solvents were obtained from Cambridge Isotope Laboratories, Inc. (Andover, MA, USA). The measurements were done at room temperature. The multiplicities are written as: s=singlet, d=doublet, q=quartet, quin=quintet, m=multiplet and b=broad. All protons were assigned by using COSY and NOESY experiments. All carbons were assigned by performing DEPT, HMQC and HMBC experiments.

Mass Spectrometry

All Mass spectra (MS) were recorded on a *Bruker esquire 3000 plus* for Electron Spray Ionisation (ESI), a *finnigan MAT 95Q* for Electron Impact (EI) or a *finnigan MAT 8400* for Fast Atom Bombardment (FAB). All High resolution mass spectras (HR-ESI-MS) were recorded by the Schürch group at the university of Berne with a LTQ Orbitrap XL (Thermo Fisher Scientific) using a nanoelectrospray ion source.

Elemental Analysis

The elemental analysis (EA) were measured on an *Perkin-Elmer Analyticator 240*.

Cyclic Voltammetry

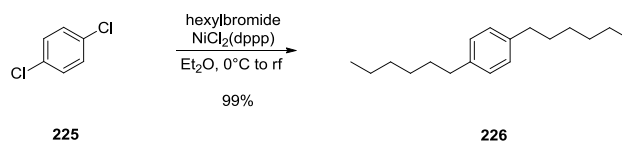
All electrochemical measurements were performed with a *Methrom Autolab PGSTAT 1*. The prepared solutions were degassed with argon prior to the experiments. The working electrodes (either glassy carbon or gold) were polished before each measurement.^[290] The platinum-net counter electrode was cauterized in a Bunsen burner flame prior to the experiment. A Ag/AgCl 3 M KCl reference electrode from *Methrom* was used.

UV/Vis Spectroscopy

UV/Vis spectra were recorded on an *Agilent 8453* diode array detector spectrophotometer using optical 114-QS Hellma cuvettes (10 mm light path) under normal atmosphere.

7.2 Synthesis of oligo-phenylene-ethynylenes

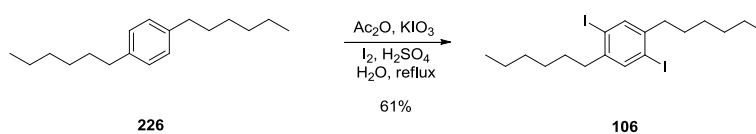
1,4-Diiodo-2,5-dihexylbenzene (**106**)^[242]



A 250 mL two necked flask equipped with a reflux condenser and a dropping funnel was charged with 1,4-dichlorobenzene (**225**) (11.9 g, 80 mmol, 1equiv.), NiCl₂(dppp) (130 mg, 0.240 mmol, 0.003equiv.) and anhydrous diethyl ether (60 ml) and cooled to 0°C. Hexylmagnesium bromide (100 ml, 200 mmol, 2.5equiv.) was added drop-wise at 0°C and the reaction mixture turned from red to yellow to green. The reaction mixture was heated to reflux for 17 hours. A precipitate was formed. The mixture was then cooled to 0°C and demin. water (20 ml) was added. Hydrochloric acid (6M in H₂O, 40 mL) was added to the reaction mixture at 0°C. The organic layer was separated and the aqueous layer was extracted with diethyl ether (3 x 50 mL). The combined organic layers were washed with brine, dried over MgSO₄ and concentrated under reduced pressure. Kugelrohrdistillation (1 mbar, 210°C) gave the product 1,4-dihexylbenzene (**226**) (19.5 g, 99%) as a colorless oil.

¹H-NMR (400 MHz, CDCl₃): δ (ppm) 7.08 (s, 4H); 2.56 (t, 4H); 1.57 (m, 4H); 1.29 (m, 12H); 0.88 (t, 6H).

¹³C-NMR (100 MHz, CDCl₃): δ (ppm) 140.3 (C_q, 2C); 128.4 (C_t, 4C); 35.8 (C_t, 2C); 32.0 (C_t, 2C); 31.8 (C_t, 2C); 29.3 (C_t, 2C); 22.8 (C_t, 2C); 14.3 (C_t, 2C).

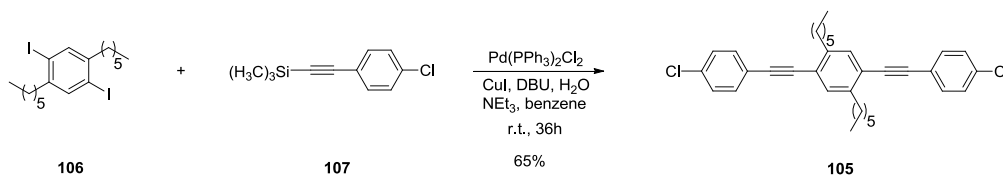


A 250 ml two-necked round-bottomed flask was charged with 1,4-dihexylbenzene **226** (9.86 g, 40 mmol, 1 equiv.) and acetic acid (130 ml). Potassium iodate (4.28 g, 20 mmol, 0.5 equiv.), iodine (11.2 g, 44 mmol, 1.1 equiv.), sulfuric acid (8.7 ml, 90 mmol, 2.25 equiv.) and water (1.31 ml, 72.8 mmol, 1.82 equiv.) were added. The resulting mixture was refluxed overnight. After 14h, the reaction mixture was cooled down to room temperature and concentrated to 50% of the initial volume. The formed precipitate was filtered off. The filter cake was dissolved in tBME and washed with aq. Na₂S₂O₄, water and brine. The organic layer was dried over MgSO₄ and concentrated under reduced pressure. The residue was filtered over a short silica pad (hexane: ethyl acetate 1:1) to afford the 1,4-diiido-2,6-dihexylbenzene (**106**) (12.1 g, 61%) as a white solid.

¹H-NMR (400 MHz, CDCl₃): δ (ppm) 7.59 (s, 2H); 2.59 (t, 4H); 1.33 (m, 4H); 1.28 (m, 12H); 0.9 (t, 6H).

¹³C-NMR (100 MHz, CDCl₃): 145.2 (C_q, 2C); 139.7 (C_t, 2C); 100.7 (C_q, 2C); 40.2 (C_s, 2C); 32.0 (C_s, 2C); 30.6 (C_s, 2C); 29.4 (C_s, 2C); 23.0 (C_s, 2C); 14.5 (C_p, 2C).

EI-MS (*m/z*) 498 (100%) [M]⁺.

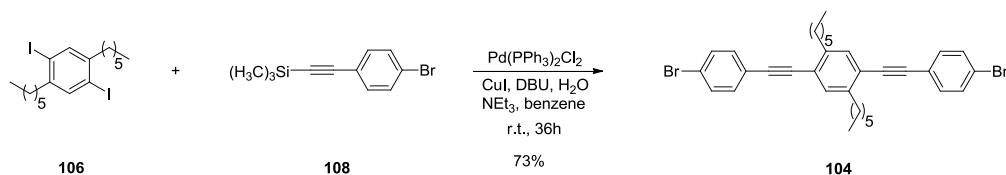
1,4-Bis[2-(4-chlorophenyl)ethynyl]-2,5-dihexylbenzene (105)


A Schlenk tube was purged with argon and charged with Pd(PPh₃)₂Cl₂ (21.3 mg, 0.03 mmol, 0.06 equiv.), CuI (19 mg, 0.1 mmol, 0.2 equiv.) and ((4-chlorophenyl)ethynyl)trimethylsilane **107** (221mg, 1.02 mmol, 2.05 equiv.). The tube was again purged with argon. Dry benzene (5 ml) and triethylamine (0.84 ml) were added. The brown suspension was degassed for 10 minutes. 1,4-dihexyl-2,5-diiodobenzene **106**^[242] (249 mg, 0.5 mmol, 1 equiv.) and 1,8-diazabicyclo[5.4.0]undec-7-ene (1.0 ml, 12 mmol, 24 equiv.) were added to the solution. Demin. water (0.0115 ml) was added and the reaction mixture was stirred at room temperature for 48h. The mixture was concentrated under reduced pressure and the residue was dissolved in CH₂Cl₂ and washed with water (2x20 ml). The organic layer was dried over MgSO₄, filtered and concentrated under reduced pressure to afford the crude product as yellow oil. The oil was purified by column chromatography (silica, cyclohexane; RF = 0.40) to afford 1,4-bis[2-(4-chlorophenyl)ethynyl]-2,5-dihexyl-benzene (**105**) (158 mg, 61.3%) as a white solid.

¹H-NMR (400 MHz, CDCl₃): δ (ppm) 7.445 (dt, ³J_{H,H}=8.8 Hz, ⁴J_{H,H}=2Hz, 4H); 7.35 (s, 2H); 7.336 (dt, ³J_{H,H}=8.8 Hz, ⁴J_{H,H}=2Hz, 4H); 2.783 (t, ³J_{H,H}=8 Hz, 4H); 1.70-1.66 (m, 4H); 1.39-1.30 (m, 12H); 0.874 (t, ³J_{H,H}=6.8 Hz, 6H).

¹³C-NMR (100 MHz, CDCl₃): 142.5 (C_q, 2C); 134.4 (C_q, 2C); 132.8 (C_t, 4C); 132.5 (C_t, 2C); 128.9 (C_t, 4C); 122.5 (C_q, 2C); 122.1 (C_q, 2C); 93.0 (C_q, 2C); 89.5 (C_q, 2C); 34.3 (C_s, 2C); 32.9 (C_s, 2C); 30.8 (C_s, 2C); 29.4 (C_s, 2C); 22.8 (C_s, 2C); 14.3 (C_p, 2C).

EI-MS (*m/z*) 514.2 (100%) [M]⁺; 443.2 (12.5%), [M-2Cl]⁺.

1,4-Bis[2-(4-bromophenyl)ethynyl]-2,5-dihexyl-benzene (104):


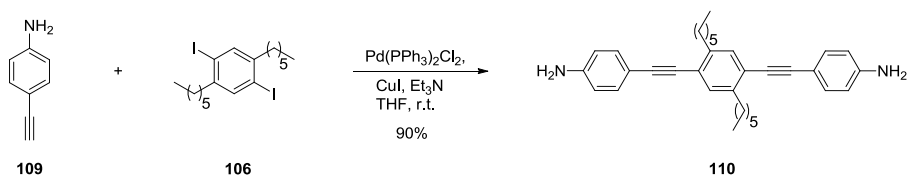
A Schlenk tube was purged with argon and charged with Pd(PPh₃)₂Cl₂ (34.12 mg, 0.048 mmol, 0.06 equiv.), CuI (30.5 mg, 0.16 mmol, 0.2 equiv.) and ((4-bromophenyl)ethynyl)trimethylsilane **108** (405 mg, 1.6 mmol, 2 equiv.). The tube was again purged with argon and dry benzene (8 ml) and triethylamine (1.35 ml) were added. The suspension was degassed for 10 minutes. 1,4-dihexyl-2,5-diiodobenzene (**106**)^[242] (400 mg, 0.8 mmol, 1 equiv.) and 1,8-diazabicyclo[5.4.0]undec-7-ene (2.9 ml, 19.2 mmol, 24 equiv.) were added to the solution which then turned green. Deion. water (0.0115 ml) was added and the reaction mixture was stirred at room temperature for 36h. The mixture was concentrated under reduced pressure and the residue was dissolved in CH₂Cl₂ and washed with water (2x20 ml). The organic layer was dried over MgSO₄, filtered and concentrated under reduced pressure to afford the crude product as dark oil. The oil was purified by column chromatography (silica, hexane) to afford 1,4-bis[2-(4-bromophenyl)ethynyl]-2,5-dihexylbenzene (**104**) (354 mg, 73.2%) as a white solid.

¹H-NMR (250 MHz, CDCl₃): δ (ppm) 7.498 (dt, ³J_{H,H}=8.25 Hz, ⁴J_{H,H}=2.25 Hz, 4H); 7.43-7.24 (m, 6H); 2.784 (t, ³J_{H,H}=7.5 Hz, 4H); 1.73-1.52 (m, 4H); 1.36-1.28 (m, 12H) 0.875 (t, ³J_{H,H}=6.75 Hz, 6H).

¹³C-NMR (100 MHz, CDCl₃): δ (ppm) 142.3 (C_q, 2C); 132.9 (C_i, 4C); 131.8 (C_i, 4C); 122.5 (C_q, 2C); 122.41 (C_q, 2C); 122.38 (C_q, 2C); 92.9 (C_q, 2C); 89.5 (C_q, 2C); 34.1 (C_s, 2C); 31.7 (C_s, 2C); 30.6 (C_s, 2C); 29.2 (C_s, 2C); 22.6 (C_s, 2C); 14.1 (C_p, 2C).

EI-MS (*m/z*) 604.1 (100%), [M]⁺.

EA: calc. C=67.56, H=6.00; found C=67.4, H=5.95.

1,4-Bis[2-(4-aminophenyl)ethynyl]-2,5-dihexyl-benzene (110):


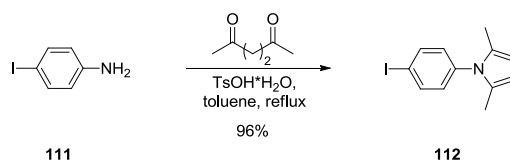
A 25 ml Schlenk tube was purged with argon and charged with 1,4-diiodo-2,5-dihexylbenzene (**106**)^[242] (996 mg, 2 mmol, 1 equiv.), Pd(PPh₃)₂Cl₂ (141 mg, 0.2 mmol, 0.1 equiv.), CuI (39.9 mg, 0.2 mmol, 0.1 equiv.), 4-ethynylaniline (**109**) (604 mg, 5 mmol, 2.5 equiv.), triethylamine (7 ml) and dry THF (10 ml). The resulting mixture was degassed for 10 min. and stirred for 16h at room temperature. The mixture was diluted with *tert*-butylmethyl ether (*t*BME) and filtered over celite. The filtrate was concentrated under reduced pressure and the residue was purified by column chromatography (silica, cyclohexane:*t*BME 1/2) to afford the pure 1,4-bis[2-(4-aminophenyl)ethynyl]-2,5-dihexyl-benzene (**110**) as a brown solid (940 mg, 98%).

¹H-NMR (400 MHz, CD₂Cl₂): δ (ppm) 7.308 (dt, ³J_{H,H}=8.4 Hz, ⁴J_{H,H}=2.4 Hz, 4H); 7.31 (s, 2H); 6.652 (dt, ³J_{H,H}=8.4 Hz, ⁴J_{H,H}=2.4 Hz, 4H); 3.94 (s, 4H); 2.774 (t, ³J_{H,H}=7.6 Hz, 4H); 1.70-1.64 (m, 4H); 1.36-1.33 (m, 12H); 0.881 (t, ³J_{H,H}=6.8 Hz, 6H).

¹³C-NMR (100 MHz, CD₂Cl₂): δ (ppm) 147.5 (C_q, 2C); 143.2 (C_q, 2C); 133.0 (C_t, 4C); 132.2 (C_t, 2C); 122.9 (C_q, 2C); 114.9 (C_t, 4C); 112.8 (C_q, 2C); 94.9 (C_q, 2C); 86.6 (C_q, 2C); 34.5 (C_s, 2C); 32.2 (C_s, 2C); 31.0 (C_s, 2C); 29.6 (C_s, 2C); 23.0 (C_s, 2C); 14.3 (C_p, 2C).

EI-MS (*m/z*) 476.3 (100%) [M]⁺.

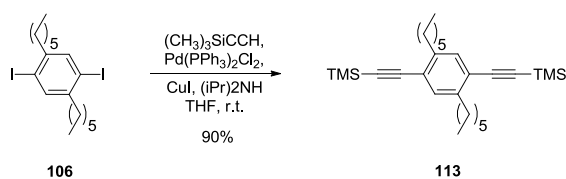
EA: calc. C=85.67, H=8.46, N=5.88; found C=85.39, H=8.38, N=5.91.

Dimethylpyrrole-iodobenzene (112):^[252]


A 25 ml flask charged with 4-iodoaniline **111** (1.314 g, 6.00 mmol, 1 equiv.), p-toluenesulfonic acid (19.4 mg, 0.102 mmol, 0.017 equiv.), acetylacetone (0.753 ml, 6.42 mmol, 1.07 equiv.) and dry toluene (16 ml). The reaction mixture was heated in a Dean-Stark apparatus for 4h. The reaction mixture was cooled down and extracted with sat. NaHCO_3 , water (5x) and brine. The organic solution was dried over MgSO_4 , filtered and concentrated under reduced pressure. The residue was dissolved in hexane: ethyl acetate (5/1) and filtered over silica. The filtrate was concentrated again to afford the desired product **112** (1.860 g, 96 %) as a brownish solid.

$^1\text{H-NMR}$ (400 MHz, CDCl_3): δ (ppm) 7.79 (dd, 2H); 6.96 (dd, 2H); 5.9 (s, 2H); 2.02 (s, 6H).

$^{13}\text{C-NMR}$ (100 MHz, CDCl_3): δ (ppm) 138.5 (C_t , 2C); 130.4 (C_t , 2C); 128.9 (C_q , 1C); 106.3 (C_t , 2C); 93.1 (C_q , 1C); 13.2 (C_p , 2C).

Building block: Di-hexyl-diacetylene-benzene (113)


A 50 ml Schlenk tube was purged with argon and charged with bis(triphenylphosphine)palladium(II)chloride (510 mg, 0.720 mmol, 0.12 equiv.), CuI (137 mg, 0.720 mmol, 0.12 equiv.) and 1,4-diiodo-2,5-dihexylbenzene **106** (2.99 g, 6.00 mmol, 1 equiv.). The tube was purged again with argon. THF (10 ml) and diisopropylamine (6 ml) were added and the resulting mixture was degassed for 10 min. Ethynyltrimethylsilane (3 ml, 21.0 mmol, 3.5 equiv.) was added and the mixture was stirred for 24h at room temperature. The reaction mixture was filtered over a silica plug and the filtrate was concentrated under reduced pressure. Hexane was added to the residue which was filtered again over silica. The filtrate was again concentrated under reduced pressure to afford a yellow oil. The crude

product was purified by column chromatography (silica, hexane) to afford the desired product **113** (2.4 g, 91%) as a yellow solid.

¹H-NMR (400 MHz, CDCl₃): δ (ppm) 7.22 (s, 2H); 2.65 (t, 4H); 1.57 (m, 4H); 1.29 (m, 12); 0.85 (t, 6H); 0.23 (s, 18H).

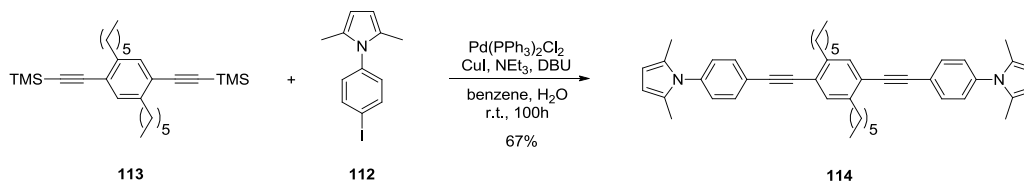
¹³C-NMR (100 MHz, CDCl₃): δ (ppm) 142.9 (C_q, 2C); 132.7 (C_t, 2C); 122.8 (C_q, 2C); 104.2 (C_q, 2C); 99.1 (C_q, 2C); 34.3 (C_s, 2C); 31.9 (C_s, 2C); 30.8 (C_s, 2C); 29.5 (C_s, 2C); 22.9 (C_s, 2C); 14.3 (C_p, 2C); 0.1 (C_p, 2C).

EI-MS (*m/z*) 438.3 (100%) [M]⁺.

Deprotection

The TMS-protected diacetylene **113** (500 mg, 1.14 mmol, 1q) was dissolved in DCM (4 ml) and methanol (35 ml, 864 mmol, 758 equiv.). Potassium carbonate (394 mg, 2.85 mmol, 2.5 equiv.) was added and the resulting mixture was stirred for 2h. The reaction mixture was concentrated under reduced pressure at room temperature. The residue was dissolved again and filtered over a short silica plug. The filtrate was concentrated to afford the product (335 mg, 99%) as a red oil.

¹H-NMR (400 MHz, CDCl₃): δ (ppm) 7.27 (s, 2H); 3.27 (s, 2H); 2.69 (t, 4H); 1.57 (m, 4H); 1.29 (m, 12H); 0.87 (t, 6H).

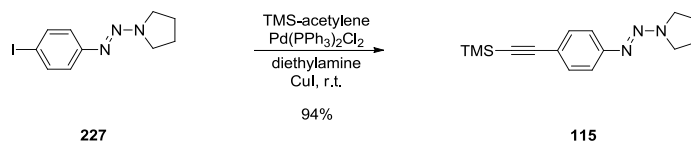
1,4-Bis[2-(4-(2,5-dimethyl-1H-pyrrol-1-yl)phenyl)ethynyl]-2,5-dihexyl-benzene (114):


An oven dried 25 ml Schlenk tube was purged with argon and charged with Pd(PPh₃)₂Cl₂ (42.5 mg, 0.06 mmol, 0.06 equiv.), CuI (38.1 mg, 0.2 mmol, 0.2 equiv.) and the TMS-protected acetylene **113**^[253] (439 mg, 1.0 mmol, 1 equiv.). The tube was again purged with argon and dry benzene (10 ml) and triethylamine (1.7 ml) were added. The yellow suspension was degassed for 10 minutes resulting in a brown solution. The dimethylpyrrole derivative **112**^[252] (624 mg, 2.1 mmol, 2.1 equiv.) and 1,8-diazabicyclo[5.4.0]undec-7-ene (3.6 ml, 24.0 mmol, 24 equiv.) were added to the solution. Demin. water (0.0144 ml) was added and the reaction mixture was stirred at room temperature for 100h. The reaction mixture was diluted with *t*BME and washed with water (2 x 20 ml) and brine. The organic layer was dried over MgSO₄, filtered and concentrated under reduced pressure to afford the crude product (1.0 g) as dark oil. The oil was purified by column chromatography (silica, cyclohexane:*t*BME 40/1) to afford the desired compound **114** (367 mg, 58%) as a white solid.

¹H-NMR (400 MHz, CDCl₃): δ (ppm) 7.615 (dt, ³J_{H,H}=8.4 Hz, ⁴J_{H,H}=1.6 Hz, 4H); 7.39 (s, 2H); 7.216 (dt, ³J_{H,H}=8.4 Hz, ⁴J_{H,H}=1.6 Hz, 4H); 5.92 (s, 4H); 2.832 (t, ³J_{H,H}=7.6 Hz, 4H); 2.06 (s, 12H); 1.74-1.71 (m, 4H) 1.43-1.26 (m, 12H); 0.876 (t, ³J_{H,H}=6.8 Hz, 6H).

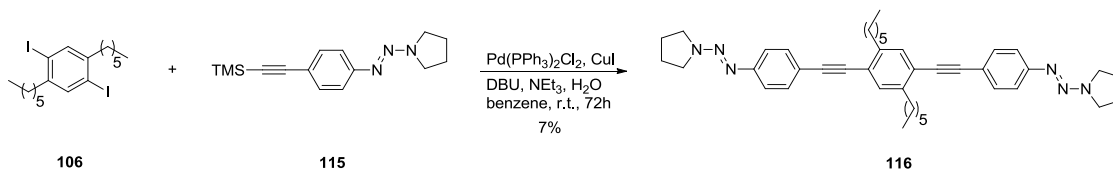
¹³C-NMR (100 MHz, CDCl₃): δ (ppm) 142.6 (C_q, 2C); 132.7 (C_q, 2C); 132.4 (C_t, 4C); 129.3 (C_t, 2C); 129.0 (C_q, 4C); 128.5 (C_t, 4C); 123.0 (C_q, 2C); 122.7 (C_q, 2C); 106.3 (C_t, 4C); 93.4 (C_q, 2C); 89.6 (C_q, 2C); 34.4 (C_s, 2C); 32.0 (C_s, 2C); 30.9 (C_s, 2C); 29.5 (C_s, 2C); 22.9 (C_s, 2C); 14.3 (C_p, 2C); 13.3 (C_p, 4C).

EI-MS (*m/z*) 632.4 (100%), [M]⁺. ESI-HRMS (*m/z*) 633.4211 [M + H]⁺ (Theo. Mass 633.4203; Δ 1.24 ppm)

1-(4-trimethylsilylethynylphenyl)-3,3-tetramethylenetriazene (115):^[256]


A 100 ml two-necked round-bottomed flask was purged with argon and charged with the (E)-1-((4-iodophenyl)diazanyl)pyrrolidine **227** (2.5 g, 8.30 mmol, 1 equiv.), diethyl amine (30 ml) and ethynyltrimethylsilane (2.4 ml, 16.6 mmol, 2 equiv.). The yellow solution was degassed for 10 min. Bis(triphenylphosphine) palladium(II) chloride (58 mg, 0.083 mmol, 0.01 equiv.) and CuI (32 mg, 0.166 mmol, 0.02 equiv.) were added. The resulting mixture was stirred overnight (17h). The reaction mixture was concentrated under reduced pressure. The brown residue was dissolved in DCM and absorbed on silica. It was then purified by column chromatography (hexane:tBME 6/1) to afford the desired compound **115** (2.11 g, 93.5%) as a brown solid.

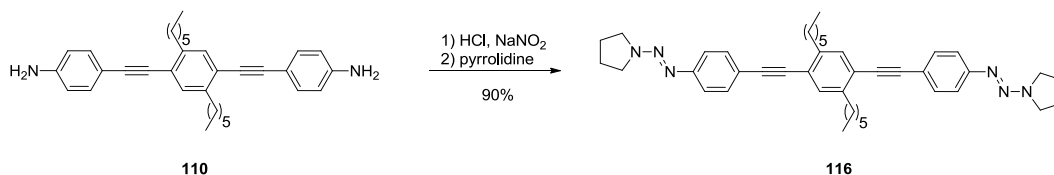
¹H-NMR (400 MHz, CDCl₃): δ (ppm) 7.43-7.39 (m, 2H); 7.33-7.31 (m, 2H); 3.77 (s, 4H); 2.01 (s, 4H); 0.22 (s, 9H).

1,4-Bis[2-(4-(3,3-tetramethylenetriazeno)phenyl)ethynyl]-2,5-dihexyl-benzene (116)
Pathway A:


Bis(triphenylphosphine)palladium(II) chloride (42.1 mg, 0.06 mmol, 0.06 equiv.), CuI (47.6 mg, 0.25 mmol, 0.2 equiv.) and 1-(4-trimethylsilylethynylphenyl)-3,3-tetramethylenetriazene (**115**)^[256] (679 mg, 2.5 mmol, 2.5 equiv.) were charged in a 50 ml Schlenk-tube and purged with argon. Benzene (12 ml) and triethylamine (1.7 ml) were added. The resulting solution was degassed for 10 minutes. 1,4-Dihexyl-2,5-diiodobenzene (**106**)^[253] (498 mg, 1.0 mmol, 1 equiv.) and 1,8-diazabicyclo[5.4.0]undec-7-ene (4.48 ml, 30 mmol, 30 equiv.) were added. Water (18 μl, 1.0 mmol, 1 equiv.) was added subsequently. The color of the reaction mixture turned green. The mixture was stirred for 24h at room temperature. The reaction mass was concentrated under reduced pressure. The residue was dissolved in CH₂Cl₂ (60 ml), extracted

with water (2 x 20 ml) and washed with brine (30 ml). The organic layer was then dried over MgSO_4 , filtered and concentrated under reduced pressure to afford a red-brown solid. The residue was purified by column chromatography (hexane/*t*BME 2:1 + 3% triethylamine) to afford the desired OPE **116** (45 mg, 7%) as a yellow powder.

Pathway B:

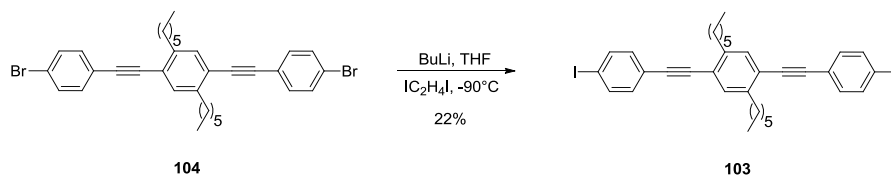


A 25 ml two-necked round-bottomed flask was purged with argon and charged with 1,4-bis[2-(4-aminophenyl)ethynyl]-2,5-dihexylbenzene (**110**) (501 mg, 1.05 mmol, 1 equiv.), water (1.5 ml), acetonitrile (1.5 ml) and hydrochloric acid 37% (0.803 ml, 9.45 mmol, 9 equiv.). The resulting mixture was cooled to 0°C and stirred for 1h. Sodium nitrite (145 mg, 2.1 mmol, 2 equiv.) dissolved in water (3.5 ml) was added and the mixture was again stirred for 1h at 0°C. The mixture was then transferred into another flask which contained potassium carbonate (1.466 mg, 10.5 mmol, 10 equiv.), water/acetonitrile 2:1 (3 ml) and pyrrolidine (0.345 ml, 4.2 mmol, 4 equiv.). The resulting mixture was stirred for 1h at 0°C and another 2h at room temperature. The mixture was then diluted with CH_2Cl_2 (100 ml). The aqueous phase was separated and washed with CH_2Cl_2 (2 x 50 ml). The organic layers were combined and washed with brine, dried with MgSO_4 and concentrated under reduced pressure to afford the crude product. Ethyl acetate was added and the slurry was put in the ultrasonic bath for 5 min. The mixture was then filtered and the solid product was dried under high vacuum to afford the desired product **116** (558 mg, 82%) as a yellow solid.

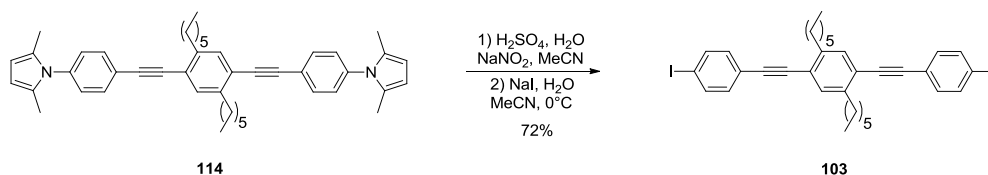
$^1\text{H-NMR}$ (400 MHz, CDCl_3): δ (ppm) 7.481(dt, $^3J_{\text{H,H}}=8.8$ Hz, $^4J_{\text{H,H}}=2$ Hz, 4H); 7.405 (dt, $^3J_{\text{H,H}}=8.8$ Hz, $^4J_{\text{H,H}}=2$ Hz, 4H); 7.34 (s, 2H); 3.80 (s, 8H); 2.801 (t, $^3J_{\text{H,H}}=7.6$ Hz, 4H); 2.04 (m_b , 8H); 1.72-1.68 (m, 4H); 1.41-1.31 (m, 12H); 0.879 (t, $^3J_{\text{H,H}}=7.2$, 6H).

$^{13}\text{C-NMR}$ (100 MHz, CDCl_3): δ (ppm) 151.4 (C_q , 2C); 142.3 (C_q , 2C); 132.4 (C_t , 4C); 132.3 (C_t , 2C); 122.8 (C_q , 2C); 120.6 (C_t , 4C); 120.0 (C_q , 2C); 94.7 (C_q , 2C); 88.6 (C_q , 2C); 34.4 (C_s , 4C); 32.0 (C_s , 2C); 30.0 (C_s , 2C); 29.5 (C_s , 2C); 24.0 (C_s , 2C); 22.9 (C_s , 4C); 14.4 (C_p , 2C).

EI-MS (m/z) 640.4 (5.5%, M^+); 543.3 (40.5, $M^+-C_4H_8N_3$); 445.2 (100%, $M^+-C_8H_{16}N_6$). ESI-HRMS (m/z) 641.4337 [$M + H$] $^+$ (Theo. Mass 641.4326; Δ 1.62 ppm)

1,4-bis[2-(4-iodophenyl)ethynyl]-2,5-dihexyl-benzene (103):
Halide exchange:


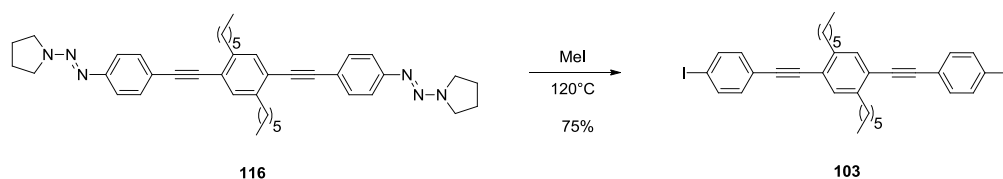
A oven dried 25 mL two necked flask was purged with argon and charged with 1,4-bis[2-(4-bromophenyl)ethynyl]-2,5-dihexyl-benzene (**104**) (100.00 mg, 0.165 mmol, 1 equiv.) and anhydrous THF (3.00 mL). The solution was cooled to -100°C . Due to the low temperature the educt was not soluble anymore. Then *n*BuLi (0.23 mL, 0.350 mmol, 2.12 equiv., 1.6 M in hexane) was slowly added to the colorless suspension so that the temperature did not exceed -90°C . The reaction mixture turned green and then yellow. The mixture was stirred for 45 min. controlled by TLC. More *n*BuLi (0.05 mL, 0.080 mmol, 0.5 equiv., 1.6 M in hexane) was added. The green reaction mixture was added drop-wise with a syringe to a precooled (-78°C) solution of 1,2-diodoethane (98.7 mg, 0.350 mmol, 2.12 equiv.) in anhydrous THF (1.50 mL). The reaction mixture turned from yellow to dark brown and was stirred overnight. The dark brown reaction mixture was poured on aq. $\text{Na}_2\text{S}_2\text{O}_3$ (15%) overlaid with diethyl ether. The ether layer was washed with aq. $\text{Na}_2\text{S}_2\text{O}_3$ (15%) twice. The aqueous layer was extracted with diethyl ether (3 x 10 mL). The combined organic layers were dried over MgSO_4 , filtered and concentrated under reduced pressure which gave a yellow residue. The crude product was purified by column chromatography (silica, hexane) to afford 1,4-bis[2-(4-iodophenyl)ethynyl]-2,5-dihexyl-benzene (**103**) (26.02 mg, 22%) as a off-white solid.

Pyrrole-strategy:


A 50 ml two-necked round-bottomed flask was purged with argon and charged with 1,4-bis[2-(4-(2,5-dimethyl-1H-pyrrol-1-yl)phenyl)ethynyl]-2,5-dihexyl-benzene (**114**) (100 mg, 0.158 mmol, 1 equiv.), MeCN (4.5 ml) and H_2SO_4 (3.32 ml, 2M, 6.64 mmol, 42 equiv.). The

mixture was cooled to -5°C . Sodium nitrite (65.4 mg, 0.948 mmol, 6 equiv.) dissolved in water (1 ml) was added drop wise at -5°C . The mixture was stirred overnight at -5°C . Then, sodium iodate (189 mg, 1.26 mmol, 8 equiv.) dissolved in water (1 ml) was added. The reaction mixture was then allowed to warm to room temperature over 1h. The mixture was briefly heated to 60°C and then stirred at room temperature for 4h. The mixture was neutralized with sat. Na_2CO_3 and then extracted with ethyl acetate (3 x 40 ml). The combined organic layers were washed with $\text{Na}_2\text{S}_2\text{O}_3$ (1N, 2 x 50 ml) and water (20 ml), dried over MgSO_4 and concentrated under reduced pressure. The crude product was purified by column chromatography (silica, hexane:*t*BME 40/1) to afford 1,4-bis[2-(4-iodophenyl)ethynyl]-2,5-dihexyl-benzene (**103**) (79 mg, 72%) as a white solid.

Triazene Strategy:



A 10 ml MW-pressure tube was purged with argon and charged with 1,4-bis[2-(4-(3,3-tetramethylenetriazeno)phenyl)ethynyl]-2,5-dihexylbenzene (**116**) (60.9 mg, 0.095 mmol, 1 equiv.) and iodomethane (4 ml). The sealed tube was heated to 120°C and stirred for 12h. The reaction mixture was then concentrated under reduced pressure. The residue was dissolved in cyclohexane and filtered over silica to afford 1,4-bis[2-(4-iodophenyl)ethynyl]-2,5-dihexylbenzene (**103**) (52 mg, 78.2%) as a white solid.

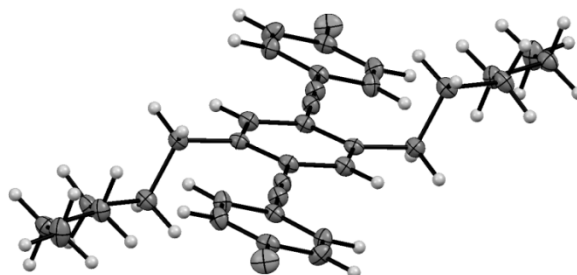
$^1\text{H-NMR}$ (400 MHz, CD_2Cl_2): δ (ppm) 7.725 (dt, $^3J_{\text{H,H}}=8.8$ Hz, $^4J_{\text{H,H}}=2$ Hz, 4H); 7.37 (s, 2H); 7.264 (dt, $^3J_{\text{H,H}}=8.8$ Hz, $^4J_{\text{H,H}}=2$ Hz, 4H); 2.795 (t, $^3J_{\text{H,H}}=7.6$ Hz, 4H); 1.70-4.64 (m, 4H); 1.42-1.31 (m, 12H); 0.881 (t, $^3J_{\text{H,H}}=6.8$ Hz, 6H).

$^{13}\text{C-NMR}$ (100 MHz, CDCl_3): δ (ppm) 143.0 (C_q , 2C); 138.2 (C_t , 4C); 133.5 (C_t , 4C); 132.9 (C_t , 2C); 123.5 (C_q , 2C); 123.0 (C_q , 2C); 94.6 (C_q , 2C); 93.6 (C_q , 2C); 90.3 (C_q , 2C); 34.6 (C_s , 2C); 32.3 (C_s , 2C); 31.2 (C_s , 2C); 29.8 (C_s , 2C); 23.2 (C_s , 2C); 14.5 (C_p , 2C).

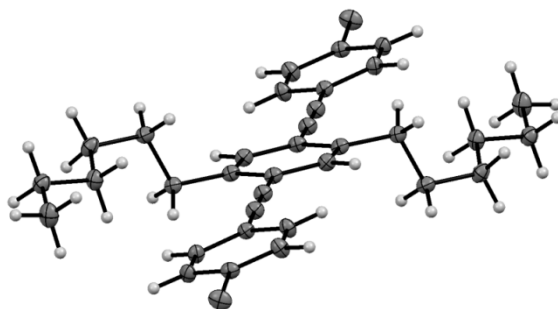
EI-MS (m/z) 697.9 (100%, M^+); 572.1 (12.5%, M^+-I).

Crystal Structures of halide end-capped OPE's

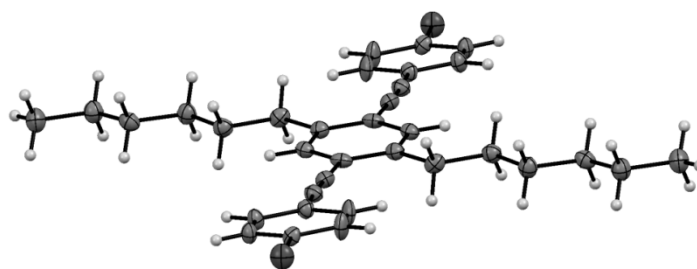
1,4-Bis[2-(4-chlorophenyl)ethynyl]-2,5-dihexylbenzene (**105**)



Crystal data for **105**: formula $C_{34}H_{36}Cl_2$, $M = 515.57$, $F(000) = 274$, colorless plate, size $0.030 \cdot 0.070 \cdot 0.180$ mm³, triclinic, space group $P \bar{1}$, $Z = 1$, $a = 5.6220(7)$ Å, $b = 8.0932(11)$ Å, $c = 15.495(2)$ Å, $\alpha = 86.859(9)^\circ$, $\beta = 83.191(9)^\circ$, $\gamma = 87.654(9)^\circ$, $V = 698.59(16)$ Å³, $D_{\text{calc.}} = 1.225$ Mg · m⁻³. The crystal was measured on a Bruker Kappa Apex2 diffractometer at 123K using graphite-monochromated Mo $K\alpha$ -radiation with $\lambda = 0.71073$ Å, $\Theta_{\text{max}} = 30.032^\circ$. Minimal/maximal transmission 0.98/0.99, $\mu = 0.253$ mm⁻¹. The Apex2 suite has been used for datacollection and integration. From a total of 13850 reflections, 4056 were independent (merging $r = 0.050$). From these, 2222 were considered as observed ($I > 2.0\sigma(I)$) and were used to refine 163 parameters. The structure was solved by direct methods using the program Superflip. Least-squares refinement against F was carried out on all non-hydrogen atoms using the program CRYSTALS. $R = 0.0402$ (observed data), $wR = 0.0823$ (all data), $GOF = 1.1125$. Minimal/maximal residual electron density = $-0.26/0.28$ e Å⁻³. Chebychev polynomial weights were used to complete the refinement. Plots were produced using CAMERON. Crystallographic data (excluding structure factors) for the structure in this paper have been deposited with the Cambridge Crystallographic Data Center, the deposition number is (CCDC 849687). Copies of the data can be obtained, free of charge, on application to the CCDC, 12 Union Road, Cambridge CB2 1EZ, UK [fax: +44-1223-336033 or e-mail: deposit@ccdc.cam.ac.uk].

1,4-Bis[2-(4-bromophenyl)ethynyl]-2,5-dihexyl-benzene (104):

Crystal data for **104**: formula $C_{34}H_{36}Br_2$, $M = 604.47$, $F(000) = 310$, colorless needle, size $0.040 \cdot 0.060 \cdot 0.270$ mm³, triclinic, space group $P -1$, $Z = 1$, $a = 5.7434(8)$ Å, $b = 8.0996(8)$ Å, $c = 15.4925(16)$ Å, $\alpha = 86.096(5)^\circ$, $\beta = 82.539(5)^\circ$, $\gamma = 87.253(4)^\circ$, $V = 712.38(14)$ Å³, $D_{calc.} = 1.409$ Mg · m⁻³. The crystal was measured on a Bruker Kappa Apex2 diffractometer at 123K using graphite-monochromated Mo $K\alpha$ -radiation with $\lambda = 0.71073$ Å, $\Theta_{max} = 37.784^\circ$. Minimal/maximal transmission 0.84/0.89, $\mu = 2.866$ mm⁻¹. The Apex2 suite has been used for datacollection and integration. From a total of 27787 reflections, 7551 were independent (merging $r = 0.033$). From these, 4999 were considered as observed ($I > 2.0\sigma(I)$) and were used to refine 163 parameters. The structure was solved by direct methods using the program Superflip. Least-squares refinement against F was carried out on all non-hydrogen atoms using the program CRYSTALS. $R = 0.0251$ (observed data), $wR = 0.0471$ (all data), $GOF = 1.0921$. Minimal/maximal residual electron density = $-0.35/0.44$ e Å⁻³. Chebychev polynomial weights were used to complete the refinement. Plots were produced using CAMERON. Crystallographic data (excluding structure factors) for the structure in this paper have been deposited with the Cambridge Crystallographic Data Center, the deposition number is (CCDC 849688). Copies of the data can be obtained, free of charge, on application to the CCDC, 12 Union Road, Cambridge CB2 1EZ, UK [fax: +44-1223-336033 or e-mail: deposit@ccdc.cam.ac.uk].

1,4-bis[2-(4-iodophenyl)ethynyl]-2,5-dihexyl-benzene (103):

Crystal data for **103**: formula $C_{34}H_{36}I_2$, $M = 740.55$, $F(000) = 740$, colorless block, size $0.040 \cdot 0.130 \cdot 0.230$ mm³, triclinic, space group $P \bar{1}$, $Z = 2$, $a = 7.2908(9)$ Å, $b = 15.0277(16)$ Å, $c = 15.3177(15)$ Å, $\alpha = 88.906(6)^\circ$, $\beta = 78.977(7)^\circ$, $\gamma = 82.784(7)^\circ$, $V = 1634.2(3)$ Å³, $D_{\text{calc.}} = 1.505$ Mg · m⁻³. The crystal was measured on a Bruker Kappa Apex2 diffractometer at 123K using graphite-monochromated Mo $K\alpha$ -radiation with $\lambda = 0.71073$ Å, $\Theta_{\text{max}} = 30.242^\circ$. Minimal/maximal transmission 0.78/0.93, $\mu = 1.947$ mm⁻¹. The Apex2 suite has been used for datacollection and integration. From a total of 32598 reflections, 9576 were independent (merging $r = 0.055$). From these, 5270 were considered as observed ($I > 2.0\sigma(I)$) and were used to refine 353 parameters. The structure was solved by direct methods using the program Superflip. Least-squares refinement against F was carried out on all non-hydrogen atoms using the program CRYSTALS. $R = 0.0558$ (observed data), $wR = 0.1018$ (all data), $GOF = 1.0652$. Minimal/maximal residual electron density = $-1.41/2.39$ e Å⁻³. Chebychev polynomial weights were used to complete the refinement. Plots were produced using CAMERON. Crystallographic data (excluding structure factors) for the structure in this paper have been deposited with the Cambridge Crystallographic Data Center, the deposition number is (CCDC 849689). Copies of the data can be obtained, free of charge, on application to the CCDC, 12 Union Road, Cambridge CB2 1EZ, UK [fax: +44-1223-336033 or e-mail: deposit@ccdc.cam.ac.uk].

STM Picture for the Dichloro-OPE 105:

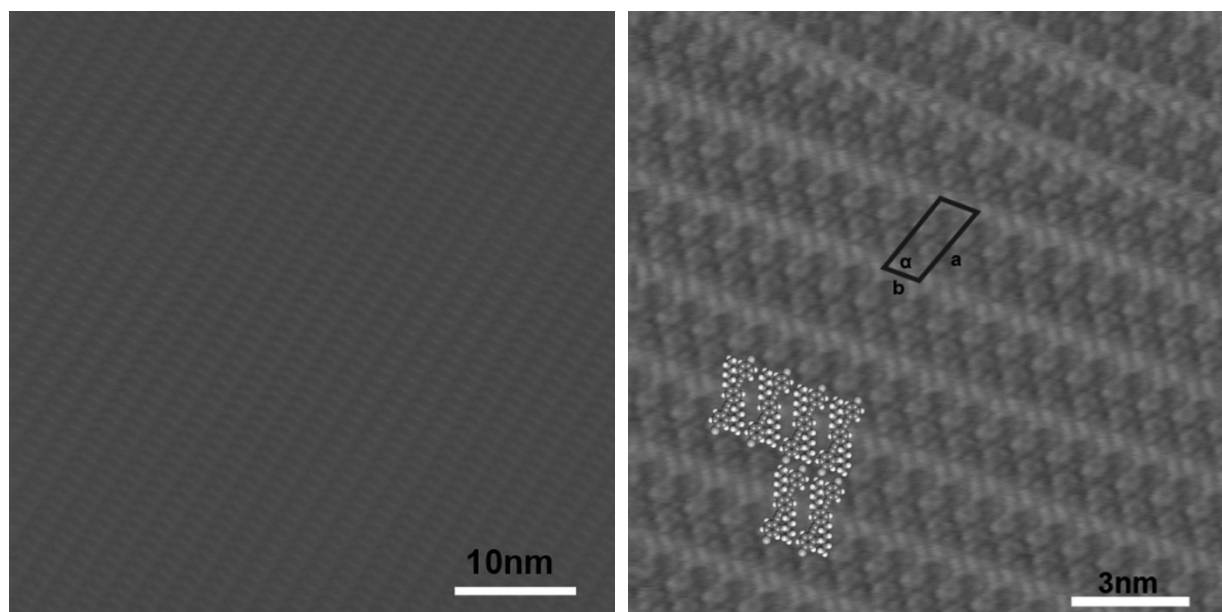


Figure 70. Left) Dichloro-OPE **105**, VB=700mV, IT=650pA. Right) Dichloro-OPE **105**, VB=585mV, IT=630pA; $a=2.0\pm 0.1\text{nm}$, $b=1.0\pm 0.1\text{nm}$, $\alpha=76\pm 2^\circ$; All the period length have been corrected.

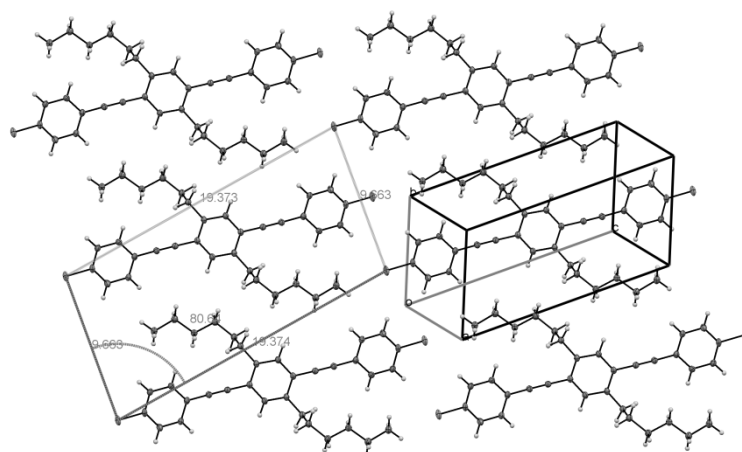


Figure 71. Planar cut through the crystal structure of OPE **105** showing the obtained unit cell and a „flat“ unit-cell representing the lateral arrangement in the sheet.

STM Picture for the Dibromo-OPE 104:

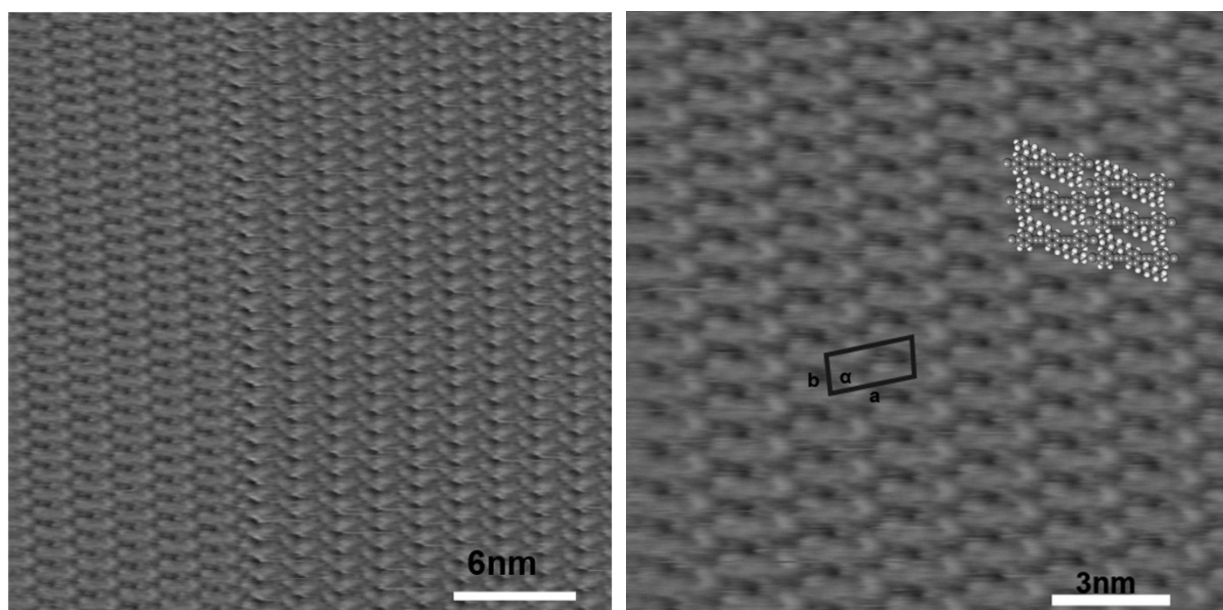


Figure 72. Left) Dibromo-OPE **104**; VB=400mV, IT=500pA. Right) Dibromo-OPE **104**; VB=400mV, IT=500pA; $a=2.0\pm 0.1\text{nm}$, $b=1.0\pm 0.1\text{nm}$, $\alpha=75\pm 4^\circ$.

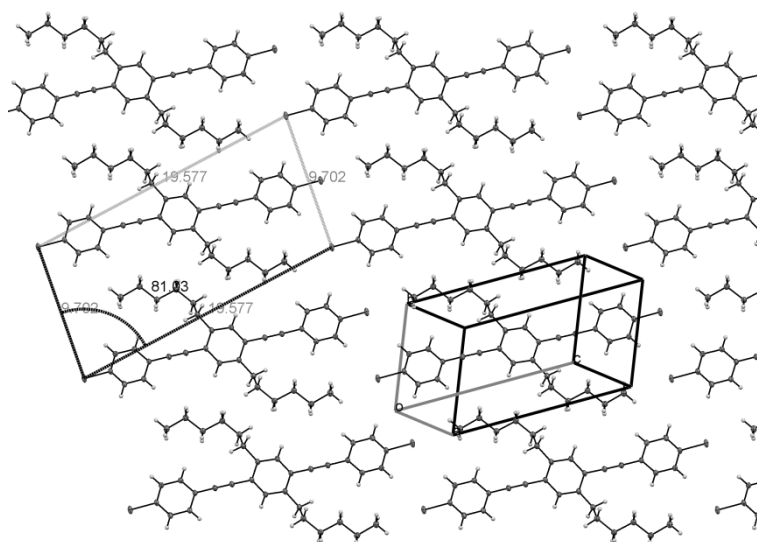


Figure 73. Planar cut through the crystal structure of OPE **104** showing the obtained unit cell and a „flat“ unit-cell representing the lateral arrangement in the sheet.

STM Picture for the Diiodo-OPE 103:

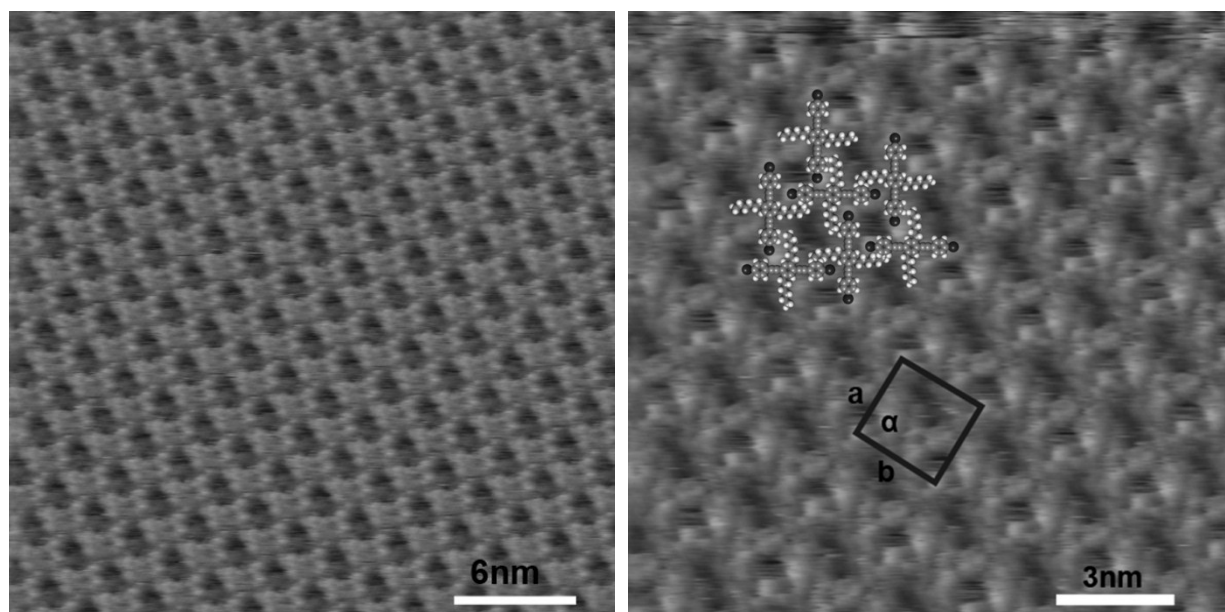


Figure 74. Left) Diiodo-OPE 103; $V_B=400\text{mV}$, $I_T=500\text{pA}$; Right) Diiodo-OPE 103; $V_B=240\text{mV}$, $I_T=500\text{pA}$; $a=2.1\pm 0.1\text{nm}$, $b=2.0\pm 0.1\text{nm}$, $\alpha=90\pm 4^\circ$

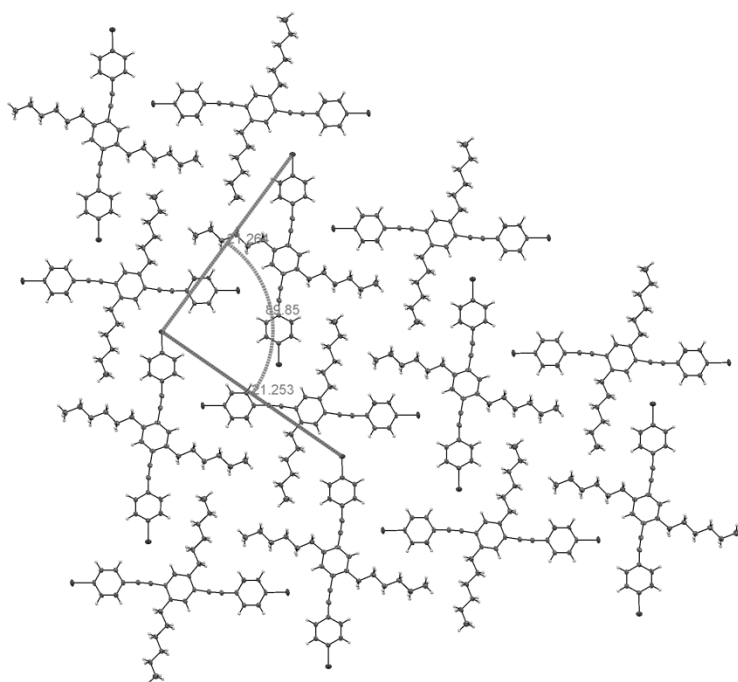
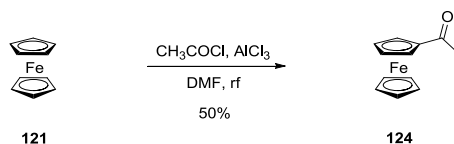


Figure 75. Planar cut through the crystal structure of OPE 103 showing the obtained unit cell and a „flat“ unit-cell representing the lateral arrangement in the sheet.

7.3 Synthesis of Ferrocene Derivatives

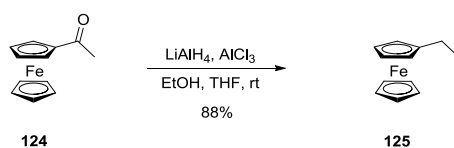
Acetylferrocene (**124**):



A 2000 ml two-necked round bottom flask was charged with acetylchloride (25.37 g, 0.32 mol, 1 equiv.), aluminium chloride (52.53 g, 0.39 mol, 1.2 equiv.) and dry DCM (500 ml). Ferrocene **121** (60.75 g, 0.32 mol, 1 equiv.) was dissolved in dry DCM (500 ml) and slowly added over a period of 2h at room temperature using an addition funnel. After the addition was complete the reaction mixture was heated to reflux and was stirred for another 3h. The mixture was then poured onto ice (600 g). The organic layer was separated and washed with water (2 x 200 ml). The organic phase was dried over MgSO₄, filtered and concentrated under reduced pressure. The residue was purified by column chromatography (1. silica, hexane/ethyl acetate 4:1; 2. Silica, DCM/MeOH 99.5:0.5) to afford the desired compound **124** (36.48 g, 50%) as a red solid.

¹H-NMR (400 MHz, CDCl₃): δ (ppm) 4.78 (t, 2H); 4.51 (t, 2H); 4.21 (s, 5H); 2.40 (s, 3H).

Ethylferrocene (**125**):



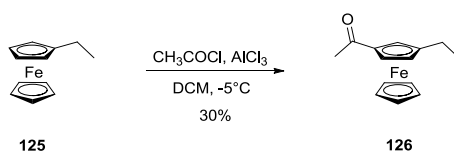
A 100 ml three necked round bottom flask was purged with argon and charged with lithium aluminiumhydride (734 mg, 18.75 mmol, 1.07 equiv.) and dry diethylether (20 ml). Aluminium chloride (2.50 g, 18.75 mmol, 1.07 equiv.) was added portion wise. Acetylferrocene **124** (4.0 g, 17.54 mmol, 1 equiv.) was dissolved in dry ethylether (30 ml) and slowly added over a period of 50 min. After the addition was complete the reaction mixture was allowed to stir for another 60 min. at room temperature. The mixture was then poured onto ice (250 g). The aqueous layer was separated and the organic phase was washed with sat. NaHCO₃ (3 x 50 ml), brine (50 ml), dried over MgSO₄, filtered and concentrated under

reduced pressure. The residue was purified by column chromatography (silica, hexane/DCM 10:1) to afford the desired compound **125** (3.318 g, 88.4%) as red oil.

$^1\text{H-NMR}$ (400 MHz, $(\text{CD}_3)_2\text{CO}$): δ (ppm) 4.09 (s, 5H); 4.07-4.06 (m, 2H); 4.02-4.01 (m, 2H); 2.36-2.30 (q, 2H); 1.16-1.12 (t, 3H).

$^{13}\text{C-NMR}$ (100 MHz, $(\text{CD}_3)_2\text{CO}$): δ (ppm) 91.76 (C_q , 1C); 69.12 (C_t , 5C); 68.17 (C_t , 2C); 67.71 (C_t , 2C); 22.90 (C_s , 1C); 15.11 (C_p , 1C).

1-Acetyl-3-ethylferrocene (**126**):



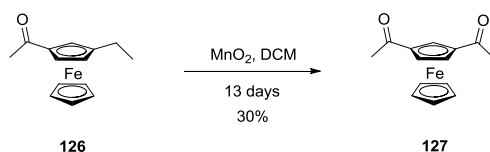
A 250 ml three necked round bottom flask was purged with argon and charged with ethylferrocene (**125**) (13.0 g, 60.72 mmol, 1 equiv.) and dry DCM (90 ml). Acetylchloride (5.3 g, 67.23 mmol, 1.1 equiv.) and aluminium chloride (9.05 g, 67.23 mmol, 1.1 equiv.) were dissolved in dry DCM (40 ml) and slowly added at room temperature. After the reaction was complete the mixture was poured onto ice. DCM (200ml) was added and the organic layer was separated. The aqueous layer was washed with DCM (3 x 50 ml). The combined organic layers were washed with brine (50 ml), dried over MgSO_4 , filtered and concentrated under reduced pressure. The residue was purified by column chromatography (1. silica, hexane/tBME 9:1; 2. silica, hexane/tBME 2,5:1) to afford the desired compound **126** (5.48 g, 35%) as a red liquid.

$^1\text{H-NMR}$ (400 MHz, $(\text{CD}_3)_2\text{CO}$): δ (ppm) 4.08 (m, 1H); 4.68-4.67 (m, 1H); 4.47-4.46 (m, 1H); 4.17 (s, 5H); 2.43-2.37 (q, 2H); 2.31 (s, 3H); 1.18 (t, 3H).

$^{13}\text{C-NMR}$ (100 MHz, $(\text{CD}_3)_2\text{CO}$): δ (ppm) 201.84 (C_q , 1C); 96.16 (C_q , 1C); 79.72 (C_q , 1C); 72.38 (C_t , 1C); 71.01 (C_t , 5C); 69.48 (C_t , 1C); 69.42 (C_t , 1C); 27.38 (C_p , 1C); 22.81 (C_s , 1C); 14.83 (C_p , 1C).

ESI-MS (m/z), MeOH: 279.3 ($\text{M}^+\text{+Na}$).

EI-MS (m/z), 256.1 (100) [M^+].

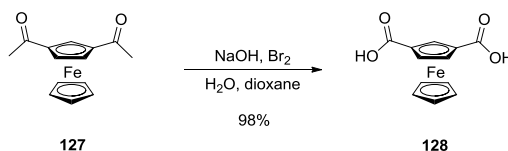
1,3-Diacetylferrocene 127:


A 100 ml two-necked round bottom flask was purged with argon and charged with 1-acetyl-3-ethylferrocene **126** (1.058 g, 4.13 mmol, 1 equiv.) and dry DCM (35 ml). Manganese(IV) oxide (5.386 g, 62 mmol, 15eq) was added and the resulting mixture was allowed to reflux overnight. Each day (for 10 days), more Manganese(IV) oxide (718 mg, 8.26 mmol, 2eq) was added to the reaction mixture. The reaction mixture was then filtered and concentrated under reduced pressure. The residue was washed with cold hexane to afford the desired compound **127** (400 mg, 35.9%) as an orange-red solid. The unreacted starting material could be re-isolated.

$^1\text{H-NMR}$ (400 MHz, $(\text{CD}_3)_2\text{CO}$): δ (ppm) 5.24 (s, 1H); 4.94 (s, 2H); 4.17 (s, 5H); 2.29 (s, 6H).

$^{13}\text{C-NMR}$ (100 MHz, $(\text{CD}_3)_2\text{CO}$): δ (ppm) 200.24 (C_q , 2C); 83.86 (C_q , 2C); 73.37 (C_t , 1C); 72.22 (C_t , 5C); 71.43 (C_t , 2C); 27.49 (C_p , 2C).

EI-MS (m/z), 270 (100%, M^+).

1,3-Ferrocenedicarboxylate 128:


A 25 ml two-necked round bottom flask was charged with sodium hydroxide (1.36 g, 33.898 mmol, 21 equiv.) and deion. water (6.5 ml). The solution was cooled to 0°C. Bromine (0.47 ml, 9.147 mmol, 5.67 equiv.) and dioxane (4,5 ml) were added subsequently. 1,3-Diacetylferrocene **127** (436 mg, 1.614 mmol, 1 equiv.) was added portion wise at 0°C. After the addition the reaction mixture was stirred for 1h. The reaction mixture was then diluted with DCM (10 ml) and the resulting organic layer was separated. The aqueous phase was washed with DCM (2 x 15 ml). The aqueous phase was acidified to pH 1 using aq. HCl and

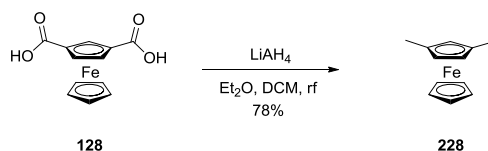
then extracted with ethyl acetate (3 x 20 ml). The combined organic layers were washed with brine, dried over MgSO₄, filtered and concentrated under reduced pressure to afford the 1,3-ferrocenedicarboxylate **128** (394 mg, 89%) as a red-brown solid.

¹H-NMR (400 MHz, (CD₃)₂CO): δ (ppm) 10.90 (s, 2H); 5.31 (s, 1H); 4.98 (s, 2H); 4.29 (s, 5H).

¹³C-NMR (100 MHz, (CD₃)₂CO): δ (ppm) 171.47 (C_q, 2C); 76.05 (C_q, 2C); 74.22 (C_t, 2C); 73.37 (C_t, 1C); 72.75 (C_t, 5C).

ESI-MS (m/z), MeOH: 273.2 (M⁻-H); 546.4 (2 x M⁻).

1,3-Dimethylferrocene **228**:

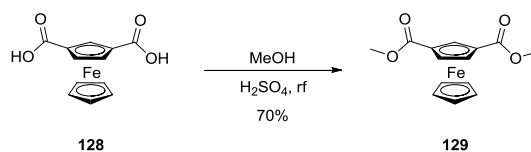


A 50 ml two-necked round bottom flask was purged with argon and charged with 1,3-ferrocenedicarboxylate **128** (394 mg, 1.438 mmol, 1 equiv.) and dry THF (20 ml). The reaction mixture was degassed for 10 min. with argon. A DiBAL-H solution (1M in hexane, 5.75 ml, 5.751 mmol, 4 equiv.) was slowly added over 30 min. After the addition was complete the reaction mixture was heated to reflux. More DiBAL-H solution (1M in hexane, 2 x 3 ml, 4 equiv.) was added until the starting material disappeared on the TLC (silica, DCM/ethyl acetate 9:1). The reaction was then quenched by adding water (25 ml). The pH was adjusted to 1 using aqueous HCl (6M). The mixture was extracted with tBME (3 x 25 ml). The combined organic layers were washed with brine, dried over MgSO₄, filtered and concentrated under reduced pressure. The residue was purified by column chromatography (silica, hexane/tBME 3:1) to afford compound **228** (239 mg, 77.7%) as an orange oil.

¹H-NMR (400 MHz, (CDCl₃): δ (ppm) 4.05 (s, 1H); 4.01 (s, 5H); 3.93 (d, J = 4 Hz, 2H); 1.95 (s, 6H).

¹³C-NMR (100 MHz, (CDCl₃): δ (ppm) 83.38 (C_q, 2C); 70.86 (C_t, 1C); 69.37 (C_t, 5C); 68.19 (C_t, 2C); 14.9 (C^p, 2C).

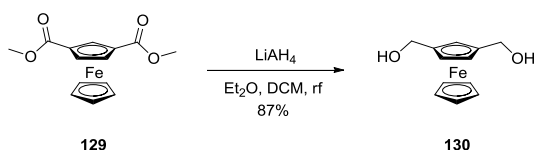
ESI-MS (m/z), MeOH: 214 (100%, M⁺).

Dimethyl-1,3-ferrocenedicarboxylate 129:

A 10 ml Schlenk tube was charged with 1,3-ferrocenedicarboxylate **128** (233 mg, 0.850 mmol), methanol (5.82 ml) and sulfuric acid (0.029 ml, 0.285 mmol). The reaction was heated to reflux and stirred for 28 h. After the reaction was complete the mixture was concentrated under reduced pressure. The residue was taken up in CHCl₃ and chromatographed over a short silica plug (benzene, then CH₂Cl₂) to afford the desired compound **129** (179 mg, 69.7%) as red oil.

¹H-NMR (400 MHz, (CD₃)₂CO): δ (ppm) 5.30-5.29 (m, 1H); 4.98 (d, 2H); 4.28 (s, 5H); 3.79 (s, 6H).

1,3-Bis(hydroxymethyl)ferrocene **130:**

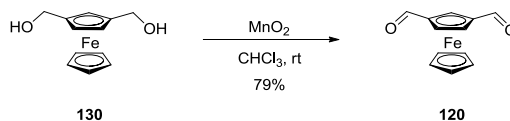


A 25 ml 3 necked round bottom flask was purged with argon and charged with lithium aluminium hydride (62.8 mg, 1.66 mmol, 4 equiv.) and dry diethyl ether (4.3 ml). Dimethyl-1,3-ferrocenedicarboxylate **129** (125 mg, 0.414 mmol, 1eq) dissolved in dry diethyl ether and dry DCM (4 ml) was added drop-wise at room temperature. After the addition was complete the reaction mixture was heated to reflux and stirred for 4h. More lithium aluminium hydride (40 mg, 1.05 mmol, 2.55eq) was added and the mixture was stirred at reflux for another 16h. After the reaction was complete the remaining LiAlH₄ was decomposed with water (4 ml). The reaction mixture was extracted with tBME (6 x 30 ml) and water. The combined organic layers were washed with brine, dried over MgSO₄, filtered and concentrated under reduced pressure to afford 1,3-bis(hydroxymethyl)ferrocene **130** (89 mg, 87.4%) as a yellow solid.

¹H-NMR (400 MHz, (CD₃)₂CO): δ (ppm) 4.31 (s, 1H); 4.30 (s, 4H); 4.265 (t, ³J_{H,H}=1.2 Hz, 2H); 4.151 (d, J=1,2 Hz, 2H); 4.12 (s, 5H).

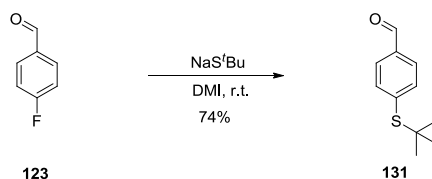
¹³C-NMR (100 MHz, (CD₃)₂CO): δ (ppm) 89.55 (C_q, 2C); 69.57 (C_t, 5C); 69.32 (C_t, 1C); 68.70 (C_t, 2C); 60.93 (C_s, 1C); 60.80 (C_s, 1C).

ESI-MS (m/z), MeOH: 246.1 (100%, M⁺).

1,3-Ferrocenedicarbaldehyde 120:

A 50 ml brominated round bottom flask was purged with argon and charged with 1,3-bis(hydroxymethyl)ferrocene **130** (85 mg, 0.345 mmol, 1 equiv.) and dry CHCl_3 (13 ml). Manganese(IV) oxide (882 mg, 8.63 mmol, 25 equiv.) was added and the reaction mixture was stirred for 18h in the absence of light. More manganese(IV) oxide (300 mg) was added until the reaction was complete. The reaction mixture was filtered and the filtrate was concentrated under reduced pressure to afford the desired 1,3-ferrocenedicarbaldehyde **120** (66 mg, 79%) as a red solid.

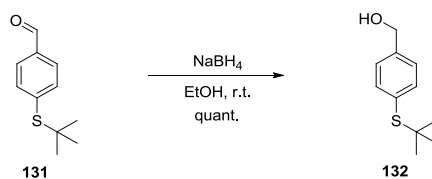
$^1\text{H-NMR}$ (400 MHz, $(\text{CD}_3)_2\text{CO}$): δ (ppm) 10.01 (s, 2H); 5.46 (s, 1H); 5.20 (s, 2H); 4.43 (s, 5H).

4-(tert-butylthio)benzaldehyde 131:

A 500 ml two-necked round bottom flask was purged with argon and charged with sodium 2-methyl-2-propanethiolate (18.7 g, 112.2 mmol, 1.5 equiv.) and dry DMI (350 ml). 4-Fluorobenzaldehyde (**123**) (12 ml, 111.2 mmol, 1 equiv.) was then slowly added to the mixture. The reaction mixture was stirred over night at room temperature. The mixture was then diluted with tBME (300 ml) and extracted with water (2 x 500 ml). The aqueous phase was extracted with tBME (3 x 150 ml). The organic layers were combined and extracted with 5% HCl aq. (2 x 500 ml), water (150 ml) and brine (150 ml). The organic phase was then dried over MgSO₄, filtered and concentrated under reduced pressure. The residue was distilled at 84°C and 3.5*10⁻² mbar to afford the desired 4-(tert-butylthio)benzaldehyde (**131**) (7.9 g, 37%) as a colorless oil.

¹H-NMR (250 MHz, CDCl₃): δ (ppm) 10.03 (s, 1H); 7.86-7.80 (m, 2H); 7.72-7.66 (m, 2H); 1.34 (s, 9H).

¹³C-NMR (100 MHz, CDCl₃): δ (ppm) 191.6 (C_t, 1C); 141.3 (C_q, 1C); 137.6 (C_t, 2C); 135.8 (C_q, 1C); 129.4 (C_t, 2C); 47.1 (C_q, 1C); 31.1 (C_p, 3C).

(4-tert-butylthio)phenyl)methanol 132:

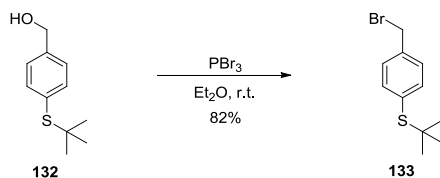
A 250 ml three necked round bottom flask was purged with argon and charged with 4-(tert-butylthio)benzaldehyde **131** (7 g, 36.0 mmol, 1 equiv.) and dry ethanol (100 ml). The mixture was cooled to 0°C. Sodium borohydride (1.51 g, 39.9 mmol, 1.1 equiv.) was added portion-wise. After the addition was complete the reaction mixture was stirred for 1h at room temperature. The mixture was then poured onto crushed ice (100 g) and aqueous HCl (4M, 60 ml). tBME was added and the aqueous phase was separated. The organic phase was then washed with water (50 ml) and brine (50 ml). Dried over MgSO₄, filtered and concentrated under reduced pressure to afford the desired (4-tert-butylthio)phenyl)methanol **132** (7.1 g, 92%) as a colorless oil.

¹H-NMR (250 MHz, CDCl₃): δ (ppm) 7.55-7.48 (m, 2H); 7.36-7.29 (m, 2H); 4.71 (s, 2H); 1.28 (s, 9H).

¹³C-NMR (100 MHz, CDCl₃): δ (ppm) 141.4; 137.6; 131.8; 126.9; 64.8; 45.9; 30.9.

EI-MS (m/z), 196 (22%, M⁺); 140 (100%, M⁺ - ^tBu); 107 (33%); 77 (12%); 57 (28%).

EA: calc.: C=67.30; H=8.22 found.: C=67.24; H=8.18

(4-(bromomethyl)phenyl)(tert-butyl)sulfane 133:

A 250 ml three necked round bottom flask was purged with argon and charged with (4-tert-butylthio)phenyl)methanol **132** (6.56 g, 33.4 mmol, 1 equiv.) and dry ether (65 ml). The reaction mixture was cooled to 0°C. PBr₃ (3.50 ml, 36.7 mmol, 1.1 equiv.) was then added within 15 minutes. The reaction mixture was stirred for another 90 min before it was quenched with water (200 ml). The layers were separated and the aqueous phase was washed

with tBME (3 x 60 ml). The organic layers were combined and washed with brine, dried over MgSO₄, filtered and concentrated under reduced pressure. The residue was purified by recrystallization using hexane/ethyl acetate to afford the desired (4-(bromomethyl)phenyl)(tert-butyl)sulfane **133** (7.1 g, 82%) as a white solid.

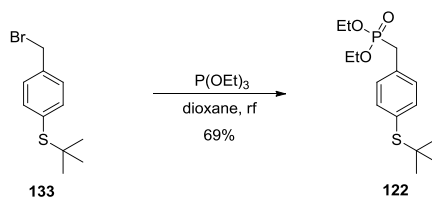
¹H-NMR (250 MHz, CDCl₃): δ (ppm) 7.53-7.47 (m, 2H); 7.38-7.31 (m, 2H); 4.49 (s, 2H); 1.29 (s, 9H).

¹³C-NMR (100 MHz, CDCl₃): δ (ppm) 138.2; 137.7; 133.1; 129.0; 46.2; 32.8; 31.0.

EI-MS (m/z), 260 (M⁺, 7%); 204 (13%); 179 (8%); 123 (100%); 78 (5%); 57 (38%).

EA: calc.: C=50.97; H=5.83 found.: C=51.87; H=5.66.

Diethyl 4-(tert-butylthio)benzylphosphonate **122**:

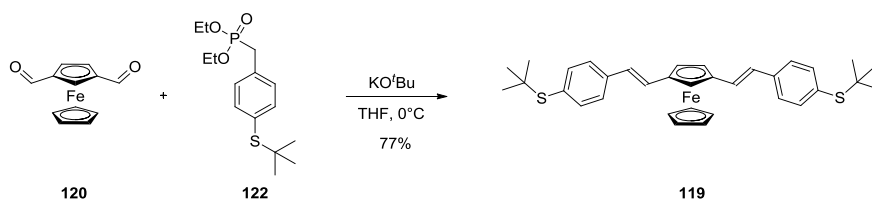


A 100 ml two-necked round bottom flask was purged with argon and charged with benzylbromide **133** (5.18 g, 20.0 mmol, 1 equiv.), triethyl-phosphite (4.4 ml, 27.3 mmol, 1.37 equiv.) and dry dioxane (30 ml). The resulting mixture was stirred at reflux for 12h. The mixture was then concentrated under reduced pressure. The residue was purified by distillation (145°C at 2.8 *10⁻² mbar) to afford the desired diethyl 4-(tert-butylthio)benzylphosphonate **122** (4.34 g, 68.7%) as a colorless oil.

¹H-NMR (400 MHz, CDCl₃): δ (ppm) 7.48-7.44 (m, 2H); 7.28-7.24 (m, 2H); 4.05-3.94 (m, 4H); 3.18 (s, 1H); 3.14 (s, 1H); 1.26 (s,9H); 1.22 (t, 6H).

¹³C-NMR (100 MHz, CDCl₃): δ (ppm) 137.5; 132.5; 131.2; 129.9; 62.2; 45.8; 34.2; 32.9; 30.9; 16.4.

EI-MS (m/z), 316 (M⁺, 14%).

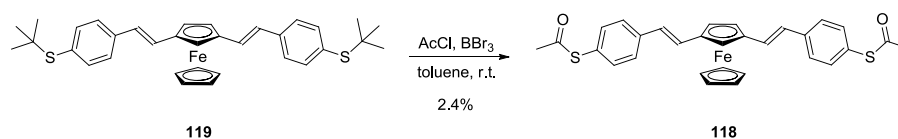
1,3-disubstituted ferrocene 119:

A 25 ml two-necked round-bottomed flask was purged with argon and charged with diethyl 4-(tert-butylthio)benzylphosphonate **122** (173 mg, 0.546 mmol, 2.2eq), 1,3-ferrocenedicarbaldehyde **120** (60 mg, 0.248 mmol, 1eq) and dry THF (5.5 ml). The resulting solution was cooled to 0°C. Potassium *tert*-butoxide (150 mg, 1.34 mmol, 5.4eq) was dissolved in THF (3 ml) and added over a period of 10min. The reaction mixture was allowed (2,5h) to warm to room temperature and was then stirred for 1h. The reaction mixture was diluted with DCM (20 ml) and extracted with water (30 ml). The aqueous phase was extracted with DCM (3 x 30 ml). The combined organic layers were washed with brine, dried over MgSO₄, filtered and concentrated under reduced pressure. The residue was purified by column chromatography (hexane/DCM 2:1) to afford the pure 1,3-ferrocene-OPV **119** (108 mg, 77%) as a red solid.

¹H-NMR (400 MHz, CDCl₃): δ (ppm) 7.50-7.39 (m, 8H); 6.931-6.898 (d, ³J_{HH}=16.5 Hz, 2H); 6.765-6.732 (d, ³J_{HH}=16.5 Hz, 2H); 4.82 (s, 1H); 4.61 (s, 2H); 4.12 (s, 5H); 1.31 (s, 18H).

¹³C-NMR (100 MHz, CDCl₃): δ (ppm) 138.3 (C_q, 2C); 138.0 (C_t, 4C); 131.2 (C_q, 2C); 127.9 (C_t, 2C); 126.0 (C_t, 4C); 125.9 (C_t, 2C); 84.4 (C_q, 2C); 70.7 (C_t, 5C); 68.5 (C_t, 2C); 65.7 (C_t, 1C); 46.3 (C_q, 2C); 31.2 (C_p, 6C).

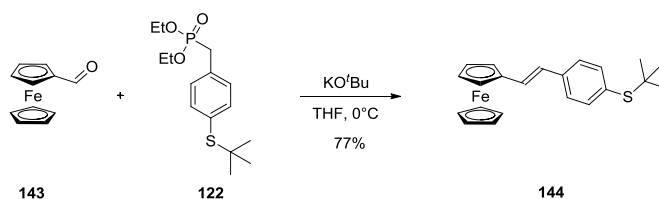
ESI-MS (m/z), MeOH: 566.0 (100%, M⁺).

1,3-disubstituted ferrocene 118:

A 100 ml two-necked round-bottomed flask was purged with argon and charged with the 1,3-disubstituted ferrocene **119** (95.2 mg, 0.168 mmol, 1eq), acetyl chloride (7.5 ml, 106 mmol, 629eq) and toluene (30 ml). The red solution was degassed for 10 min. A boron tribromide solution (0.4 ml, 0.4 mmol, 2.38eq, 1M in DCM) was added dropwise over 10 min. The reaction mixture turned dark-red after the addition was complete. The reaction mixture was stirred at room temperature for 3h. After the reaction was complete it was quenched with ice-water. The aqueous phase was separated and extracted with toluene (3 x 20 ml). The combined organic layers were washed with brine, dried over MgSO₄ and concentrated under reduced pressure. The crude product was purified by column chromatography (1st column: hexane/EA 5:1, RF: 0.24; 2nd column: DCM, RF 0.9) to afford the desired target structure **118** (2.2 mg, 2.4%) as a red solid.

¹H-NMR (400 MHz, (CD₃)₂CO): δ (ppm) 7.46-7.34 (m, 8H); 6.93-6.89 (d, ³J_{HH}=16 Hz, 2H); 6.74-6.70 (d, ³J_{HH}=16 Hz, 2H); 4.08 (m, 1H); 4.596-4.593 (d, ³J_{HH}=1.2 Hz, 2H); 4.09 (s, 5H); 2.41 (s, 6H).

ESI-MS (m/z), MeOH: 538.0 (100%, M⁺).

Mono-substituted ferrocene 144:


A 25 ml two-necked round-bottomed flask was purged with argon and charged with Diethyl 4-(tert-butylthio)benzylphosphonate (**122**) (174 mg, 0.550 mmol, 1.1 equiv.), aldehyde ferrocene **143** (109 mg, 0.500 mmol, 1 equiv.) and dry THF (7 ml). The resulting solution was cooled to 0°C. Potassium tert-butoxide (151 mg, 1.35 mmol, 2.7eq), dissolved in dry THF (5 ml), was added over a period of 10min. The reaction mixture was slowly (30 min.) allowed to reach room temperature. The reaction mixture was diluted with DCM (20 ml) and extracted with water (3 x 30 ml). The aqueous phase was extracted with DCM (3 x 30 ml). The combined organic layers were washed with brine, dried over MgSO₄ and concentrated under reduced pressure. The residue was filtered over a short plug of silica (hexane/DCM 2:1) to afford the desired ferrocene **144** (188 mg, 99%) as a red solid.

¹H-NMR (400 MHz, CDCl₃): δ (ppm) 7.49-7.37 (m, 4H); 6.93-6.89 (d, ³J_{HH}=16 Hz, 1H); 6.71-6.67 (d, ³J_{HH}=16 Hz, 1H); 4.47 (t, ³J_{HH}=2 Hz, 2H); 4.30 (t, ³J_{HH}=2 Hz, 2H); 4.14 (s, 5H); 1.30 (s, 9H).

¹³C-NMR (125 MHz, CDCl₃): δ (ppm) 138.4 (C_q, 1C); 137.9 (C_t, 2C); 130.9 (C_q, 1C); 128.2 (C_t, 1C); 125.9 (C_t, 2C); 125.4 (C_t, 1C); 83.4 (C_q, 1C); 69.5 (C_t, 5C) 69.4 (C_t, 2C); 67.1 (C_t, 2C); 46.2 (C_q, 1C); 31.1 (C_p, 3C).

ESI-MS (m/z), MeOH: 376.0 (100%, M⁺).

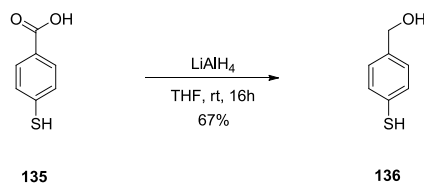
Mono-substituted ferrocene 142:

A 100 ml two-necked round-bottomed flask was purged with argon and charged with ferrocene **144** (94.1 mg, 0.250 mmol, 1 equiv.), acetyl chloride (5.35 ml, 75.0 mmol, 300 equiv.) and dry toluene (30 ml). The red solution was degassed for 10 min. Boron tribromide (0.0287 ml, 74.5 mmol, 1.19 equiv.) in DCM (1 ml) was added dropwise over 10 min. The reaction mixture was stirred at room temperature overnight. The reaction was then quenched with ice-water and the aqueous phase was separated and extracted with toluene (3 x 20 ml). The combined organic layers were washed with brine, dried over MgSO₄ and concentrated under reduced pressure. The residue was filtered over a short silica plug (hexane/ethyl acetate 5:1, no vacuum suction) to afford the slightly impure product (34 mg). The crude product was purified by column chromatography (DCM/hexane 1:1) to afford the desired compound **142** (33 mg, 36%) as a red solid.

¹H-NMR (500 MHz, CDCl₃): δ (ppm) 7.47-7.45 (d, ³J_{HH}=8 Hz, 2H); 7.36-7.34 (d, ³J_{HH}=8 Hz, 2H); 6.95-6.92 (d, ³J_{HH}=16 Hz, 1H); 6.70-6.67 (d, ³J_{HH}=16 Hz, 1H); 4.47 (s, 2H); 4.31 (s, 2H); 4.14 (s, 5H); 2.43 (s, 3H).

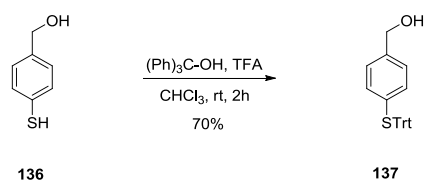
¹³C-NMR (126 MHz, CDCl₃): δ (ppm) 193.68 (C_q, 1C); 139.35 (C_q, 1C); 134.90 (C_t, 2C); 129.00 (C_t, 1C); 126.59 (C_t, 2C); 125.06 (C_t, 1C); 82.91 (C_q, 1C); 78.80 (C_q, 1C); 69.46 (C_t, 2C); 69.41 (C_t, 5C); 67.20 (C_t, 2C); 30.33 (C_p, 1C).

ESI-MS (m/z), MeOH: 362.0 (100%, M⁺).

(4-mercaptophenyl)methanol 136:

A 250 ml three-necked round bottom flask was purged with argon and charged with lithium aluminium hydride (4.42 g, 117 mmol, 5 equiv.) and dry THF (40 ml). A solution of 4-mercapto-benzoic acid **135** (4.0 g, 23.3 mmol, 1 equiv.) in dry THF (25 ml) was added dropwise within 45 min. The resulting mixture was stirred at room temperature for 16h. The formation of a sticky cum ball could be observed during that time. Water (20 ml) was slowly added to quench the reaction. The mixture was then acidified with 1M HCl. The mixture was extracted with *t*BME (3 x 50 ml) and the combined organic layers were washed with brine, dried over MgSO₄, filtered and concentrated under reduced pressure. The crude product (3.979 g) was purified by recrystallization to afford the desired compound **136** (1.976 g, 60.5%) as a white solid.

¹H-NMR (400 MHz, CD₂Cl₂): δ (ppm) 7.28-7.22 (m, 4H); 4.61 (s, 2H); 4.06 (s, 1H); 3.54 (s, 1H).

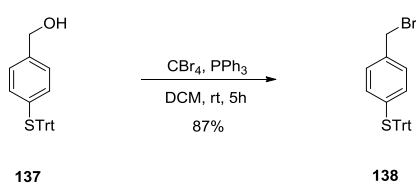
(4-(tritylthio)phenyl)methanol 137:

To a solution of (4-mercaptophenyl)methanol **136** (0.979 g, 6.98 mmol, 1 equiv.) in dry CHCl₃ (50 ml), triphenylmethanol (2.25 g, 8.38 mmol, 1.2 equiv.) and TFA (1.67 ml, 14.7, 2.1eq) were added. The mixture was stirred at room temperature for 2h. Saturated aq. NaHCO₃ was then added to quench the reaction. The organic solvent was evaporated and the residue extracted with DCM (3 x 30 ml). The organic layers were combined and washed with brine (15 ml), dried over MgSO₄, filtered and concentrated under reduced pressure. The crude product was purified by column chromatography (hexane/*t*BME 2:1) to afford the desired product **137** as colorless oil (1.27 g, 47.6%).

$^1\text{H-NMR}$ (400 MHz, CD_2Cl_2): δ (ppm) 7.42-7.39 (m, 6H); 7.27-7.18 (m, 9H); 7.000 (dt, $^3\text{J}_{\text{H,H}}=8.4$ Hz, $^4\text{J}_{\text{H,H}}=1.6$ Hz, 2H); 6.934 (dt, $^3\text{J}_{\text{H,H}}=8.4$ Hz, $^4\text{J}_{\text{H,H}}=1.6$ Hz, 2H); 4.535 (d, $^3\text{J}_{\text{H,H}}=5.6$ Hz, 2H); 3.16 (s, 1H).

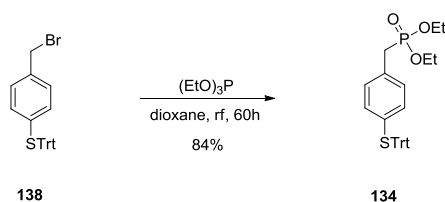
$^{13}\text{C-NMR}$ (100 MHz, CD_2Cl_2): δ (ppm) 144.9; 141.4; 134.9; 130.3; 128.1; 127.1; 126.8; 64.8; 27.1.

(4-(bromomethyl)phenyl)(trityl)sulfane 138:



A 100 ml two-necked round bottomed flask was purged with argon and charged with 4-(tritylthio)phenylmethanol **137** (1.20 g, 3.15 mmol, 1 equiv.), carbon tetrabromide (1.16 g, 3.47 mmol, 1.1 equiv.) and dry DCM (25 ml). The resulting solution was cooled to 0°C . Triphenylphosphine (0.918 g, 3.47 mmol, 1.1 equiv.) was added portion wise over 30 min. The resulting mixture was then allowed to reach room temperature and was stirred for another 5h. The mixture was poured into brine and the organic layer was separated. The aqueous phase was extracted with DCM (3 x 20 ml). The combined organic layers were dried over Na_2SO_4 , filtered and concentrated under reduced pressure. The crude product (3.469 g) was purified by column chromatography to afford the 4-(bromomethyl)phenyl(trityl)sulfane **138** (1.226 g, 87.4%) as a white solid.

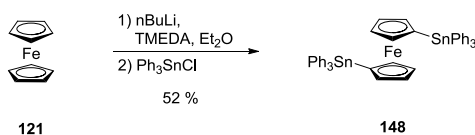
$^1\text{H-NMR}$ (400 MHz, CD_2Cl_2): δ (ppm) 7.41-7.38 (m, 6H); 7.30-7.18 (m, 9H); 7.022 (dt, $^3\text{J}_{\text{H,H}}=8.4$ Hz, $^4\text{J}_{\text{H,H}}=2.4$ Hz, 2H); 6.909 (dt, $^3\text{J}_{\text{H,H}}=8.4$ Hz, $^4\text{J}_{\text{H,H}}=2.4$ Hz, 2H); 4.37 (s, 2H).

Diethyl 4-(tritylthio)benzylphosphonate **134:**

A two-necked round bottomed flask was purged with argon and charged with (4-(bromomethyl)phenyl) (trityl)sulfane **138** (1g, 2.24 mmol, 1 equiv.) and dioxane (20 ml). Triethyl phosphite (0.55 ml, 3.07 mmol, 1.37 equiv.) was added and the resulting solution was heated to reflux for 60h. The reaction mixture was then concentrated under reduced pressure and the residue was purified by column chromatography (DCM/EA 10:1) to afford the desired product **134** (717 mg, 63%) as a white solid.

$^1\text{H-NMR}$ (400 MHz, CD_2Cl_2): δ (ppm) 7.41-7.38 (m, 6H); 7.26-7.17 (m, 9H); 6.95-6.89 (m, 4H); 4.00-3.86 (m, 4H); 2.981 (d, $^2J_{\text{H,H}}=21.6$ Hz, 2H); 1.192 (t, $^3J_{\text{H,H}}=7.2$ Hz, 6H).

$^{13}\text{C-NMR}$ (125 MHz, CD_2Cl_2): δ (ppm) 145.06 (C_q , 3C); 135.06 (C_t , 2C); 133.19 (C_q , 1C); 132.54 (C_q , 1C); 130.49 (C_t , 6C); 130.04 (C_t , 2C); 128.22 (C_t , 6C); 127.24 (C_t , 3C); 70,70 (C_q , 1C); 62.59 (C_s , 2C); 34.33 (C_s , 1C); 16.77 (C_p , 2C).

1,1'-bis(triphenylstannyl)ferrocene (148**):**

A 500 ml two-necked round-bottomed flask was purged with argon and charged with TMEDA (11.3 ml, 74.0 mmol, 2.47 equiv.) and dry diethylether (10 ml). The mixture was cooled with an ice bath and *n*-BuLi (46.3 ml, 74.0 mmol, 2.47 equiv., 1.6M in hexane) was added via syringe. The mixture was warmed to room temperature. After 10 min. a ferrocene **121** solution (5.6 g, 30.0 mmol, 1 equiv., in 250 ml diethylether) was added over a period of 30 min. The reaction mixture was stirred for an additional 6h, during which time orange crystals were observed to be formed. The slurry was cooled to 0°C. Triphenyltin chloride (25.2 g, 63.3 mmol, 2.11 equiv.) was added. The reaction mixture was warmed to room temperature and stirred overnight. The mixture was transferred into a 2L separation funnel,

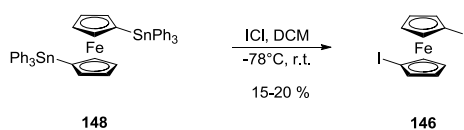
diluted with *t*BME/toluene (300/100 ml) and washed with water (500 ml) and brine (300 ml). The organic phase was dried over MgSO₄, filtered and concentrated under reduced pressure to afford the crude product as red oil which solidified upon standing. The crude product was dissolved in DCM and adsorbed on b-Alox and then directly purified by column chromatography (silica, hexane:DCM, 5:1) to afford the desired compound **148** (13.7 g, 52 %) as an orange solid.

¹H-NMR (400 MHz, CD₂Cl₂): δ (ppm) 7.68-7.53 (m, 12H); 7.42-7.36 (m, 18H); 4.19 (t, 4H); 4.10 (t, 4H).

¹³C-NMR (125 MHz, CD₂Cl₂): δ (ppm) 138.9 (C_q, 6C); 137.2 (C_t, 12C); 129.2 (C_q, 6C); 128.7 (C_t, 12C); 76.8 (C_t, 4C); 75.0 (C_t, 4C); 66.3 (C_q, 2C).

ESI-MS, (MeOH, pos. mode) m/z: 884.3 (M⁺); 907.3 (M⁺+Na).

1,1'-diiodoferrocene (**146**):

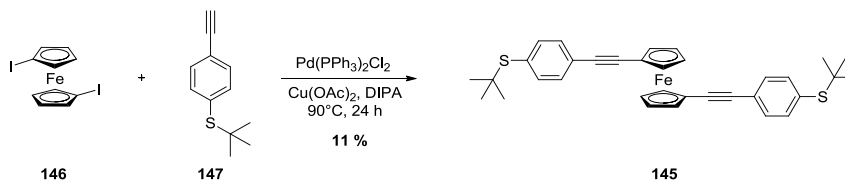


A 25 ml two-necked round-bottomed flask was purged with argon and charged with compound **148** (4.1 g, 4.64 mmol, 1 equiv.) and dry DCM (15 ml). The solution was cooled to -78°C and degassed for 10 min. Iodine monochloride (1M in DCM, 9.74 ml, 9.74 mmol, 2.1 equiv.) was then added quickly with a syringe. The resulting black solution was allowed to reach room temperature and was stirred overnight. The reaction mass was diluted with *t*BME and extracted with sat. Na₂S₂O₃, water and brine. The organic solution was dried over MgSO₄, filtered and concentrated under reduced pressure. The residue was dissolved in cyclohexane and filtered over a silica plug. The crude product was purified by column chromatography (RP-18, acetonitrile:water 5:1) to afford the desired 1,1'-diiodoferrocene (**146**) (405 mg, 20 %) as red oil.

¹H-NMR (400 MHz, CD₂Cl₂): δ (ppm) 4.37 (t, 4H); 4.18 (t, 4H).

¹³C-NMR (125 MHz, CDCl₃): δ (ppm) 78.1 (C_t, 4C); 77.4 (C_t, 4C); 72.9 (C_q, 2C).

ESI-MS, (MeOH, pos. mode) m/z: 437.8 (M⁺). EI-MS (70 eV), m/z (%): 437.8 (100) [M⁺]; 310.8 (9.2) [M⁺-I].

1,1'-bis[2-(4-*tert*-butylthiophenyl)ethynyl]-ferrocene **145:**


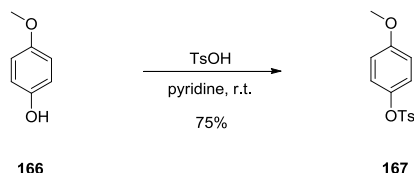
A 10 ml Schlenk-tube was purged with argon and charged with bis(triphenylphosphine)palladium(II) chloride (8.4 mg, 0.012 mmol, 0.08 equiv.) and Cu(OAc)_2 (2.2 mg, 0.012 mmol, 0.08 equiv.). 1,1'-diiodoferrocene **146** (65.7 mg, 0.15 mmol, 1 equiv.), 1-*tert*-butylthio-4-ethynylbenzene **147** (65.7 mg, 0.345 mmol, 2.3 equiv.) and diisopropylamine (1 ml) were added. The resulting dark solution was heated to 90°C and stirred overnight. The reaction mixture was concentrated under reduced pressure and the residue was purified by column chromatography (silica, cyclohexane/DCM 2:1) to afford the desired product **145** (9 mg, 10.7%) as a red solid.

$^1\text{H-NMR}$ (400 MHz, CDCl_3): δ (ppm) 7.437 (dt, $^3J_{\text{H,H}}=8.4$ Hz, $^4J_{\text{H,H}}=1,6$ Hz, 4H); 7.390 (dt, $^3J_{\text{H,H}}=8.4$ Hz, $^4J_{\text{H,H}}=1,6$ Hz, 4H); 4.551 (t, $^3J_{\text{H,H}}=2$ Hz, 2H); 4.339 (t, $^3J_{\text{H,H}}=2$ Hz, 2H); 1.288 (s, 18H).

$^{13}\text{C-NMR}$ (125 MHz, CDCl_3): δ (ppm) 137.2 (C_t , 4C); 132.7 (C_q , 2C); 131.4 (C_t , 4C); 124.3 (C_q , 2C); 73.1 (C_t , 4C); 71.1 (C_t , 4C); 66.8 (C_q , 2C); 46.2 (C_q , 2C); 30.7 (C_p , 6C).

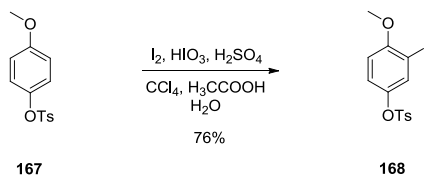
7.4 Synthesis of a Interlinked Molecular Wire

4-Methoxyphenyl *p*-Toluenesulfonate **167**:



A 500 ml round bottom flask was purged with argon and charged with 4-methoxyphenol **166** (49.7 g, 400 mmol, 1 equiv.), tosyl chloride (76.3 g, 400 mmol, 1 equiv.) and dry THF (200 ml). Pyridine (31.6 g, 32.3 ml, 400 mmol, 1 equiv.) was added at room temperature and the reaction mixture was stirred for 12h. The mixture was poured into a mixture of water (300 ml) and diethyl ether (1200 ml). The organic layer was separated and extracted with 10% sodium hydroxide (4 x 250 ml), washed with water (200 ml) and brine (200 ml). The organic layer was then dried over MgSO₄, filtered and concentrated under reduced pressure. The residue was recrystallized from methanol to afford the desired compound **167** (53.04 g, 47 %) as a white solid.

¹H-NMR (250 MHz, CDCl₃): δ (ppm) 7.67 (d, 2H); 7.29 (d, 2H); 6.88 (d, 2H); 6.78-6.75 (m, 2H); 3.77 (s, 3H); 2.45 (s, 3H).

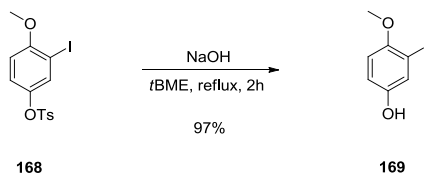
3-iodo-4-methoxyphenyl *p*-Toluenesulfonate 168:

A 250 ml round bottom flask was purged with argon and charged with 4-methoxyphenyl *p*-Toluenesulfonate **167** (53.0 g, 190.5 mmol, 1 equiv.), iodine (38.7 g, 152 mmol, 0.8 equiv.), iodic acid (13.4 g, 76.2 mmol, 0.4 equiv.), sulfuric acid (7.8 ml, 143 mmol, 0.75 equiv.), carbon tetrachloride (38.7 g, 400 mmol, 2.1 equiv.), acetic acid (91.6 ml, 1600 mmol, 8.4 equiv.) and water (45.6 ml). The mixture was heated to reflux and stirred for 3 days. After cooling to room temperature the mixture was poured into diethylether (1000 ml) and water (300 ml). The organic layer was extracted with water (150 ml), aqueous sodium thiosulfate (4 x 200 ml), 10 % aqueous sodium hydroxide (2 x 200 ml), water (200 ml) and brine (200 ml). The organic phase was dried over MgSO₄, filtered and concentrated under reduced pressure. The residue was recrystallized from methanol to afford the desired compound **168** (58.4 g, 76 %) as an off-white solid.

¹H-NMR (CD₂Cl₂, 400 MHz) δ (ppm): 7.67 (d, J = 8.4 Hz, 2H); 7.34-7.37 (m, 3H); 6.94 (dd, ³J = 9.0 Hz, ⁴J = 2.8 Hz, 1H); 6.71 (d, J = 9.0 Hz, 1H); 3.83 (s, 3H); 2.45 (s, 3H).

¹³C-NMR (CD₂Cl₂, 100.6 MHz): δ (ppm) 158.01; 146.71; 143.83; 133.92; 132.69; 130.64; 129.27; 124.01; 111.33; 85.57; 57.49; 22.23.

EI-MS (70 eV), m/z (%): 404 (33.1) [M⁺], 249 (100) [M⁺ - C₇H₇O₂S].

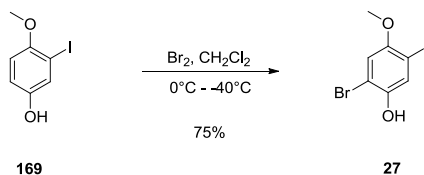
3-Iodo-4-methoxyphenol 169:

A 250 ml round bottom flask was charged with sodium hydroxide (20.0 g, 0.5 mol) and water (80 ml). The solution was degassed for 10 min. with argon. Another round bottom flask was purged with argon and charged with 3-iodo-4-methoxyphenyl-*p*-toluenesulfonate **168** (56.0 g, 138.54 mmol, 1 equiv.) and *t*BME (75 ml). The solution was also degassed for 10 min. The sodium hydroxide solution was then added drop wise. After the addition was complete the reaction mixture was heated to reflux for 2h. The mixture was cooled to room temperature and then acidified with aq. HCl (10 %, 150 ml). The mixture was poured into a mixture of *t*BME (550 ml) and water (200 ml). The aqueous phase was separated and the organic layer was washed with aq. NaOH (10 %, 4 x 180 ml). The aqueous layers were combined, acidified with aq. HCl (10 %, 750 ml) and extracted with *t*BME (4 x 180 ml). the combined organic layers were washed with brine (300 ml), dried over MgSO₄, filtered and concentrated under reduced pressure to afford the desired compound **169** (33.82 g, 97.7 %) as a white solid.

¹H-NMR (CD₂Cl₂, 250 MHz): δ (ppm) 7.30 (d, 1H); 6.84-6.82 (dd, 1H); 6.75-6.73 (d, 1H); 4.83 (s, 1H); 3.79 (s, 3H).

¹³C-NMR (CD₂Cl₂, 100.6 MHz): δ (ppm) 153.32; 150.70; 126.66; 116.50; 112.30; 86.20; 57.43.

EI-MS (70 eV), m/z (%): 250 (100) [M⁺], 235 (56.81) [M⁺ -CH₃], 108 (16) [M⁺ -CH₃ -I].

2-Bromo-5-iodo-4-methoxyphenol 27:

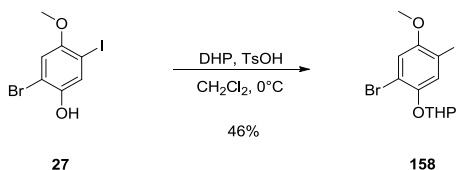
A 500 ml round bottom flask was purged with argon and charged with 3-iodo-4-methoxyphenol **169** (33.77 g, 135.04 mmol) and dry CH₂Cl₂ (250 ml). A bromine solution (21.58 g, 135.04 mmol, 40 ml CH₂Cl₂) was added drop wise at 0°C. The reaction mixture was then cooled to -40°C and was stirred overnight. Dry CH₂Cl₂ (20 ml) and chloroform (20 ml) were added and the reaction mixture was stirred for another 2h at room temperature. The mixture was then poured into *t*BME (550 ml) and water (270 ml). The organic layer was washed 2 times with water (270 ml), 4 times with 17 % aqueous sodium thiosulphate and brine (270 ml). Drying over MgSO₄ and evaporation of the solvent yielded in 42.02 g of a brown solid. Recrystallization from heptane afforded the desired compound **27** (33.30 g, 75.2 %) as a brown solid.

¹H-NMR (CDCl₃, 400 MHz): δ (ppm) 7.46 (s, 1H); 6.89 (s, 1H); 5.10 (s, 1H); 3.82 (s, 3H).

¹³C-NMR (CDCl₃, 100.6 MHz): δ (ppm) 147.55; 126.56; 114.33; 98.98; 85.72; 57.55.

EI-MS (70 eV), m/z (%): 327.9 (100) [M⁺], 312.9 (63.3) [M⁺ -CH₃], 186 (15.1) [M⁺ -CH₃ -I], 79 (5.4) [Br⁺].

2-Bromo-5-iodo-4-methoxy-1-(3,4-tetrahydro-2H-pyran-2-yloxy)benzene 158:

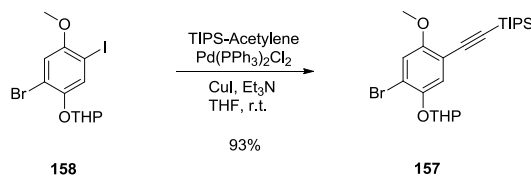


A 100 ml round bottom flask was charged with 2-bromo-5-iodo-4-methoxyphenol **27** (33.30 g, 101.23 mmol) and dry DCM (25 ml). *p*TsOH (0.022 g, 0.106 mmol) was added and the mixture was cooled to 0°C. 3,4-Dihydropyran (13.625 g, 161.97 mmol) was added drop wise over 20 min and the reaction mixture stirred for 1 h at 0°C and an additional hour at room temperature. The mixture was poured into *t*BME (50 ml) and 10 % sodium hydroxide. The organic layer was extracted with 10 % sodium hydroxide (3 x 20 mL), water (25 ml) and brine (30 ml). The organic phase was then dried over MgSO₄, filtered and concentrated under reduced pressure to afford 44.50 g of a brown solid. Two fold recrystallization from *n*-hexane afforded the desired compound **158** (18.90 g, 45.8 %) as a slightly yellow solid.

¹H-NMR (CDCl₃, 400 MHz): δ (ppm) 7.56 (s, 1H); 6.89 (s, 1H); 5.36 (t, 1H); 3.94-3.89 (tt, 1H); 3.38 (s, 3H); 3.65-3.62 (dd, 1H); 2.06-1.60 (m, 6H).

¹³C-NMR (CDCl₃): δ (ppm) 153.89; 148.44; 128.01; 115.42; 113.76; 98.02; 84.23; 62.07; 57.18; 30.31; 25.33; 18.46.

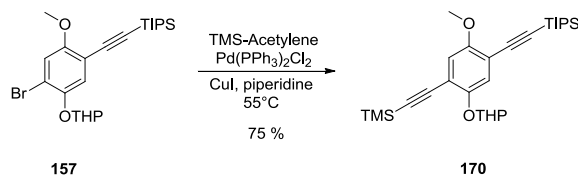
EI-MS (70 eV), *m/z* (%): 412 (0.47) [M⁺], 327.9 (100) [M⁺ - DHP], 85.1 (97.4) [DHP⁺].

4-Methoxy-1-(tetrahydro-2H-pyran-2-yloxy)-2-(triisopropylsilylethynyl)-5-bromobenzene 157:

A 100 ml Schlenk tube was purged with argon and charged with 2-bromo-5-iodo-4-methoxy-1-(3,4-tetrahydro-2H-pyran-2-yloxy)benzene **158** (2.003 g, 4.85 mmol, 1 equiv.), bis(triphenylphosphine) palladium chloride (170 mg, 0.243 mmol, 0.05 equiv.), CuI (92.8 mg, 0.485 mmol, 0.1 equiv.), dry THF (20 ml) and DIEA (4.8 ml). The mixture was degassed with argon for 10 min. Then, (triisopropylsilyl) acetylene (1.26 ml, 5.34 mmol, 1.1 equiv.) was added to the orange solution and the reaction mixture was stirred for 15h at room temperature. After the reaction was completed *t*BME was added and the suspension was filtered through Celite. The filtrate was concentrated under reduced pressure. The residue was purified by column chromatography (silica, cyclohexane:ethyl acetate 35/1 + 5% triethylamine) to afford the desired compound **157** as a slightly yellow oil (2.15 g, 93.5 %).

¹H-NMR (CDCl₃, 400 MHz): δ (ppm) 7.19 (s, 1H); 7.03 (s, 1H); 5.39 (t, 3H); 3.97-3.91 (tt, 1H); 3.81 (s, 3H); 3.64-3.61 (dd, 1H); 2.08-1.61 (m, 6H); 1.09 (s, 21H).

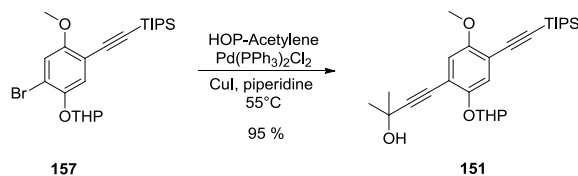
¹³C-NMR (CDCl₃): δ (ppm) 156.50; 147.46; 122.18; 116.68; 114.67; 113.29; 102.56; 97.99; 94.06; 62.28; 57.04; 30.59; 25.64; 19.06; 18.76; 11.73.

4-Methoxy-1-(tetrahydro-2H-pyran-2-yloxy)-2-(2-triisopropylsilylethynyl)-5-(2-trimethylsilylethynyl)benzene 170:

A 50 ml Schlenk tube was purged with argon and charged with 4-methoxy-1-(tetrahydro-2H-pyran-2-yloxy)-2-(triisopropylsilylethynyl)-5-bromobenzene **157** (1.730 g, 3.70 mmol, 1 equiv.), piperidine (12 ml), Pd(PPh₃)₂Cl₂ (129.9 mg, 0.185 mmol, 0.05 equiv.) and CuI (35.2 mg, 0.185 mmol, 0.05 equiv.). the resulting mixture was degassed with argon for 10 min. Ethynyltrimethylsilane (0.727 g, 7.402 mmol, 2 equiv.) was then added to the solution and the reaction mixture was stirred at 55°C for 15h. The reaction was diluted with *t*BME and filtered over celite. The filtrate was concentrated under reduced pressure. The residue was dissolved in *t*BME (100 ml) and extracted with aqueous NH₄Cl (4 x 25 ml). The aqueous phase was acidified with aq. 1N HCl and extracted with *t*BME (50 ml). The organic layers were combined and washed with brine, dried over MgSO₄, filtered and concentrated under reduced pressure. The residue was purified by column chromatography (silica, cyclohexane/*t*BME 40:1) to afford the desired compound **170** (1.36 g, 75.8 %) as yellow oil.

¹H-NMR (CDCl₃, 400 MHz) δ (ppm) = 7.13 (s, 1H), 6.87 (s, 1H), 5.46 (s, 1H), 4.05-3.99 (tt, 1H), 3.82 (s, 3H), 3.62-3.59 (dd, 1H), 2.06-1.62 (m, 7H), 1.12 (s, 21H), 0.25 (s, 9H).

4-(5-methoxy-2-((tetrahydro-2H-pyran-2-yl)oxy)-4-((triisopropylsilyl)ethynyl)phenyl)-2-methylbut-3-yn-2-ol **151:**

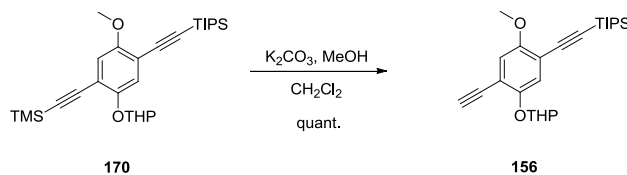


A 50 ml Schlenk tube was purged with argon and charged with 4-methoxy-1-(tetrahydro-2H-pyran-2-yloxy)-2-(triisopropylsilylethynyl)-5-bromobenzene **157** (2.583 g, 5.53 mmol, 1eq), bis(triphenylphosphine) palladium chloride (194 mg, 0.276 mmol, 0.05eq), CuI (84.6 mg, 0.442 mmol, 0.08eq) and piperidine (25 ml). The solution was degassed for 10 min. with argon. The mixture was heated to 55°C and 2-methyl-3-butyn-2-ol (1.08 ml, 11.1 mmol, 2eq) was added. The reaction was stirred for 17h at 55°C. After the reaction was complete *t*BME was added and the mixture was filtered over celite. The filtrate was concentrated under reduced pressure. The residue was purified by column chromatography (silica, cyclohexane/*t*BME 5:1 → 1:1 + 5 % triethylamine) to afford the desired compound **151** (3.88 g, 94.8 %) as yellowish oil.

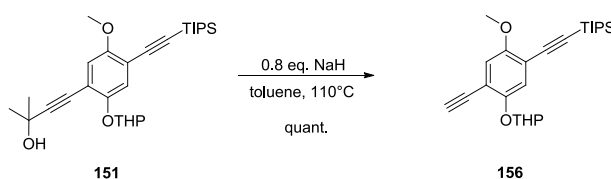
$^1\text{H-NMR}$ (CDCl_3 , 400 MHz) δ (ppm) = 7.259 (s, 1H); 6.835 (s, 1H); 5.431 (t, $^3J_{\text{H,H}} = 2.8$ Hz, 1H); 3.999 (dt, $^3J_{\text{H,H}} = 10.8$ Hz, $^2J_{\text{H,H}} = 2.8$ Hz, 1H); 3.799 (s, 3H); 3.64-3.59 (m, 1H); 1.918-1.626 (m, 12 H); 1.123 (s, 21 H).

$^{13}\text{C-NMR}$ (CDCl_3 , 100.6 MHz) δ (ppm) = 155.7; 151.3; 121.8; 115.4; 114.8; 114.3; 102.7; 99.1; 97.6; 97.1; 78.8; 65.9; 61.9; 56.6; 49.6; 31.6; 30.4; 27.1; 25.4; 18.8; 18.5; 11.5.

FAB-MS, (8 kV) m/z (%): 471 (10.4) [$\text{M}^+ + \text{H}$], 453 (19.8) [$\text{M}^+ - \text{OH}$], 386 (65.1) [$\text{M}^+ - \text{C}_5\text{H}_8\text{O}$], 369 (100) [$\text{M}^+ - \text{C}_5\text{H}_8\text{O}_2$].

Deprotection method of compound 170: (TMS-protected acetylene)


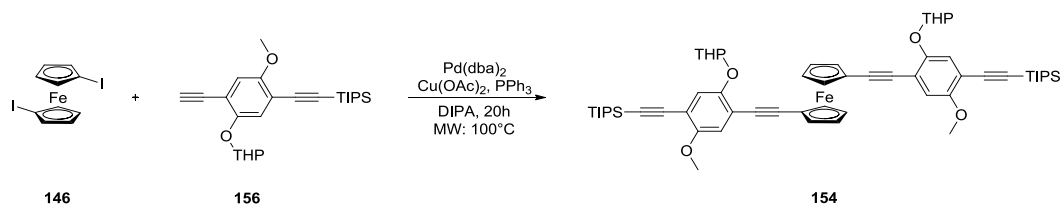
A 100 ml two-necked round-bottomed flask was purged with argon and charged with compound **170** (1.47 g, 3.04 mmol, 1 equiv.), dry DCM (5 ml) and dry methanol (55 ml). The resulting solution was degassed for 5 min. Potassium carbonate (721 mg, 5.16 mmol, 1.7 equiv.) was added and the reaction mixture was stirred overnight. The reaction mixture was concentrated under reduced pressure. A Cyclohexane:*t*BME mixture (3/1) was added to the residue and then filtered over a short silica plug. The filtrate was again concentrated to afford the desired product **156** (1.277 g, quant.) as brown oil.

Deprotection method of compound 151: (HOP-protected acetylene)


A 50 ml three-necked round bottom flask was purged with argon and charged with compound **151** (1.158 g, 2.46 mmol, 1 equiv.) and dry toluene (30 ml). The resulting solution was degassed with argon for 10 min. Sodium hydride (78.7 mg, 1.97 mmol, 60 %, 0.8 equiv.) was added and the resulting mixture was heated to reflux for 45 min. The reaction was cooled to room temperature and was directly filtered over silica (cyclohexane) and then eluted with cyclohexane/*t*BME 20:1. The filtrate was concentrated under reduced pressure. The residue was purified by column chromatography (silica, cyclohexane/ethyl acetate 1:1) to afford the desired compound **156** (1.02 g, quant.) as a yellow solid.

$^1\text{H-NMR}$ (CD_2Cl_2 , 400 MHz) δ (ppm) = 7.14 (s, 1H); 6.94 (s, 1H); 5.40 (t, 1H); 3.93 (m, 1H); 3.81 (s, 3H); 3.59 (m, 1H); 3.38 (s, 1H); 1.88-1.85 (m, 6H); 1.13 (s, 21H).

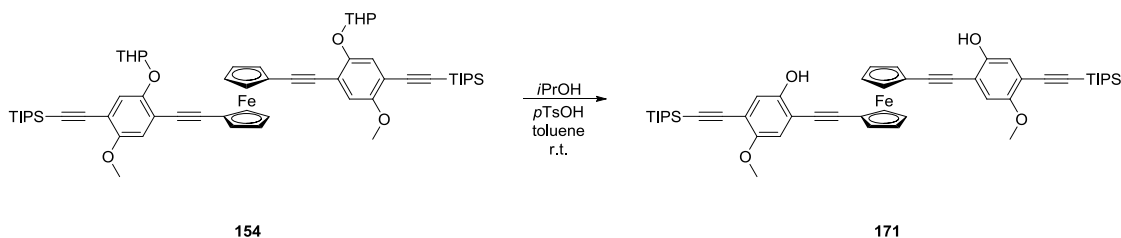
$^{13}\text{C-NMR}$ (CD_2Cl_2 , 100.6 MHz) δ (ppm) = 155.7; 152.1; 121.7; 116.3; 114.3; 97.9; 82.6; 80.2; 62.3; 56.8; 30.6; 27.3; 25.6; 18.9; 18.8; 11.7.

Compound 154:

A 20 ml microwave tube was purged with argon and charged with compound **146** (157 mg, 0.358 mmol, 1 equiv.), compound **156** (369 mg, 0.895 mmol, 2.5 equiv.), bis(dibenzylideneacetone)palladium (32.9 mg, 0.0573 mmol, 0.16 equiv.), copper acetate (10.5 mg, 0.0573 mmol, 0.16 equiv.), triphenylphosphine (60.1 mg, 0.229 mmol, 0.64 equiv.) and diisopropylamine (16 ml). The resulting mixture was degassed for 5 minutes. The reaction was carried out using the microwave reactor at 100°C for 20h. The reaction mixture was then diluted with *t*BME and filtered over celite. The filtrate was concentrated under reduced pressure. The residue was purified by column chromatography (silica, cyclohexane/DCM 1:1) to afford the desired product **154** (202 mg, 56 %) as a red solid.

¹H-NMR (CD₂Cl₂, 400 MHz) δ (ppm) = 7.13 (s, 2H); 6.88 (s, 2H); 5.445 (t, ³J_{H,H} = 2.8 Hz, 2H); 4.549 (t, ³J_{H,H} = 2 Hz, 4H); 4.38-4.37 (m, 4H); 4.007 (dt, ³J_{H,H} = 11.2 Hz, ⁴J_{H,H} = 3.2 Hz, 2H); 3.78 (s, 6H); 3.62-3.59 (m, 2H); 2.24-1.68 (m, 12H); 1.15 (s, 42H).

ESI-MS, (MeOH, pos. mode) m/z: 1006.8 (M⁺); 1029.8 (M⁺+Na).

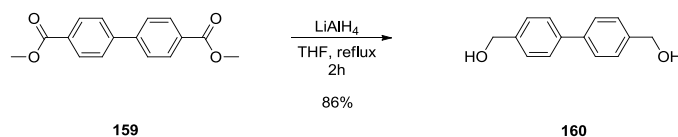
Compound 171:

A 100 ml two-necked round-bottomed flask was purged with argon and charged with compound **154** (232 mg, 0.23 mmol, 1eq), toluene (2 ml) and *iso*-propanol (44 ml). An orange precipitate was formed. Previously dried *p*-TsOH·H₂O (6.6 mg, 0.0345 mmol, 0.15eq) was added and the mixture was stirred overnight. The mixture was then diluted with *t*BME (150 ml) and washed with water (2 x 25 ml) and brine (2 x 20 ml). The organic layer was dried over MgSO₄, filtered and concentrated under reduced pressure. The residue was purified by column chromatography (silica, cyclohexane/DCM 1:2) to afford the desired product **171** (158 mg, 81.9 %) as a red solid.

¹H-NMR (CD₂Cl₂, 400 MHz) δ (ppm) = 6.979 (s, 2H); 6.829 (s, 2H); 5.622 (s, 2H); 4.585 (t, J_{H,H} = 1.6 Hz, 4H); 4.417 (t, J_{H,H} = 1.6 Hz, 4H, 4H); 3.764 (s, 6H); 1.135 (s, 42H).

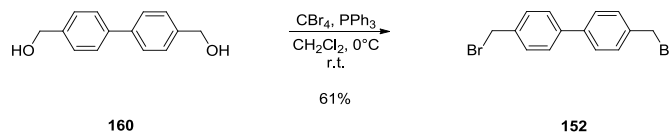
¹³C-NMR (CD₂Cl₂, 100.6 MHz) δ (ppm) = 154.4 (C_q, 2C); 150.2 (C_q, 2C); 119.3 (C_t, 2C); 114.5 (C_q, 2C); 113.5 (C_t, 2C); 110.8 (C_q, 2C); 102.7 (C_q, 2C); 80.6 (C_q, 2C); 73.7 (C_q, 2C); 71.4 (C_t, 4C); 69.3 (C_q, 2C); 62.8 (C_q, 2C); 59.9 (C_q, 2C); 56.5 (C_p, 2C), 29.7 (C_t, 6C); 26.7 (C_p, 12C).

EI-MS, (MeOH, pos. mode) m/z: 861.6 (M⁺+Na)

[1,1'-biphenyl]-4,4'-diyl dimethanol (160):

A 100 ml two-necked round-bottomed flask was purged with argon and charged with LiAlH₄ (659 mg, 16.5 mmol, 1.1 equiv.) and dry THF (23 ml). The resulting suspension was cooled with an ice bath while dimethylbiphenyl-4,4'-dicarboxylate (**159**) (4.1 g, 15 mmol, 1eq) was added portion-wise. After the addition was complete the mixture was allowed to reflux for 2h. The reaction mixture was then cooled to room temperature and carefully treated with water (25 ml) and H₂SO₄ (2N). The resulting mixture was diluted with Ethyl acetate and the precipitate was filtered off. The aqueous phase was extracted with ethyl acetate (3 x 50 ml). The organic phases were combined and washed with brine, dried over MgSO₄, filtered and concentrated under reduced pressure to afford the desired product **160** (2.77 g, 86 %) as a white solid.

¹H-NMR (CDCl₃, 400 MHz) δ (ppm) = 7.60 (dt, ³J_{H,H} = 8.0 Hz, ⁴J_{H,H} = 2.0 Hz, 4H); 7.451 (dt, ³J_{H,H} = 8.0 Hz, ⁴J_{H,H} = 2.0 Hz, 4H); 4.753 (s, 4H).

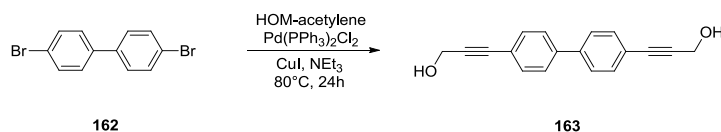
4,4'-bis(bromomethyl)-1,1'-biphenyl (152):


A 100 ml two-necked round-bottomed flask was purged with argon and charged with [1,1'-biphenyl]-4,4'-diyldimethanol (**160**) (1.07 g, 5 mmol, 1 equiv.), carbon tetrabromide (4.02 g, 12 mmol, 2.4 equiv.) and dry DCM (70 ml). The suspension was stirred at room temperature while the triphenylphosphine (3.24 g, 12 mmol, 2.4 equiv.) was added portion wise. The resulting solution was stirred for 24 hours. The reaction mixture was then concentrated under reduced pressure. The residue was dissolved in cyclohexane and *t*BME (3:1) and was filtered over a short silica plug. The crude product was purified by column chromatography (silica, cyclohexane:DCM 3/1) to afford the desired product **152** (1.037 g, 61%) as white crystals.

$^1\text{H-NMR}$ (CDCl_3 , 400 MHz) δ (ppm) = 7.557 (dt, $^3J_{\text{H,H}} = 8.0$ Hz, $^4J_{\text{H,H}} = 1.6$ Hz, 4H); 7.468 (dt, $^3J_{\text{H,H}} = 8.0$ Hz, $^4J_{\text{H,H}} = 1.6$ Hz, 4H); 4.547 (s, 4H).

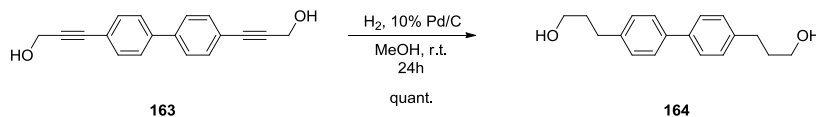
$^{13}\text{C-NMR}$ (CDCl_3 , 100.6 MHz) δ (ppm) = 140.7 (C_q ; 2C); 137.3 (C_q ; 2C); 129.7 (C_i ; 4C); 127.7 (C_i ; 4C); 33.4 (C_s ; 2C).

EI-MS (70 eV), m/z (%): 339.9 (7.9) [M^+]; 259 (81.9) [$\text{M}^+ - \text{Br}$]; 180 (100) [$\text{M}^+ - 2\text{Br}$].

3,3'-([1,1'-biphenyl]-4,4'-diyl)bis(prop-2-yn-1-ol) (163):


A 50 ml Schenk tube was purged with argon and charged with 4,4'-dibromobiphenyl (**162**) (1.092 g, 3.5 mmol, 1 equiv.), bis(triphenylphosphine)palladium (II) chloride (123 mg, 0.175 mmol, 0.05 equiv.), CuI (67 mg, 0.35 mmol, 0.1 equiv.) and triethylamine (30 ml). The resulting mixture was degassed for 10 min. Propargylalcohol (0.434 ml, 7.35 mmol, 2.1 equiv.) was added and the reaction mixture was heated to 80°C and stirred for 24 hours. After aqueous workup and filtration over silica, the slightly impure product **163** was directly used for the next reaction step.

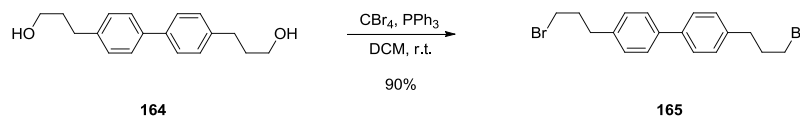
$^1\text{H-NMR}$ (CD_2Cl_2 , 400 MHz) δ (ppm) = 7.578 (dt, $^3J_{\text{H,H}} = 8.8$ Hz, $^4J_{\text{H,H}} = 1.6$ Hz, 4H); 7.516 (dt, $^3J_{\text{H,H}} = 8.4$ Hz, $^4J_{\text{H,H}} = 1.6$ Hz, 4H); 4.490 (d, $^3J_{\text{H,H}} = 6.0$ Hz, 4H).

3,3'-([1,1'-biphenyl]-4,4'-diyl)bis(propan-1-ol) (164):


An approximately 20 ml vial was charged with palladium/10% on activated carbon (31.9 mg, 0.03 mmol, 0.1eq), 3,3'-([1,1'-biphenyl]-4,4'-diyl)bis(prop-2-yn-1-ol) (**163**) (78.7 mg, 0.3 mmol, 1eq), methanol abs. (10 ml) and benzene abs. (5 ml). The starting material **163** could not be completely dissolved. The vial was put into an autoclave and exposed to H_2 (4 bars) for 24h at room temperature. The reaction mixture was then filtered through celite and concentrated under reduced pressure. The residue was absorbed on silica and purified by column chromatography (silica, ethyl acetate: cyclohexane 1/1 \rightarrow ethyl acetate) to afford the desired product **164** (72 mg, 88.8%) as a white solid.

$^1\text{H-NMR}$ (CD_2Cl_2 , 400 MHz) δ (ppm) = 7.553 (d, $^3J_{\text{H,H}} = 8.4$ Hz, 4H); 7.310 (d, $^3J_{\text{H,H}} = 8.4$ Hz, 4H); 3.698 (t, $^3J_{\text{H,H}} = 6.8$ Hz, 4H); 2.763 (t, $^3J_{\text{H,H}} = 7.6$ Hz, 4H); 1.947-1.908 (m, 4H).

$^{13}\text{C-NMR}$ (CD_2Cl_2 , 100.6 MHz) δ (ppm) = 147.1 (C_q , 2C); 129.2 (C_t , 2C); 127.1 (C_t , 4C); 120.4 (C_q , 4C); 62.5 (C_s , 2C); 34.8 (C_s , 2C); 32.0 (C_s , 2C).

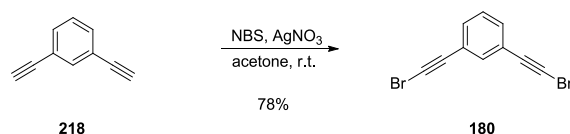
4,4'-bis(3-bromopropyl)-1,1'-biphenyl (165):


A 100 ml two-necked round-bottomed flask was purged with argon and charged with 3,3'-([1,1'-biphenyl]-4,4'-diyl)bis(propan-1-ol) (**164**) (67.6 mg, 0.25 mmol, 1 equiv.), carbon tetrabromide (285 mg, 0.85 mmol, 3.4 equiv.) and dry DCM (70 ml). The suspension was stirred at room temperature while the triphenylphosphine (223 mg, 0.85 mmol, 3.4 equiv.) was added portion wise. The resulting solution was stirred for 24 hours. The reaction mixture was then concentrated under reduced pressure and the residue was purified by column chromatography (silica, cyclohexane: ethyl acetate 3/1) to afford the desired product **165** (89 mg, 90 %) as white crystals.

$^1\text{H-NMR}$ (CD_2Cl_2 , 400 MHz) δ (ppm) = 7.525 (dt, $^3J_{\text{H,H}} = 8.0$ Hz, $^4J_{\text{H,H}} = 2.0$ Hz, 4H); 7.276 (dt, $^3J_{\text{H,H}} = 8.0$ Hz, $^4J_{\text{H,H}} = 2.0$ Hz, 4H); 3.443 (t, $^3J_{\text{H,H}} = 6.8$ Hz, 4H); 2.807 (t, $^3J_{\text{H,H}} = 7.6$ Hz, 4H); 2.227-2.157 (m, 4H).

$^{13}\text{C-NMR}$ (CD_2Cl_2 , 100.6 MHz) δ (ppm) = 140.3 (C_q , 2C); 139.3 (C_q , 2C); 129.6 (C_t , 4H); 127.5 (C_t , 4H); 34.8 (C_s , 2C); 34.2 (C_s , 2C); 33.9 (C_s , 2C).

EI-MS (70 eV), m/z (%): 396 (85) [M^+]; 287 (100) [$\text{M}^+ - \text{C}_2\text{H}_4\text{Br}$].

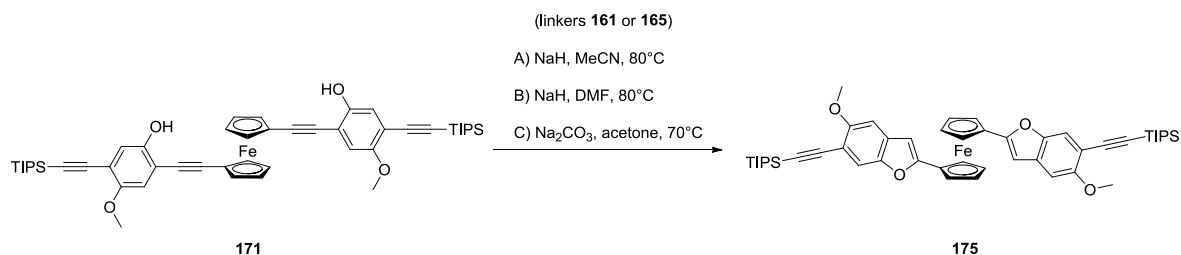
1,3-bis(bromoethynyl)benzene 180:

A 50 ml round bottom flask was purged with argon and charged with 1,3-diethynylbenzene (**218**) (501 mg, 3.85 mmol, 1 equiv.), *N*-bromosuccinimide (1.959 g, 10.9 mmol, 2.83 equiv.), silver nitrate (114 mg, 0.674 mmol, 0.175 equiv.) and dry acetone (40 ml). The reaction mixture was stirred for 2h at room temperature. After the reaction was complete the mixture was adsorbed on silica and purified by column chromatography (silica, cyclohexane: *t*BME 20/1) to afford the desired product **180** (85.6 mg, 78 %) as white solid.

¹H-NMR (CD₂Cl₂, 400 MHz) δ (ppm) = 7.519 (dt, *J*_{H,H} = 1.6 Hz, 1H); 7.433 (dd, ³*J*_{H,H} = 7.6 Hz, 4*J*_{H,H} = 2.0 Hz, 2H); 7.290 (dt, ³*J*_{H,H} = 7.6 Hz, 4*J*_{H,H} = 0.8 Hz, 1H).

¹³C-NMR (CD₂Cl₂, 100.6 MHz) δ (ppm) = 135.7 (C_t, 1C); 132.7 (C_t, 2C); 129.2 (C_t, 1C); 123.6 (C_q, 2C); 79.4 (C_q, 2C); 51.4 (C_q, 2C).

EI-MS (70 eV), *m/z* (%): 282 (100) [M⁺].

Compound 175:


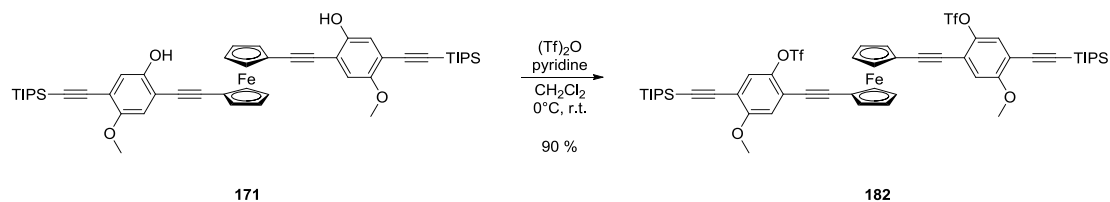
General procedure for **175** = 0.0274 mmol:

A 50 ml three-necked round bottom flask was purged with argon and charged with base (40 equiv.) and dry solvent (10 ml). Compound **171** (1 equiv.) and compound **161** or **165** (not necessary for the reaction) (1 equiv.) were each dissolved in dry solvent (10 ml) and taken up into two 10 ml syringes. The reaction mixture was heated to 50-70°C. Compound **171** and **161** or **165** were then slowly added using a syringe pump (0.02 mm/min \approx 40h). After the addition was complete the reaction was stirred for three days until no changes in the reaction progress was observed (TLC control). The reaction mixture was extracted with water (25 ml) and brine (25 ml), dried over MgSO₄, filtered and concentrated under reduced pressure. The residue was purified by column chromatography to afford product **175**.

¹H-NMR (CD₂Cl₂, 400 MHz) δ (ppm) = 7.39 (s, 2H); 6.17 (s, 2H); 6.08 (s, 2H); 4.929 (t, ³J_{H,H} = 2 Hz, 4H); 4.343 (t, ³J_{H,H} = 2 Hz, 4H); 3.77 (s, 6H); 1.75-1.70 (m, 42H).

¹³C-NMR (CD₂Cl₂, 100.6 MHz) δ (ppm) = 157.1 (C_q, 2C); 148.7 (C_q, 2C); 148.7 (C_q, 2C); 130.4 (C_q, 2C); 113.9 (C_t, 2C); 107.8 (C_q, 2C); 104.5 (C_q, 2C); 101.5 (C_t, 2C); 100.4 (C_t, 2C); 94.1 (C_q, 2C); 78.9 (C_q, 2C); 70.1 (C_t, 4C); 66.9 (C_t, 4C); 55.8 (C_p, 2C); 18.4 (C_p, 12C); 11.6 (C_t, 6C).

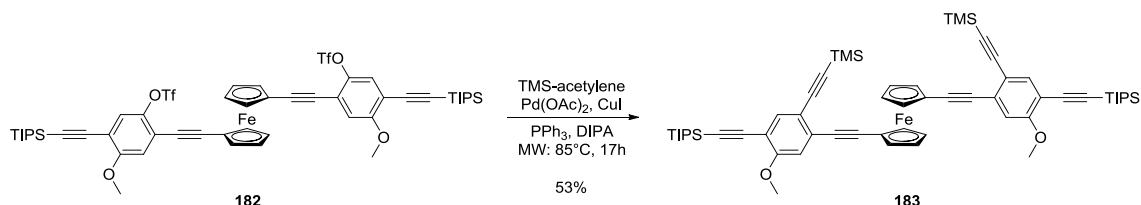
ESI-MS, (MeOH, pos. mode) m/z: 838 [M⁺]

Compound 182:


A 10 ml two-necked round bottom flask was purged with argon and charged with compound **171** (104 mg, 0.124 mmol, 1 equiv.) and dry DCM (6 ml). The solution was degassed for 5 min. and then cooled to 0°C. Pyridine (80.2 μl , 0.992 mmol, 8 equiv.) in dry DCM (1 ml) and triflic anhydride (83.4 μl , 0.496 mmol, 4 equiv.) in dry DCM (1 ml) were added subsequently. After the addition was complete the reaction mixture was allowed to warm to room temperature and was stirred for 1h. The mixture was then diluted with *t*BME and washed with 10% HCl, 50% Na_2CO_3 , water and brine. The organic solution was dried over MgSO_4 , filtered and concentrated under reduced pressure. The residue was purified by column chromatography (silica, cyclohexane/*t*BME 3:1; $R_F = 0.65$) to afford the desired product **182** (130 mg, 95 %) as a red solid.

$^1\text{H-NMR}$ (CD_2Cl_2 , 400 MHz) δ (ppm) = 7.26 (s, 2H); 6.92 (s, 2H); 4.660 (t, $^3J_{\text{H,H}} = 1.6$ Hz, 4H); 4.449 (t, $^3J_{\text{H,H}} = 1.6$ Hz, 4H); 3.80 (s, 6H); 1.14 (s, 42H).

MALDI-MS, (RP mode, 2',4',6'-trihydroxyacetophenone monohydrate) m/z : 1102.3 [M^+].

Compound 183:


A 3 ml micro-wave tube was purged with argon and charged with compound **182** (44.1 mg, 0.04 mmol, 1 equiv.), $\text{Pd}(\text{OAc})_2$ (1.8 mg, 0.008 mmol, 0.2 equiv.), triphenylphosphine (8.39 mg, 0.032 mmol, 0.8 equiv.), CuI (1.53 mg, 0.008 mmol, 0.2 equiv.) and DIPA (2.8 ml). The resulting mixture was degassed with argon for 5 min. The reaction vial was then put in the microwave reactor (85°C, 17h). After the reaction was complete *t*BME was added and the

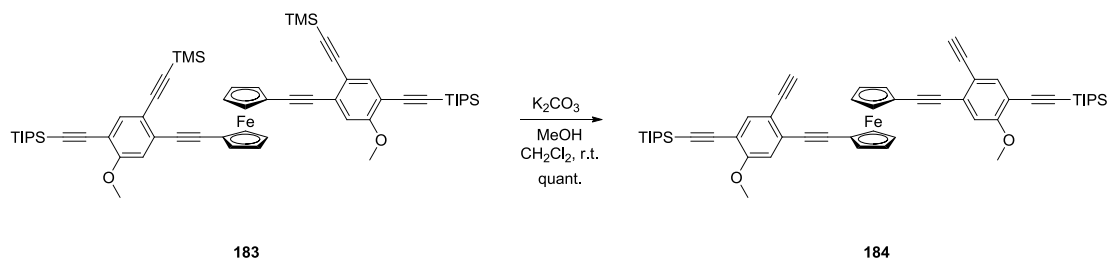
suspension was filtered over Celite. The filtrate was concentrated under reduced pressure. The residue was purified by column chromatography (1st column: silica, cyclohexane:tBME 20:1; RF = 0.47. 2nd column: RP18-silica, acetonitrile:THF 3:1→1:1; RF = 0.1) to afford the desired compound **183** (21 mg, 53 %) as a red solid.

¹H-NMR (CD₂Cl₂, 400 MHz) δ (ppm) = 7.34 (s, 2H); 6.72 (s, 2H); 4.444 (t, ³J_{H,H} = 1.6 Hz, 4H); 4.252 (t, ³J_{H,H} = 1.6 Hz, 4H) 3.64 (s, 6H); 0.97 (s, 42H); 0.125 (s, 18H).

¹³C-NMR (CD₂Cl₂, 100.6 MHz) δ (ppm) = 160.6 (C_q, 2C); 138.1 (C_t, 2C); 128.2 (C_q, 2C); 117.9 (C_t, 2C); 114.1 (C_q, 2C); 113.4 (C_q, 2C); 103.5 (C_q, 2C); 102.5 (C_q, 2C); 97.8 (C_q, 2C); 97.4 (C_q, 2C); 94.0 (C_q, 2C); 85.9 (C_q, 2C); 73.8 (C_t, 4C); 72.6 (C_t, 4C); 66.8 (C_q, 2C); 19.0 (C_p, 12C); 11.9 (C_t, 6C); 0.5 (C_p, 6C).

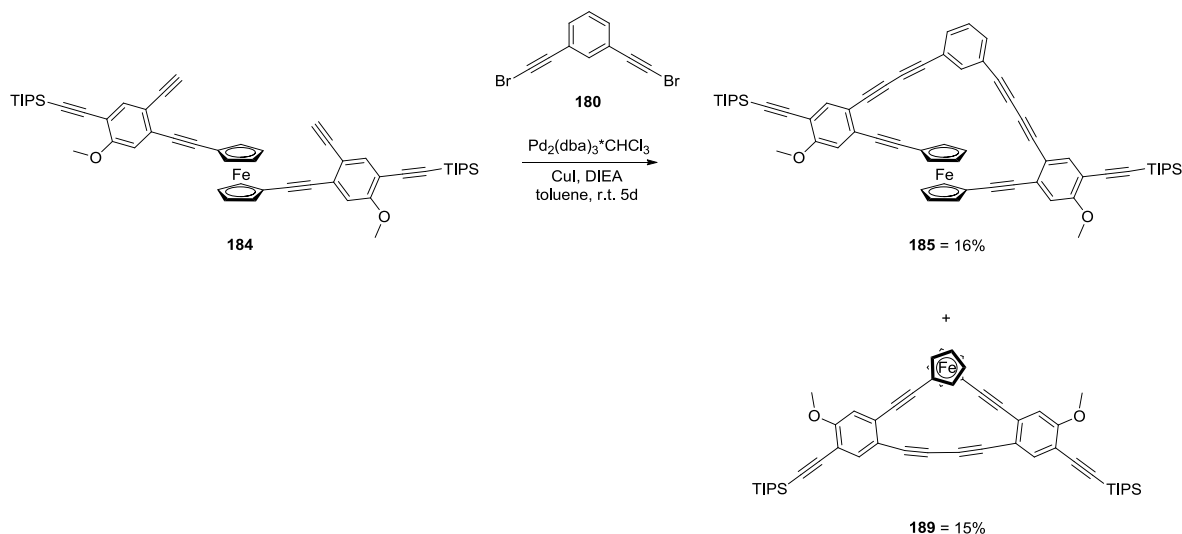
MALDI-MS, (RP mode, 2',4',6'-trihydroxyacetophenone monohydrate) m/z: 998.4 [M⁺].

Compound 184:



A 5 ml round bottom flask was purged with argon and charged with compound **183** (5 mg, 0.005 mmol, 1 equiv.), dry DCM (1 ml) and methanol (1 ml). The mixture was degassed and potassium carbonate (1.4 mg, 0.01 mmol, 2 equiv.) was added. The reaction mixture was stirred for 3h at room temperature. After the reaction was complete a filtration over silica eluting with cyclohexane:tBME (20:1) gave the desired product **184** (3.5 mg, 81.9 %) as orange solid.

¹H-NMR (CD₂Cl₂, 400 MHz) δ (ppm) = 7.550 (s, 2H); 6.937 (s, 2H); 4.597 (t, 4H); 4.424 (t, 4H); 3.837 (s, 6H); 3.331 (s, 2H); 1.151-1.139 (m, 42H).

Compounds 185 and 189:


A 250 ml three-necked round bottom flask was purged with argon and charged with dry toluene (112 ml) and DIEA (1.24 ml). The resulting mixture was degassed for 10 min. Tris(dibenzylideneacetone)dipalladium-chloroform (10.1 mg, 0.00975 mmol, 0.325 equiv.) and CuI (4.77 mg, 0.0249 mmol, 0.833 equiv.) were added. Compound **184** (25.7 mg, 0.03 mmol, 1 equiv.) and compound **180** (8.52 mg, 0.03 mmol, 1 equiv.) were each dissolved in toluene (5 ml) and slowly added at room temperature using a syringe pump (0.01 mm/min, 10 ml syringe). After the addition was complete the reaction mixture was stirred for 4 days. The mixture was then extracted with water (50 ml) and brine (2 x 50 ml), dried over MgSO_4 , filtered and concentrated under reduced pressure. The residue was purified by column chromatography (1st: silica, cyclohexane:tBME 10:1; 2nd: RP18, acetonitrile:THF 2:1) to afford the desired product **185** (4.3 mg, 16%) as an orange solid and a second product **189** (4.0 mg, 15%).

185:

$^1\text{H-NMR}$ (CD_2Cl_2 , 400 MHz) δ (ppm) = 8.103-8.094 (m, 1H); 7.518 (s, 2H); 7.489-7.482 (m, 2H); 7.402-7.364 (m, 1H); 6.972 (m, 2H); 4.883 (t, 4H); 4.547 (t, 4H); 3.899 (s, 6H); 1.148-1.127 (m, 42H).

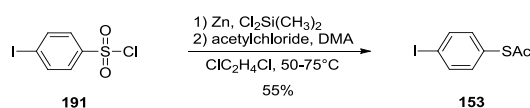
$^{13}\text{C-NMR}$ (CD_2Cl_2 , 100.6 MHz) δ (ppm) = 140.7; 136.5; 130.8; 129.6; 113.2; 74.9; 74.2; 73.7; 70.7; 56.5; 18.8; 11.7.

MALDI-MS, (RP mode, 2',4',6'-trihydroxyacetophenone monohydrate) m/z: 976.89 [M^+].

189:

$^1\text{H-NMR}$ (CD_2Cl_2 , 400 MHz) δ (ppm) = 7.577 (s, 2H); 6.996 (s, 2H); 4.457 (t, 4H); 4.408 (t, 4H); 3.898 (6H); 1.142 (s, 42H).

MALDI-MS, (RP mode, 2',4',6'-trihydroxyacetophenone monohydrate) m/z : 852.27 [M^+].

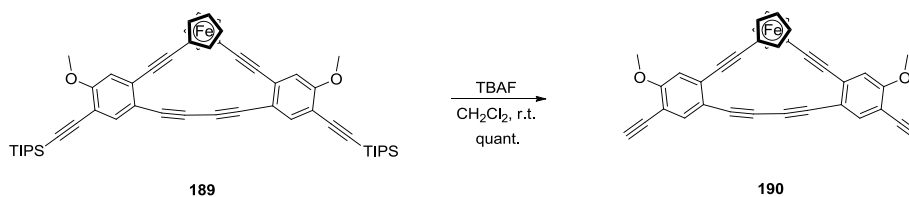
Compound 153:


To a stirred suspension of zinc powder (3.92 g, 59.94 mmol, 3.53 equiv.) and dichlorodimethylsilane (7.00 mL, 58.00 mmol, 3.42 equiv.) in 1,2-dichloroethane (20 mL) was added a solution of 4-iodobenzenesulfonylchloride **191** (5.13 g, 16.96 mmol, 1 equiv.) and *N,N*-dimethylacetamide (4.65 mL, 50.00 mmol, 2.95 equiv.) in dichloroethane (20 mL). The mixture was stirred at 75 °C for 2 hours until the zinc powder was no longer visible. The reaction mixture was cooled to 50 °C, and acetyl chloride (1.53 mL, 21.50 mmol, 1.27 equiv.) was added. After 15 minutes, the mixture was poured into water, and extracted with DCM (3 x 50 mL). The combined organic layers were dried over MgSO_4 , filtered, concentrated in vacuo and purified by flash chromatography (cyclohexane:DCM 1/1) to provide **153** (2.59 g, 54.9 %) as a colorless oil which solidified at -20 °C.

$^1\text{H-NMR}$ (CDCl_3 , 400 MHz) δ (ppm) = 7.740 (d, $^3J_{\text{H,H}} = 8$ Hz, 2H); 7.128 (d, $^3J_{\text{H,H}} = 8$ Hz, 2H); 2.423 (s, 3H).

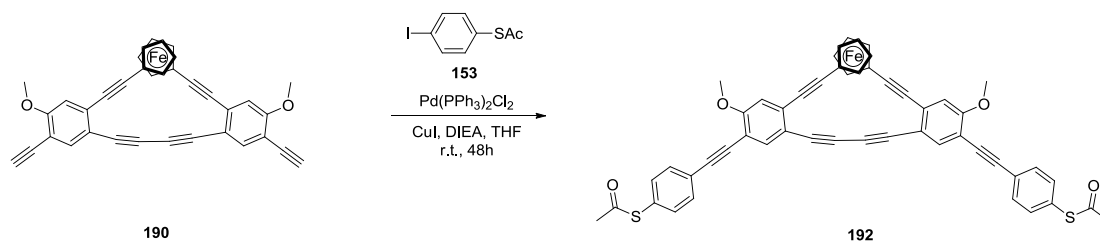
$^{13}\text{C-NMR}$ (CD_2Cl_2 , 100.6 MHz) δ (ppm) = 193.4 (C_q , 1C); 138.6 (C_t , 2C); 136.2 (C_t , 2C); 128.0 (C_q , 1C); 96.2 (C_q , 1C); 30.5 (C_q , 1C).

EI-MS (70 eV), m/z (%): 278 (24) [M^+]; 236 (100) [$\text{M}^+ - \text{OCCH}_3$].

Compound 190:

A 10 ml round bottom flask was purged with argon and charged with compound **189** (6.4 mg, 0.0075 mmol, 1 equiv.) and dry DCM (2 ml). The solution was degassed for 5 min. A TBAF solution (1M in THF, 0.0165 ml, 0.0165 mmol, 2.2 equiv.) was added at room temperature and the resulting mixture was stirred for 1h. The reaction was quenched with water/*t*BME and extracted. The organic layer was dried over MgSO₄, filtered and concentrated under reduced pressure to afford the desired compound **190** (5 mg, quant.) as an orange solid.

¹H-NMR (CD₂Cl₂, 400 MHz) δ (ppm) = 7.597 (s, 2H); 7.028 (s, 2H) 4.465 (t; 4H); 4.410 (t, 4H); 3.919 (s, 6H); 3.414 (s, 2H).

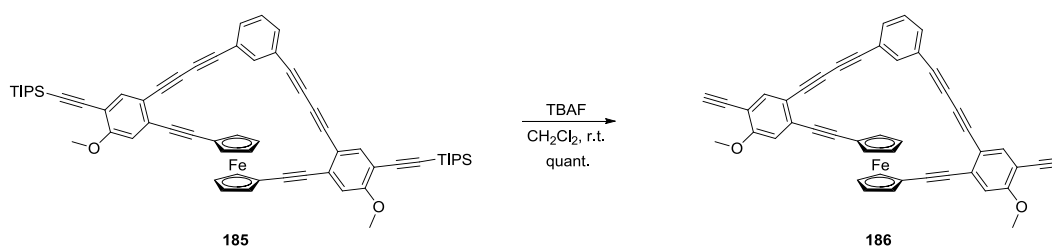
Compound 192:


A 10 ml Schlenk tube was purged with argon and charged with compound **190** (4.05 mg, 0.075 mmol, 1 equiv.), compound **153** (4.8 mg, 0.0173 mmol, 2.3 equiv.), bis(triphenylphosphine)palladium chloride (0.211 mg, 0.0003 mmol, 0.04 equiv.), CuI, 0.057 mg, 0.0003 mmol, 0.04 equiv.) and *N*-ethyldiisopropylamine (0.03 ml). The resulting mixture was degassed with argon for 10 min and stirred for 48 hours at room temperature. The reaction mixture was then diluted with *t*BME and filtered over celite. The filtrate was concentrated under reduced pressure. The residue was purified by column chromatography (RP18, acetonitrile:THF 4:1) to afford the desired compound **192** (1.85 mg, 30.6) as red solid.

$^1\text{H-NMR}$ (CD_2Cl_2 , 400 MHz) δ (ppm) = 7.661 (s, 2H); 7.587 (d, $^3J_{\text{H,H}} = 8.4$ Hz, 4H); 7.427 (d, $^3J_{\text{H,H}} = 8.4$ Hz, 4H); 7.064 (s, 2H); 4.480 (t, 4H); 4.429 (t, 4H); 3.962 (s, 6H); 2.428 (s, 6H).

$^{13}\text{C-NMR}$ (CD_2Cl_2 , 100.6 MHz) δ (ppm) = 149.6 (C_q , 2C); 160.5 (C_q , 2C); 136.5 (C_t , 2C); 134.8 (C_t , 4C); 132.4 (C_t , 4C); 130.5 (C_q , 2C); 129.2 (C_q , 2C); 124.6 (C_q , 2C); 113.2 (C_t , 2C); 112.5 (C_q , 2C); 95.9 (C_q , 2C); 94.6 (C_q , 2C); 86.7 (C_q , 2C); 85.4 (C_q , 2C); 81.0 (C_q , 2C); 77.4 (C_q , 2C); 75.2 (C_t , 4C); 71.0 (C_t , 4C); 67.1 (C_q , 2C); 56.6 (C_p , 2C); 30.5 (C_p , 2C).

MALDI-MS, (RP mode, 2',4',6'-trihydroxyacetophenone monohydrate) m/z : 840.36 $[\text{M}^+]$.

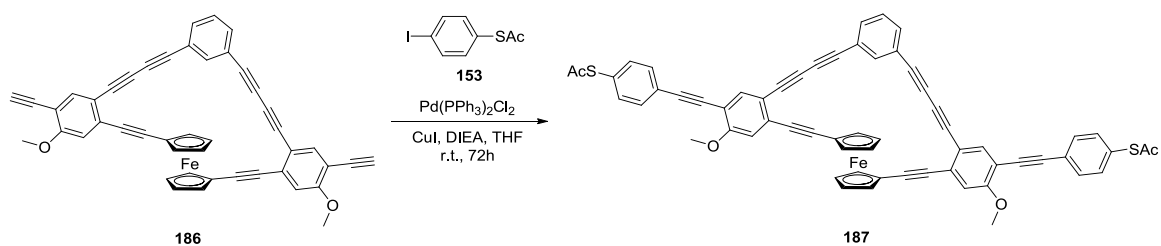
Compound 186:


A 10 ml round bottom flask was purged with argon and charged with compound **185** (6.3 mg, 0.0065 mmol, 1 equiv.) and dry DCM (2 ml). The solution was degassed for 5 min. A TBAF

solution (1M in THF, 0.0149 ml, 0.0149 mmol, 2.3 equiv.) was added at room temperature and the resulting mixture was stirred for 1h. The reaction was quenched with water/*t*BME and extracted. The organic layer was dried over MgSO₄, filtered and concentrated under reduced pressure to afford the desired compound **186** (5 mg, quant.) as an orange solid.

¹H-NMR (C₄D₈O, 400 MHz) δ (ppm) = 10.895 (s, 1H); 8.193 (t, 1H); 7.569-7.549 (m, 3H); 7.493-7.462 (m, 1H); 7.140 (s, 2H); 4.934 (t, 4H); 4.563 (t, 4H); 3.938 (s, 6H); 3.841 (s, 2H).

Compound 187:



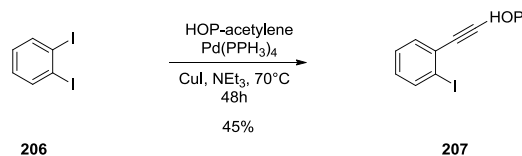
A 10 ml Schlenk tube was purged with argon and charged with compound **186** (4.32 mg, 0.065 mmol, 1 equiv.), compound **153** (4.52mg, 0.0163 mmol, 2.5 equiv.), bis(triphenylphosphine) palladium chloride (0.183 mg, 0.00026 mmol, 0.04 equiv.), CuI, 0.0498 mg, 0.00026 mmol, 0.04 equiv.) and N-ethyl-diisopropylamine (0.15 ml). The resulting mixture was degassed with argon for 10 min and stirred for 72 hours at room temperature. The reaction mixture was then diluted with THF and filtered over celite. The filtrate was concentrated under reduced pressure. The residue was purified by column chromatography (RP18, acetonitrile:THF 4:1 → CHCl₃) to afford the desired compound **187** (0.3 mg, <5 %) as red solid.

¹H-NMR (CD₂Cl₂, 400 MHz) δ (ppm) = 8.06-7.40 (arom. signals); 4.40-4.00 (Cp signals); 3.65 (OMe).

MALDI-MS, (RP mode, 2',4',6'-trihydroxyacetophenone monohydrate) m/z: 962 [M⁺].

7.5 Synthesis of a Car-jack Molecule

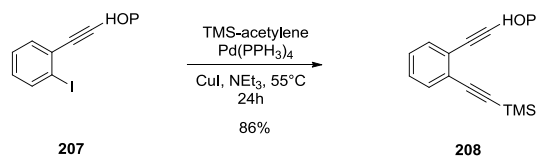
4-(2-iodophenyl)-2-methylbut-3-yn-2-ol (**207**):



A 100 ml Schlenk tube was purged with argon and charged with tetrakis(triphenylphosphine)palladium(0) (190 mg, 0.164 mmol, 0.02 equiv.), CuI (16 mg, 0.082 mmol, 0.01 equiv.), 1,2-diodobenzene **206** (2.71 g, 8.2 mmol, 1 equiv.) and triethylamine (40 ml). The resulting mixture was degassed with argon for 10 min. 2-Methyl-3-butyn-2-ol (0.841 ml, 8.61 mmol, 1.05 equiv.) was added to the yellow solution and the mixture was then quickly heated to 70°C. A white precipitate was formed after 10 min. The reaction mixture was stirred for 48h at 70°C. The reaction mixture was then concentrated under reduced pressure. The residue was diluted in *t*BME and filtered over celite. The filtrate was again concentrated under reduced pressure. The crude product was then dissolved in cyclohexane and filtered over a short silica pad (1st cyclohexane, 2nd cyclohexane/*t*BME 5:1, 3rd cyclohexane/*t*BME 1:1). The filtrate containing the product was then purified by column chromatography to afford the desired compound **207** (1.06 g, 45 %) as yellow-orange oil.

¹H-NMR (CDCl₃, 400 MHz) δ (ppm): 7.834 (dd, ³J_{H,H} = 6.8 Hz, ⁴J_{H,H} = 1.2 Hz, 1H); 7.420 (dd, ³J_{H,H} = 6 Hz, ⁴J_{H,H} = 1.6 Hz, 1H); 7.286 (dt, ³J_{H,H} = 7.6 Hz, ⁴J_{H,H} = 1.2 Hz, 1H); 6.990 (dt, ³J_{H,H} = 6 Hz, ⁴J_{H,H} = 1.6 Hz, 1H); 1.66 (s, 6H).

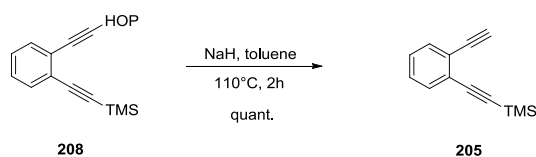
¹³C-NMR (CDCl₃, 100.6 MHz): δ (ppm) 138.8 (C_t, 1C); 132.5 (C_t, 1C); 129.6 (C_t, 1C); 127.9 (C_t, 1C); 101.4 (C_q, 1C); 97.7 (C_q, 1C); 84.7 (C_q, 1C); 82.0 (C_q, 1C); 65.5 (C_q, 1C); 31.4 (C_p, 2C).

2-methyl-4-(2-((trimethylsilyl)ethynyl)phenyl)but-3-yn-2-ol (208):


A 25 ml Schlenk tube was purged with argon and charged with tetrakis(triphenylphosphine)palladium (11.6 mg, 0.01 mmol, 0.01 equiv.), CuI (2 mg, 0.01 mmol, 0.01 equiv.), compound **207** (286 mg, 1 mmol, 1 equiv.) and triethylamine (5 ml). The mixture was degassed with argon for 20 min. Trimethylsilylacetylene (0.29 ml, 2 mmol, 2 equiv.) was added and the mixture was heated to 65°C and stirred overnight. The reaction mixture was concentrated under reduced pressure and the residue was purified by column chromatography (silica, cyclohexane:*t*BME 3:1) to afford the desired compound **208** (550 mg, 86 %) as yellow oil.

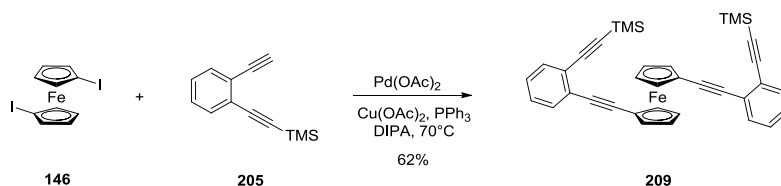
$^1\text{H-NMR}$ (CD_2Cl_2 , 400 MHz) δ (ppm): 7.47-7.40 (m, 2H); 7.30-7.25 (m, 2H); 1.61 (s, 6H); 0.26 (s, 9H).

$^{13}\text{C-NMR}$ (CD_2Cl_2 , 100.6 MHz): δ (ppm) 132.8 (C_t , 1C); 132.4 (C_t , 1C); 128.8 (C_t , 1C); 128.6 (C_t , 1C); 126.0 (C_q , 1C); 125.8 (C_q , 1C); 66.0 (C_q , 1C); 31.9 (C_p , 2C); 0.23 (C_p , 3C).

((2-ethynylphenyl)ethynyl)trimethylsilane (205):


A 50 ml two-necked round-bottomed flask equipped with a reflux condenser was purged with argon and charged with compound **208** (510 mg, 1.99 mmol, 1 equiv.) and dry toluene (20 ml). The solution was degassed with argon for 15 min. Sodium hydride (88 mg, 2.19 mmol, 1.1 equiv.) was added and the resulting mixture heated to reflux for 2h. The reaction mixture was then filtered through a small silica plug. The filtrate was slowly concentrated under reduced pressure to afford the desired product **205** (400 mg, quant.) as yellow oil.

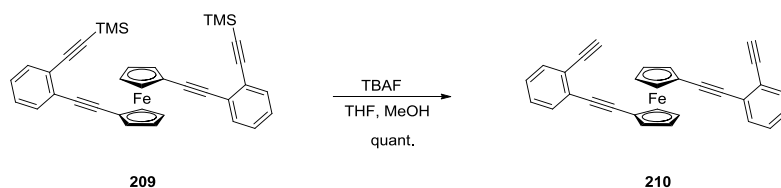
$^1\text{H-NMR}$ (CDCl_3 , 400 MHz) δ (ppm): 7.48-7.46 (m, 2H); 7.28-7.26 (m, 2H); 3.30 (s, 1H); 0.27 (s, 9H).

Compound 209:


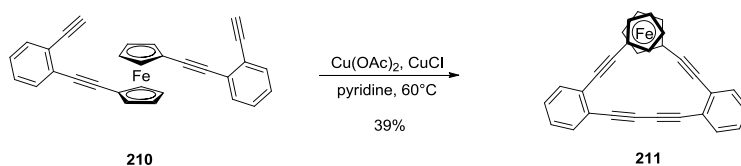
A 10 ml Schlenk tube was purged with argon and charged with palladium acetate (1.8 mg, 0.008 mmol, 0.08 equiv.), copper acetate (1.47 mg, 0.008 mmol, 0.08 equiv.), triphenylphosphine (8.4 mg, 0.032 mmol, 0.32 equiv.), compound **146** (43.8 mg, 0.1 mmol, 1 equiv.) and diisopropylamine (1 ml). The resulting mixture was degassed for 10 min and slowly heated to 70°C. Compound **205** (86.8 mg, 0.35 mmol, 3.5 equiv.) dissolved in diisopropylamine (1 ml) was then added. The mixture was stirred over night at 70°C. After 42h the mixture was diluted with *t*BME and passed through a celite pad. The filtrate was concentrated and the residue was purified by column chromatography (silica, cyclohexane:DCM 5:1) to afford the desired compound **209** (36 mg, 62.2%) as a red solid.

$^1\text{H-NMR}$ (CDCl_3 , 400 MHz) δ (ppm): 7.45-7.39 (m, 4H); 7.21-7.18 (m, 4H); 4.58 (t, 4H), 4.36 (t, 4H); 0.30 (s, 18H).

ESI-MS, (MeOH, pos. mode) m/z : 578.2 (M^+).

Compound 210:


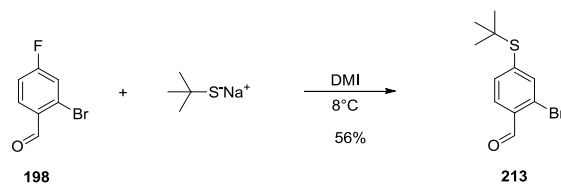
A 25 ml two-necked round-bottomed flask was purged with argon and charged with compound **209** (46.3 mg, 0.08 mmol, 1 equiv.), THF (8 ml) and MeOH (0.5 ml). TBAF (1M in THF, 0.28 ml, 0.28 mmol, 3.5 equiv.) was added at room temperature. The mixture was stirred for 45 min. The reaction mixture was concentrated under reduced pressure and the residue was dissolved in cyclohexane/DCM (5:1) and filtered over silica. The filtrate was concentrated and the residue was directly used in the next step.

Compound 211:

A 100 ml three-necked round-bottomed flask was purged with argon and charged with copper(II) acetate (367 mg, 2 mmol, 25eq), copper(I) chloride (158 mg, 1.6 mmol, 20eq) and pyridine (25 ml). The mixture was heated to 60°C. Compound **210** (34.7 mg, 0.08 mmol, 1eq, dissolved in 10 ml pyridine) was then added over a period of 9h. After 24h the reaction mixture was concentrated under reduced pressure. The residue was dissolved in DCM and filtered over a short silica pad. The filtrate was again concentrated to afford the desired product **211** (27 mg, 39 %) as red solid.

¹H-NMR (CDCl₃, 400 MHz) δ (ppm): 7.55-7.49 (m, 4H); 7.36-7.27 (m, 4H); 4.41 (s, 8H).

ESI-MS, (MeOH, pos. mode) m/z: 432.1 (M⁺).

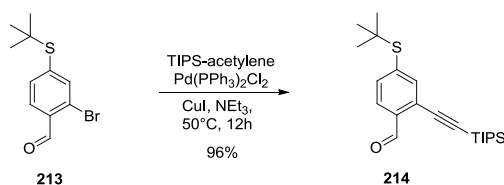
Compound 213:


A 500 ml three-necked round bottom flask was purged with argon and charged with 2-bromo-4-fluorobenzaldehyde (**198**) (5.8 g, 28 mmol, 1 equiv.) and DMI (240 ml). Sodium 2-methyl-2-propanethiolate (3.3 g, 29.4 mmol, 1.05 equiv.) was dissolved in DMI (60 ml) and slowly added over a period of 1h at 8°C. The reaction was then stirred for 6h at 8°C. The mixture was diluted with *t*BME and extracted with water (5 x 50 ml) and brine (50 ml). The combined organic layers were dried over MgSO₄, filtered and concentrated under reduced pressure. The residue was purified by column chromatography (silica, cyclohexane: *t*BME 10:1; RF = 0.52) to afford the desired product **213** (4.25 g, 56 %) as colorless oil.

¹H-NMR (CD₂Cl₂, 400 MHz) δ (ppm): 10.33 (s, 1H); 7.82 (d, 2H); 7.58 (d, 1H); 1.35 (s, 9H).

¹³C-NMR (CD₂Cl₂, 100.6 MHz): δ (ppm) 192.5 (C_t, 1C); 143.3 (C_q, 1C); 141.0 (C_t, 1C); 135.9 (C_t, 1C); 133.4 (C_q, 1C); 129.6 (C_t, 1C); 126.6 (C_q, 1C); 48.0 (C_q, 1C); 31.3 (C_p, 3C).

EI-MS (70 eV), m/z (%): 272 (9.7) [M⁺]; 216 (47.6) [M⁺ - *t*Bu].

Compound 214:


A 100 ml Schlenk tube was purged with argon and charged with compound **213** (2.5 g, 9.15 mmol, 1 equiv.), bis(triphenylphosphine)palladium chloride (129 mg, 0.183 mmol, 0.02 equiv.), triethylamine (37 ml) and triisopropylsilylacetylene (2.33 ml, 10.1 mmol, 1.1 equiv.). The resulting mixture was degassed for 5 min. CuI (17.5 mg, 0.0915 mmol, 0.01eq) was then added and the resulting mixture was heated to 50°C and stirred overnight. The mixture was diluted with *t*BME and filtered over celite. The filtrate was concentrated and the crude

product was purified by column chromatography (silica, cyclohexane:*t*BME 10:1; RF = 0.57) to afford the desired product **214** (3.31 g, 96.6 %) as a yellow oil.

¹H-NMR (CDCl₃, 400 MHz) δ (ppm): 10.6 (s, 1H); 7.85 (d, 1H); 7.72 (s, 1H); 7.57 (d, 1H); 1.36 (s, 9H); 1.15 (s, 21H).

¹³C-NMR (CDCl₃, 100.6 MHz): δ (ppm) 191.4 (C_t, 1C); 141.3 (C_t, 1C); 141.0 (C_q, 1C); 136.7 (C_t, 1C); 135.8 (C_q, 1C); 127.2 (C_q, 1C); 126.8 (C_t, 1C); 101.6 (C_q, 1C); 100.0 (C_q, 1C); 47.6 (C_q, 1C); 31.3 (C_p, 3C); 18.8 (C_p, 6C); 11.4 (C_t, 3C).

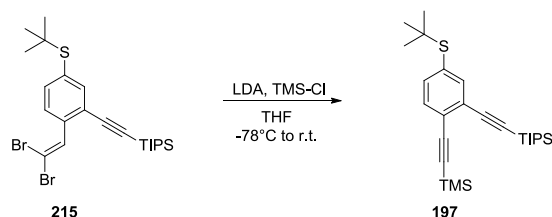
Compound 215:



A 10 ml 2-necked-round bottom flask was purged with argon and charged with compound **214** (2.0 g, 5.34 mmol, 1 equiv.), triphenylphosphine (5.6 g, 21.4 mmol, 4 equiv.) and dry DCM (25 ml). The mixture was cooled to 0°C and carbon tetrabromide (3.58 g, 10.7 mmol, 2 equiv.) was added portion wise. The reaction mixture was stirred for 4h and then filtered through a silica pad eluting with cyclohexane:*t*BME (5/1; RF = 0.71). The filtrate was concentrated under reduced pressure to afford the desired compound **215** as yellow oil (2.46 g, 86.9 %) which solidified upon standing.

¹H-NMR (CDCl₃, 400 MHz) δ (ppm): 7.84 (s, 1H); 7.76 (d, 1H); 7.64 (d, 1H); 7.49 (d, 1H); 1.31 (s, 9H); 1.15 (s, 21H).

¹³C-NMR (CDCl₃, 100.6 MHz): δ (ppm) 140.7; 136.8; 135.3; 127.6; 121.1; 91.7; 88.1; 46.6; 31.1; 18.7; 11.3.

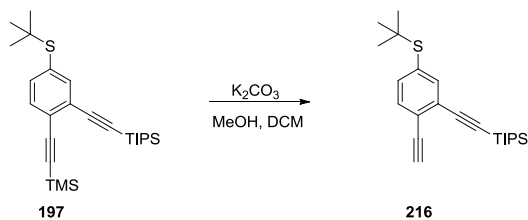
Compound 197:

A 10 ml 2-necked-round bottom flask was purged with argon and charged with compound **215** (2.355 g, 4.44 mmol, 1 equiv.) and dry THF (30 ml). The solution was degassed for 5 minutes and then cooled to -78°C . A lithium diisopropylamine solution (2M in THF/n-heptane, 8.88 ml, 17.8 mmol, 4 equiv.) was slowly added. The color immediately turned red. The resulting mixture was stirred for 2.5 h at -78°C . Trimethylsilyl chloride (3.47 ml, 26.6 mmol, 6 equiv.) was then added and the resulting mixture was stirred for 1h at -78°C and for another hour at room temperature. After a aqueous workup and a filtration over a silica plug eluting with cyclohexane:*t*BME (10:1) the desired product **197** (1.63 g, 83.1 %) was isolated as yellow oil.

$^1\text{H-NMR}$ (CD_2Cl_2 , 400 MHz) δ (ppm): 7.63 (s, 1H); 7.41 (s, 2H); 1.28 (s, 9H); 1.15 (s, 21H); 0.24 (s, 9H).

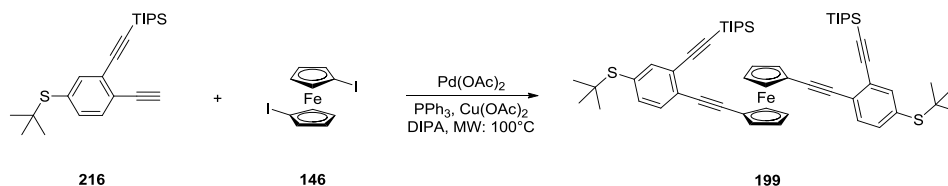
$^{13}\text{C-NMR}$ (CD_2Cl_2 , 100.6 MHz): δ (ppm) 141.6 (C_t , 1C); 137.3 (C_t , 1C); 134.1 (C_q , 1C); 133.2 (C_t , 1C); 126.4 (C_q , 1C); 126.2 (C_q , 1C); 105.2 (C_q , 1C); 103.4 (C_q , 1C); 100.5 (C_q , 1C); 96.3 (C_q , 1C); 47.2 (C_q , 1C); 31.3 (C_p , 3C); 19.1 (C_p , 6C); 11.9 (C_t , 3C); 0.1 (C_p , 3C).

EI-MS (70 eV), m/z (%): 442.2 (72) [M^+]; 357.1 (74.9) [$\text{M}^+ - 2 \times i\text{Pr}$].

Compound 216:

A 25 ml round bottom flask was purged with argon and charged with compound **197** (328 mg, 0.74 mmol, 1 equiv.), dry DCM (3 ml) and methanol (13.5 ml). The resulting mixture was degassed for 5 minutes. Potassium carbonate (176 mg, 1.26 mmol, 1.7 equiv.) was then added and the mixture was stirred for 2h at room temperature. The reaction mixture was filtered over a short silica plug eluting with cyclohexane:*t*BME (10:1) to afford the desired compound **216** (274 mg, quant.) as yellow oil.

$^1\text{H-NMR}$ (CDCl_3 , 400 MHz) δ (ppm): 7.64 (s, 1H); 7.42 (s, 2H); 3.32 (s, 1H); 1.30 (s, 9H); 1.14 (s, 21H).

Compound 199:

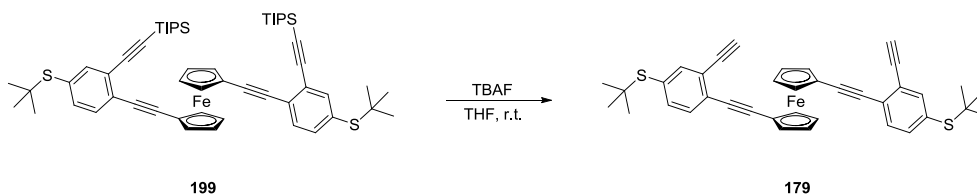
A 5 ml microwave tube was purged with argon and charged with palladium acetate (0.934 mg, 0.00416 mmol, 0.08 equiv.), copper acetate (0.763 mg, 0.00416 mmol, 0.08 equiv.), triphenylphosphine (4.36 mg, 0.0166 mmol, 0.32 equiv.), compound **146** (22.8 mg, 0.052 mmol, 1 equiv.), diisopropylamine (3 ml) and compound **216** (67.5 mg, 0.182 mmol, 3.5 equiv.). The resulting mixture was degassed for 5 min. and then heated to 100°C for 4.5h. The reaction mixture was diluted with *t*BME and washed with water. The combined organic layers were washed with brine, dried over MgSO₄, filtered and concentrated under reduced pressure. The residue was purified by column chromatography (silica, cyclohexane:DCM 5:1) to afford the desired product **199** (27 mg, 56%) as a red solid.

¹H-NMR (CD₂Cl₂, 400 MHz) δ (ppm): 7.59 (s, 2H); 7.40-7.35 (m, 4H); 4.55 (t, 4H); 4.35 (t, 4H); 1.29 (s, 18H); 1.16 (s, 42H).

¹³C-NMR (CD₂Cl₂, 100.6 MHz): δ (ppm) 141.0 (C_t, 2C); 136.7 (C_t, 2C); 131.9 (C_t, 2C); 73.1 (C_t, 4C); 71.4 (C_t, 4C); 46.4 (C_q, 2C); 39.7 (C_q, 2C); 30.7 (C_p, 6C); 18.6 (C_p, 12C); 11.3 (C_t, 6C).

ESI-MS, (MeOH, pos. mode) m/z: 922 (M⁺); 945 (M⁺+Na).

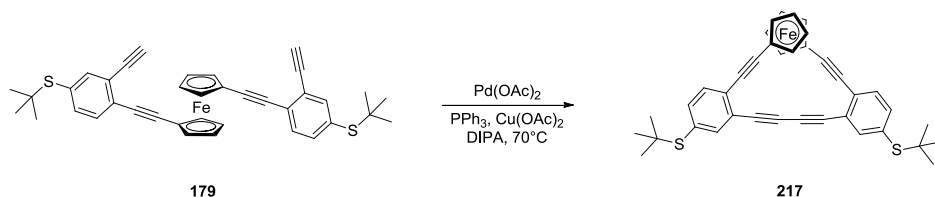
Compound 179:



A 10 ml two-necked round-bottomed flask was purged with argon and charged with compound **199** (27 mg, 0.029 mmol, 1 equiv.) and dry THF (4 ml). TBAF (1M in THF, 0.102 ml, 0.102 mmol, 3.5 equiv.) was added at room temperature. The mixture was stirred for 45 min. The reaction mixture was concentrated under reduced pressure and the residue was dissolved in cyclohexane/DCM (5:1) and filtered over silica. The filtrate was concentrated to afford the desired compound **179** (17 mg, 96 %) as orange solid.

¹H-NMR (CD₂Cl₂, 400 MHz) δ (ppm): 7.66 (s, 2H); 7.42-7.39 (m, 4H); 4.59 (t, 4H); 3.45 (s, 2H); 1.29 (s, 18H).

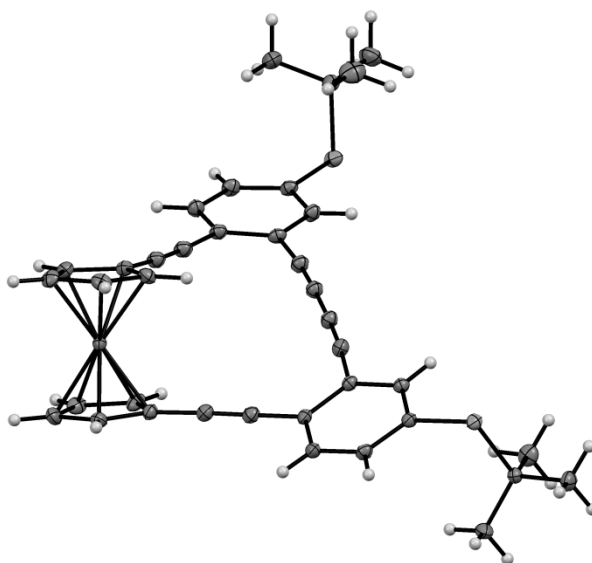
MALDI-MS, (RP mode, 2',4',6'-trihydroxyacetophenone monohydrate) m/z: 610.15 [M⁺].

Compound 217:

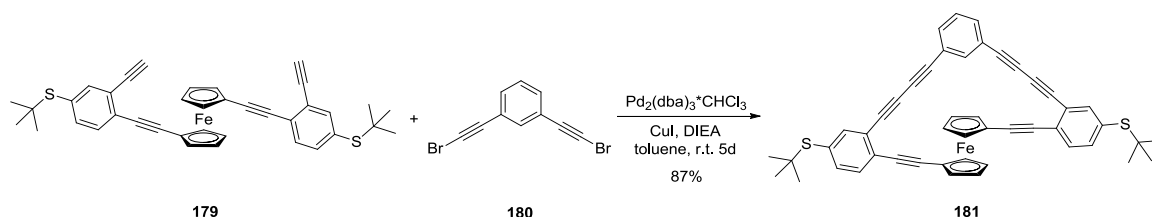
A 25 ml three necked round bottom flask was purged with argon and charged with palladium acetate (110 mg, 0.49 mmol, 5 equiv.), copper acetate (9 mg, 0.049 mmol, 0.5 equiv.), triphenylphosphine (514 mg, 1.96 mmol, 20 equiv.) and diisopropylamine (11 ml). The resulting mixture was degassed for 10 min and heated to 70°C. Compound **179** (59.8 mg, 0.098 mmol 1 equiv.) and compound **146** (42.9 mg, 0.098 mmol, 1 equiv.) were each dissolved in diisopropylamine (2 x 10 ml) and slowly added using a syringe pump (0.02 mm/min) to the prepared solution. After the addition was complete the mixture was stirred for 24h. The reaction mixture was then concentrated under reduced pressure and the residue was purified by column chromatography (silica, cyclohexane:*t*BME 20:1; RF = 0.43) to afford the desired product **217** (25 mg, 42 %) as red solid.

¹H-NMR (CDCl₃, 400 MHz) δ (ppm): 7.70 (s, 2H); 7.46 (q, 4H); 4.44-4.42 (m, 8H); 1.32 (s, 18H).

MALDI-MS, (RP mode, 2',4',6'-trihydroxyacetophenone monohydrate) m/z: 608.1 [M⁺].

Crystal Data for compound 217:

Crystal data for **217**: formula $C_{38}H_{32}Fe_1S_2$, $M = 608.65$, $F(000) = 1272$, orange needle, size $0.030 \cdot 0.040 \cdot 0.240 \text{ mm}^3$, monoclinic, space group $P 2_1/c$, $Z = 4$, $a = 6.0771(4) \text{ \AA}$, $b = 18.8976(11) \text{ \AA}$, $c = 26.7586(15) \text{ \AA}$, $\alpha = 90^\circ$, $\beta = 95.372(3)^\circ$, $\gamma = 90^\circ$, $V = 3059.5(3) \text{ \AA}^3$, $D_{\text{calc.}} = 1.321 \text{ Mg} \cdot \text{m}^{-3}$. The crystal was measured on a Nonius KappaCCD diffractometer at 123K using graphite-monochromated Mo K_α -radiation with $\lambda = 0.71073 \text{ \AA}$, $\Theta_{\text{max}} = 33.728^\circ$. Minimal/maximal transmission 0.97/0.98, $\mu = 0.655 \text{ mm}^{-1}$. The COLLECT suite has been used for datacollection and integration. From a total of 80989 reflections, 12203 were independent (merging $r = 0.045$). From these, 8432 were considered as observed ($I > 2.0\sigma(I)$) and were used to refine 370 parameters. The structure was solved by Other methods using the program Superflip. Least-squares refinement against F was carried out on all non-hydrogen atoms using the program CRYSTALS. $R = 0.0320$ (observed data), $wR = 0.0496$ (all data), $GOF = 1.0293$. Minimal/maximal residual electron density = $-0.33/0.50 \text{ e \AA}^{-3}$. Chebychev polynomial weights were used to complete the refinement. Plots were produced using CAMERON.

Compound 181:

A 250 ml three-necked round bottom flask was purged with argon and charged with dry toluene (105 ml) and DIEA (1.5 ml). The resulting mixture was degassed for 10 min. Tris(dibenzylideneacetone)dipalladium-chloroform (9.42 mg, 0.0091 mmol, 0.325 equiv.) and CuI (4.45 mg, 0.0232 mmol, 0.833 equiv.) were added. Compound **179** (17.1 mg, 0.028 mmol, 1 equiv.) and compound **180** (7.95 mg, 0.028 mmol, 1 equiv.) were each dissolved in toluene (5 ml) and slowly added at room temperature using a syringe pump (0.01 mm/h, 10 ml syringe). After the addition was complete the reaction mixture was stirred for 4 days. The mixture was extracted with water (2 x 50 ml) and brine (50 ml), dried over MgSO₄, filtered and concentrated under reduced pressure. The crude product was purified by column chromatography (silica, cyclohexane:*t*BME 20:1; RF = 0.43) to afford the desired product **181** (18 mg, 87 %) as a red solid.

¹H-NMR (CDCl₃, 400 MHz) δ (ppm): 7.85-7.56 (m, 10H); 4.58-4.56 (m, 4H); 4.45-4.43 (m, 4H); 1.33 (s, 9H); 1.18 (s, 9H).

ESI-MS, (MeOH, pos. mode) *m/z*: 677 (M⁺*i*Pr).

8 Bibliography

- [1] N. Weibel, S. Grunder, M. Mayor, *Org. Biomol. Chem.* **2007**, *5*, 2343–2353.
- [2] R. P. Feynman, *Engineering and Science* **1960**, 22–36.
- [3] C. J. Muller, J. M. van Ruitenbeek, L. J. de Jongh, *Phys. Rev. Lett.* **1992**, *69*, 140–143.
- [4] M. A. Reed, C. Zhou, C. J. Muller, T. P. Burgin, J. M. Tour, *Science* **1997**, *278*, 252–254.
- [5] N. Agraït, A. L. Yeyati, J. M. van Ruitenbeek, *Physics Reports* **2003**, *377*, 81–279.
- [6] S. Wu, Electrical conductance of single conjugated oligomers, Basel, **2009**.
- [7] G. Binnig, H. Rohrer, C. Gerber, E. Weibel, *Phys. Rev. Lett.* **1982**, *49*, 57–61.
- [8] G. Binnig, C. F. Quate, C. Gerber, *Phys. Rev. Lett.* **1986**, *56*, 930–933.
- [9] A. Aviram, C. Joachim, M. Pomerantz, *Chemical Physics Letters* **1988**, *146*, 490–495.
- [10] S. M. Lindsay, Y. Li, J. Pan, T. Thundat, L. A. Nagahara, P. Oden, J. A. DeRose, U. Knipping, J. W. White, in *Proceedings of the International Conference on Scanning Tunneling Microscopy/Spectroscopy*, Avs, **1991**, S. 1096–1101.
- [11] B. Xu, *Science* **2003**, *301*, 1221–1223.
- [12] R. J. Nichols, W. Haiss, S. J. Higgins, E. Leary, S. Martin, D. Bethell, *Phys. Chem. Chem. Phys.* **2010**, *12*, 2801–2815.
- [13] A. Ciesielski, C. Palma, M. Bonini, P. Samorì, *Adv. Mater.* **2010**, *22*, 3506–3520.
- [14] N. M. Jenny, H. Wang, M. Neuburger, H. Fuchs, L. Chi, M. Mayor, *European Journal of Organic Chemistry* **2012**, *14*, 2738–2747.
- [15] L. Kampschulte, M. Lackinger, A.-K. Maier, R. S. K. Kishore, S. Griessl, M. Schmittel, W. M. Heckl, *J. Phys. Chem. B* **2006**, *110*, 10829–10836.
- [16] Y. Noguchi, T. Nagase, T. Kubota, T. Kamikado, S. Mashiko, *Thin Solid Films* **2006**, *499*, 90–94.
- [17] H. S. J. Van der Zant, E. A. Osorio, M. Poot, K. O’Neill, *physica status solidi (b)* **2006**, *243*, 3408–3412.
- [18] E. A. Osorio, T. Bjørnholm, J. M. Lehn, M. Ruben, H. S. J. Van Der Zant, *J. Phys.: Condens. Matter* **2008**, *20*, 374121.
- [19] K. Moth-Poulsen, T. Bjørnholm, *Nat Nano* **2009**, *4*, 551–556.
- [20] E. A. Osorio, K. O’Neill, N. Stuhr-Hansen, O. F. Nielsen, T. Bjørnholm, H. S. J. van der Zant, *Advanced Materials* **2007**, *19*, 281–285.
- [21] L. H. Yu, Z. K. Keane, J. W. Ciszek, L. Cheng, J. M. Tour, T. Baruah, M. R. Pederson, D. Natelson, *Phys. Rev. Lett.* **2005**, *95*, 256803.
- [22] E. A. Osorio, K. O’Neill, M. Wegewijs, N. Stuhr-Hansen, J. Paaske, T. Bjørnholm, H. S. J. van der Zant, *Nano Lett.* **2007**, *7*, 3336–3342.
- [23] H. B. Heersche, Z. de Groot, J. A. Folk, H. S. J. van der Zant, C. Romeike, M. R. Wegewijs, L. Zobbi, D. Barreca, E. Tondello, A. Cornia, *Phys. Rev. Lett.* **2006**, *96*, 206801.

-
- [24] M.-H. Jo, J. E. Grose, K. Baheti, M. M. Deshmukh, J. J. Sokol, E. M. Rumberger, D. N. Hendrickson, J. R. Long, H. Park, D. C. Ralph, *Nano Lett.* **2006**, *6*, 2014–2020.
- [25] H. B. Heersche, G. Lientschnig, K. O’Neill, H. S. J. van der Zant, H. W. Zandbergen, *Applied Physics Letters* **2007**, *91*, 072107–072107.
- [26] T. Taychatanapat, K. I. Bolotin, F. Kuemmeth, D. C. Ralph, *Nano Lett.* **2007**, *7*, 652–656.
- [27] S. Kubatkin, A. Danilov, M. Hjort, J. Cornil, J.-L. Brédas, N. Stuhr-Hansen, P. Hedegard, T. Bjørnholm, *Nature* **2003**, *425*, 698–701.
- [28] S. Kubatkin, A. Danilov, M. Hjort, J. Cornil, J.-L. Brédas, N. Stuhr-Hansen, P. Hedegård, T. Bjørnholm, *Current Applied Physics* **2004**, *4*, 554–558.
- [29] A. R. Champagne, A. N. Pasupathy, D. C. Ralph, *Nano Lett.* **2005**, *5*, 305–308.
- [30] Z. Li, I. Pobelov, B. Han, T. Wandlowski, A. Błaszczuk, M. Mayor, *Nanotechnology* **2007**, *18*, 044018.
- [31] N. J. Tao, *Nature Nanotechnology* **2006**, *1*, 173–181.
- [32] T. Dadoosh, Y. Gordin, R. Krahne, I. Khivrich, D. Mahalu, V. Frydman, J. Sperling, A. Yacoby, I. Bar-Joseph, *Nature* **2005**, *436*, 677–680.
- [33] H. Park, J. Park, A. K. L. Lim, E. H. Anderson, A. P. Alivisatos, P. L. McEuen, *Nature* **2000**, *407*, 57–60.
- [34] S. Kubatkin, A. Danilov, M. Hjort, J. Cornil, J. L. Brédas, N. Stuhr-Hansen, P. Hedegard, T. Bjørnholm, *Nature* **2003**, *425*, 698–701.
- [35] A. Danilov, S. Kubatkin, S. Kafanov, P. Hedegard, N. Stuhr-Hansen, K. Moth-Poulsen, T. Bjørnholm, *Nano Lett.* **2007**, *8*, 1–5.
- [36] S. Y. Quek, L. Venkataraman, H. J. Choi, S. G. Louie, M. S. Hybertsen, J. B. Neaton, *Nano Lett.* **2007**, *7*, 3477–3482.
- [37] F. Chen, X. Li, J. Hihath, Z. Huang, N. Tao, *J. Am. Chem. Soc.* **2006**, *128*, 15874–15881.
- [38] R. Huber, M. T. González, S. Wu, M. Langer, S. Grunder, V. Horhoiu, M. Mayor, M. R. Bryce, C. Wang, R. Jitchati, u. a., *J. Am. Chem. Soc.* **2008**, *130*, 1080–1084.
- [39] Y. S. Park, A. C. Whalley, M. Kamenetska, M. L. Steigerwald, M. S. Hybertsen, C. Nuckolls, L. Venkataraman, *J. Am. Chem. Soc.* **2007**, *129*, 15768–15769.
- [40] S. Wu, M. T. Gonzalez, R. Huber, S. Grunder, M. Mayor, C. Schonenberger, M. Calame, *Nat Nano* **2008**, *3*, 569–574.
- [41] L. Patrone, S. Palacin, J. P. Bourgoin, *Appl. Surf. Sci.* **2003**, *212-213*, 446–451.
- [42] L. Patrone, S. Palacin, J. Charlier, F. Armand, J. P. Bourgoin, H. Tang, S. Gauthier, *Phys. Rev. Lett.* **2003**, *91*, 096802.
- [43] S. Yasuda, S. Yoshida, J. Sasaki, Y. Okutsu, T. Nakamura, A. Taninaka, O. Takeuchi, H. Shigekawa, *J. Am. Chem. Soc.* **2006**, *128*, 7746–7747.
- [44] C. A. Martin, D. Ding, J. K. Sørensen, T. Bjørnholm, J. M. van Ruitenbeek, H. S. J. van der Zant, *J. Am. Chem. Soc.* **2008**, *130*, 13198–13199.
- [45] Kim, J. M. Beebe, Y. Jun, X.-Y. Zhu, C. D. Frisbie, *J. Am. Chem. Soc.* **2006**, *128*, 4970–4971.
-

- [46] A. Mishchenko, L. A. Zotti, D. Vonlanthen, M. Bürkle, F. Pauly, J. C. Cuevas, M. Mayor, T. Wandlowski, *J. Am. Chem. Soc.* **2011**, *133*, 184–187.
- [47] D. Gao, F. Scholz, H.-G. Nothofer, W. E. Ford, U. Scherf, J. M. Wessels, A. Yasuda, F. von Wrochem, *J. Am. Chem. Soc.* **2011**, *133*, 5921–5930.
- [48] M. Carrara, F. Nüesch, L. Zuppiroli, *Synthetic Metals* **2001**, *121*, 1633–1634.
- [49] N. Weibel, S. Grunder, M. Mayor, *Org. Biomol. Chem.* **2007**, *5*, 2343–2353.
- [50] F. Chen, N. J. Tao, *Acc. Chem. Res.* **2011**, *42*, 429–438.
- [51] A. Salomon, D. Cahen, S. Lindsay, J. Tomfohr, V. B. Engelkes, C. D. Frisbie, *Advanced Materials* **2003**, *15*, 1881–1890.
- [52] V. Kaliginedi, P. Moreno-García, H. Valkenier, W. Hong, V. M. García-Suárez, P. Buitter, J. L. H. Otten, J. C. Hummelen, C. J. Lambert, T. Wandlowski, *J. Am. Chem. Soc.* **2012**, *134*, 5262–5275.
- [53] M. Mayor, M. Büschel, K. M. Fromm, J.-M. Lehn, J. Daub, *Annals of the New York Academy of Sciences* **2006**, *960*, 16–28.
- [54] S. N. Yaliraki, M. A. Ratner, *Annals of the New York Academy of Sciences* **2006**, *960*, 153–162.
- [55] Marcel Mayor, H. B. Weber, J. Reichert, M. Elbing, C. von Hänisch, D. Beckmann, M. Fischer, *Angew. Chem. Int. Ed.* **2003**, *42*, 5834–5838.
- [56] I.-W. P. Chen, M.-D. Fu, W.-H. Tseng, C. Chen, C.-M. Chou, T.-Y. Luh, *Chem. Commun.* **2007**, 3074.
- [57] L. Venkataraman, J. E. Klare, C. Nuckolls, M. S. Hybertsen, M. L. Steigerwald, *Nature* **2006**, *442*, 904–907.
- [58] H. H. Jaffé, M. Orchin, *Theory and Applications of Ultraviolet Spectroscopy*, Wiley-vch, **1962**.
- [59] D. Vonlanthen, *Biphenyl-Cyclophanes: The Molecular Control over Conductivity of Single-Molecule Junctions*, Basel, **2010**.
- [60] D. Vonlanthen, A. Mishchenko, M. Elbing, M. Neuburger, T. Wandlowski, M. Mayor, *Angew. Chem. Int. Ed.* **2009**, *48*, 8886–8890.
- [61] J. F. Smalley, S. B. Sachs, C. E. D. Chidsey, S. P. Dudek, H. D. Sikes, S. E. Creager, C. J. Yu, S. W. Feldberg, M. D. Newton, *J. Am. Chem. Soc.* **2004**, *126*, 14620–14630.
- [62] M. D. Newton, J. F. Smalley, *Phys. Chem. Chem. Phys.* **2007**, *9*, 555.
- [63] A. Tsuda, A. Osuka, *Science* **2001**, *293*, 79–82.
- [64] J. Chen, M. . Reed, *Chemical Physics* **2002**, *281*, 127–145.
- [65] J. Taylor, M. Brandbyge, K. Stokbro, *Phys. Rev. B* **2003**, *68*, 121101.
- [66] J. Chen, M. A. Reed, A. M. Rawlett, J. M. Tour, *Science* **1999**, *286*, 1550–1552.
- [67] A. Błaszczuk, M. Chadim, C. von Hänisch, M. Mayor, *Eur. J. Org. Chem.* **2006**, 3809–3825.
- [68] M. Elbing, R. Ochs, M. Koentopp, M. Fischer, C. Von Hänisch, F. Weigend, F. Evers, H. B. Weber, M. Mayor, *PNAS* **2005**, *102*, 8815–8820.
- [69] A. Aviram, M. A. Ratner, *Chemical Physics Letters* **1974**, *29*, 277–283.
- [70] R. M. Metzger, *Chem. Rev.* **2003**, *103*, 3803–3834.

- [71] H. Werner, *Angew. Chem. Int. Ed.* **2012**, 2–9.
- [72] G. Wilkinson, M. Rosenblum, M. C. Whiting, R. B. Woodward, *J. Am. Chem. Soc.* **1952**, *74*, 2125–2126.
- [73] L. F. N. A. Qune, K. Tamada, M. Hara, *e-Journal of Surface Science and Nanotechnology* **2008**, *6*, 119–123.
- [74] D. Bao, B. Millare, W. Xia, B. G. Steyer, A. A. Gerasimenko, A. Ferreira, A. Contreras, V. I. Vullev, *J. Phys. Chem. A* **2009**, *113*, 1259–1267.
- [75] T. Yamamoto, T. Morikita, T. Maruyama, K. Kubota, M. Katada, *Macromolecules* **1997**, *30*, 5390–5396.
- [76] T. Morikita, T. Yamamoto, *Journal of Organometallic Chemistry* **2001**, 637–639, 809–812.
- [77] S. Creager, C. J. Yu, C. Bamdad, S. O'Connor, T. MacLean, E. Lam, Y. Chong, G. T. Olsen, J. Luo, M. Gozin, u. a., *J. Am. Chem. Soc.* **1999**, *121*, 1059–1064.
- [78] S. Getty, C. Engtrakul, L. Wang, R. Liu, S.-H. Ke, H. Baranger, W. Yang, M. Fuhrer, L. Sita, *Phys. Rev. B* **2005**, *71*, DOI 10.1103/PhysRevB.71.241401.
- [79] S. Datta, *Nanotechnology* **2004**, *15*, 433–451.
- [80] C. Engtrakul, L. R. Sita, *Organometallics* **2008**, *27*, 927–937.
- [81] J. Ma, M. Vollmann, H. Menzel, S. Pohle, H. Butenschön, *Journal of Inorganic and Organometallic Polymers and Materials* **2008**, *18*, 41–50.
- [82] X. Xiao, D. Brune, J. He, S. Lindsay, C. B. Gorman, N. Tao, *Chemical Physics* **2006**, *326*, 138–143.
- [83] J. J. Davis, B. Peters, W. Xi, J. Appel, A. Kros, T. J. Aartsma, R. Stan, G. W. Canters, *J. Phys. Chem. Lett.* **2010**, *1*, 1541–1546.
- [84] S. Grunder, *New Functional Molecules in Molecular Junctions*, Basel, **2009**.
- [85] D. S. Seferos, S. A. Trammell, G. C. Bazan, J. G. Kushmerick, *PNAS* **2005**, *102*, 8821–8825.
- [86] F. Davis, S. Higson, in *Macrocycles: Construction, Chemistry and Nanotechnology Applications*, John Wiley & Sons, Ltd, **2011**, S. 381–517.
- [87] T. J. J. Müller, U. H. F. Bunz, *Functional Organic Materials*, Wiley, Weinheim, **2007**.
- [88] V. Balzani, M. Gómez-López, J. F. Stoddart, *Acc. Chem. Res.* **1998**, *31*, 405–414.
- [89] E. R. Kay, D. A. Leigh, F. Zerbetto, *Angewandte Chemie International Edition* **2006**, *46*, 72–191.
- [90] W. R. Browne, B. L. Feringa, *Nature Nanotechnology* **2006**, *1*, 25–35.
- [91] M. Iyoda, J. Yamakawa, M. J. Rahman, *Angewandte Chemie International Edition* **2011**, *50*, 10522–10553.
- [92] R. Gleiter, H. Hopf, *Modern Cyclophane Chemistry*, Wiley-vch, Weinheim, **2004**.
- [93] M. Müri, K. C. Schuermann, L. De Cola, M. Mayor, *Eur. J. Org. Chem.* **2009**, *2009*, 2562–2575.
- [94] A. Błaszczuk, M. Chadim, C. von Hänisch, M. Mayor, *Eur. J. Org. Chem.* **2006**, *2006*, 3809–3825.
- [95] N. M. Jenny, M. Mayor, T. R. Eaton, *Eur. J. Org. Chem.* **2011**, *26*, 4965–4983.

- [96] T. J. J. Müller, U. H. F. Bunz, Hrsg., *Functional Organic Materials – Syntheses, Strategies and Applications*, Wiley-vch, Weinheim, **2007**.
- [97] E. Negishi, L. Anastasia, *Chem. Rev.* **2003**, *103*, 1979–2018.
- [98] X. F. Wu, P. Anbarasan, H. Neumann, M. Beller, *Angew. Chem. Int. Ed.* **2010**, *49*, 9047–9050.
- [99] „The Nobel Prize in Chemistry 2010 - Scientific Background“, can be found under http://nobelprize.org/nobel_prizes/chemistry/laureates/2010/sci.html, **2010**.
- [100] F. Diederich, P. J. Stang, R. R. Tykwinski, Hrsg., *Acetylene Chemistry - Chemistry, Biology and Material Science*, Wiley-vch, **2005**.
- [101] K. Sonogashira, *J. Organomet. Chem.* **2002**, *653*, 46–49.
- [102] R. R. Tykwinski, *Angew. Chem. Int. Ed.* **2003**, *42*, 1566–1568.
- [103] K. Sonogashira, Y. Tohda, N. Hagihara, *Tetrahedron Lett.* **1975**, *16*, 4467–4470.
- [104] N. Weibel, S. Grunder, M. Mayor, *Org. Biomol. Chem.* **2007**, *5*, 2343–2353.
- [105] J. N. Wilson, U. H. F. Bunz, *J. Am. Chem. Soc.* **2005**, *127*, 4124–4125.
- [106] M. Fischer, G. Lieser, A. Rapp, I. Schnell, W. Mamdouh, S. De Feyter, F. C. De Schryver, S. Höger, *J. Am. Chem. Soc.* **2004**, *126*, 214–222.
- [107] K. C. Nicolaou, P. G. Bulger, D. Sarlah, *Angew. Chem. Int. Ed.* **2005**, *44*, 4442–4489.
- [108] A. L. K. Shi Shun, E. T. Chernick, S. Eisler, R. R. Tykwinski, *J. Org. Chem.* **2003**, *68*, 1339–1347.
- [109] M. Kivala, F. Diederich, *Pure Appl. Chem.* **2008**, *80*, 411–427.
- [110] J. P. Hermes, F. Sander, P. Torsten, C. Cioffi, P. Ringler, T. Pfohl, M. Mayor, *Small* **2011**, *7*, 920–929.
- [111] A. Schaate, M. Schulte, M. Wiebcke, A. Godt, P. Behrens, *Inorg. Chim. Acta* **2009**, *362*, 3600–3606.
- [112] D. Evrard, F. Lambert, C. Policar, V. Balland, B. Limoges, *Chem. Eur. J.* **2008**, *14*, 9286–9291.
- [113] J. E. Reeve, H. A. Collins, K. D. Mey, M. M. Kohl, K. J. Thorley, O. Paulsen, K. Clays, H. L. Anderson, *J. Am. Chem. Soc.* **2009**, *131*, 2758–2759.
- [114] N. Miyaura, A. Suzuki, *J. Chem. Soc., Chem. Commun.* **1979**, 866.
- [115] D. Milstein, J. K. Stille, *J. Am. Chem. Soc.* **1978**, *100*, 3636–3638.
- [116] S. Chopin, F. Chaignon, E. Blart, F. Odobel, *J. Mater. Chem.* **2007**, *17*, 4139.
- [117] U. H. F. Bunz, *Macromol. Rapid Commun.* **2009**, *30*, 772–805.
- [118] C. Wang, A. S. Batsanov, M. R. Bryce, *J. Org. Chem.* **2006**, *71*, 108–116.
- [119] Y. Cakmak, E. U. Akkaya, *Org. Lett.* **2009**, *11*, 85–88.
- [120] T. E. O. Screen, I. M. Blake, L. H. Rees, W. Clegg, S. J. Borwick, H. L. Anderson, *J. Chem. Soc., Perkin Trans. 1* **2002**, 320–329.
- [121] M. B. Nielsen, F. Diederich, *Chem. Record* **2002**, *2*, 189–198.
- [122] C. D. Simpson, J. D. Brand, A. J. Berresheim, L. Przybilla, H. J. Räder, K. Müllen, *Chem. Eur. J.* **2002**, *8*, 1424–1429.
- [123] J. S. Moore, *Accounts Chem. Res.* **1997**, *30*, 402–413.

- [124] B. Schmaltz, A. Rouhanipour, H. J. Räder, W. Pisula, K. Müllen, *Angew. Chem. Int. Ed.* **2009**, *48*, 720–724.
- [125] L. Shu, M. Mayor, *Chem. Commun.* **2006**, 4134–4136.
- [126] L. Shu, M. Müri, R. Krupke, M. Mayor, *Org. Biomol. Chem.* **2009**, *7*, 1081–1092.
- [127] Z. Wu, S. Lee, J. S. Moore, *J. Am. Chem. Soc.* **1992**, *114*, 8730–8732.
- [128] T. C. Bedard, J. S. Moore, *J. Am. Chem. Soc.* **1995**, *117*, 10662–10671.
- [129] N. Weibel, A. Mishchenko, T. Wandlowski, M. Neuburger, Y. Leroux, M. Mayor, *Eur. J. Org. Chem.* **2009**, 6140–6150.
- [130] A. Błaszczuk, M. Chadim, C. von Hänisch, M. Mayor, *Eur. J. Org. Chem.* **2006**, 3809–3825.
- [131] K. Sato, T. Yoshimura, M. Shindo, K. Shishido, *J. Org. Chem.* **2001**, *66*, 309–314.
- [132] M. Kivala, C. Boudon, J.-P. Gisselbrecht, P. Seiler, M. Gross, F. Diederich, *Angew. Chem. Int. Ed.* **2007**, *46*, 6357–6360.
- [133] H. C. Kolb, M. G. Finn, K. B. Sharpless, *Angew. Chem. Int. Ed.* **2001**, *40*, 2004–2021.
- [134] P. Siemsen, R. C. Livingston, F. Diederich, *Angew. Chem. Int. Ed.* **2000**, *39*, 2632–2657.
- [135] E. J. Corey, *Chem. Soc. Rev.* **1988**, *17*, 111.
- [136] A. L. Kanibolotsky, I. F. Perepichka, P. J. Skabara, *Chem. Soc. Rev.* **2010**, *39*, 2695–2728.
- [137] T. Narita, M. Takase, T. Nishinaga, M. Iyoda, K. Kamada, K. Ohta, *Chem. Eur. J.* **2010**, *16*, 12108–12113.
- [138] M. Mayor, J.-M. Lehn, *J. Am. Chem. Soc.* **1999**, *121*, 11231–11232.
- [139] M. Mayor, C. Didschies, *Angew. Chem. Int. Ed.* **2003**, *42*, 3176–3179.
- [140] B. M. Trost, M. T. Sorum, C. Chan, G. Rühler, *J. Am. Chem. Soc.* **1997**, *119*, 698–708.
- [141] R. Chinchilla, C. Nájera, *Chem. Rev.* **2007**, *107*, 874–922.
- [142] P. Fitton, M. P. Johnson, J. E. McKeon, *Chem. Commun.* **1968**, 6–7.
- [143] P. Fitton, E. A. Rick, *J. Organomet. Chem.* **1971**, *28*, 287–291.
- [144] C. Amatore, A. Jutand, *Acc. Chem. Res.* **2000**, *33*, 314–321.
- [145] C. Amatore, S. Bensalem, S. Ghalem, A. Jutand, Y. Medjour, *Eur. J. Org. Chem.* **2004**, 366–371.
- [146] C. Amatore, A. Jutand, *J. Organomet. Chem.* **1999**, *576*, 254–278.
- [147] L. Xue, Z. Lin, *Chem. Soc. Rev.* **2010**, *39*, 1692.
- [148] G. P. McGlacken, I. J. S. Fairlamb, *Eur. J. Org. Chem.* **2009**, 4011–4029.
- [149] S. Wu, M. T. Gonzalez, R. Huber, S. Grunder, M. Mayor, C. Schönenberger, M. Calame, *Nat. Nanotechnol.* **2008**, *3*, 569–574.
- [150] R. L. Carroll, C. B. Gorman, *Angew. Chem. Int. Ed.* **2002**, *41*, 4378–4400.
- [151] V. P. W. Böhm, W. A. Herrmann, *Eur. J. Org. Chem.* **2000**, 3679–3681.
- [152] A. C. Hillier, G. A. Grasa, M. S. Viciu, H. M. Lee, C. Yang, S. P. Nolan, *J. Organomet. Chem.* **2002**, *653*, 69–82.

- [153] A. F. Littke, G. C. Fu, *Angew. Chem. Int. Ed.* **2002**, *41*, 4176–4211.
- [154] C. Torborg, J. Huang, T. Schulz, B. Schöffner, A. Zapf, A. Spannenberg, A. Börner, M. Beller, *Chem. Eur. J.* **2009**, *15*, 1329–1336.
- [155] S. Cacchi, P. G. Ciattini, E. Morera, G. Ortar, *Tetrahedron Lett.* **1986**, *27*, 3931–3934.
- [156] S. Darses, G. Michaud, J.-P. Genêt, *Eur. J. Org. Chem.* **1999**, 1875–1883.
- [157] G. Fabrizi, A. Goggiamani, A. Sferrazza, S. Cacchi, *Angew. Chem. Int. Ed.* **2010**, 4067–4070.
- [158] D. Sahoo, S. Thiele, M. Schulte, N. Ramezani, A. Godt, *Beilstein J. Org. Chem.* **2010**, *6*, DOI 10.3762/bjoc.6.57.
- [159] H. Kukula, S. Veit, A. Godt, *Eur. J. Org. Chem.* **1999**, 277–286.
- [160] S. Höger, *Liebigs Ann./Recl.* **1997**, 273–277.
- [161] S. Höger, A. D. Meckenstock, S. Müller, *Chem. Eur. J.* **1998**, *4*, 2423–2434.
- [162] F. M. Irvine, J. C. Smith, *J. Chem. Soc.* **1927**, 74.
- [163] M. Schelhaas, H. Waldmann, *Angew. Chem. Int. Ed.* **1996**, *35*, 2056–2083.
- [164] U. Ziener, A. Godt, *J. Org. Chem.* **1997**, *62*, 6137–6143.
- [165] P. Wuts, T. Greene, *Greene's Protective Groups in Organic Synthesis*, Wiley-vch, **2006**.
- [166] T. Kamikawa, T. Hayashi, *J. Org. Chem.* **1998**, *63*, 8922–8925.
- [167] T. Sandmeyer, *Ber. Dtsch. Chem. Ges.* **1884**, *17*, 1633–1635.
- [168] J. Louie, J. F. Hartwig, *Tetrahedron Lett.* **1995**, *36*, 3609–3612.
- [169] A. S. Guram, R. A. Rennels, S. L. Buchwald, *Angew. Chem. Int. Ed.* **1995**, *34*, 1348–1350.
- [170] H. Ku, J. R. Barrio, *J. Org. Chem.* **1981**, *46*, 5239–5241.
- [171] N. Satyamurthy, J. R. Barrio, *J. Org. Chem.* **1983**, *48*, 4394–4396.
- [172] J. S. Moore, E. J. Weinstein, Z. Wu, *Tetrahedron Lett.* **1991**, *32*, 2465–2466.
- [173] J. Zhang, J. S. Moore, Z. Xu, R. A. Aguirre, *J. Am. Chem. Soc.* **1992**, *114*, 2273–2274.
- [174] E. J. Corey, P. L. Fuchs, *Tetrahedron Lett.* **1972**, *13*, 3769–3772.
- [175] J. C. Gilbert, U. Weerasooriya, *J. Org. Chem.* **1979**, *44*, 4997–4998.
- [176] E. Negishi, A. O. King, J. M. Tour, *Org. Synth.* **1986**, *64*, 44.
- [177] L. R. Jones, J. S. Schumm, J. M. Tour, *J. Org. Chem.* **1997**, *62*, 1388–1410.
- [178] F. Thiemann, T. Piehler, D. Haase, W. Saak, A. Lützen, *Eur. J. Org. Chem.* **2005**, *2005*, 1991–2001.
- [179] I. Wallmann, M. Schiek, R. Koch, A. Lützen, *Synthesis* **2008**, 2446–2450.
- [180] S. Takahashi, Y. Kuroyama, K. Sonogashira, N. Hagihara, *Synthesis* **1980**, 627–630.
- [181] R. Eastmond, D. R. M. Walton, *Tetrahedron* **1972**, *28*, 4591–4599.
- [182] U. Halbes-Letinois, J.-M. Weibel, P. Pale, *Chem. Soc. Rev.* **2007**, *36*, 759–769.
- [183] R. Severin, J. Reimer, S. Doye, *J. Org. Chem.* **2010**, *75*, 3518–3521.
- [184] S. Höger, K. Bonrad, *J. Org. Chem.* **2000**, *65*, 2243–2245.

- [185] W. E. Davidsohn, M. C. Henry, *Chem. Rev.* **1967**, *67*, 73–106.
- [186] F. Diederich, Y. Rubin, O. L. Chapman, N. S. Goroff, *Helv. Chim. Acta* **1994**, *77*, 1441–1457.
- [187] S. Höger, A.-D. Meckenstock, *Chem. Eur. J.* **1999**, *5*, 1686–1691.
- [188] S. Kim, B. Kim, J. In, *Synthesis* **2009**, *2009*, 1963–1968.
- [189] G. Gaefke, S. Höger, *Synthesis* **2008**, *2008*, 2155–2157.
- [190] A. Ernst, L. Gobbi, A. Vasella, *Tetrahedron Lett.* **1996**, *37*, 7959–7962.
- [191] Y. Li, C. M. Santos, A. Kumar, M. Zhao, A. I. Lopez, G. Qin, A. M. McDermott, C. Cai, *Chem. Eur. J.* **2011**, *17*, 2656–2665.
- [192] C. Cai, A. Vasella, *Helv. Chim. Acta* **1995**, *78*, 732–757.
- [193] N. A. Bumagin, A. B. Ponomaryov, I. P. Beletskaya, *Synthesis* **1984**, 728–729.
- [194] S. J. Havens, P. M. Hergenrother, *J. Org. Chem.* **1985**, *50*, 1763–1765.
- [195] M. J. Dabdoub, V. B. Dabdoub, E. J. Lenardão, *Tetrahedron Lett.* **2001**, *42*, 1807–1809.
- [196] J. G. Rodríguez, J. Esquivias, A. Lafuente, C. Díaz, *J. Org. Chem.* **2003**, *68*, 8120–8128.
- [197] O. H. Omar, F. Babudri, G. M. Farinola, F. Naso, A. Operamolla, *Eur. J. Org. Chem.* **2011**, 529–537.
- [198] S. Goeb, R. Ziessele, *Org. Lett.* **2007**, *9*, 737–740.
- [199] J. G. Rodríguez, J. L. Tejedor, T. La Parra, C. Díaz, *Tetrahedron* **2006**, *62*, 3355–3361.
- [200] A. Khatyr, R. Ziessele, *J. Org. Chem.* **2000**, *65*, 3126–3134.
- [201] R. Ziessele, S. Diring, P. Retailleau, *Dalton T.* **2006**, 3285–3290.
- [202] J. Luo, Q. Yan, Y. Zhou, T. Li, N. Zhu, C. Bai, Y. Cao, J. Wang, J. Pei, D. Zhao, *Chem. Commun.* **2010**, *46*, 5725–5727.
- [203] N. Zhu, W. Hu, S. Han, Q. Wang, D. Zhao, *Org. Lett.* **2008**, *10*, 4283–4286.
- [204] M. M. Haley, M. L. Bell, J. J. English, C. A. Johnson, T. J. R. Weakley, *J. Am. Chem. Soc.* **1997**, *119*, 2956–2957.
- [205] M. J. Mio, L. C. Kopel, J. B. Braun, T. L. Gadzikwa, K. L. Hull, R. G. Brisbois, C. J. Markworth, P. A. Grieco, *Org. Lett.* **2002**, *4*, 3199–3202.
- [206] H.-F. Chow, C.-W. Wan, K.-H. Low, Yeung, *J. Org. Chem.* **2001**, *66*, 1910–1913.
- [207] P. N. W. Baxter, *Chem. Eur. J.* **2003**, *9*, 5011–5022.
- [208] A. M. McDonagh, C. E. Powell, J. P. Morrall, M. P. Cifuentes, M. G. Humphrey, *Organometallics* **2003**, *22*, 1402–1413.
- [209] Y. Zhao, Y. Shirai, A. D. Slepko, L. Cheng, L. B. Alemany, T. Sasaki, F. A. Hegmann, J. M. Tour, *Chem. Eur. J.* **2005**, *11*, 3643–3658.
- [210] Y. Shirai, Y. Zhao, L. Cheng, J. M. Tour, *Org. Lett.* **2004**, *6*, 2129–2132.
- [211] K. C. Nicolaou, S. E. Webber, *J. Am. Chem. Soc.* **1984**, *106*, 5734–5736.
- [212] D. Bonifazi, S. Mohnani, A. Llanes-Pallas, *Chem. Eur. J.* **2009**, *15*, 7004–7025.

- [213] J. V. Barth, *Annu. Rev. Phys. Chem.* **2007**, *58*, 375–407.
- [214] C.-A. Palma, J. Bjork, M. Bonini, M. S. Dyer, A. Llanes-Pallas, D. Bonifazi, M. Persson, P. Samori, *J. Am. Chem. Soc.* **2009**, *131*, 13062–13071.
- [215] P. Politzer, J. S. Murray, T. Clark, *Phys. Chem. Chem. Phys.* **2010**, *12*, 7748–7757.
- [216] J. P. Rabe, S. Buchholz, *Science* **1991**, *253*, 424–427.
- [217] Z. Mu, Q. Shao, J. Ye, Z. Zeng, Y. Zhao, H. H. Hng, F. Y. C. Boey, J. Wu, X. Chen, *Langmuir* **2011**, *27*, 1314–1318.
- [218] A. S. Klymchenko, J. Slevin, K. Binnemans, S. De Feyter, *Langmuir* **2006**, *22*, 723–728.
- [219] T. Takami, D. P. Arnold, A. V. Fuchs, G. D. Will, R. Goh, E. R. Waclawik, J. M. Bell, P. S. Weiss, K. Sugiura, W. Liu, u. a., *J. Phys. Chem. B* **2006**, *110*, 1661–1664.
- [220] J. Gomez-Segura, I. Diez-Perez, N. Ishikawa, M. Nakano, J. Veciana, D. Ruiz-Molina, *Chem. Commun.* **2006**, 2866–2868.
- [221] K. Tahara, S. Lei, W. Mamdouh, Y. Yamaguchi, T. Ichikawa, H. Uji-i, M. Sonoda, K. Hirose, F. C. De Schryver, S. De Feyter, u. a., *J. Am. Chem. Soc.* **2008**, *130*, 6666–6667.
- [222] S. Lei, K. Tahara, X. Feng, S. Furukawa, F. C. De Schryver, K. Müllen, Y. Tobe, S. De Feyter, *J. Am. Chem. Soc.* **2008**, *130*, 7119–7129.
- [223] S. Furukawa, H. Uji-i, K. Tahara, T. Ichikawa, M. Sonoda, F. C. De Schryver, Y. Tobe, S. De Feyter, *J. Am. Chem. Soc.* **2006**, *128*, 3502–3503.
- [224] Z. Mu, L. Shu, H. Fuchs, M. Mayor, L. Chi, *Langmuir* **2011**, *27*, 1359–1363.
- [225] Z. Mu, L. Shu, H. Fuchs, M. Mayor, L. Chi, *J. Am. Chem. Soc.* **2008**, *130*, 10840–10841.
- [226] K. Yoosaf, A. R. Ramesh, J. George, C. H. Suresh, K. G. Thomas, *J. Phys. Chem. C* **2009**, *113*, 11836–11843.
- [227] P. Metrangolo, F. Meyer, T. Pilati, G. Resnati, G. Terraneo, *Angew. Chem. Int. Ed.* **2008**, *47*, 6114–6127.
- [228] O. Hassel, *Science* **1970**, *170*, 497–502.
- [229] G. R. Desiraju, R. Parthasarathy, *J. Am. Chem. Soc.* **2011**, *133*, 8725–8726.
- [230] G. R. Desiraju, *J. Chem. Sci.* **2010**, *122*, 667–675.
- [231] G. R. Desiraju, *Acc. Chem. Res.* **2002**, *35*, 565–573.
- [232] P. Metrangolo, H. Neukirch, T. Pilati, G. Resnati, *Acc. Chem. Res.* **2005**, *38*, 386–395.
- [233] A. Mukherjee, G. R. Desiraju, *Crystal Growth & Design* **2011**, *11*, 3735–3739.
- [234] V. R. Pedireddi, D. S. Reddy, B. S. Goud, D. C. Craig, A. D. Rae, G. R. Desiraju, *J. Chem. Soc., Perkin Trans. 2* **1994**, 2353–2360.
- [235] C. B. Aakeröy, K. R. Seddon, *Chem. Soc. Rev.* **1993**, *22*, 397–407.
- [236] S. K. Nayak, M. K. Reddy, T. N. Guru Row, D. Chopra, *Crystal Growth & Design* **2011**, *11*, 1578–1596.
- [237] I. Saraogi, V. G. Vijay, S. Das, K. Sekar, T. N. Guru Row, *Crystal Engineering* **2003**, *6*, 69–77.

- [238] O. Ermer, *J. Am. Chem. Soc.* **1988**, *110*, 3747–3754.
- [239] G. R. Desiraju, *Angew. Chem. Int. Ed.* **2007**, *46*, 8342–8356.
- [240] R. Banerjee, R. Mondal, J. A. K. Howard, G. R. Desiraju, *Crystal Growth & Design* **2006**, *6*, 999–1009.
- [241] M. J. Mio, L. C. Kopel, J. B. Braun, T. L. Gadzikwa, K. L. Hull, R. G. Brisbois, C. J. Markworth, P. A. Grieco, *Org. Lett.* **2002**, *4*, 3199–3202.
- [242] D. Mössinger, S.-S. Jester, E. Sigmund, U. Müller, S. Höger, *Macromolecules* **2009**, *42*, 7974–7978.
- [243] P. Fitton, M. P. Johnson, J. E. McKeon, *Chem. Commun.* **1968**, 6–7.
- [244] P. Fitton, E. A. Rick, *J. Organomet. Chem.* **1971**, *28*, 287–291.
- [245] U. Ziener, A. Godt, *J. Org. Chem.* **1997**, *62*, 6137–6143.
- [246] C. Xue, F.-T. Luo, *Tetrahedron* **2004**, *60*, 6285–6294.
- [247] T. Sandmeyer, *Ber. Dtsch. Chem. Ges.* **1884**, *17*, 1633–1635.
- [248] M. Schiek, K. Al-Shamery, A. Lützen, *Synthesis* **2007**, *2007*, 613–621.
- [249] D. V. Kosynkin, J. M. Tour, *Org. Lett.* **2001**, *3*, 993–995.
- [250] A. J. Deeming, G. Hogarth, M. (Venus) Lee, M. Saha, S. P. Redmond, H. (Taya) Phetmung, A. G. Orpen, *Inorg. Chim. Acta* **2000**, *309*, 109–122.
- [251] F. Thiemann, T. Piehler, D. Haase, W. Saak, A. Lützen, *Eur. J. Org. Chem.* **2005**, 1991–2001.
- [252] I. Wallmann, M. Schiek, R. Koch, A. Lützen, *Synthesis* **2008**, *2008*, 2446–2450.
- [253] M. S. Maji, T. Pfeifer, A. Studer, *Chem. Eur. J.* **2010**, *16*, 5872–5875.
- [254] J. S. Moore, E. J. Weinstein, Z. Wu, *Tetrahedron Lett.* **1991**, *32*, 2465–2466.
- [255] J. Zhang, J. S. Moore, Z. Xu, R. A. Aguirre, *J. Am. Chem. Soc.* **1992**, *114*, 2273–2274.
- [256] A. Godt, *J. Org. Chem.* **1997**, *62*, 7471–7474.
- [257] C. Laurence, M. Berthelot, *Perspectives in drug discovery and design* **2000**, *18*, 39–60.
- [258] N. Weibel, A. Mishchenko, T. Wandlowski, M. Neuburger, Y. Leroux, M. Mayor, *Eur. J. Org. Chem.* **2009**, *2009*, 6140–6150.
- [259] D. Vonlanthen, A. Mishchenko, M. Elbing, M. Neuburger, T. Wandlowski, M. Mayor, *Angew. Chem. Int. Ed.* **2009**, *48*, 8886–8890.
- [260] M. T. González, S. Wu, R. Huber, S. J. van der Molen, C. Schönenberger, M. Calame, *Nano Letters* **2006**, *6*, 2238–2242.
- [261] M. Calame, *Chimia* **2010**, *64*, 391–397.
- [262] Huang, F. Chen, P. A. Bennett, Tao, *J. Am. Chem. Soc.* **2007**, *129*, 13225–13231.
- [263] L. A. Zotti, T. Kirchner, J. C. Cuevas, F. Pauly, T. Huhn, E. Scheer, A. Erbe, *Small* **2010**, *6*, 1529–1535.
- [264] A. Danilov, S. Kubatkin, S. Kafanov, P. Hedegard, N. Stuhr-Hansen, K. Moth-Poulsen, T. Bjørnholm, *Nano Letters* **2008**, *8*, 1–5.
- [265] C. A. Martin, D. Ding, J. K. Sørensen, T. Bjørnholm, J. M. van Ruitenbeek, H. S. J. van der Zant, *J. Am. Chem. Soc.* **2008**, *130*, 13198–13199.

- [266] J. K. Sørensen, J. Fock, A. H. Pedersen, A. B. Petersen, K. Jennum, K. Bechgaard, K. Kilså, V. Geskin, J. Cornil, T. Bjørnholm, u. a., *J. Org. Chem.* **2010**, *76*, 245–263.
- [267] S. Grunder, D. Muñoz Torres, C. Marquardt, A. Błaszczuk, R. Krupke, M. Mayor, *Eur. J. Org. Chem.* **2011**, *2011*, 478–496.
- [268] K. Moth-Poulsen, T. Bjørnholm, *Nat Nano* **2009**, *4*, 551–556.
- [269] D. I. Gittins, D. Bethell, D. J. Schiffrin, R. J. Nichols, *Nature* **2000**, *408*, 67–69.
- [270] W. Haiss, H. van Zalinge, S. J. Higgins, D. Bethell, H. Höbenreich, D. J. Schiffrin, R. J. Nichols, *J. Am. Chem. Soc.* **2003**, *125*, 15294–15295.
- [271] Xu, Xiao, X. Yang, L. Zang, Tao, *J. Am. Chem. Soc.* **2005**, *127*, 2386–2387.
- [272] X. Xiao, D. Brune, J. He, S. Lindsay, C. B. Gorman, N. Tao, *Chemical Physics* **2006**, *326*, 138–143.
- [273] S. Lindsay, *J. Chem. Educ.* **2005**, *82*, 727.
- [274] F. Chen, N. J. Tao, *Acc. Chem. Res.* **2009**, *42*, 429–438.
- [275] H. Valkenier, E. H. Huisman, P. A. van Hal, D. M. de Leeuw, R. C. Chiechi, J. C. Hummelen, *J. Am. Chem. Soc.* **2011**, 4930–4939.
- [276] W. S. Wadsworth, W. D. Emmons, *J. Am. Chem. Soc.* **1961**, *83*, 1733–1738.
- [277] A. Kasahara, *Bull. Chem. Soc. Jpn.* **1982**, *55*, 1901–1906.
- [278] M. Hisatome, O. Tachikawa, M. Sasho, K. Yamakawa, *Journal of Organometallic Chemistry* **1981**, *217*, C17–C20.
- [279] A. N. Nesmeyanov, E. V. Leonova, N. S. Kochetkova, A. I. Malkova, A. G. Makarovskaya, *Journal of Organometallic Chemistry* **1975**, *96*, 275–278.
- [280] B. Ferber, S. Top, R. Welter, G. Jaouen, *Chem. Eur. J.* **2006**, *12*, 2081–2086.
- [281] N. Stühr-Hansen, J. B. Christensen, N. Harrit, T. Bjørnholm, *J. Org. Chem.* **2003**, *68*, 1275–1282.
- [282] K. L. Kees, Fitzgerald, K. E. Steiner, J. F. Mattes, B. Mihan, T. Tosi, D. Mondoro, M. L. McCaleb, *Journal of Medicinal Chemistry* **1996**, *39*, 3920–3928.
- [283] E. F. Pratt, J. F. V. D. Castle, *J. Org. Chem.* **1961**, *26*, 2973–2975.
- [284] A. Michelis, R. Kaehne, *Chem. Ber.* **1898**, 1048–1055.
- [285] A. Arbuzov, *J. Russ. Phys. Chem. Soc.* **1906**, 395.
- [286] R. Appel, *Angew. Chem. Int. Ed.* **1975**, *14*, 801–811.
- [287] A. Błaszczuk, M. Elbing, M. Mayor, *Org. Biomol. Chem.* **2004**, *2*, 2722.
- [288] I. R. Butler, S. B. Wilkes, S. J. McDonald, L. J. Hobson, A. Taralp, C. P. Wilde, *Polyhedron* **1993**, *12*, 129–131.
- [289] K. A. Winship, *Adverse Drug React Acute Poisoning Rev* **1988**, *7*, 19–38.
- [290] D. E. Weisshaar, T. Kuwana, *Anal. Chem.* **1985**, *57*, 378–379.
- [291] S. Ranganathan, T.-C. Kuo, R. L. McCreery, *Anal. Chem.* **1999**, *71*, 3574–3580.
- [292] S. M. Batterjee, M. I. Marzouk, M. E. Aazab, M. A. El-Hashash, *Appl. Organometal. Chem.* **2003**, *17*, 291–297.
- [293] J. K. Pudelski, M. R. Callstrom, *Organometallics* **1994**, *13*, 3095–3109.

- [294] S. Höger, *Liebigs Ann./Recl.* **1997**, 1997, 273–277.
- [295] S. Percec, R. Getty, W. Marshall, G. Skidd, R. French, *Journal of Polymer Science Part A: Polymer Chemistry* **2004**, 42, 541–550.
- [296] T. A. Halgren, *J. Am. Chem. Soc.* **1992**, 114, 7827–7843.
- [297] T. A. Halgren, *Journal of Computational Chemistry* **1996**, 17, 490–519.
- [298] T. A. Halgren, *Journal of Computational Chemistry* **1996**, 17, 520–552.
- [299] T. A. Halgren, *Journal of Computational Chemistry* **1996**, 17, 553–586.
- [300] J. Ma, B. Kühn, T. Hackl, H. Butenschön, *Chem. Eur. J.* **2010**, 16, 1859–1870.
- [301] J. K. Pudelski, M. R. Callstrom, *Organometallics* **1992**, 11, 2757–2759.
- [302] J. K. Pudelski, M. R. Callstrom, *Organometallics* **1994**, 13, 3095–3109.
- [303] J. E. Baldwin, *J. Chem. Soc., Chem. Commun.* **1976**, 734.
- [304] J. E. Baldwin, R. C. Thomas, L. I. Kruse, L. Silberman, *J. Org. Chem.* **1977**, 42, 3846–3852.
- [305] B. VanVeller, D. Robinson, T. M. Swager, *Angew. Chem. Int. Ed.* **2012**, 51, 1182–1186.
- [306] P. Cadiot, W. Chodkiewicz, in *Chemistry of Acetylenes*, Viehe, New York, **1969**, S. 597–647.
- [307] L. Shu, M. Müri, R. Krupke, M. Mayor, *Org. Biomol. Chem.* **2009**, 7, 1081–1092.
- [308] F. A. Carey, R. J. Sundberg, *Structure and Mechanisms*, Springer, **2007**.
- [309] G. P. Briner, J. Miller, M. Liveris, P. G. Lutz, *J. Chem. Soc.* **1954**, 1265–1266.
- [310] E. J. Corey, P. L. Fuchs, *Tetrahedron Lett.* **1972**, 13, 3769–3772.

9 Appendix

9.1 Abbreviations

a	Acceptor
Å	Angstrom
Ar	Aryl
Bu	Butyl
cos	cosine
CMOS	Complementary metal-oxide-semiconductor
COSY	Correlation spectroscopy
<i>Cp</i>	Cyclopentadienyl
<i>C_p</i>	Primary carbon
<i>C_q</i>	Quaternary carbon
<i>C_s</i>	Secondary carbon
<i>C_t</i>	Tertiary carbon
CV	Cyclic voltammetry
d	Donor
DCM	Dichloromethane
DIEA	Diisopropylethylamine
DIPA	Diisopropylamine
DMF	<i>N,N</i> -dimethylformamide
DMI	1,3-dimethylimidazolidin-2-one
EA	Elemental analysis
EI	Electron impact
equiv.	Equivalent
ESI	Electron spray ionization
Et	Ethyl
Fc	Ferrocene
HMBC	Heteronuclear multiple bond coherence

HMQC	Heteronuclear multiple quantum coherence
HOMO	Highest occupied molecular orbital
HOPG	Highly oriented pyrolytic graphite
HWE	Horner-Wadsworth-Emmons
LDA	Lithium diisopropylamine
LUMO	Lowest unoccupied molecular orbital
m/z	Mass per charge
MALDI	Matrix-assisted laser desorption/ionization
MCBJ	Mechanically controlled break junction
MMFF	Merck molecular force field
MS	Mass spectrometry
NMR	Nuclear magnetic resonance
NOESY	Nuclear Overhauser effect spectroscopy
OPE	Oligo-phenylene-ethynylene
OPV	Oligo-phenylene-vinylene
PG	Protecting group
Ph	Phenyl
ppm	Parts per million
Pr	Propyl
quant.	Quantitative
<i>p</i> -TsOH	<i>para</i> -Toluenesulfonic acid
R _f	Retention factor
r.t.	Room temperature
STM	Scanning tunneling microscopy
TBAF	Tetrabutylammonium fluoride
TBAH	Tetrabutylammonium hydroxide
TBAPF ₆	Tetrabutylammonium hexafluorophosphate
<i>t</i> BME	Tertiary-butyl methyl ether
THF	Tetrahydrofuran
TIPS	Triisopropylsilyl
TLC	Thin layer chromatography

TMEDA	<i>N,N,N',N'</i> -tetramethylenediamine
TMS	Trimethylsilyl
Trt	Trityl
UV/vis	Ultraviolet/visible
X-ray	X-ray specrometry

9.2 Contributions

During their ‘Wahlpraktikum’ Fabian Schmid and Andreas Spielhofer helped to synthesize important building blocks to assemble halide end-capped OPEs. Daniel Ebner did a scale up of the synthesis for building block **27**. The MCBJ measurements were performed by Jan Brunner from the group of Prof. Dr. Michel Calame at the University of Basel. The STM images were recorded by Hong Wang from the group of Prof. Dr. Lifeng Chi at the University of Muenster. All X-ray structures were measured by Dr. Markus Neuburger. EI and FAB-MS measurements were performed by Dr. Heinz Nadig. Elemental Analysis were measured by Werner Kirsch. 2D-NMR spectra were recorded by Heiko Gsellinger from the group of PD Dr. Daniel Häusinger at the University of Basel.

9.3 Spectra of target structures

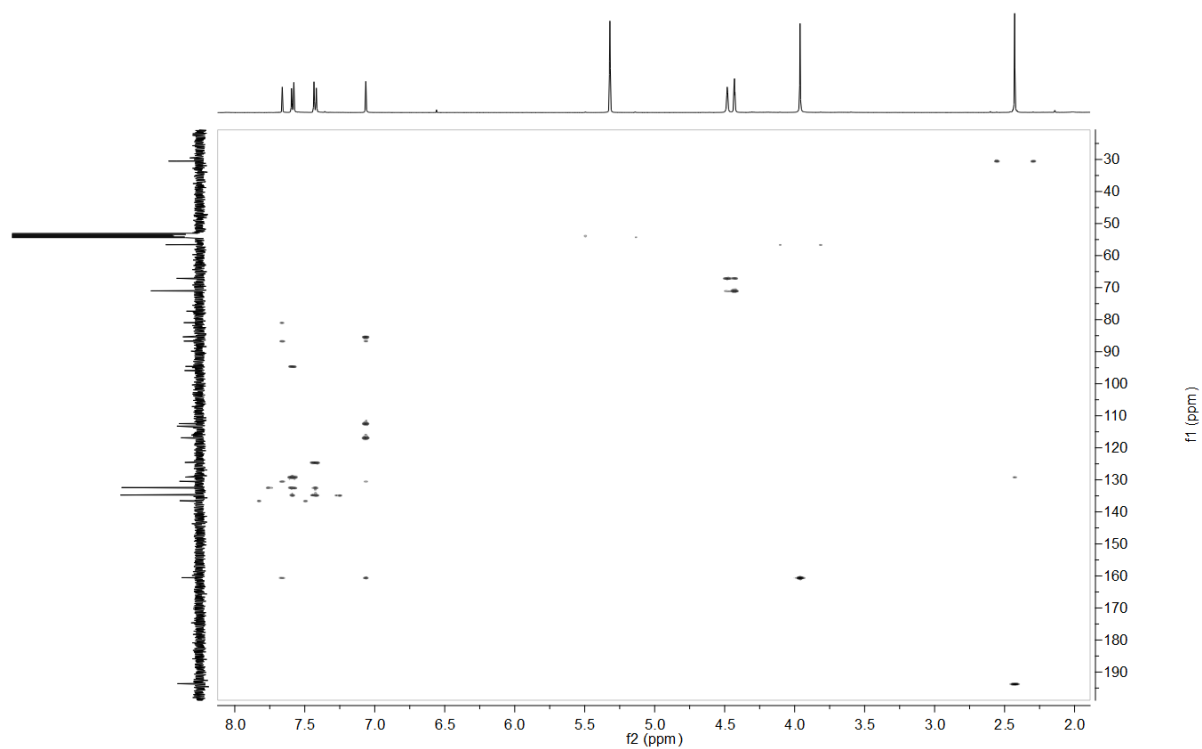


Figure 76. HMBC of compound 192.

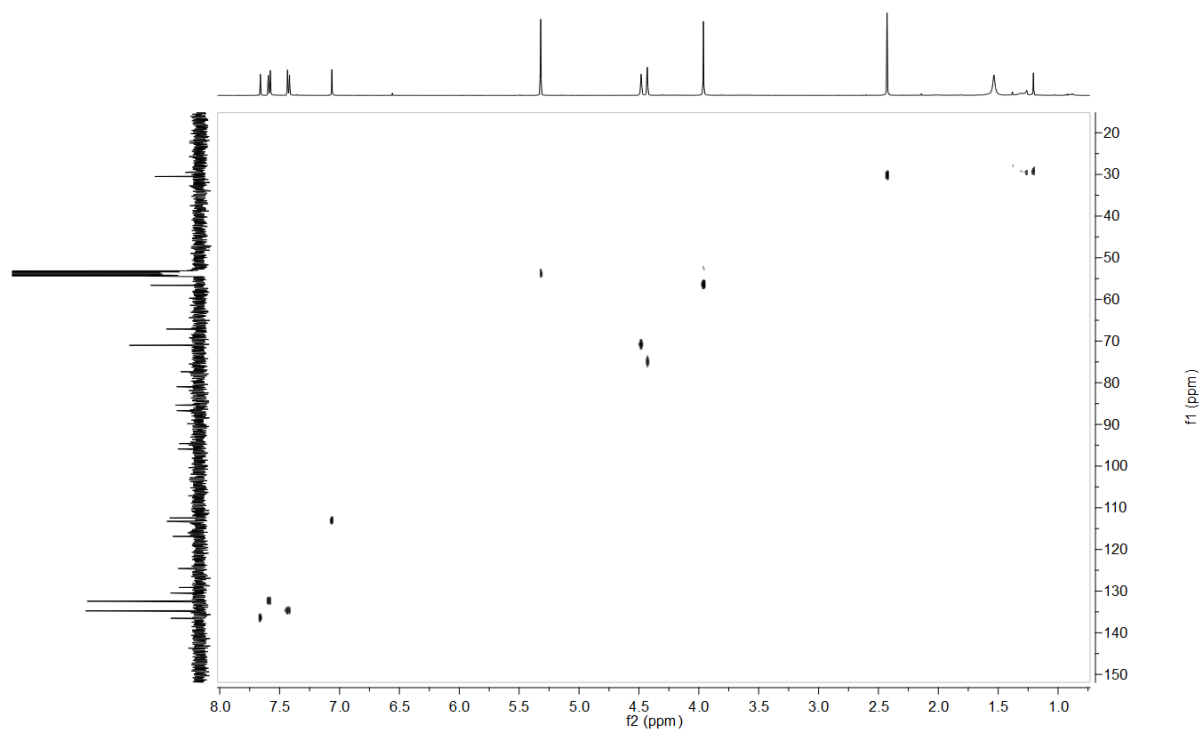


Figure 77. HMQC of compound 192:

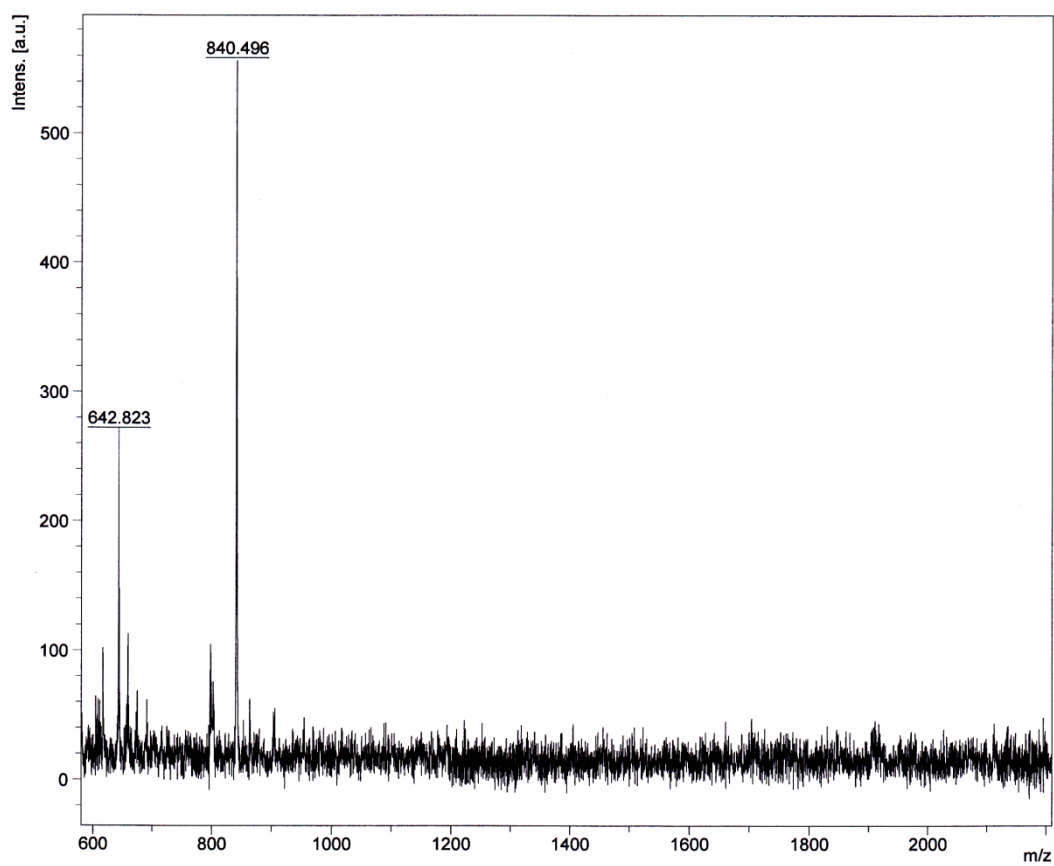


Figure 78. MALDI-MS of compound **192** (expected mass: 840).

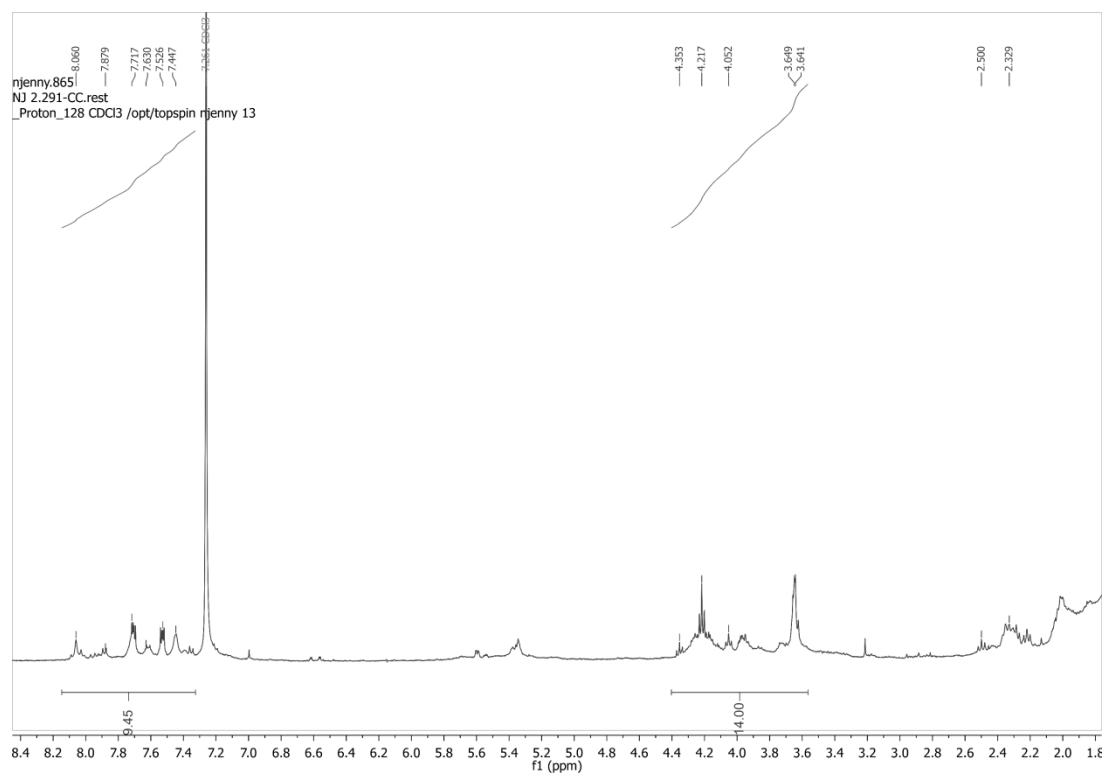


Figure 79. ¹H-NMR spectrum of compound **187**.

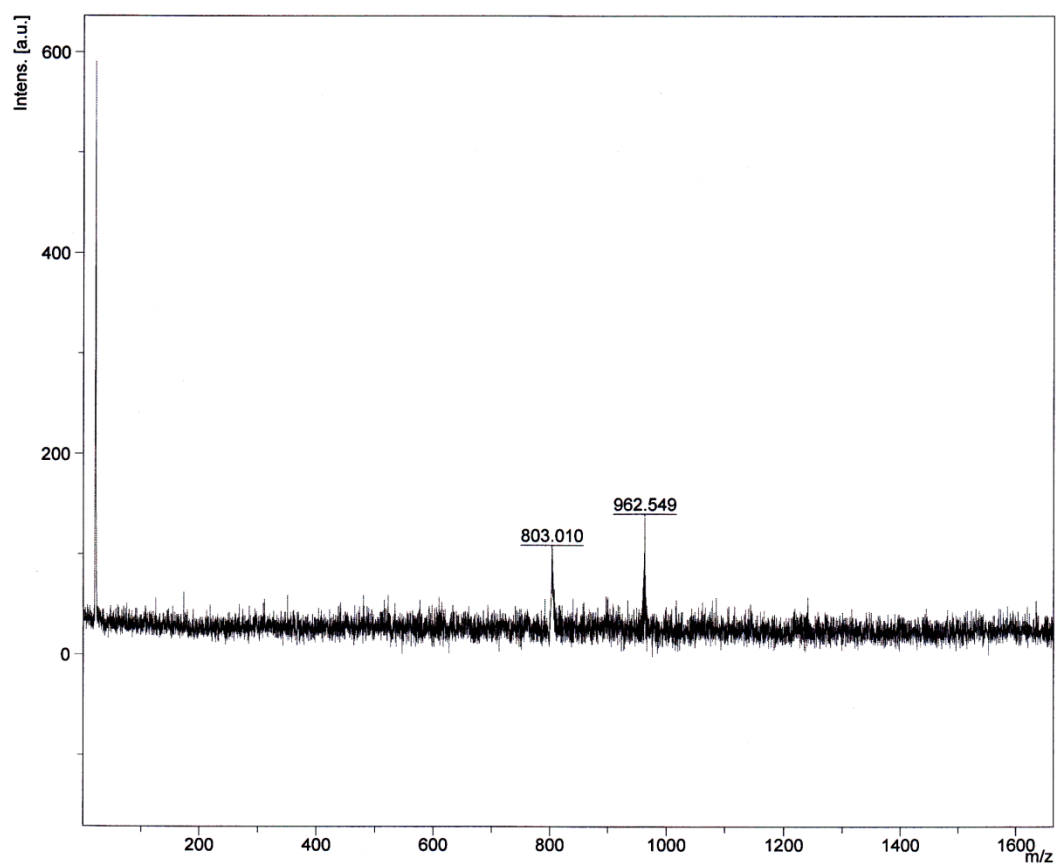


Figure 80. MALDI-MS of compound **187** (expected mass: 964).

Nicolas Marco Jenny

Date of birth: December 24th 1981

Nationality: Swiss

Education

PhD candidate 2008-2012

University of Basel, Department of organic Chemistry

Thesis: *Synthesis of New Functional Molecules for Molecular Electronics*, under the supervision of Prof. Dr. Marcel Mayor, University of Basel. 2008-2012

Publications:

N. M. Jenny et al., Phenyl–Acetylene Bond Assembly: A Powerful Tool for the Construction of Nanoscale Architectures, *Eur. J. Org. Chem.* **2011**, 26, 4965–4983.

N. M. Jenny et al., Synthesis and Solid State Investigations of Oligo-Phenylene-Ethynylene Structures with Halide End-Groups, *Eur. J. Org. Chem.* **2012**, 14, 2738-2747.

Master of Science in Chemistry 2007

University of Basel, Department of organic Chemistry.

Master Thesis: *Towards the synthesis of a push-pull Lander: Designed for integration into a surface decoupled STM-setup*, under the supervision of Prof. Dr. Marcel Mayor, University of Basel. 2006-2007

Chemist FH 2006

University of Applied Sciences (FHBB), Muttenz.

Diploma Thesis: *Substrat- und Reaktionsbreite des peptidischen Katalysators H-Pro-Pro-Asp-Ahx-PEG in Aldolreaktionen*, under the supervision of Prof. Dr. Helma Wennemers, University of Basel. 2002-2006

Professional Maturity 1997-2000

Ausbildungszentrum Muttenz.

Apprenticeship as laboratory technician 1997-2000

Ciba Specialty Chemicals Basel.

Professional Experience

Ciba Specialty Chemicals, Pratteln, Switzerland 2001-2002

R&D, Coating Effects, Schweizerhalle.

Ciba Specialty Chemicals, MacIntosh, Alabama, United States 2000-2001

R&D, Tinuvin® Focus Factory.